Nonlinear Wave Propagation and Imaging in Deterministic and Random Media

by

Wei Li

A dissertation submitted in partial fulfillment
of the requirements for the degree of
Doctor of Philosophy
(Applied and Interdisciplinary Mathematics)
in the University of Michigan
2016

Doctoral Committee:
Professor Liliana Borcea, Co-Chair
Professor John C. Schotland, Co-Chair
Professor Peter D. Miller
Professor Theodore B. Norris
Emeritus Professor Jeffrey B. Rauch

Acknowledgements

I would like to express my sincere gratitude to my advisors Professor Liliana Borcea and Professor John C. Schotland, for all the time that they invested, all the support that they offered and all the guidance and insight that they provided.

I would also like to thank the rest of my committee members, Professor Peter D. Miller, Professor Theodore B. Norris and Professor Jeffrey B. Rauch, for their valuable discussions and suggestions.

Table of Contents

List of Figures

Abstract

This thesis consists of three projects that attempt to understand and identify applications for optical scattering from small nonlinear scatterers.

In the first part of the thesis we consider the direct scattering problem from a collection of small nonlinear scatterers. We considered all common types of quadratic and cubic nonlinearities within the scalar wave theory. We assume that the scatterers are small compared to the incident wavelength, thus the Lippman-Schwinger integral equations can be converted to algebraic equations. We further assume that the nonlinearity is weak, thus the scattering amplitudes can be calculated by solving the algebraic equations perturbatively. We apply this method to explore the redistribution of energy among the frequency components of the field, the modifications of scattering resonances and the mechanism of optical bistability for the Kerr nonlinearity.

In the second part of the thesis we generalized the optical theorem to nonlinear scattering processes. The optical theorem is a conservation law which has only been shown to hold in linear media. We show that the optical theorem holds exactly for polarizations as arbitrary functions of the electric field, which includes nonlinear media as a special case. As an application, we develop a model for apertureless near-field scanning optical microscopy. We model the sample as a collection of small linear scatterers, and introduce a nonlinear metallic scatterer as the near-field tip. We show that this imaging method is background-free and achieves subwavelength resolution. This work is done for the full Maxwell model.

In the third part of the thesis we consider the imaging of small nonlinear scatterers in random media. We analyze the problem of locating small nonlinear scatterers in weakly scattering random media which respond linearly to light. We show that for propagation distances within a few transport mean free paths, we can obtain robust images using the coherent interferometry (CINT) imaging functions. We also show that imaging the quadratic susceptibility with CINT yields better result, because that the CINT imaging function for the linear susceptibility has noisy peaks in a region that depends on the geometry of the aperture and the cone of incident directions.

Chapter 1

Introduction

This thesis consists of three projects that attempt to understand and identify applications for optical scattering from systems consisting of small nonlinear scatterers. Nonlinear optics is a rich and rapidly developing field of study that is concerned with the nonlinear interaction of light and optical materials. The fundamental physical principle underlying nonlinear optics is that the electric polarization of material media responds nonlinearly to applied fields, thus leading to the presence of nonlinear terms in the Maxwell equations. These nonlinear terms give rise to many interesting effects, including the generation of new harmonics and the coupling of fields at different frequencies. These phenomena are the building blocks of optical amplifiers, frequency converters, phase conjugation mirrors, self focusing lens, soliton transmission systems and optical computing units [17, 81, 77]. Optical nonlinearity also poses great mathematical challenges. Despite well-known existence and uniqueness results for the nonlinear Maxwell equations [6, 5], few exact solutions are known except in one dimension [17, 81, 77].

In the first part of the thesis we consider the problem of scattering from a collection of small nonlinear scatterers. We begin by investigating the case of a single spherical scatterer. This problem was solved by Mie in 1908 when the scatterer is linear [59], but there are

no results when the scatterer is nonlinear [71]. To simplify the problem, we assume that the nonlinearity is weak and the scatterers are small compared to the incident wavelength. Thus the scattering amplitude can be calculated perturbatively. Note that for sufficiently small particles, quantum effects may become important [97], which we do not take into consideration in this thesis. We apply this method to typical quadratic and cubic frequency mixing processes in the presence of one or two small scatterers, including second harmonic generation, three wave mixing, the Kerr effect, third harmonic generation and four wave mixing. We characterize the redistribution of energy among the frequency components of the field. We also discover modifications of scattering resonances, depending on the type of nonlinearity. An important finding is that the developed method also reveals the mechanism of optical bistability for the Kerr nonlinearity in the presence of one scatterer. The results in this part of the thesis are derived within the scalar theory of electromagnetic scattering, but can be readily generalized to the Maxwell equations.

The second part of the thesis is concerned with the generalization of the optical theorem to nonlinear scattering processes. The optical theorem relates the extinguished power in a scattering process to the scattering amplitude in the forward direction. It has been formulated in a variety of settings including quantum mechanics, acoustics and electromagnetic theory. However, all of the existing formulations of the optical theorem assume that the medium is linear [16]. Using a similar approach to [21], we show that the optical theorem holds when the polarization is an arbitrary function of the electric field. As a special case, this relation holds for nonlinear media.

As an application of the generalized optical theorem, we develop a model for apertureless near-field scanning optical microscopy (NSOM). NSOM is a widely used tool to overcome the diffraction limit by exploiting the fast oscillating evanescent waves in the near field of the sample. A typical experiment involves illuminating the sample by an incident field from the far field, scanning a tip in the near field of the sample and recording the scattered field

by a detector placed in the far field of the sample and tip. The image is formed by plotting the intensity as the position of the tip is varied. Recent experiments have utilized nonlinear metallic scatterers as near-field tips [41]. The key advantage of this approach is that the tip acts as a source of a background-free field. We model the imaging system as a collection of small scatterers: the tip is a small nonlinear metal particle and the sample consists of small linear dielectric particles. Thus the field at the tip can be calculated by the methods developed in this thesis. We study in detail the achievable resolution compared to the case of a linear tip.

In the third part of the thesis we consider the imaging of small nonlinear scatterers in random media. Many imaging systems involve background media which vary randomly in space, such as the atmosphere, the ocean, and biological tissues. The effects of these media on the propagation of light depend on factors including the spatial size and structure of the inhomogeneities, the magnitude of the fluctuation, and the distance over which the light propagates. The imaging of small linear scatterers in random media has been extensively studied for decades [43, 44]. However, the imaging of nonlinear scatterers has only recently been considered. For instance, in [2] nonlinear imaging of a random medium exhibiting second harmonic generation was studied by employing the method of Kirchoff migration. In that work, a two-dimensional systems was studied in which the electromagnetic field at the fundamental frequency was taken to have transverse-electric polarization, while the second-harmonic field had transverse-magnetic polarization. In contrast, we consider the full three-dimensional problem within the scalar theory developed in chapter 1. We consider a scattering background medium with many weak inhomogeneities. The effect of an individual inhomogeneity is too weak to be observed, but the cumulative effect of all the inhomogeneities is not negligible over long propagation distances. To account for the scattering from the inhomogeneities, we model the background medium as one realization of a random process. In addition to investigating Kirchoff migration in this setting, we also

study imaging methods that make use of correlations. We show that the migration images of both linear and nonlinear susceptibilities focus well in homogeneous media. But in random media, when the propagation distance exceeds a few scattering mean free paths, the migration images become unstable. This means that the image in one realization of the random medium may be difficult to interpret, and the location of the peaks of the images change significantly in different realizations of the random medium. To obtain stable images for longer propagation distance, we derive a coherent interferometry (CINT) imaging function for the linear and quadratic susceptibilities [15]. We show for propagation distances between a few scattering mean free paths and a few transport mean free paths, the CINT imaging functions stabilize the images of both linear and quadratic susceptibilities, at the expense of resolution. However the CINT imaging function for the linear susceptibility has large peaks in a region that depends on the geometry of the aperture and the cone of incident directions. This region covers a larger proportion of the imaging domain as the size of the aperture or the incident cone grows. Thus the linear susceptibility of the scatterers is not visible in the images if the scatterers are located in this region. This problem is due to the fact that the randomized incident wave can not be eliminated as a component of the recorded data. In the meanwhile, the CINT image of the quadratic susceptibility does not suffer from this problem because that there is no incident wave at the second harmonic frequency. Thus, imaging the quadratic susceptibility with CINT yields the best result.

Chapter 2

Point Scatterers in Nonlinear Optics

2.1 Introduction

The scattering of waves by spherical particles, or collections of such particles, is a topic of fundamental interest. It is also of considerable applied importance in fields ranging from atmospheric science to nano-optics. The problem arises in various settings, including in quantum mechanics, acoustics and electromagnetism. Indeed, entire volumes have been devoted to its study [39, 89, 65]. For the case of a single sphere, it is well known that the scattered field can be expressed as a superposition of partial waves [59, 33]. If the radius of the sphere is large compared to the wavelength, the evaluation of such sums is both numerically complex and physically unrevealing. Thus the use of asymptotic methods is essential to understand phenomena such as Mie resonances and the approach to the diffraction limit [65]. In the opposite limit of a small sphere, which we will refer to as a point scatterer, integral equation methods can be employed to calculate the scattered field [92]. This approach can also be extended to treat the case of multiple point scatterers [36, 50, 73]. Here there are applications to surface plasmon polaritons in nanoparticle waveguides [18, 54, 55, 29, 57, 38], propagation of excitons in molecular chains [37], and spontaneous emission of molecules

in the vicinity of nanostructures [24, 3, 20].

The problem of scattering from spheres has also been addressed in the context of nonlinear optics. In addition to allowing for a much greater variety of physical phenomena, nonlinear effects introduce considerable mathematical complexity. For instance, in the case of the Kerr nonlinearity, exact solutions to the problem of scattering from a sphere are not known. The same is true for the case of second-harmonic generation (SHG). However, the fact that SHG is forbidden in the bulk of centrosymmetric systems and takes place only at interfaces can be used, in some instances, to obtain approximate solutions to the problem of scattering from spherical particles [31, 30, 66, 71, 79].

In this chapter we consider the problem of scattering from point objects in nonlinear optics. By making use of integral equation methods, we find exact solutions to a large class of problems with both second- and third-order nonlinearities. In particular, we study in detail the processes of second-harmonic generation, sum- and difference-frequency generation, three-wave mixing, Kerr effect, third-harmonic generation and four-wave mixing. The theory is developed both for single point-scatterers and collections of point-scatterers. In each case, we calculate the scattering amplitude and characterize the associated scattering resonances. For simplicity, we work within the scalar theory of electromagnetic scattering. The extension to the vector theory poses no particular problems and was partially described in previous work on the optical theorem in nonlinear optics [52].

The remainder of this chapter is organized as follows. In Sec. 2.2 the necessary background in nonlinear optics is recalled. In addition, the integral equation formulation of scattering theory that we use throughout the chapter is derived. In Secs. 2.3 and 2.4 we consider separately the cases of second- and third-order nonlinearities, respectively. Numerical illustrations of our results are described in Sec. 2.5. Finally, we summarize our results in Sec. 2.6. Several appendices include the mathematical details of calculations that are too long to be presented in the body of the chapter.

2.2 Preliminaries

In the scalar theory of electromagnetic fields, the scalar electric field $u(\mathbf{r}, t)$ obeys the wave equation

$$\Delta u(\mathbf{r}, t) - \frac{1}{c^2}\frac{\partial^2 u(\mathbf{r}, t)}{\partial t^2} = \frac{4\pi}{c^2}\frac{\partial^2 P(\mathbf{r}, t)}{\partial t^2}, \tag{2.1}$$

where P is the polarization density [81, 17]. This is a good approximation when the dielectric susceptibilities of the medium are slowly varying, the nonlinear coupling between distinct components of the electric fields is weak, and the boundary conditions are imposed far from the region of interest.

We adopt the following Fourier transformation convention:

$$f(\mathbf{r}, \omega) = \int f(\mathbf{r}, t) e^{i\omega t} dt \ , \tag{2.2}$$

$$f(\mathbf{r}, t) = \frac{1}{2\pi}\int f(\mathbf{r}, \omega) e^{-i\omega t} d\omega \ , \tag{2.3}$$

where the time and frequency dependences are differentiated by the names of the relevant variables. Note that if $f(\mathbf{r}, t)$ is real-valued, then $f(\mathbf{r}, -\omega) = f^*(\mathbf{r}, \omega)$. Performing the Fourier transform of (2.1), we obtain

$$\Delta u(\mathbf{r}, \omega) + k^2(\omega) u(\mathbf{r}, \omega) = -4\pi k^2(\omega) P(\mathbf{r}, \omega), \tag{2.4}$$

where $k(\omega) = \omega/c$. Throughout this chapter, we consider incident fields that are monochromatic with frequency ω.

The polarization may be expanded in powers of the electric field. In principle, the expansion involves infinitely many terms, but only the first few terms are of practical importance. In this chapter, we restrict our attention to linear, quadratic and cubic media. A medium is

linear if

$$P(\mathbf{r},\omega) = \chi^{(1)}(\mathbf{r},\omega)u(\mathbf{r},\omega) \ , \tag{2.5}$$

where the coefficient $\chi^{(1)}(\mathbf{r},\omega)$ is the first-order susceptibility. A medium is said to be quadratically nonlinear if

$$P(\mathbf{r},\omega) = \chi^{(1)}(\mathbf{r},\omega)u(\mathbf{r},\omega) + \sum_{\omega_1+\omega_2=\omega} \chi^{(2)}(\mathbf{r},\omega_1,\omega_2)u(\mathbf{r},\omega_1)u(\mathbf{r},\omega_2) \ , \tag{2.6}$$

where $\chi^{(2)}(\mathbf{r},\omega_1,\omega_2)$ are the second-order susceptibilities. The summation implies that the electric field at the frequencies ω_1 and ω_2 contributes to the polarization at the frequency ω if $\omega_1 + \omega_2 = \omega$. A medium is cubically nonlinear if

$$P(\mathbf{r},\omega) = \chi^{(1)}(\mathbf{r},\omega)u(\omega) + \sum_{\omega_1+\omega_2+\omega_3=\omega} \chi^{(3)}(\mathbf{r},\omega_1,\omega_2,\omega_3)u(\mathbf{r},\omega_1)u(\mathbf{r},\omega_2)u(\mathbf{r},\omega_3) \ , \tag{2.7}$$

where $\chi^{(3)}(\mathbf{r},\omega_1,\omega_2,\omega_3)$ are the third-order susceptibilities. Materials with inversion symmetry have zero second-order susceptibilities and thus fall into this category.

We will assume that the susceptibilities have full permutation symmetry. Thus, the quadratic susceptibilities satisfy the conditions

$$\begin{aligned} &\chi^{(2)}(\mathbf{r},\omega_2,\omega_3) = \chi^{(2)}(\mathbf{r},\omega_3,\omega_2) = \chi^{(2)}(\mathbf{r},\omega_1,-\omega_3) \\ &= \chi^{(2)}(\mathbf{r},-\omega_3,\omega_1) = \chi^{(2)}(\mathbf{r},\omega_1,-\omega_2) = \chi^{(2)}(\mathbf{r},-\omega_2,\omega_1) \ , \end{aligned} \tag{2.8}$$

provided that $\omega_1 = \omega_2 + \omega_3$. The cubic susceptibilities satisfy

$$\begin{aligned}
&\chi^{(3)}(\mathbf{r}, \omega_2, \omega_3, \omega_4) = \chi^{(3)}(\mathbf{r}, \omega_2, \omega_4, \omega_3) = \chi^{(3)}(\mathbf{r}, \omega_3, \omega_2, \omega_4) \\
&= \chi^{(3)}(\mathbf{r}, \omega_3, \omega_4, \omega_2) = \chi^{(3)}(\mathbf{r}, \omega_4, \omega_2, \omega_3) = \chi^{(3)}(\mathbf{r}, \omega_4, \omega_3, \omega_2) \\
&= \chi^{(3)}(\mathbf{r}, \omega_1, -\omega_2, -\omega_3) = \chi^{(3)}(\mathbf{r}, \omega_1, -\omega_2, -\omega_4) = \chi^{(3)}(\mathbf{r}, \omega_1, -\omega_3, -\omega_4)
\end{aligned} \tag{2.9}$$

provided that $\omega_1 = \omega_2 + \omega_3 + \omega_4$. This assumption is known to be true for non resonant frequencies in the anharmonic oscillator model [17].

Suppose that a source generates an incident wave $u_i(\mathbf{r}, \omega)$. The solution to the wave equation (2.4) can be expressed as the sum of the incident field and the scattered field $u_s(\mathbf{r}, \omega)$:

$$u(\mathbf{r}, \omega) = u_i(\mathbf{r}, \omega) + u_s(\mathbf{r}, \omega) \ . \tag{2.10}$$

It follows that the incident field satisfies the equation

$$\Delta u_i(\mathbf{r}, \omega) + k^2(\omega) u_i(\mathbf{r}, \omega) = 0 \ , \tag{2.11}$$

and the scattered field obeys

$$\Delta u_s(\mathbf{r}, \omega) + k^2(\omega) u_s(\mathbf{r}, \omega) = -4\pi k^2(\omega) P(\mathbf{r}, \omega) \ . \tag{2.12}$$

We then have that the field is given by

$$u(\mathbf{r}, \omega) = u_i(\mathbf{r}, \omega) + \int dr' G(\mathbf{r}, \mathbf{r}', \omega) P(\mathbf{r}', \omega) \ . \tag{2.13}$$

Here the Green's function $G(\mathbf{r}, \mathbf{r}', \omega)$ obeys

$$(\Delta + k^2(\omega)) G(\mathbf{r}, \mathbf{r}', \omega) = -4\pi \delta(\mathbf{r} - \mathbf{r}') \tag{2.14}$$

and is of the form

$$G(\mathbf{r}, \mathbf{r}', \omega) = \frac{e^{ik(\omega)|\mathbf{r}-\mathbf{r}'|}}{|\mathbf{r}-\mathbf{r}'|} \ . \tag{2.15}$$

The asymptotic form of the Green's function in the far field is

$$G(\mathbf{r}, \mathbf{r}', \omega) \sim \frac{e^{ik(\omega)r}}{r} e^{-ik(\omega)\hat{\mathbf{r}}\cdot\mathbf{r}'} \ , \quad \text{for} \quad r \gg r' \ . \tag{2.16}$$

Thus the scattered field behaves as an outgoing spherical wave of the form

$$u_s(\mathbf{r}, \omega) \sim \frac{e^{ik(\omega)r}}{r} A(\mathbf{r}, \omega) \ , \tag{2.17}$$

where the scattering amplitude is defined by

$$A = k^2(\omega) \int_V e^{-ik(\omega)\hat{\mathbf{r}}\cdot\mathbf{r}'} P(\mathbf{r}', \omega) d^3r' \ . \tag{2.18}$$

2.3 Second-order nonlinearities

In this section we study second-order nonlinear effects including second-harmonic generation (SHG), sum-difference frequency generation (SDFG) and three-wave mixing (TWM) for a medium consisting of one or two small spherical inclusions. We assume that the nonlinear susceptibilities are sufficiently weak that the condition

$$\sum_{\omega_1+\omega_2=\omega} \chi^{(2)}(\mathbf{r}, \omega_1, \omega_2) u(\mathbf{r}, \omega_1) u(\mathbf{r}, \omega_2) \ll \chi^{(1)}(\mathbf{r}, \omega) u(\mathbf{r}, \omega) \tag{2.19}$$

is obeyed.

2.3.1 Second-harmonic generation

We consider SHG excited by a monochromatic incident field of frequency Ω. We then find that the wave equation (2.1) together with (2.6) and (2.8) gives rise to the pair of coupled wave equations for the electric fields at the frequencies Ω and 2Ω:

$$\Delta u(\mathbf{r},\Omega) + k^2(\Omega)(1 + 4\pi\chi^{(1)}(\mathbf{r},\Omega)))u(\mathbf{r},\Omega) = -4\pi k^2(\Omega)2\chi^{(2)}(2\Omega,-\Omega)u(\mathbf{r},2\Omega)u^*(\mathbf{r},\Omega) \tag{2.20}$$

$$\Delta u(\mathbf{r},2\Omega) + k^2(2\Omega)(1 + 4\pi\chi^{(1)}(\mathbf{r},2\Omega))u(\mathbf{r},2\Omega) = -4\pi k^2(2\Omega)^2\chi^{(2)}(\Omega,\Omega)u(\mathbf{r},\Omega)^2 \ . \tag{2.21}$$

Note that we have not accounted for the formation of higher harmonics, consistent with the condition (2.19). It follows immediately from (2.13) that the solutions to (2.20) and (2.21) are given by

$$\begin{aligned} u(\mathbf{r},\Omega) &= u_i(\mathbf{r},\Omega) + k^2(\Omega)\int d^3r'\chi^{(1)}(\mathbf{r}',\Omega)G(\mathbf{r},\mathbf{r}',\Omega)u(\mathbf{r}',\Omega) \\ &\quad +2k^2(\Omega)\int d^3r'\chi^{(2)}(\mathbf{r}',2\Omega,-\Omega)G(\mathbf{r},\mathbf{r}',\Omega)u(\mathbf{r}',2\Omega)u^*(\mathbf{r}',\Omega) \ , \qquad (2.22) \\ u(\mathbf{r},2\Omega) &= k^2(2\Omega)\int d^3r'\chi^{(1)}(\mathbf{r}',2\Omega)G(\mathbf{r},\mathbf{r}',2\Omega)u(\mathbf{r}',2\Omega) \\ &\quad +k^2(2\Omega)\int d^3r'\chi^{(2)}(\mathbf{r}',\Omega,\Omega)G(\mathbf{r},\mathbf{r}',2\Omega)u(\mathbf{r}',\Omega)u(\mathbf{r}',\Omega) \ . \qquad (2.23) \end{aligned}$$

SHG with one point scatterer

Suppose that the scattering medium is a small ball of radius a with $k(\Omega)a \ll 1$ and $k(2\Omega)a \ll 1$. The susceptibilities are taken to be $\chi^{(1)}(\mathbf{r},\omega) = \eta^{(1)}$ and $\chi^{(2)}(\mathbf{r},\omega) = \eta^{(2)}$ for $|\mathbf{r}| \leq a$ and

to vanish for $|\mathbf{r}| > a$. Eqs. (2.22) and (2.23) thus become

$$\begin{aligned} u(\mathbf{r},\Omega) &= u_i(\mathbf{r},\Omega) + k^2(\Omega)\eta^{(1)} \int_{|\mathbf{r}'|<a} d^3r' G(\mathbf{r},\mathbf{r}',\Omega)u(\mathbf{r}',\Omega) \\ &\quad +2k^2(\Omega)\eta^{(2)} \int_{|\mathbf{r}'|<a} d^3r' G(\mathbf{r},\mathbf{r}',\Omega)u(\mathbf{r}',2\Omega)u^*(\mathbf{r}',\Omega) \ , \qquad (2.24) \\ u(\mathbf{r},2\Omega) &= k^2(2\Omega)\eta^{(1)} \int_{|\mathbf{r}'|<a} d^3r' G(\mathbf{r},\mathbf{r}',\Omega)u(\mathbf{r}',2\Omega) \\ &\quad +k^2(2\Omega)\eta^{(2)} \int_{|\mathbf{r}'|<a} d^3r' G(\mathbf{r},\mathbf{r}',\Omega)u(\mathbf{r}',\Omega)u(\mathbf{r}',\Omega) \ . \qquad (2.25) \end{aligned}$$

Using the asymptotic form of the Green's function given in (2.16), we find that the scattered fields are of the form

$$\begin{aligned} u_s(\mathbf{r},\Omega) &= A(\mathbf{r},\Omega)\frac{e^{ik(\Omega)r}}{r} \ , \qquad (2.26) \\ u_s(\mathbf{r},2\Omega) &= A(\mathbf{r},2\Omega)\frac{e^{ik(2\Omega)r}}{r} \ , \qquad (2.27) \end{aligned}$$

where the scattering amplitudes are defined by

$$\begin{aligned} A(\mathbf{r},\Omega) &= \frac{4\pi}{3}a^3k^2(\Omega)(\eta^{(1)}u(\mathbf{0},\Omega) + 2\eta^{(2)}u(\mathbf{0},2\Omega)u^*(\mathbf{0},\Omega)) \ , \qquad (2.28) \\ A(\mathbf{r},2\Omega) &= \frac{4\pi}{3}a^3k^2(2\Omega)(\eta^{(1)}u(\mathbf{0},2\Omega) + \eta^{(2)}u(\mathbf{0},\Omega)u(\mathbf{0},\Omega)) \ . \qquad (2.29) \end{aligned}$$

Here we have used the fact that the radius of the scatterer is small, along with the identity

$$\int_{|\mathbf{r}'|<a} d^3r' e^{-ik(\omega)\hat{\mathbf{r}}\cdot\mathbf{r}'} g(k(\omega)\mathbf{r}') = \frac{4\pi}{3}a^3 g(\mathbf{0})(1 + O(k(\omega)a)) \ , \qquad (2.30)$$

for an arbitrary function g. To proceed, we must now calculate the local fields $u(\mathbf{0},\Omega)$ and $u(\mathbf{0},2\Omega)$. To do so, we set $\mathbf{r}=\mathbf{0}$ in (2.24) and (2.25) and thus obtain

$$\begin{aligned} u(\mathbf{0},\Omega) &= u_i(\mathbf{0},\Omega)+k^2(\Omega)\eta^{(1)}\int_{|\mathbf{r}'|<a} d^3r' G(\mathbf{0},\mathbf{r}',\Omega)u(\mathbf{r}',\Omega) \\ &\quad +2k^2(\Omega)\eta^{(2)}\int_{|\mathbf{r}'|<a} d^3r' G(\mathbf{0},\mathbf{r}',\Omega)u(\mathbf{r}',\Omega)u^*(\mathbf{r}',2\Omega)\ , \qquad (2.31) \\ u(\mathbf{0},2\Omega) &= k^2(2\Omega)\eta^{(1)}\int_{|\mathbf{r}'|<a} d^3r' G(\mathbf{0},\mathbf{r}',\Omega)u(\mathbf{r}',2\Omega) \\ &\quad +k^2(\Omega)\eta^{(2)}\int_{|\mathbf{r}'|<a} d^3r' G(\mathbf{0},\mathbf{r}',\Omega)u(\mathbf{r}',\Omega)u(\mathbf{r}',\Omega))\ . \qquad (2.32) \end{aligned}$$

Next, we use the fact that for an arbitrary function g

$$\begin{aligned} &\int_{|\mathbf{r}'|<a} d^3r' G(\mathbf{0},\mathbf{r}',\omega)g(\mathbf{r}',\omega) \\ &= 4\pi a^2\left(\frac{1}{2}+i\frac{1}{3}k(\omega)a+O((k(\omega)a)^2)\right)g(\mathbf{0},\omega)\,(1+O(k(\omega)a))\ . \qquad (2.33) \end{aligned}$$

We then find that (2.31) and (2.32) lead to a system of nonlinear algebraic equations for the local fields which are of the form

$$\begin{aligned} u(\mathbf{0},\Omega) &= u_i(\mathbf{0},\Omega)+\frac{4\pi}{3}a^3k^2(\Omega)G_R(\Omega)(\eta^{(1)}u(\mathbf{0},\Omega)+2\eta^{(2)}u(\mathbf{0},2\Omega)u^*(\mathbf{0},\Omega))\ , \qquad (2.34) \\ u(\mathbf{0},2\Omega) &= \frac{4\pi}{3}a^3k^2(2\Omega)G_R(2\Omega)(\eta^{(1)}u(\mathbf{0},2\Omega)+\eta^{(2)}u(\mathbf{0}',\Omega)u(\mathbf{0},\Omega))\ , \qquad (2.35) \end{aligned}$$

where

$$G_R(\omega)=\frac{3}{2a}+ik(\omega)\ . \qquad (2.36)$$

To solve the above equations we proceed perturbatively. We thus introduce a small parameter ϵ to scale the nonlinear terms in (2.34) and (2.35):

$$u(\mathbf{0},\Omega) = u_i(\mathbf{0},\Omega) + \frac{4\pi}{3}a^3k^2(\Omega)G_R(\Omega)(\eta^{(1)}u(\mathbf{0},\Omega) + 2\epsilon\eta^{(2)}u(\mathbf{0},2\Omega)u^*(\mathbf{0},\Omega)) \ , \quad (2.37)$$

$$u(\mathbf{0},2\Omega) = \frac{4\pi}{3}a^3k^2(2\Omega)G_R(2\Omega)(\eta^{(1)}u(\mathbf{0},2\Omega) + \epsilon\eta^{(2)}u(\mathbf{0},\Omega)u(\mathbf{0},\Omega)) \ . \quad (2.38)$$

We then introduce formal expansions for the fields of the form

$$u(0,\Omega) = u^{(0)}(0,\Omega) + \epsilon u^{(1)}(0,\Omega) + \epsilon^2 u^{(2)}(0,\Omega) + \cdots \ , \quad (2.39)$$

$$u(0,2\Omega) = u^{(0)}(0,2\Omega) + \epsilon u^{(1)}(0,2\Omega) + \epsilon^2 u^{(2)}(0,2\Omega) + \cdots \ . \quad (2.40)$$

For simplicity, we assume that the direction of observation is taken to be $\widehat{\mathbf{z}}$. To simplify the notation, we set $\Omega_1 = \Omega$, $\Omega_2 = 2\Omega$, and write $u_j = u(\mathbf{0},\Omega_j)$, $k_j = \Omega_j/c$ and $G_{Rj} = G_R(\Omega_j)$. Then (2.37) and (2.38) become

$$u_1 = u_i + \frac{4\pi}{3}a^3k_1^2G_{R1}(\eta^{(1)}u_1 + 2\eta^{(2)}u_1^*u_2) \ , \quad (2.41)$$

$$u_2 = \frac{4\pi}{3}a^3k_2^2G_{R2}(\eta^{(1)}u_2 + \eta^{(2)}u_1u_1) \ . \quad (2.42)$$

Next, we expand the fields $u_{1,2}$ according to (2.39) and (2.40) and collect like powers of ϵ. At $O(1)$ we have that

$$u_1^{(0)} = u_i^{(0)} + \frac{4\pi}{3}a^3k_1^2G_{R1}\eta^{(1)}u_1^{(0)} \ , \quad (2.43)$$

$$u_2^{(0)} = 0 \ . \quad (2.44)$$

Thus

$$u_1^{(0)} = \frac{1}{1 - \frac{4\pi}{3}a^3k_1^2G_{R1}\eta^{(1)}} \ . \quad (2.45)$$

At $O(\epsilon)$ we have

$$u_1^{(1)} = \frac{4\pi}{3} a^3 k_1^2 G_{R1} \eta^{(1)} u_1^{(1)} \ , \tag{2.46}$$

$$u_2^{(1)} = \frac{4\pi}{3} a^3 k_2^2 G_{R2} (\eta^{(1)} u_2^{(1)} + \eta^{(2)} u_1^{(0)} u_1^{(0)}) \ , \tag{2.47}$$

which gives

$$u_2^{(1)} = \frac{4\pi}{3} a^3 k_2^2 G_{R2} (\eta^{(1)} u_2^{(1)} + \eta^{(2)} u_1^{(0)} u_1^{(0)}) \ . \tag{2.48}$$

Thus

$$u_2^{(1)} = \frac{\frac{4\pi}{3} a^3 k_2^2 G_{R2} \eta^{(2)} u_1^{(0)} u_1^{(0)}}{1 - \frac{4\pi}{3} a^3 k_2^2 G_{R2} \eta^{(1)}} \ . \tag{2.49}$$

At $O(\epsilon^2)$ we obtain

$$u_1^{(2)} = \frac{4\pi}{3} a^3 k_1^2 G_{R1} (\eta^{(1)} u_1^{(2)} + 2\eta^{(2)} (u_1^{(0)})^* u_2^{(1)}) \ , \tag{2.50}$$

which gives

$$u_1^{(2)} = \frac{4\pi}{3} a^3 k_1^2 G_{R1} (\eta^{(1)} u_1^{(2)} + 2\eta^{(2)} u_2^{(1)} (u_1^*)^{(0)}) \ . \tag{2.51}$$

Thus

$$u_1^{(2)} = \frac{\frac{4\pi}{3} a^3 k_1^2 G_{R1} 2\eta^{(2)} (u_1^*)^{(0)} u_2^{(1)}}{1 - \frac{4\pi}{3} a^3 k_1^2 G_{R1} \eta^{(1)}} \ . \tag{2.52}$$

We can now calculate the scattering amplitude from (2.28). We find that

$$A(\mathbf{r},\Omega) = \frac{4\pi}{3}a^3k_1^2(\eta^{(1)}u_1^{(0)}+\eta^{(1)}u_1^{(2)}+2\eta^{(2)}(u_1^*)^{(0)}u_2^{(1)})u_i^*+\cdots\ , \tag{2.53}$$

$$A(\mathbf{r},2\Omega) = \frac{4\pi}{3}a^3k_2^2\eta^{(2)}(u_1^{(0)})^2+\cdots\ . \tag{2.54}$$

Restoring our original notation, we obtain

$$\begin{aligned} A(\mathbf{r},\Omega) &= \frac{4\pi}{3}a^3k^2(\Omega)((\eta^{(1)}u^{(0)}(\mathbf{0},\Omega)+\eta^{(1)}u^{(2)}(\mathbf{0},\Omega) \\ &\quad +2\eta^{(2)}(u^{(0)}(\mathbf{0},\Omega))^*u^{(1)}(\mathbf{0},2\Omega))u_i(\mathbf{0},\Omega)^*)+\cdots\ , \end{aligned} \tag{2.55}$$

$$A(\mathbf{r},2\Omega) = \frac{4\pi}{3}a^3k^2(2\Omega)\eta^{(2)}(u^{(0)}(\mathbf{0},\Omega))^2+\cdots\ . \tag{2.56}$$

Second-harmonic generation with two point Scatterers

Suppose that two scatterers of radius a are placed at the points $\mathbf{r}_1 = (l,0,0)$ and $\mathbf{r}_2 = (-l,0,0)$. Thus, the susceptibilities are taken to be $\chi^{(1)}(\mathbf{r},\omega) = \eta^{(1)}$ and $\chi^{(2)}(\mathbf{r},\omega) = \eta^{(2)}$ for $|\mathbf{r}-\mathbf{r}_1| \le a$ and $|\mathbf{r}-\mathbf{r}_2| \le a$ and to vanish everywhere else. The solutions to the wave equations (2.20) and (2.21) become

$$\begin{aligned} u(\mathbf{r},\Omega) &= u_i(\mathbf{r},\Omega)+k^2(\Omega)\eta^{(1)}\int_{|\mathbf{r}'-\mathbf{r}_1|<a}d^3r'G(\mathbf{r},\mathbf{r}',\Omega)u(\mathbf{r}',\Omega) \\ &\quad +k^2(\Omega)\eta^{(1)}\int_{|\mathbf{r}'-\mathbf{r}_2|<a}d^3r'G(\mathbf{r},\mathbf{r}',\Omega)u(\mathbf{r}',\Omega) \\ &\quad +2k^2(\Omega)\eta^{(2)}\int_{|\mathbf{r}'-\mathbf{r}_1|<a}d^3r'G(\mathbf{r},\mathbf{r}',\Omega)u(\mathbf{r}',2\Omega)u^*(\mathbf{r}',\Omega) \\ &\quad +2k^2(\Omega)\eta^{(2)}\int_{|\mathbf{r}'-\mathbf{r}_2|<a}d^3r'G(\mathbf{r},\mathbf{r}',\Omega)u(\mathbf{r}',2\Omega)u^*(\mathbf{r}',\Omega)\ , \end{aligned} \tag{2.57}$$

$$
\begin{aligned}
u(\mathbf{r},2\Omega) &= k^2(2\Omega)\eta^{(1)}\int_{|\mathbf{r}'-\mathbf{r}_1|<a} d^3r' G(\mathbf{r},\mathbf{r}',\Omega)u(\mathbf{r}',2\Omega) \\
&\quad + k^2(2\Omega)\eta^{(1)}\int_{|\mathbf{r}'-\mathbf{r}_2|<a} d^3r' G(\mathbf{r},\mathbf{r}',\Omega)u(\mathbf{r}',2\Omega) \\
&\quad + k^2(2\Omega)\eta^{(2)}\int_{|\mathbf{r}'-\mathbf{r}_1|<a} d^3r' G(\mathbf{r},\mathbf{r}',\Omega)u(\mathbf{r}',\Omega)u(\mathbf{r}',\Omega) \\
&\quad + k^2(2\Omega)\eta^{(2)}\int_{|\mathbf{r}'-\mathbf{r}_2|<a} d^3r' G(\mathbf{r},\mathbf{r}',\Omega)u(\mathbf{r}',\Omega)u(\mathbf{r}',\Omega)\ . \qquad (2.58)
\end{aligned}
$$

Using (2.16) and (2.30), we find that the scattered fields are of the form

$$
u_s(\mathbf{r},\Omega) = A(\mathbf{r},\Omega)\frac{e^{ik(\Omega)r}}{r}\ , \qquad (2.59)
$$

$$
u_s(\mathbf{r},2\Omega) = A(\mathbf{r},2\Omega)\frac{e^{ik(2\Omega)r}}{r}\ , \qquad (2.60)
$$

where the scattering amplitudes are defined by

$$
\begin{aligned}
A(\mathbf{r},\Omega) &= \frac{4\pi}{3}a^3k^2(\Omega)(\eta^{(1)}u(\mathbf{r}_1,\Omega)+2\eta^{(2)}u(\mathbf{r}_1,2\Omega)u^*(\mathbf{r}_1,\Omega))e^{ik(\Omega)\widehat{\mathbf{r}}\cdot\mathbf{r}_1} \\
&\quad + \frac{4\pi}{3}a^3k^2(\Omega)(\eta^{(1)}u(\mathbf{r}_2,\Omega)+2\eta^{(2)}u(\mathbf{r}_2,2\Omega)u^*(\mathbf{r}_2,\Omega))e^{ik(\Omega)\widehat{\mathbf{r}}\cdot\mathbf{r}_2}\ , \qquad (2.61) \\
A(\mathbf{r},2\Omega) &= \frac{4\pi}{3}a^3k^2(2\Omega)(\eta^{(1)}u(\mathbf{r}_1,2\Omega)+\eta^{(2)}u(\mathbf{r}_1,\Omega)u(\mathbf{r}_1,\Omega))e^{ik(2\Omega)\widehat{\mathbf{r}}\cdot\mathbf{r}_1} \\
&\quad + \frac{4\pi}{3}a^3k^2(2\Omega)(\eta^{(1)}u(\mathbf{r}_1,2\Omega)+\eta^{(2)}u(\mathbf{r}_1,\Omega)u(\mathbf{r}_1,\Omega))e^{ik(2\Omega)\widehat{\mathbf{r}}\cdot\mathbf{r}_1}\ . \qquad (2.62)
\end{aligned}
$$

To calculate the local fields $u(\mathbf{r}_1,\Omega)$, $u(\mathbf{r}_1,2\Omega)$ $u(\mathbf{r}_1,\Omega)$ and $u(\mathbf{r}_1,2\Omega)$, we set $\mathbf{r}=\mathbf{r}_1$ and $\mathbf{r}=\mathbf{r}_2$ in (2.57) and (2.58) and thus obtain a system of nonlinear algebraic equations for the local fields of the form

$$
\begin{aligned}
u(\mathbf{r}_1,\Omega) &= u_i(\mathbf{r}_1,\Omega)+\frac{4\pi}{3}a^3k^2(\Omega)G_R(\Omega)(\eta^{(1)}u(\mathbf{r}_1,\Omega)+2\eta^{(2)}u(\mathbf{r}_1,2\Omega)u^*(\mathbf{r}_1,\Omega)) \\
&\quad + \frac{4\pi}{3}a^3k^2(\Omega)G(\mathbf{r}_1,\mathbf{r}_2,\Omega)(\eta^{(1)}u(\mathbf{r}_2,\Omega)+2\eta^{(2)}u(\mathbf{r}_2,2\Omega)u^*(\mathbf{r}_2,\Omega))\ , \qquad (2.63)
\end{aligned}
$$

$$
\begin{aligned}
u(\mathbf{r}_1,2\Omega) &= \frac{4\pi}{3}a^3k^2(2\Omega)G_R(2\Omega)(\eta^{(1)}u(\mathbf{r}_1,2\Omega)+\eta^{(2)}u(\mathbf{r}_1,\Omega)u(\mathbf{r}_1,\Omega)) \\
&\quad +\frac{4\pi}{3}a^3k^2(2\Omega)G(\mathbf{r}_1,\mathbf{r}_2,2\Omega)(\eta^{(1)}u(\mathbf{r}_2,2\Omega)+\eta^{(2)}u(\mathbf{r}_2,\Omega)u(\mathbf{r}_2,\Omega)) \ , \quad (2.64) \\
u(\mathbf{r}_2,\Omega) &= u_i(\mathbf{r}_2,\Omega)+\frac{4\pi}{3}a^3k^2(\Omega)G_R(\Omega)(\eta^{(1)}u(\mathbf{r}_2,\Omega)+2\eta^{(2)}u(\mathbf{r}_2,2\Omega)u^*(\mathbf{r}_2,\Omega)) \\
&\quad +\frac{4\pi}{3}a^3k^2(\Omega)G(\mathbf{r}_2,\mathbf{r}_1,\Omega)(\eta^{(1)}u(\mathbf{r}_1,\Omega)+2\eta^{(2)}u(\mathbf{r}_1,2\Omega)u^*(\mathbf{r}_1,\Omega)) \ , \quad (2.65) \\
u(\mathbf{r}_2,2\Omega) &= \frac{4\pi}{3}a^3k^2(2\Omega)G_R(2\Omega)(\eta^{(1)}u(\mathbf{r}_2,2\Omega)+\eta^{(2)}u(\mathbf{r}_2,\Omega)u(\mathbf{r}_2,\Omega)) \\
&\quad +\frac{4\pi}{3}a^3k^2(2\Omega)G(\mathbf{r}_2,\mathbf{r}_1,2\Omega)(\eta^{(1)}u(\mathbf{r}_1,2\Omega)+\eta^{(2)}u(\mathbf{r}_1,\Omega)u(\mathbf{r}_1,\Omega)) \ . \quad (2.66)
\end{aligned}
$$

As before, we solve the above set of nonlinear equations perturbatively. Accordingly, we introduce a parameter ϵ to scale the nonlinear terms in (2.63):

$$
\begin{aligned}
u(\mathbf{r}_1,\Omega) &= u_i(\mathbf{r}_1,\Omega)+\frac{4\pi}{3}a^3k^2(\Omega)G_R(\Omega)(\eta^{(1)}u(\mathbf{r}_1,\Omega)+2\epsilon\eta^{(2)}u(\mathbf{r}_1,2\Omega)u^*(\mathbf{r}_1,\Omega)) \\
&\quad +\frac{4\pi}{3}a^3k^2(\Omega)G(\mathbf{r}_1,\mathbf{r}_2,\Omega)(\eta^{(1)}u(\mathbf{r}_2,\Omega)+2\epsilon\eta^{(2)}u(\mathbf{r}_2,2\Omega)u^*(\mathbf{r}_2,\Omega)) \ , \quad (2.67) \\
u(\mathbf{r}_1,2\Omega) &= \frac{4\pi}{3}a^3k^2(2\Omega)G_R(2\Omega)(\eta^{(1)}u(\mathbf{r}_1,2\Omega)+\epsilon\eta^{(2)}u(\mathbf{r}_1,\Omega)u(\mathbf{r}_1,\Omega)) \\
&\quad +\frac{4\pi}{3}a^3k^2(2\Omega)G(\mathbf{r}_1,\mathbf{r}_2,2\Omega)(\eta^{(1)}u(\mathbf{r}_2,2\Omega)+\epsilon\eta^{(2)}u(\mathbf{r}_2,\Omega)u(\mathbf{r}_2,\Omega)) \ , \quad (2.68) \\
u(\mathbf{r}_2,\Omega) &= u_i(\mathbf{r}_2,\Omega)+\frac{4\pi}{3}a^3k^2(\Omega)G_R(\Omega)(\eta^{(1)}u(\mathbf{r}_2,\Omega)+2\epsilon\eta^{(2)}u(\mathbf{r}_2,2\Omega)u^*(\mathbf{r}_2,\Omega)) \\
&\quad +\frac{4\pi}{3}a^3k^2(\Omega)G(\mathbf{r}_2,\mathbf{r}_1,\Omega)(\eta^{(1)}u(\mathbf{r}_1,\Omega)+2\epsilon\eta^{(2)}u(\mathbf{r}_1,2\Omega)u^*(\mathbf{r}_1,\Omega)) \ , \quad (2.69) \\
u(\mathbf{r}_2,2\Omega) &= \frac{4\pi}{3}a^3k^2(2\Omega)G_R(2\Omega)(\eta^{(1)}u(\mathbf{r}_2,2\Omega)+\epsilon\eta^{(2)}u(\mathbf{r}_2,\Omega)u(\mathbf{r}_2,\Omega)) \\
&\quad +\frac{4\pi}{3}a^3k^2(2\Omega)G(\mathbf{r}_2,\mathbf{r}_1,2\Omega)(\eta^{(1)}u(\mathbf{r}_1,2\Omega)+\epsilon\eta^{(2)}u(\mathbf{r}_1,\Omega)u(\mathbf{r}_1,\Omega)) \ . \quad (2.70)
\end{aligned}
$$

We then introduce formal expansions for the fields of the form

$$
\begin{aligned}
u(\mathbf{r},\Omega) &= u^{(0)}(\mathbf{r},\Omega)+\epsilon u^{(1)}(0,\Omega)+\epsilon^2u^{(2)}(\mathbf{r},\Omega)+\cdots \ , \quad (2.71) \\
u(\mathbf{r},2\Omega) &= u^{(0)}(\mathbf{r},2\Omega)+\epsilon u^{(1)}(\mathbf{r},2\Omega)+\epsilon^2u^{(2)}(\mathbf{r},2\Omega)+\cdots \ . \quad (2.72)
\end{aligned}
$$

To simplify the notation, we set $\Omega_1 = \Omega$, $\Omega_2 = 2\Omega$, and write $u_j(\mathbf{r}) = u(\mathbf{r}, \Omega_j)$, $k_j = \Omega_j/c$, $G_{Rj} = G_R(\Omega_j)$ and $G_{12,j} = G(\mathbf{r}_2, \mathbf{r}_1, \Omega_j)$. Then (2.67) becomes

$$\begin{aligned}
u_1(\mathbf{r}_1) &= u_i(\mathbf{r}_1) + \frac{4\pi}{3}a^3k_1^2G_{R1}(\eta^{(1)}u_1(\mathbf{r}_1) + 2\epsilon\eta^{(2)}u_2(\mathbf{r}_1)u_1^*(\mathbf{r}_1) \\
&\quad + \frac{4\pi}{3}a^3k_1^2G_{12,1}(\eta^{(1)}u_1(\mathbf{r}_2) + 2\epsilon\eta^{(2)}u_2(\mathbf{r}_2)u_1^*(\mathbf{r}_2)) \ , \qquad (2.73) \\
u_2(\mathbf{r}_1) &= \frac{4\pi}{3}a^3k_2^2G_{R2}(\eta^{(1)}u_2(\mathbf{r}_1) + \epsilon\eta^{(2)}u_1(\mathbf{r}_1)u_1(\mathbf{r}_1)) \\
&\quad + \frac{4\pi}{3}a^3k_2^2G_{12,2}(\eta^{(1)}u_2(\mathbf{r}_2) + \epsilon\eta^{(2)}u_1(\mathbf{r}_2)u_1(\mathbf{r}_2)) \ , \qquad (2.74) \\
u_1(\mathbf{r}_2) &= u_i(\mathbf{r}_2) + \frac{4\pi}{3}a^3k_1^2G_{R1}(\eta^{(1)}u_1(\mathbf{r}_2) + 2\epsilon\eta^{(2)}u_2(\mathbf{r}_2)u_1^*(\mathbf{r}_2)) \\
&\quad + \frac{4\pi}{3}a^3k_1^2G_{12,1}(\eta^{(1)}u_1(\mathbf{r}_1) + 2\epsilon\eta^{(2)}u_2(\mathbf{r}_1)u_1^*(\mathbf{r}_1)) \ , \qquad (2.75) \\
u_2(\mathbf{r}_2) &= \frac{4\pi}{3}a^3k_2^2G_{R2}(\eta^{(1)}u_2(\mathbf{r}_2) + \epsilon\eta^{(2)}u_1(\mathbf{r}_2)u_1(\mathbf{r}_2)) \\
&\quad + \frac{4\pi}{3}a^3k_2^2G_{12,2}(\eta^{(1)}u_2(\mathbf{r}_1) + \epsilon\eta^{(2)}u_1(\mathbf{r}_1)u_1(\mathbf{r}_1)) \ . \qquad (2.76)
\end{aligned}$$

The $O(1)$ terms in the expansion are

$$\begin{aligned}
u_1^{(0)}(\mathbf{r}_1) &= u_{inc,1}(\mathbf{r}_1) + \frac{4\pi}{3}a^3k_1^2G_{R1}\eta^{(1)}u_1^{(0)}(\mathbf{r}_1) + \frac{4\pi}{3}a^3k_1^2G_{12,1}\eta^{(1)}u_1^{(0)}(\mathbf{r}_2) \ , \qquad (2.77) \\
u_1^{(0)}(\mathbf{r}_2) &= u_{inc,2}(\mathbf{r}_2) + \frac{4\pi}{3}a^3k_1^2G_{12,1}\eta^{(1)}u_1^{(0)}(\mathbf{r}_1) + \frac{4\pi}{3}a^3k_1^2G_{R1}\eta^{(1)}u_1^{(0)}(\mathbf{r}_2) \ , \qquad (2.78) \\
u_2^{(0)}(\mathbf{r}_1) &= \frac{4\pi}{3}a^3k_2^2G_{R2}\eta^{(1)}u_2^{(0)}(\mathbf{r}_1) + \frac{4\pi}{3}a^3k_2^2G_{12,2}\eta^{(1)}u_2^{(0)}(\mathbf{r}_2) \ , \qquad (2.79) \\
u_2^{(0)}(\mathbf{r}_2) &= \frac{4\pi}{3}a^3k_2^2G_{12,2}\eta^{(1)}u_2^{(0)}(\mathbf{r}_1) + \frac{4\pi}{3}a^3k_2^2G_{R2}\eta^{(1)}u_2^{(0)}(\mathbf{r}_2) \ . \qquad (2.80)
\end{aligned}$$

These equations can be put in the matrix form

$$Mj \begin{pmatrix} u_j^{(0)}(\mathbf{r}_1) \\ u_j^{(0)}(\mathbf{r}_2) \end{pmatrix} = \begin{pmatrix} u_{inc,j}(\mathbf{r}_1) \\ u_{inc,j}(\mathbf{r}_2) \end{pmatrix} \ ,$$

where

$$M_j = \begin{pmatrix} 1 - \frac{4\pi}{3} a^3 k_j^2 G_{Rj} \eta^{(1)} & -\frac{4\pi}{3} a^3 k_j^2 G_{12,j} \eta^{(1)} \\ -\frac{4\pi}{3} a^3 k_j^2 G_{12,j} \eta^{(1)} & 1 - \frac{4\pi}{3} a^3 k_j^2 G_{Rj} \eta^{(1)} \end{pmatrix}.$$

Similarly, higher order terms in the expansion are uniquely determined as long as the M_j's are nonsingular. Hence we are able to calculate the scattering amplitude using (2.61).

2.3.2 Sum- and difference-frequency generation

Consider a source with two frequency components Ω_1 and Ω_2 with $\Omega_1 > \Omega_2$, The strongest nonlinear response is called sum- and difference-frequency generation, where waves at frequencies $\Omega_3 = \Omega_1 + \Omega_2$ and $\Omega_4 = \Omega_1 - \Omega_2$ are generated. The electric fields at the corresponding frequencies obey the equations

$$\begin{aligned}
\Delta u(\mathbf{r}, \Omega_1) &+ k^2(\Omega_1)(1 + 4\pi\chi^{(1)}(\mathbf{r}, \Omega_1))u(\mathbf{r}, \Omega_1) \\
&= -4\pi S(\mathbf{r}, \Omega_1) - 4\pi k^2(\Omega_1)(2\chi^{(2)}(\mathbf{r}, \Omega_3, -\Omega_2)u(\mathbf{r}, \Omega_3)u^*(\mathbf{r}, \Omega_2) \\
&+ 2\chi^{(2)}(\mathbf{r}, \Omega_4, \Omega_2)u(\mathbf{r}, \Omega_4)u(\mathbf{r}, \Omega_2)) \ , \qquad (2.81) \\
\Delta u(\mathbf{r}, \Omega_2) &+ k^2(\Omega_2)(1 + 4\pi\chi^{(1)}(\mathbf{r}, \Omega_2))u(\mathbf{r}, \Omega_2) \\
&= -4\pi S(\mathbf{r}, \Omega_2) - 4\pi k^2(\Omega_2)(2\chi^{(2)}(\mathbf{r}, \Omega_3, -\Omega_1)u(\mathbf{r}, \Omega_3)u^*(\mathbf{r}, \Omega_1) \\
&+ 2\chi^{(2)}(\mathbf{r}, \Omega_1, -\Omega_4)u(\mathbf{r}, \Omega_1)u^*(\mathbf{r}, \Omega_4)) \ , \qquad (2.82) \\
\Delta u(\mathbf{r}, \Omega_3) &+ k^2(\Omega_3)(1 + 4\pi\chi^{(1)}(\mathbf{r}, \Omega_3))u(\mathbf{r}, \Omega_3) \\
&= -4\pi k^2(\Omega_3)2\chi^{(2)}(\mathbf{r}, \Omega_1, \Omega_2)u(\mathbf{r}, \Omega_1)u(\mathbf{r}, \Omega_2) \ , \qquad (2.83) \\
\Delta u(\mathbf{r}, \Omega_4) &+ k^2(\Omega_4)(1 + 4\pi\chi^{(1)}(\mathbf{r}, \Omega_4))u(\mathbf{r}, \Omega_4) \\
&= -4\pi k^2(\Omega_4)2\chi^{(2)}(\mathbf{r}, \Omega_1, -\Omega_2)u(\mathbf{r}, \Omega_1)u^*(\mathbf{r}, \Omega_2) \ . \qquad (2.84)
\end{aligned}$$

Eq (2.81) can be solved perturbatively as described in Appendix 2.B.

2.3.3 Three-wave mixing

Consider an incident field consisting of frequency components Ω_1, Ω_2 and Ω_3 with $\Omega_1 + \Omega_2 = \Omega_3$. In this case, the strongest nonlinear effect is referred to as three-wave mixing. The electric fields at the corresponding frequencies obey

$$\begin{aligned}
\Delta u(\mathbf{r},\Omega_1) &+ k^2(\Omega_1)(1+4\pi\chi^{(1)}(\mathbf{r},\Omega_1))u_1(\mathbf{r},\Omega_1) = -4\pi S(\mathbf{r},\Omega_1) \\
&- 4\pi k^2(\Omega_1)2\chi^{(2)}(\mathbf{r},\Omega_3,-\Omega_2)u(\mathbf{r},\Omega_3)u_2^*(\mathbf{r},\Omega_2)\ , \qquad (2.85)\\
\Delta u(\mathbf{r},\Omega_2) &+ k^2(\Omega_2)(1+4\pi\chi^{(1)}(\mathbf{r},\Omega_2))u(\mathbf{r},\Omega_2) = -4\pi S(\mathbf{r},\Omega_2) \\
&- 4\pi k^2(\Omega_2)2\chi^{(2)}(\mathbf{r},\Omega_3,-\Omega_1)u(\mathbf{r},\Omega_3)u^*(\mathbf{r},\Omega_1)\ , \qquad (2.86)\\
\Delta u(\mathbf{r},\Omega_3) &+ k^2(\Omega_3)(1+4\pi\chi^{(1)}(\mathbf{r},\Omega_3))u(\mathbf{r},\Omega_3) = -4\pi S(\mathbf{r},\Omega_3) \\
&- 4\pi k^2(\Omega_3)2\chi^{(2)}(\mathbf{r},\Omega_1,\Omega_2)u(\mathbf{r},\Omega_1)u(\mathbf{r},\Omega_2)\ . \qquad (2.87)
\end{aligned}$$

Eq. (2.85) can be solved perturbatively as shown in Appendix 2.C.

2.4 Third-order nonlinearities

In this section we study third-order nonlinearities including the Kerr effect, third-harmonic generation (THG) and four-wave mixing (FWM). We assume that the nonlinear susceptibilities are sufficiently weak that the condition

$$\sum_{\omega_1+\omega_2+\omega_3=\omega} \chi^{(3)}(\mathbf{r},\omega_1,\omega_2,\omega_3)u(\mathbf{r},\omega_1)u(\mathbf{r},\omega_2)u(\mathbf{r},\omega_3) \ll \chi^{(1)}(\mathbf{r},\omega)u(\mathbf{r},\omega) \qquad (2.88)$$

is obeyed.

2.4.1 Kerr effect

Suppose a source of frequency Ω is incident upon a cubic nonlinear medium. The strongest nonlinear effect is the Kerr effect. The electric field obeys the wave equation

$$\begin{aligned} \Delta u(\mathbf{r},\Omega) + k^2(\Omega)u(\mathbf{r},\Omega) &= -4\pi k^2(\Omega)\chi^{(1)}(\mathbf{r},\Omega)u(\mathbf{r},\Omega) \\ &- 4\pi k^2(\Omega)3\chi^{(3)}(\mathbf{r},\omega,\Omega,\Omega,-\Omega)u(\mathbf{r},\Omega)u(\mathbf{r},\Omega)u^*(\mathbf{r},\Omega) \end{aligned} \quad (2.89)$$

It follows immediately from (2.13) that the solution to (2.89) is given by

$$\begin{aligned} u(\mathbf{r},\Omega) &= u_i(\mathbf{r},\Omega) + 4\pi k^2(\Omega)\int dr'\chi^{(1)}(\mathbf{r}',\Omega)u(\mathbf{r}',\Omega) \\ &+k^2(\Omega)\int dr'\chi^{\Omega(3)}(\mathbf{r}',\Omega,\Omega,-\Omega)u(\mathbf{r}',\Omega)u(\mathbf{r}',dr)u^*(\mathbf{r}',dr)\ . \end{aligned} \quad (2.90)$$

Single point scatterer

Suppose that the scattering medium is a small ball of radius a with $k(\Omega)a \ll 1$. The susceptibilities are taken to be $\chi^{(1)}(\mathbf{r},\omega) = \eta^{(1)}$ and $\chi^{(3)}(\mathbf{r},\omega) = \eta^{(3)}$ for $|\mathbf{r}| \leq a$ and to vanish for $|\mathbf{r}| > a$. Eq. (2.90) thus become

$$\begin{aligned} u(\mathbf{r},\Omega) &= u_i(\mathbf{r},\Omega) + 4\pi k^2(\Omega)\eta^{(1)}\int_{|\mathbf{r}'|<a} dr'u(\mathbf{r}',\Omega) \\ &+k^2(\Omega)\eta^{(3)}\int_{|\mathbf{r}'|<a} dr'u(\mathbf{r}',\Omega)u(\mathbf{r}',dr)u^*(\mathbf{r}',dr)\ . \end{aligned} \quad (2.91)$$

Using the asymptotic form of the Green's function given in (2.16), we find that the scattered field is of the form

$$u_s(\mathbf{r},\Omega) = A(\mathbf{r},\Omega)\frac{e^{ik(\Omega)r}}{r}\ . \quad (2.92)$$

where the scattering amplitude is defined by

$$A(\mathbf{r},\Omega) = \frac{4\pi}{3}a^3k^2(\Omega)(\eta^{(1)}u(\mathbf{0},\Omega)+3\eta^{(3)}u(\mathbf{0},\Omega)u(\mathbf{0},\Omega))u^*(\mathbf{0},\Omega)) \ , \tag{2.93}$$

We must now calculate the local field $u(\mathbf{0},\Omega)$. To proceed, we set $\mathbf{r}=0$ in (2.91) and thus obtain

$$\begin{aligned} u(\mathbf{0},\Omega) &= u_i(\mathbf{0},\Omega)+k^2(\Omega)\eta^{(1)}\int_{|\mathbf{r}'|<a} d^3r' G(\mathbf{0},\mathbf{r}',\Omega)u(\mathbf{r}',\Omega) \\ &\quad +3k^2(\Omega)\eta^{(3)}\int_{|\mathbf{r}'|<a} d^3r' G(\mathbf{0},\mathbf{r}',\Omega)u(\mathbf{r}',\Omega)u(\mathbf{r}',\Omega)u^*(\mathbf{r}',\Omega)) \ . \end{aligned} \tag{2.94}$$

We then find that (2.94) leads to a nonlinear algebraic equation for the local field which is of the form

$$\begin{aligned} u(\mathbf{0},\Omega) &= u_i(\mathbf{0},\Omega)+\frac{4\pi}{3}a^3k^2(\Omega)G_R(\Omega)(\eta^{(1)}u(\mathbf{0},\Omega) \\ &\quad +3\eta^{(3)}u^*(\mathbf{0},\Omega)u(\mathbf{0},\Omega)u(\mathbf{0},\Omega)) \ . \end{aligned} \tag{2.95}$$

Eq. (2.95) is a nonlinear algebraic equation that we solve perturbatively. As before, we introduce a parameter ϵ to scale the nonlinear terms in (2.95):

$$\begin{aligned} u(\mathbf{0},\Omega) &= u_i(\mathbf{0},\Omega)+\frac{4\pi}{3}a^3k^2(\Omega)G_R(\Omega)(\eta^{(1)}u(\mathbf{0},\Omega) \\ &\quad +3\epsilon\eta^{(3)}u^*(\mathbf{0},\Omega)u(\mathbf{0},\Omega)u(\mathbf{0},\Omega)) \ . \end{aligned} \tag{2.96}$$

We then introduce formal expansions for the field of the form

$$u(0,\Omega) = u^{(0)}(0,\Omega)+\epsilon u^{(1)}(0,\Omega)+\epsilon^2u^{(2)}(0,\Omega)+\cdots \ . \tag{2.97}$$

To simplify the notation, we write $u=u(\mathbf{0},\Omega)$, $k=\Omega/c$ and $G_R=G_R(\Omega)$. Then (2.96)

becomes

$$u = u_i + \frac{4\pi}{3} a^3 k^2 G_R (\eta^{(1)} u + \epsilon 3 \eta^{(3)} u^* u u) \ . \tag{2.98}$$

Next, we expand the fields u according to (2.97) and collect like powers of ϵ. At $O(1)$ we have

$$u^{(0)} = u_i + \frac{4\pi}{3} a^3 k^2 G_R \eta^{(1)} u^{(0)} \ . \tag{2.99}$$

Thus

$$u^{(0)} = \frac{1}{1 - \frac{4\pi}{3} a^3 k^2 G_R \eta^{(1)}} \ . \tag{2.100}$$

At $O(\epsilon)$ we have

$$u^{(1)} = \frac{4\pi}{3} a^3 k^2 G_R (\eta^{(1)} u^{(1)} + 3 \eta^{(3)} (u^*)^{(0)} u^{(0)} u^{(0)}) \ . \tag{2.101}$$

Thus

$$u^{(1)}(\mathbf{0}) = \frac{3 \frac{4\pi}{3} a^3 k^2 G_R \eta^{(3)} (u^*)^{(0)}(0) u^{(0)}(0) u^{(0)}(0))}{1 - \frac{4\pi}{3} a^3 k^2 G_R \eta^{(1)} u^{(1)}(0)} \ . \tag{2.102}$$

We can now calculate the scattering amplitude. We find that

$$A(\mathbf{r}, \Omega) = \frac{4\pi}{3} a^3 k^2 \left((\eta^{(1)} u^{(0)} + \eta^{(1)} u^{(1)} + 3 \eta^{(2)} (u^*)^{(0)} u^{(0)} u^{(0)}) u_i \right) + \cdots \ . \tag{2.103}$$

Restoring our original notation, we obtain

$$\begin{aligned} A(\mathbf{r},\Omega) &= \frac{4\pi}{3}a^3k^2(\Omega)((\eta^{(1)}u^{(0)}(\mathbf{0},\Omega)+\eta^{(1)}u^{(1)}(\mathbf{0},\Omega) \\ &\quad +3\eta^{(2)}(u^*)^{(0)}(\mathbf{0},\Omega)u^{(0)}(\mathbf{0},\Omega)u^{(0)}(\mathbf{0},\Omega))u_i(\mathbf{0},\Omega)) \ . \end{aligned} \tag{2.104}$$

Two point scatterers

Suppose two scatterers of radius a are placed at $\mathbf{r}_1 = (l,0,0)$ and $\mathbf{r}_2 = (-l,0,0)$,. That is, the susceptibilities are taken to be $\chi^{(1)}(\mathbf{r},\omega) = \eta^{(1)}$ and $\chi^{(3)}(\mathbf{r},\omega) = \eta^{(3)}$ for $|\mathbf{r}-\mathbf{r}_1| \le a$ and $|\mathbf{r}-\mathbf{r}_2| \le a$ and to vanish everywhere else. Then the solution to the wave equation (2.89) becomes

$$\begin{aligned} u(\mathbf{r},\Omega) &= u_i(\mathbf{r},\Omega) + k^2(\Omega)\eta^{(1)}\int_{|\mathbf{r}'-\mathbf{r}_1|<a} d^3r' G(\mathbf{r},\mathbf{r}',\Omega)u(\mathbf{r}',\Omega) \\ &\quad +k^2(\Omega)\eta^{(1)}\int_{|\mathbf{r}'-\mathbf{r}_2|<a} d^3r' G(\mathbf{r},\mathbf{r}',\Omega)u(\mathbf{r}',\Omega) \\ &\quad +3k^2(\Omega)\eta^{(3)}\int_{|\mathbf{r}'-\mathbf{r}_1|<a} d^3r' G(\mathbf{r},\mathbf{r}',\Omega)u(\mathbf{r}',\Omega)u(\mathbf{r}',\Omega)u^*(\mathbf{r}',\Omega) \\ &\quad +3k^2(\Omega)\eta^{(3)}\int_{|\mathbf{r}'-\mathbf{r}_2|<a} d^3r' G(\mathbf{r},\mathbf{r}',\Omega)u(\mathbf{r}',\Omega)u(\mathbf{r}',\Omega)u^*(\mathbf{r}',\Omega) \ . \end{aligned} \tag{2.105}$$

Using the asymptotic form of the Green's function in (2.16) and (2.30), we find that the scattered fields are of the form

$$u_s(\mathbf{r},\Omega) = A(\mathbf{r},\Omega)\frac{e^{ik(\Omega)r}}{r} \ , \tag{2.106}$$

where the scattering amplitudes are defined by

$$\begin{aligned} A_i(\mathbf{r},\Omega) &= \frac{4\pi}{3}a^3k^2(\Omega)(\eta^{(1)}u(\mathbf{r}_1,\Omega)+3\eta^{(3)}u(\mathbf{r}_1,\Omega)u(\mathbf{r}_1,\Omega)u^*(\mathbf{r}_1,\Omega))e^{ik(\Omega)\widehat{\mathbf{r}}\cdot\mathbf{r}_1} \\ &\quad +\frac{4\pi}{3}a^3k^2(\Omega)(\eta^{(1)}u(\mathbf{r}_2,\Omega)+3\eta^{(3)}u(\mathbf{r}_2,\Omega)u(\mathbf{r}_1,\Omega)u^*(\mathbf{r}_2,\Omega))e^{ik(\Omega)\widehat{\mathbf{r}}\cdot\mathbf{r}_2} \ . \end{aligned} \tag{2.107}$$

To calculate the fields $u(\mathbf{r}_1,\Omega)$ and $u(\mathbf{r}_1,\Omega)$, we set $\mathbf{r}=\mathbf{r}_1$ and $\mathbf{r}=\mathbf{r}_2$ in (2.57) and (2.58) and thus obtain a system of nonlinear algebraic equations for the local fields:

$$\begin{aligned} u(\mathbf{r}_1,\Omega) &= u_i(\mathbf{r}_1,\Omega)+\frac{4\pi}{3}a^3k^2(\Omega)G_R(\Omega)(\eta^{(1)}u(\mathbf{r}_1,\Omega)+3\eta^{(3)}u(\mathbf{r}_1,\Omega)u(\mathbf{r}_1,\Omega)u^*(\mathbf{r}_1,\Omega)) \\ &\quad+\frac{4\pi}{3}a^3k^2(\Omega)G(\mathbf{r}_1,\mathbf{r}_2,\Omega)(\eta^{(1)}u(\mathbf{r}_2,\Omega)+3\eta^{(3)}u(\mathbf{r}_2,\Omega)u(\mathbf{r}_2,\Omega)u^*(\mathbf{r}_2,\Omega))\ , \qquad (2.108) \\ u(\mathbf{r}_2,\Omega) &= u_i(\mathbf{r}_2,\Omega)+\frac{4\pi}{3}a^3k^2(\Omega)G_R(\Omega)(\eta^{(1)}u(\mathbf{r}_2,\Omega)+3\eta^{(3)}u(\mathbf{r}_2,\Omega)u(\mathbf{r}_2,\Omega)u^*(\mathbf{r}_2,\Omega)) \\ &\quad+\frac{4\pi}{3}a^3k^2(\Omega)G(\mathbf{r}_2,\mathbf{r}_1,\Omega)(\eta^{(1)}u(\mathbf{r}_1,\Omega)+3\eta^{(3)}u(\mathbf{r}_1,\Omega)u(\mathbf{r}_1,\Omega)u^*(\mathbf{r}_1,\Omega))\ . \qquad (2.109) \end{aligned}$$

Note that (2.108) accounts for self interaction, which is omitted by the equation used in Ref. [40].

We solve this set of nonlinear algebraic equations perturbatively. To proceed, we introduce a parameter ϵ to scale the nonlinear terms in (2.63):

$$\begin{aligned} u(\mathbf{r}_1,\Omega) &= u_i(\mathbf{r}_1,\Omega)+\frac{4\pi}{3}a^3k^2(\Omega)G_R(\Omega)(\eta^{(1)}u(\mathbf{r}_1,\Omega)+3\epsilon\eta^{(3)}u(\mathbf{r}_1,\Omega)u(\mathbf{r}_1,\Omega)u^*(\mathbf{r}_1,\Omega)) \\ &\quad+\frac{4\pi}{3}a^3k^2(\Omega)G(\mathbf{r}_1,\mathbf{r}_2,\Omega)(\eta^{(1)}u(\mathbf{r}_2,\Omega)+3\epsilon\eta^{(3)}u(\mathbf{r}_2,\Omega)u(\mathbf{r}_2,\Omega)u^*(\mathbf{r}_2,\Omega))\ , \qquad (2.110) \\ u(\mathbf{r}_2,\Omega) &= u_i(\mathbf{r}_2,\Omega)+\frac{4\pi}{3}a^3k^2(\Omega)G_R(\Omega)(\eta^{(1)}u(\mathbf{r}_2,\Omega)+3\epsilon\eta^{(3)}u(\mathbf{r}_2,\Omega)u(\mathbf{r}_2,\Omega)u^*(\mathbf{r}_2,\Omega)) \\ &\quad+\frac{4\pi}{3}a^3k^2(\Omega)G(\mathbf{r}_2,\mathbf{r}_1,\Omega)(\eta^{(1)}u(\mathbf{r}_1,\Omega)+3\epsilon\eta^{(3)}u(\mathbf{r}_1,\Omega)u(\mathbf{r}_1,\Omega)u^*(\mathbf{r}_1,\Omega))\ . \qquad (2.111) \end{aligned}$$

We then introduce formal expansions for the fields of the form

$$u(\mathbf{r},\Omega) \;=\; u^{(0)}(\mathbf{r},\Omega)+\epsilon u^{(1)}(0,\Omega)+\epsilon^2u^{(2)}(\mathbf{r},\Omega)+\cdots\ . \qquad (2.112)$$

To simplify the notation, we write $u(\mathbf{r})=u(\mathbf{r},\Omega)$, $k=\Omega/c$, $G_R=G_R(\Omega)$ and $G_{12}=G(\mathbf{r}_2,\mathbf{r}_1,\Omega)$. Then (2.110) becomes

$$
\begin{aligned}
u(\mathbf{r}_1) &= u_i(\mathbf{r}_1) + \frac{4\pi}{3}a^3k^2G_R(\eta^{(1)}u(\mathbf{r}_1) + 3\epsilon\eta^{(3)}u(\mathbf{r}_1)u(\mathbf{r}_1)u^*(\mathbf{r}_1)) \\
&\quad + \frac{4\pi}{3}a^3k^2G_{12}(\eta^{(1)}u(\mathbf{r}_2) + 3\epsilon\eta^{(3)}u(\mathbf{r}_2)u(\mathbf{r}_2)u^*(\mathbf{r}_2)) \ , \qquad (2.113) \\
u(\mathbf{r}_2) &= u_i(\mathbf{r}_2) + \frac{4\pi}{3}a^3k^2G_R(\eta^{(1)}u(\mathbf{r}_2) + 3\epsilon\eta^{(3)}u(\mathbf{r}_2)u(\mathbf{r}_2)u^*(\mathbf{r}_2)) \\
&\quad + \frac{4\pi}{3}a^3k^2G_{12}(\eta^{(1)}u(\mathbf{r}_1) + 3\epsilon\eta^{(3)}u(\mathbf{r}_1)u(\mathbf{r}_1)u^*(\mathbf{r}_1)) \ . \qquad (2.114)
\end{aligned}
$$

The $O(1)$ terms in the expansion are

$$
\begin{aligned}
u^{(0)}(\mathbf{r}_1) &= u_i(\mathbf{r}_1) + \frac{4\pi}{3}a^3k^2G_R\eta^{(1)}u_1^{(0)}(\mathbf{r}_1) + \frac{4\pi}{3}a^3k_1^2G_{12}\eta^{(1)}u^{(0)}(\mathbf{r}_2) \ , \qquad (2.115) \\
u^{(0)}(\mathbf{r}_2) &= u_i(\mathbf{r}_2) + \frac{4\pi}{3}a^3k^2G_{12}\eta^{(1)}u_1^{(0)}(\mathbf{r}_1) + \frac{4\pi}{3}a^3k_1^2G_R\eta^{(1)}u^{(0)}(\mathbf{r}_2) \ . \qquad (2.116)
\end{aligned}
$$

These equations can be put in the matrix form

$$
M \begin{pmatrix} u^{(0)}(\mathbf{r}_1) \\ u^{(0)}(\mathbf{r}_2) \end{pmatrix} = \begin{pmatrix} u_i(\mathbf{r}_1) \\ u_i(\mathbf{r}_2) \end{pmatrix} \ ,
$$

where

$$
M = \begin{pmatrix} 1 - \frac{4\pi}{3}a^3k^2G_R\eta^{(1)} & -\frac{4\pi}{3}a^3k^2G_{12}\eta^{(1)} \\ -\frac{4\pi}{3}a^3k^2G_{12}\eta^{(1)} & 1 - \frac{4\pi}{3}a^3k^2G_R\eta^{(1)} \end{pmatrix} .
$$

Similarly, higher order terms in the expansion are uniquely determined as long as the M is nonsingular. Hence we are able to calculate the scattering amplitude using (2.106).

2.4.2 Bistability

Eq. (2.98) is a nonlinear algebraic equation for the local field u. As shown in Appendix 2.A, (2.98) may have one, two or three roots depending on the choice of the parameters $\eta^{(1)}$,

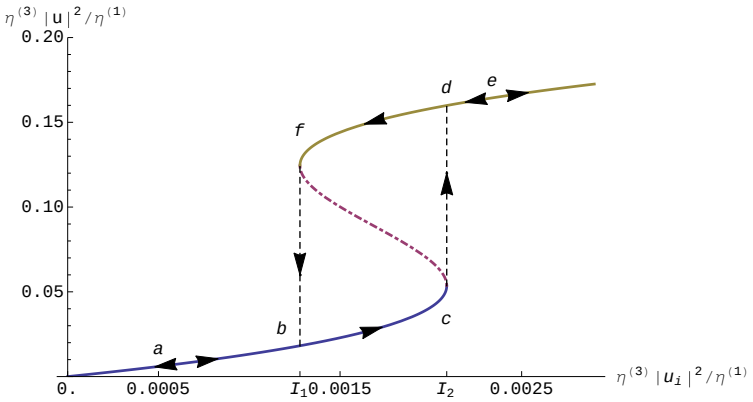

Figure 2.1: Optical bistability. One input intensity may give rise to multiple output intensities. Here $ka = 0.15$ and $\eta^{(1)} = 5$.

$\eta^{(3)}$, ka and $|u_i|^2$. As an example, in Fig. 2.1 we plot the quantity the normalized intensity $I = \eta_3|u|^2/\eta_1$ as a function of the incident intensity $I_i = \eta_3|u_i|^2/\eta_1$ for $ka = 0.15$ and $\eta^{(1)} = 5$. We see that when I_i exceeds a critical threshold I_1, the function I becomes multivalued. The resulting nonuniqueness of the solution occurs in the interval $I_1 \leq I_i \leq I_2$. The phenomenon when more than one intensity is possible for a given incident intensity is known as bistability [81, 17]. We note that bistability for the Kerr nonlinearity in one-dimensional systems has been studied in [26, 27, 48, 56, 93].

Evidently, bistability leads to hysteresis. Suppose that I_i is initially smaller than I_1 and is slowly increased to a value larger than I_2. Then the output intensity I is follows the path $a \to b \to c \to d \to e$. If I_i is initially larger then I_2 and is slowly decreased to a value less than I_1, then I follows the path $e \to d \to f \to b \to a$. We note that the dash-dotted branch is unstable in the sense that if the system is initially on this branch, it can jump to another branch under a small perturbation in I_i.

We have found the values of ka and $\eta^{(1)}$ which permit optical bistability, namely those that satisfy the constraint

$$\left|1 - \frac{9}{8\pi\eta^{(1)}(ka)^2(9/4 + (ka)^2)}\right| > \sqrt{27}\left|\frac{ka}{4\pi\eta^{(1)}(ka)^2(9/4 + (ka)^2)}\right| \ . \tag{2.117}$$

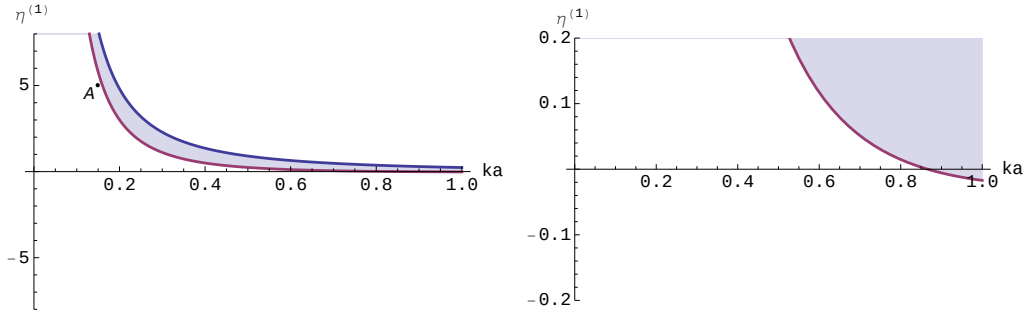

(a) (b)

Figure 2.2: Illustrating the unshaded region which allows bistability. The values of ka and $\eta^{(1)}$ for Fig. 2.1 is given by the point A. The zoomed in region in (b) shows that some negative values of $\eta^{(1)}$ do not permit bistability.

These values are represented by the unshaded region in Fig. 2.2(a). It is possible to obtain formulas for I_1 and I_2, the initial and end points of the folded region in Fig 2.1, when ka and $\eta^{(1)}$ lies in the unshaded region in Fig. 2.2(a). We do not present these formulas since they are elementary and cumbersome to display. See Appendix 2.A for further details.

2.4.3 Third-harmonic generation

Consider an incident field of frequency Ω. Then a wave at frequency 3Ω is generated in the process of third-harmonic generation. The electric fields at the corresponding frequencies obey

$$\begin{aligned} \Delta u(\mathbf{r},\Omega) &+ k^2(\Omega)(1+4\pi\chi^{(1)}(\mathbf{r},\Omega))u(\mathbf{r},\Omega) = -4\pi k^2(\Omega_1)3\chi^{(3)}(\mathbf{r},\Omega,\Omega,-\Omega)u^2(\mathbf{r},\Omega))u(\mathbf{r},\Omega)^* \\ &- 4\pi k^2(\Omega)3\chi^{(3)}(3\Omega,-\Omega,-\Omega)u(\mathbf{r},3\Omega))(u^*(\mathbf{r},\Omega)))^2 \qquad (2.118) \\ \Delta u(\mathbf{r},3\Omega) &+ k^2(3\Omega)(1+4\pi\chi^{(1)}(\mathbf{r},3\Omega))u(\mathbf{r},3\Omega)) = -4\pi k^2(3\Omega)\chi^{(3)}(\mathbf{r},\Omega,\Omega,\Omega)u^3(\mathbf{r},\Omega)\ . \\ & \qquad (2.119) \end{aligned}$$

Eq. (2.118) can be solved perturbatively as described in Appendix 2.D.

2.4.4 Four-wave mixing

Consider an incident field consisting of frequencies Ω_1, Ω_2, Ω_3 and Ω_4 with $\Omega_1+\Omega_2+\Omega_3 = \Omega_4$. The strongest nonlinear effect is known as four-wave mixing. The wave equations for the electric fields at the corresponding frequencies are of the form

$$\begin{aligned}
&\Delta u(\mathbf{r},\Omega_1) + k^2(\Omega_1)(1+4\pi\chi^{(1)}(\mathbf{r},\Omega_1))u(\mathbf{r},\Omega_1) = \\
&\qquad\qquad -4\pi k^2(\Omega_1)6\chi^{(3)}(\mathbf{r},\Omega_4,-\Omega_3,-\Omega_2)u(\mathbf{r},\Omega_4)u^*(\mathbf{r},\Omega_3)u^*(\mathbf{r},\Omega_2)\ , \\
&\Delta u(\mathbf{r},\Omega_2) + k^2(\Omega_2)(1+4\pi\chi^{(1)}(\mathbf{r},\Omega_2))u(\mathbf{r},\Omega_2) = \\
&\qquad\qquad -4\pi k^2(\Omega_2)6\chi^{(3)}(\mathbf{r},\Omega_4,-\Omega_3,-\Omega_1)u(\mathbf{r},\Omega_4)u^*(\mathbf{r},\Omega_3)u^*(\mathbf{r},\Omega_1) \\
&\Delta u(\mathbf{r},\Omega_3) + k^2(\Omega_3)(1+4\pi\chi^{(1)}(\mathbf{r},\Omega_3))u(\mathbf{r},\Omega_3) = \\
&\qquad\qquad -4\pi k^2(\Omega_3)6\chi^{(3)}(\mathbf{r},\Omega_4,-\Omega_2,-\Omega_1)u(\mathbf{r},\Omega_4)u^*(\mathbf{r},\Omega_2)u^*(\mathbf{r},\Omega_1) \\
&\Delta u(\mathbf{r},\Omega_4) + k^2(\Omega_4)(1+4\pi\chi^{(1)}(\mathbf{r},\Omega_4))u(\mathbf{r},\Omega_4) = \\
&\qquad\qquad -4\pi k^2(\Omega_4)6\chi^{(3)}(\mathbf{r},\Omega_1,\Omega_2,\Omega_3)u(\mathbf{r},\Omega_1)u(\mathbf{r},\Omega_2)u(\mathbf{r},\Omega_3)\ . \qquad (2.120)
\end{aligned}$$

Equation (2.120) can be solved perturbatively as described in Appendix 2.E.

2.5 Numerical results

In this section we present numerical results for the nonlinear effects described in Secs. 2.3 and 2.4. We will discuss the following three cases:

1. A single scatterer of radius a centered at the origin.

2. Two scatterers of radii a centered at the points $\mathbf{r}_1$ and $\mathbf{r}_2$ on the z-axis. The distance between the centers of the scatterers is taken to be $3a$.

3. Two scatterers of radii a centered at the points $\mathbf{r}_1$ and $\mathbf{r}_2$ on the x-axis. The distance

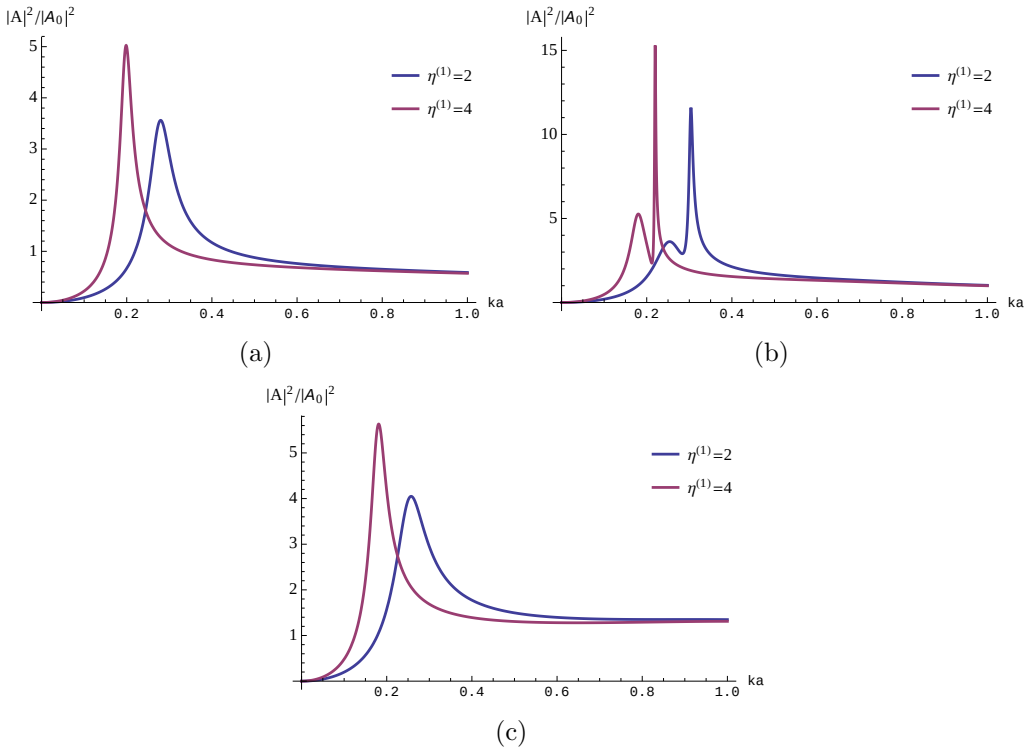

Figure 2.3: The frequency dependence of the scattering amplitude for linear scatterers. (a) One scatterer, (b) Two scatterers parallel to the incident wave, (c) Two scatterers perpendicular to the incident wave.

between the centers of the scatterers is taken to be $3a$

In all cases the incident fields are plane waves of the form $u_i = u_0 \exp(ik_0 \widehat{\mathbf{z}} \cdot \mathbf{r})$. Since the wave vector of the incident field is in the $\widehat{\mathbf{z}}$ direction, case 2 above is referred to as parallel illumination and case 3 is referred to as perpendicular illumination.

2.5.1 Linear dielectric

We suppose that the medium consists of one linear scatterer with linear susceptibility $\chi^{(1)}$ given by

$$\chi^{(1)}(\mathbf{r}) = \begin{cases} \eta^{(1)} & \text{if } |\mathbf{r}| \leq a \\ 0 & \text{if } |\mathbf{r}| > 0 \ . \end{cases} \tag{2.121}$$

Using (2.28), the scattering amplitude becomes

$$A = k^2 u_0 \left(\frac{\frac{4\pi}{3} a^3 \eta^{(1)}}{1 - \frac{4\pi}{3} a^3 k^2 \eta^{(1)} G_R} \right) \ . \tag{2.122}$$

We can write the above formula in a more familiar form in terms of the renormalized polarizability α, which is defined as

$$\alpha = \frac{\alpha_0}{1 - k^2 \alpha_0 (\frac{3}{2a} + ik)} \ . \tag{2.123}$$

Here α_0 is the zero-frequency polarizability, which is defined in terms of the linear dielectric permittivity $\epsilon^{(1)}$, where

$$\alpha_0 = \frac{4\pi}{3} a^3 \eta^{(1)} \ , \tag{2.124}$$

and $\epsilon^{(1)} = 1 + 4\pi\eta^{(1)}$. We find that (2.122) becomes

$$A = k^2 u_0 \alpha \ . \tag{2.125}$$

In Figure 2.3(a) we illustrate the frequency dependence of the scattering amplitude for a dielectric scatterer. We see that there is a scattering resonance at $ka \approx 0.3$ when $\eta^{(1)} = 2$, and a stronger resonance at $ka \approx 0.2$ when $\eta^{(1)} = 4$. Note that the resonance shifts to lower frequencies for stronger scatterering.

In Figure 2.3(b) we illustrate the frequency dependence of the scattering amplitude for two scatterers in the case of parallel illumination. We see that for $\eta^{(1)} = 2$, there is a primary resonance at $ka \approx 0.3$ and a secondary resonance at $ka \approx 0.25$. For $\eta^{(1)} = 4$, there are two resonances as well. We note that the amplitude increases and the resonances shift to lower frequencies. In Figure 2.3(c) we illustrate the frequency dependence of the scattering amplitude in the case of perpendicular illumination. We see that for $\eta^{(1)} = 2$, there is a

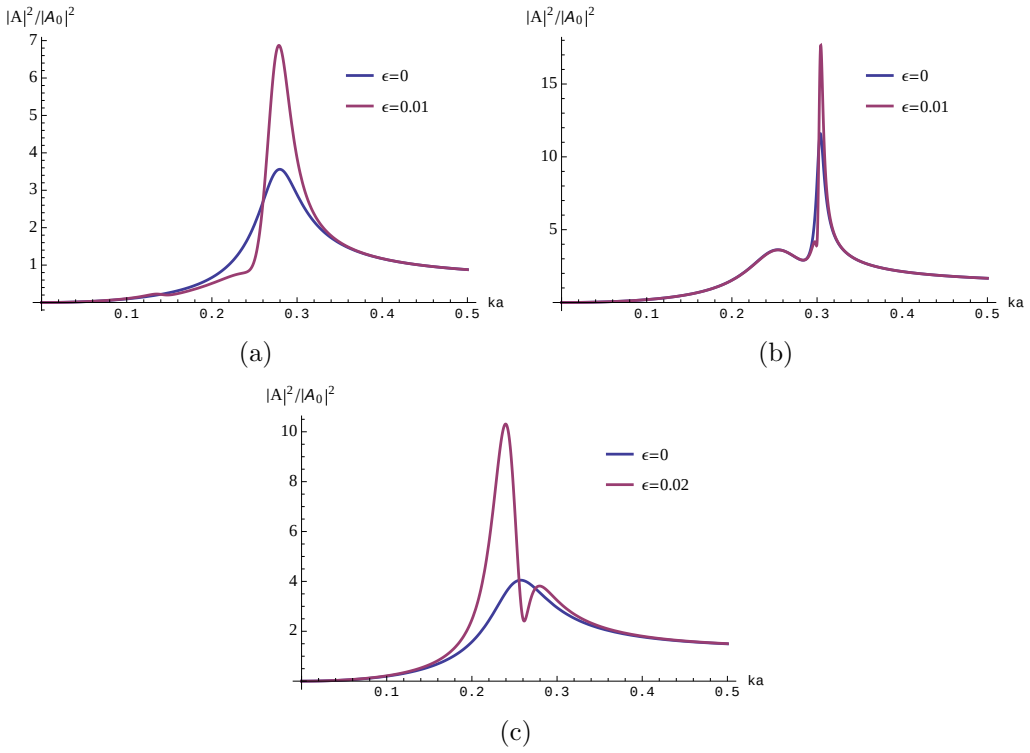

Figure 2.4: Frequency dependence of the scattering amplitude at the incident frequency in SHG. The parameters are given by $\eta^{(1)} = 2$, $\epsilon = \eta^{(2)} u_0 / \eta^{(1)}$. (a) One scatterer, (b) Two scatterers parallel to the incident wave, (c) Two scatterers perpendicular to the incident wave.

resonance at $ka \approx 0.28$. For $\eta^{(1)} = 4$, the resonance does not split. As before, the amplitude increases and the resonance shifts to a lower frequency.

2.5.2 Second-harmonic generation

We begin with the case of a single scatterer and suppose that the second-order susceptibility $\chi^{(2)}$ given by

$$\chi^{(2)}(\mathbf{r}) = \begin{cases} \eta^{(2)} & \text{if } |\mathbf{r}| \leq a \\ 0 & \text{if } |\mathbf{r}| > 0 \ , \end{cases} \tag{2.126}$$

which corresponds to a homogeneous sphere of radius a centered at the origin. We also introduce the small parameter $\epsilon = \eta^{(2)} u_0 / \eta^{(1)}$. In Figure 2.4(a) we illustrate the frequency

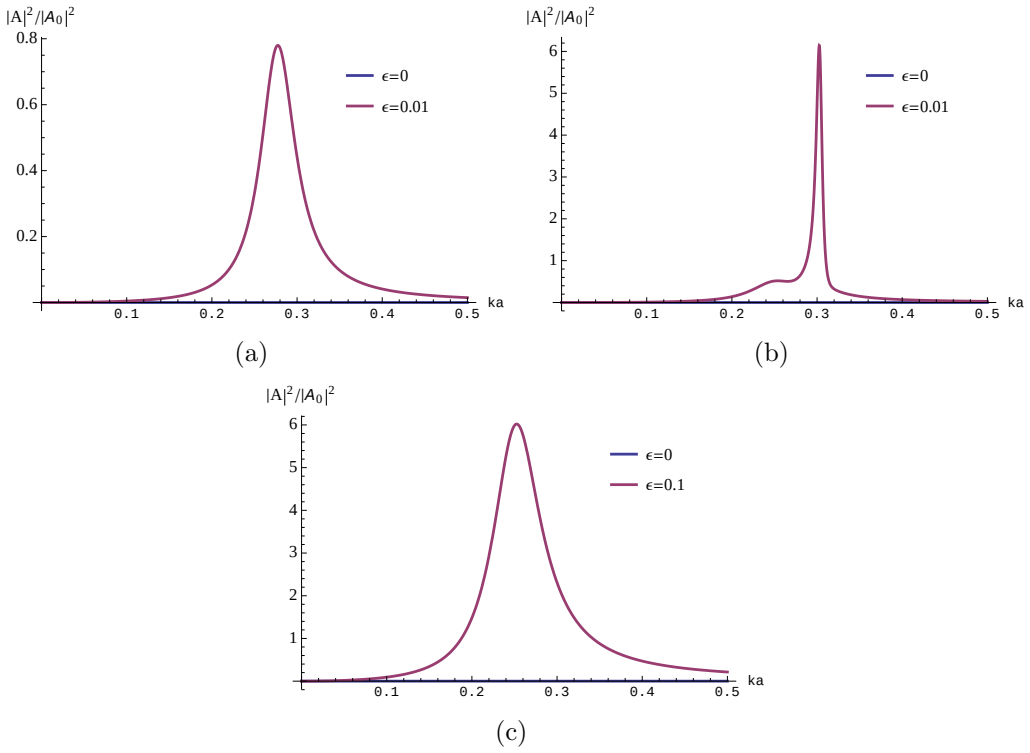

Figure 2.5: Frequency dependence of the scattering amplitude in SHG. The parameters are as in Fig. 2.4. (a) One scatterer, (b) Two scatterers parallel to the incident wave, (c) Two scatterers perpendicular to the incident wave.

dependence of the scattering amplitude at the incident frequency for $\epsilon = 0.01$. We see that the scattering amplitude increases and the resonance appears at approximately the same frequency as in the linear case with $\epsilon = 0$. The frequency dependence of the second-harmonic scattering amplitude is shown in Figure 2.5(a).

Next we consider the case of two scatterers. In Figure 2.4(b) we illustrate the frequency dependence of the scattering amplitude at the incident frequency in the case of parallel illumination. We see that when $\epsilon = 0.01$, the primary resonance acquires a larger amplitude and shifts to a slightly higher frequency, while the secondary resonance is as in the linear case. We note that a weak third resonance forms at in intermediate frequency. The frequency dependence of the second-harmonic scattering amplitude is shown in Figure 2.5(b).

Finally, in Figure 2.4(c) we show the frequency dependence of the scattering amplitude

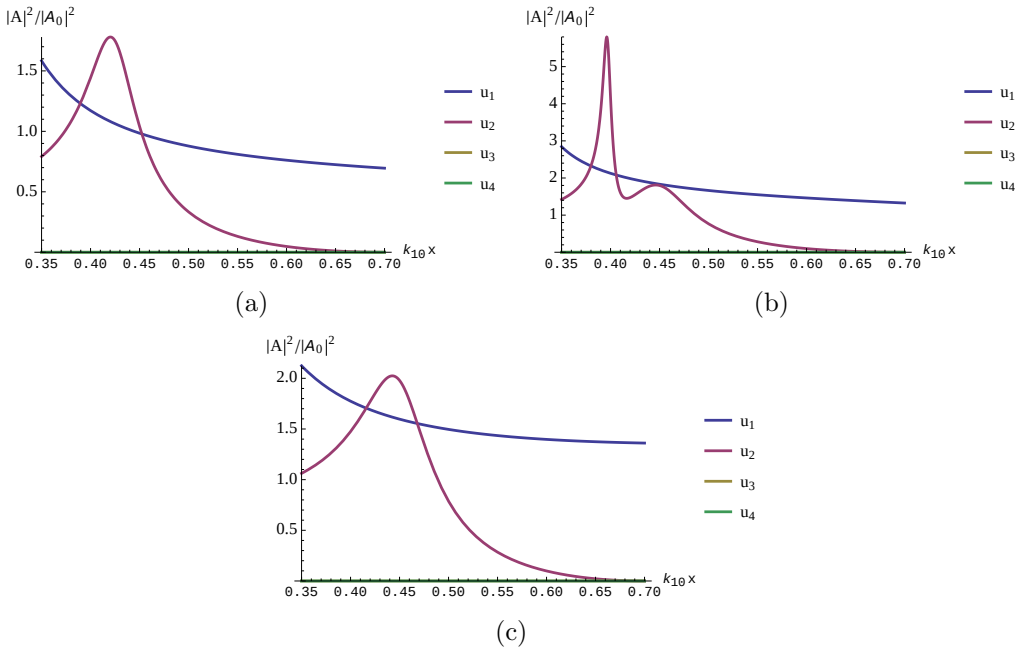

Figure 2.6: Frequency dependence of the scattering amplitudes when two plane waves are incident upon linear scatterers. The linear susceptibility is $\eta^{(1)} = 2$. (a) One scatterer, (b) Two scatterers parallel to the incident wave, (c) Two scatterers perpendicular to the incident wave.

at the incident frequency in the case of perpendicular illumination. We see that the primary resonance acquires a large amplitude and shifts to a slightly lower frequency. A weak secondary resonance also forms at a higher frequency. The frequency dependence of the second-harmonic scattering amplitude is shown in Figure 2.5(c).

2.5.3 Sum-difference frequency generation

We consider two incident waves in the $\widehat{\mathbf{z}}$ direction: $u_{1i} = u_{10}\exp(ik_{10}\widehat{\mathbf{z}}\cdot\mathbf{r})$ and $u_{2i} = u_{20}\exp(ik_{20}\widehat{\mathbf{z}}\cdot\mathbf{r})$. Let $k_{30} = k_{10} + k_{20}$ and $k_{40} = k_{10} - k_{20}$. We then consider the following set of parameters. The quantity $k_{30}a = 0.7$, so the wave numbers are all functions of k_{10}. That is, $k_{20}a = 0.7 - k_{10}a$ and $k_{40}a = 2k_{10}a - 0.7$. Results are shown for $0.35 < k_{10}a < 0.7$, so that all the wave numbers are positive. The field amplitude u_{20} is taken to be $u_{20} = u_{10}/2$.

We first consider the linear case with $\epsilon = \eta^{(2)}u_0/\eta^{(1)} = 0$ and $\eta^{(1)} = 2$. In Figure 2.6(a) we

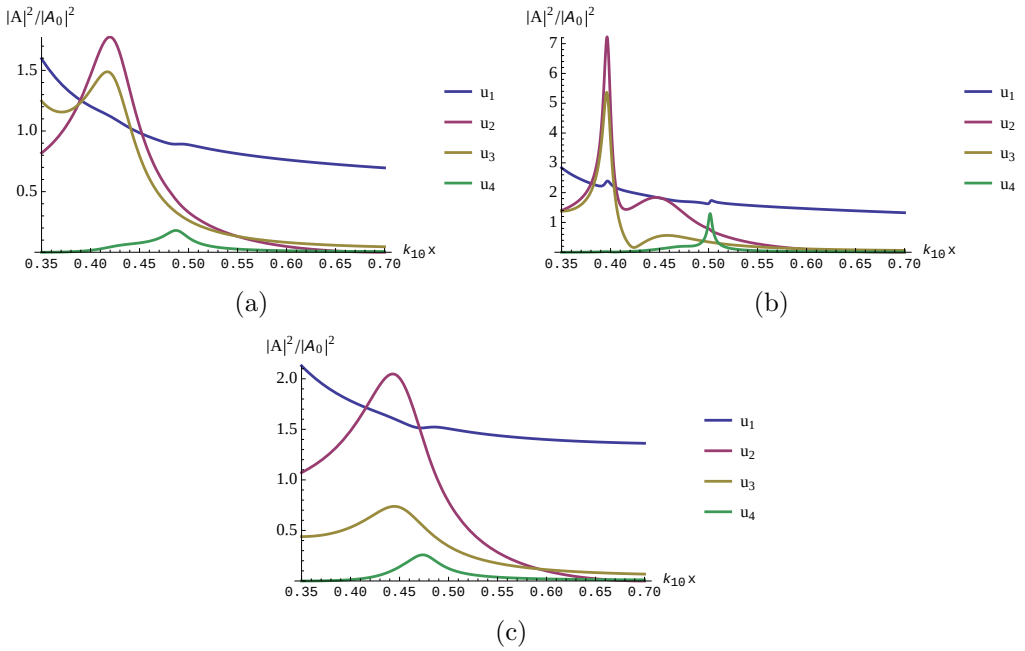

Figure 2.7: Frequency dependence of the scattering amplitudes in SDFG. The parameters are given by $\eta^{(1)} = 2$, $\epsilon = \eta^{(2)} u_0/\eta^{(1)} = 0.05$. (a) One scatterer, (b) Two scatterers parallel to the incident wave, (c) Two scatterers perpendicular to the incident wave.

illustrate the frequency dependence of the scattering amplitude for a single linear scatterer. We see that u_1 decreases for all frequencies shown, u_2 has a resonance at $k_{10}a \approx 0.43$, and $u_3 = u_4 = 0$. This result is consistent with Figure 2.3(a). Next we consider the case of two scatterers with parallel and perpendicular illumination. In Figure 2.6(b) we illustrate the frequency dependence of the scattering amplitude for the case of parallel illumination. We see that u_1 decreases for all frequencies, u_2 has a primary resonance at $k_{10}a \approx 0.39$ and a secondary resonance at $k_{10}a \approx 0.45$, and $u_3 = u_4 = 0$. This is again consistent with Figure 2.3(b). In Figure 2.6(c) we illustrate the frequency dependence of the scattering amplitude for the case of perpendicular illumination. We see that u_1 decreases on the entire domain, u_2 has a resonance at $k_{10}a \approx 0.45$, and $u_3 = u_4 = 0$. This is consistent with Figure 2.3(c).

Next we consider the nonlinear case with $\epsilon = 0.2$. In Figure 2.7(a) we plot the scattering amplitude for a single scatterer. We see that u_3 has a resonance at $k_{10}a \approx 0.42$, u_4 has a

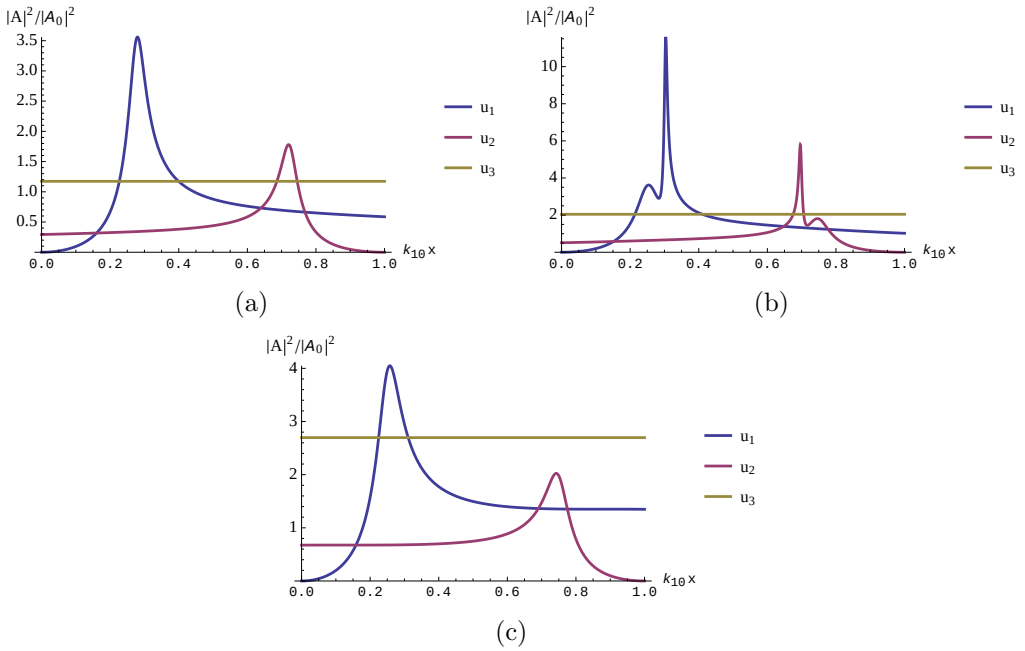

Figure 2.8: Frequency dependence of the scattering amplitudes when three plane waves with wave numbers $k_{10} + k_{20} = k_{30}$ are incident upon linear scatterers. The linear susceptibility is $\eta^{(1)} = 2$. (a) One scatterer, (b) Two scatterers parallel to the incident wave, (c) Two scatterers perpendicular to the incident wave.

resonance at $k_{10}a \approx 0.49$. In Figure 2.7(b) we plot the scattering amplitude for the case of parallel illumination. We see that u_3 has a primary resonance at $k_{10}a \approx 0.39$ and a secondary resonance at $k_{10}a \approx 0.45$, u_4 picks up a resonance at $k_{10}a \approx 0.5$, and u_1 picks up two tiny resonances at $k_{10}a \approx 0.4$ and $k_{10}a \approx 0.5$. In Figure 2.7(c) we plot the scattering amplitude for the case of perpendicular illumination. We see that u_3 develops a resonance at $k_{10}a \approx 0.45$ and u_4 has a resonance at $k_{10}a \approx 0.47$.

2.5.4 Three-wave mixing

We consider three incident waves in the $\widehat{\mathbf{z}}$ direction: $u_{1i} = u_{10}\exp(ik_{10}\widehat{\mathbf{z}}\cdot\mathbf{r})$, $u_{2i} = u_{20}\exp(ik_{20}\widehat{\mathbf{z}}\cdot\mathbf{r})$ and $u_{3i} = u_{30}\exp(ik_{30}\widehat{\mathbf{z}}\cdot\mathbf{r})$, satisfying the three-wave mixing condition $k_{10} + k_{20} = k_{30}$. We then consider the following set of parameters. The quantity $k_{30}a$ is fixed to be 1, so the three-wave mixing condition implies that $k_{20}a = 1 - k_{10}a$. We also assume that $u_{20} = u_{10}/2$

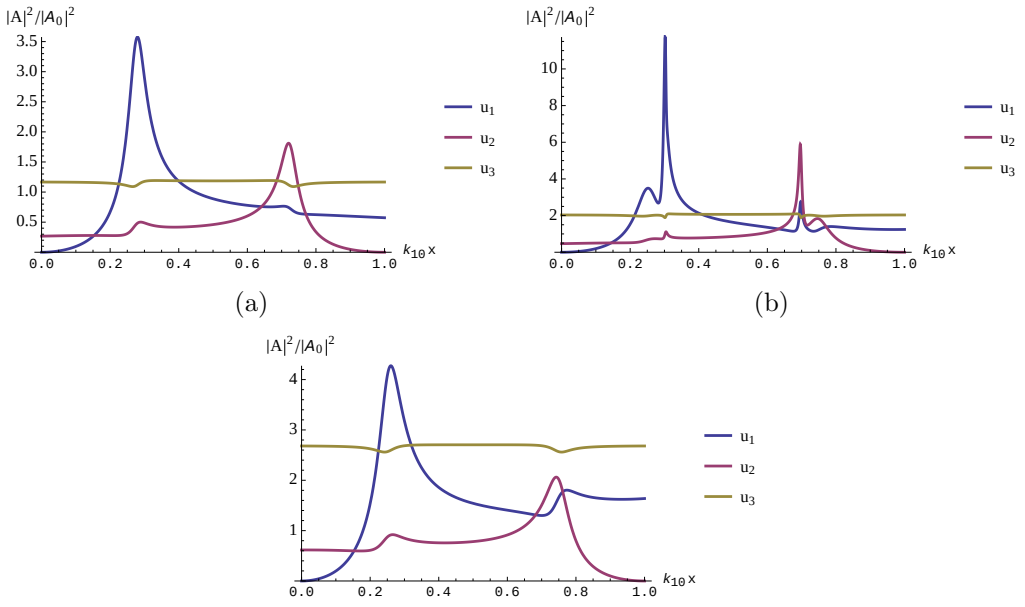

Figure 2.9: Frequency dependence of the scattering amplitudes in TWM. The parameters are given by $\eta^{(1)} = 2$, $\epsilon = \eta^{(2)}u_0/\eta^{(1)} = 0.2$. (a) One scatterer, (b) Two scatterers parallel to the incident wave, (c) Two scatterers perpendicular to the incident wave.

and $u_{30} = 2u_{10}$.

We first consider the linear case with $\epsilon = \eta^{(2)}u_0/\eta^{(1)} = 0$ and $\eta^{(1)} = 2$. In Figure 2.8(a) we plot the scattering amplitude for a single scatterer. We see that u_1 has a resonance at $k_{10}a \approx 0.3$, u_2 has a resonance at $k_{10}a \approx 0.7$, and u_3 is a constant since $k_{30}a = 1$ is independent of $k_{10}a$. Next we consider the case of two scatterers with parallel and perpendicular illumination. In Figure 2.8(b) we plot the scattering amplitude for the case of parallel illumination. We see that u_1 has a primary resonance at $k_{10}a \approx 0.3$ and a secondary resonance at $k_{10}a \approx 0.25$, u_2 has a primary resonance at $k_{10}a \approx 0.7$ and a secondary resonance at $k_{10}a \approx 0.75$, and u_3 is a constant. In Figure 2.8(c) we plot the scattering amplitude for the case of perpendicular illumination. We see that u_1 has a resonance at $k_{10}a \approx 0.3$, u_2 has a resonance at $k_{10}a \approx 0.7$, and u_3 is a constant.

Next we consider the nonlinear case with $\epsilon = 0.2$. In Figure 2.9(a) we plot the frequency dependence of the scattering amplitude for a single scatterer. We see that a second resonance

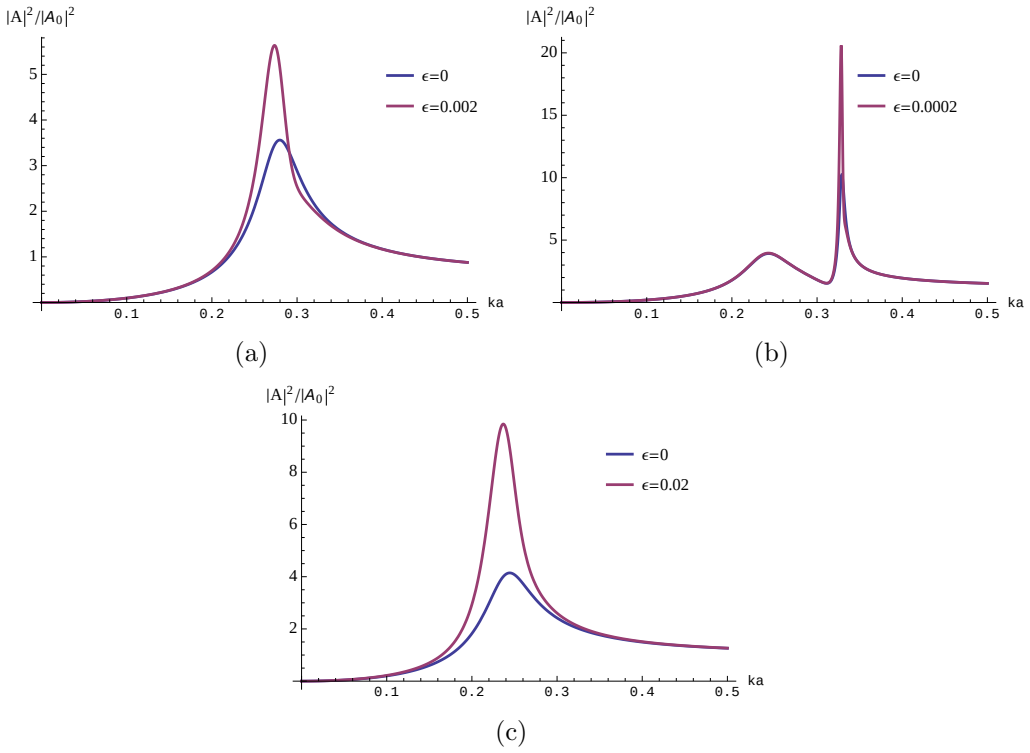

Figure 2.10: Frequency dependence of the scattering amplitude in the Kerr effect. The parameters are given by $\eta^{(1)} = 2$, $\epsilon = \eta^{(3)} u_0/\eta^{(1)}$. (a) One scatterer, (b) Two scatterers parallel to the incident wave, (c) Two scatterers perpendicular to the incident wave.

of u_1 appears at $k_{10}a \approx 0.7$, a second resonance of u_2 appears at $k_{10}a \approx 0.3$, and u_3 has two antiresonances at $k_{10}a = 0.3$ and $k_{10}a = 0.7$. In Figure 2.9(b) we plot the frequency dependence of the scattering amplitude for the case of parallel illumination. We see that a third resonance of u_1 appears at $k_{10}a \approx 0.7$, a third resonance of u_2 appears at $k_{10}a \approx 0.3$, and u_3 has two antiresonances at $k_{10}a = 0.3$ and $k_{10}a = 0.7$. In Figure 2.9(c) we plot the scattering amplitude for the case of perpendicular illumination. We see that a second resonance of u_1 appears at $k_{10}a \approx 0.7$, a second resonance of u_2 appears at $k_{10}a \approx 0.3$, and u_3 has two antiresonances at $k_{10}a = 0.3$ and $k_{10}a = 0.7$.

2.5.5 Kerr effect

We consider an incident field of the form $u_i = u_0 \exp(ik_0 \widehat{\mathbf{z}} \cdot \mathbf{r})$ and define the small parameter $\epsilon = \eta^{(3)} u_0^2 / \eta^{(1)}$. In Figure 2.10(a) we plot the scattering amplitude for a single scatterer with $\epsilon = 0.002$. We see that in the presence of the nonlinearity, the amplitude increases and the resonance shifts to a lower frequency. Next we consider two linear scatterers with parallel and perpendicular illumination. In Figure 2.10(b) we plot the scattering amplitude for the case of parallel illumination for $\epsilon = 0$ and $\epsilon = 0.0002$. We see that in the presence of the nonlinearity, the primary resonance acquires a larger amplitude without a shift and the secondary resonance is nearly unchanged from the linear case. In Figure 2.10(c) we plot the scattering amplitude for the case of perpendicular illumination for $\epsilon = 0.02$. We see that in the presence of the nonlinearity, the primary resonance acquires a larger amplitude and shifts to a slightly lower frequency.

2.5.6 Third-harmonic generation

We consider an incident field of the form $u_i = u_0 \exp(ik_0 \widehat{\mathbf{z}} \cdot \mathbf{r})$ and define the small parameter $\epsilon = \eta^{(3)} u_0^2 / \eta^{(1)}$. Note that to obtain third-harmonic generation, we must work to order $O(\epsilon^2)$. In Figure 2.11(a) we plot the scattering amplitude at the incident frequency for a single scatterer with $\epsilon = 0.002$. We see that in the presence of the nonlinearity, the amplitude increases, the resonance shifts to a lower frequency with $k_0 a \approx 0.26$ and a secondary resonance appears at $k_0 a \approx 0.3$. The frequency dependence of the third-harmonic amplitude is shown in Figure 2.12(a). Next we consider the case of two scatterers in parallel and perpendicular illumination. In Figure 2.11(b) we plot the scattering amplitude for the case of parallel illumination for $\epsilon = 0.002$. We see that in the presence of the nonlinearity, the primary resonance grows in amplitude and the secondary resonance is unchanged from the linear case. The frequency dependence of the third-harmonic scattering amplitude is shown

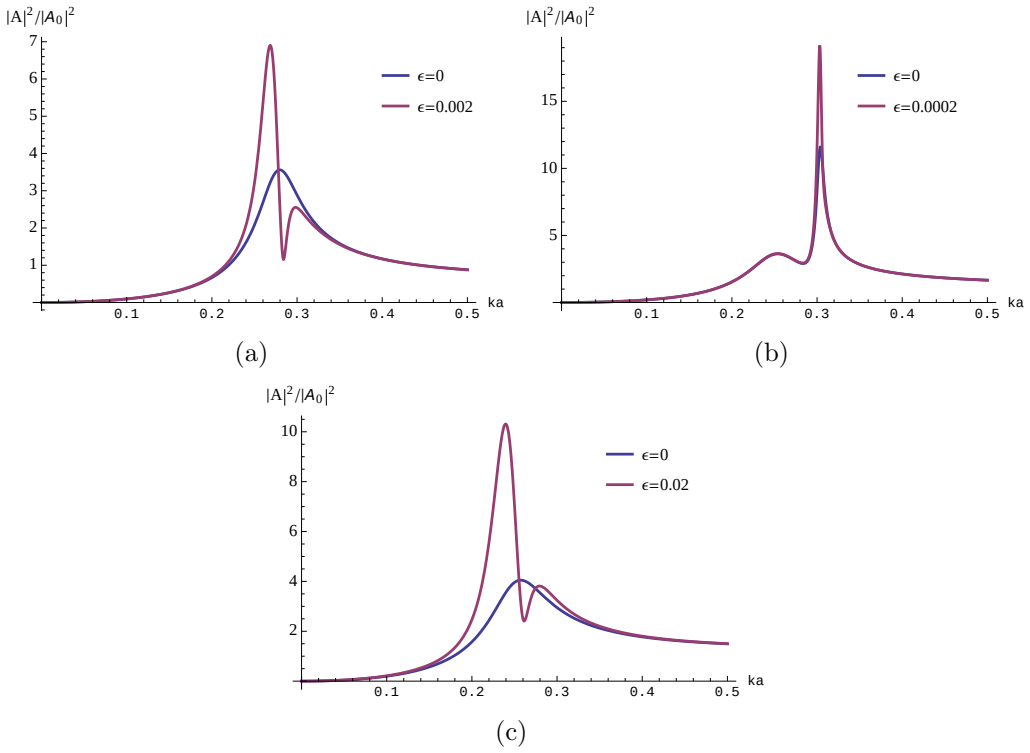

Figure 2.11: Frequency dependence of the scattering amplitude at the incident frequency in THG. The parameters are as in Fig. 2.10. (a) One scatterer, (b) Two scatterers parallel to the incident wave, (c) Two scatterers perpendicular to the incident wave.

in Figure 2.12(b). In Figure 2.11(c) we plot the the scattering amplitude for the case of perpendicular illumination for $\epsilon = 0.02$. We see that in the presence of the nonlinearity, the primary resonance acquires a larger amplitude and shifts to a lower frequency at $k_0 a \approx 0.23$. A weak secondary resonance also forms at $k_0 a \approx 0.3$. The frequency dependence of the third-harmonic scattering amplitude is shown in Figure 2.12(c).

2.5.7 Four-wave mixing

We consider four incident waves in the $\widehat{\mathbf{z}}$ direction: $u_{1i} = u_{10}\exp(ik_{10}\widehat{\mathbf{z}}\cdot\mathbf{r})$, $u_{2i} = u_{20}\exp(ik_{20}\widehat{\mathbf{z}}\cdot\mathbf{r})$, $u_{3i} = u_{30}\exp(ik_{30}\widehat{\mathbf{z}}\cdot\mathbf{r})$ and $u_{4i} = u_{40}\exp(ik_{40}\widehat{\mathbf{z}}\cdot\mathbf{r})$, satisfying the four-wave mixing condition $k_{10}+k_{20}+k_{30} = k_{40}$. We further consider the following set of parameters. We take $k_{30}a$ to be fixed at 0.5 and $k_{40}a$ set to 1. Thus the four-wave mixing condition implies that

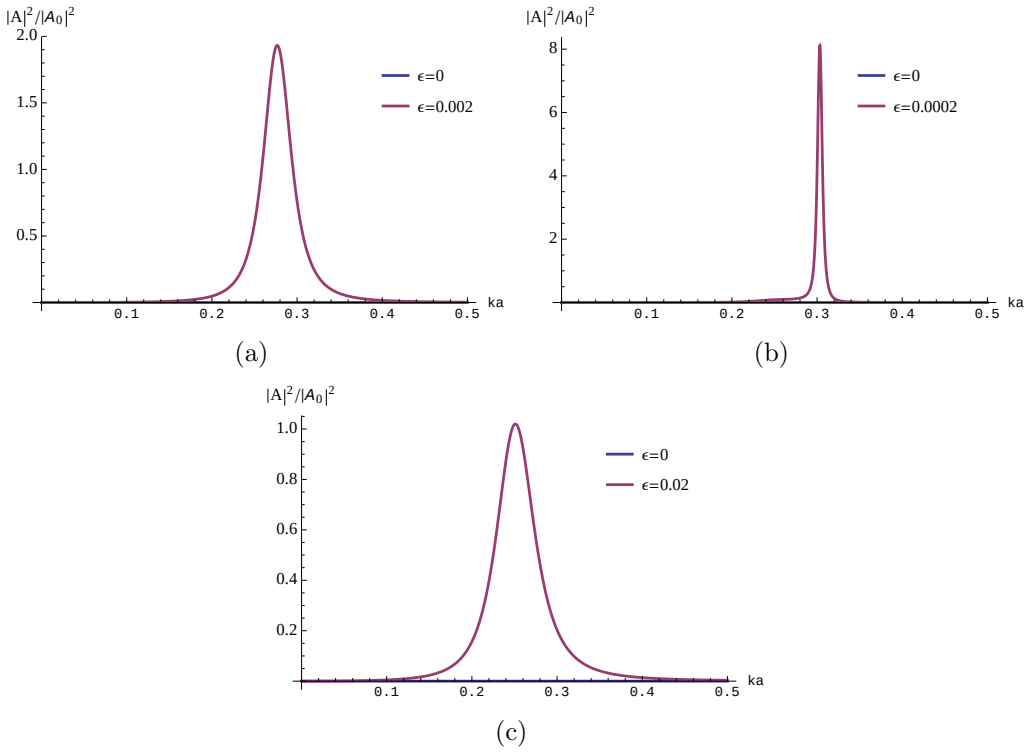

Figure 2.12: Frequency dependence of the scattering amplitude at the third-harmonic frequency in THG. The parameters are as in Fig. 2.10. (a) One scatterer, (b) Two scatterers parallel to the incident wave, (c) Two scatterers perpendicular to the incident wave.

$k_{20}a = 0.5 - k_{10}a$. We assume that $u_{20} = u_{10}/2$, $u_{30} = 2u_{10}$ and $u_{40} = u_{10}$. We introduce the small parameter $\epsilon = \eta^{(3)}u_0^2/\eta^{(1)}$ with $\eta^{(1)} = 2$.

We first consider the linear case with $\epsilon = 0$ In Figure 2.13(a) we plot the scattering amplitude for a single scatterer. We see that u_1 has a resonance at $k_{10}a \approx 0.3$, u_2 has a resonance at $k_{10}a \approx 0.2$, and u_3 and u_4 are constant since $k_{30}a = 0.5$ and $k_{40}a = 1$ are independent of $k_{10}a$. In Figure 2.13(b) we illustrate the frequency dependence of the scattering amplitude for two linear scatterers placed parallel to the incident waves. We see that u_1 has a primary resonance at $k_{10}a \approx 0.3$ and a secondary resonance at $k_{10}a \approx 0.25$, u_2 has a primary resonance at $k_{10}a \approx 0.2$ and a secondary resonance at $k_{10}a \approx 0.25$, and u_3 and u_4 are constants. In Figure 2.13(c) we plot the scattering amplitude for two linear scatterers placed perpendicular to the incident waves. We see that u_1 has a resonance at $k_{10}a \approx 0.3$,

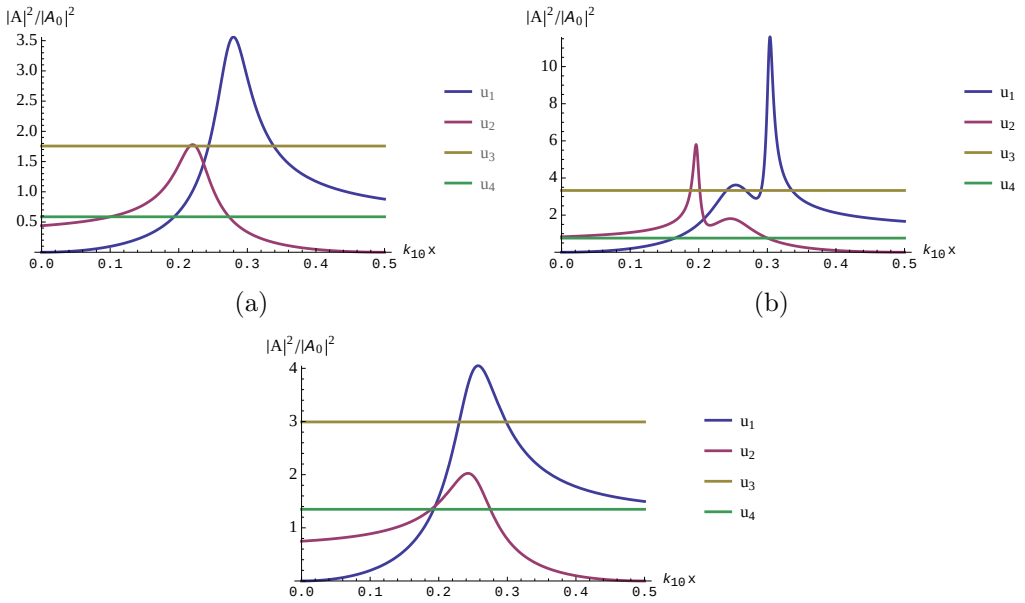

Figure 2.13: Frequency dependence of the scattering amplitudes when four plane waves with wave numbers $k_{10} + k_{20} + k_{30} = k_{40}$ are incident upon linear scatterers. The linear susceptibility is given by $\eta^{(1)} = 2$. (a) One scatterer, (b) Two scatterers parallel to the incident wave, (c) Two scatterers perpendicular to the incident wave.

u_2 has a resonance at $k_{10}a \approx 0.25$, and u_3 and u_4 are constants.

Next we consider the effects of nonlinearity with $\epsilon = 0.1$. In Figure 2.14(a) we plot the scattering amplitude for a single scatterer. We see that u_3 and u_4 develop small resonances at $k_{10}a \approx 0.22$ and $k_{10}a \approx 0.28$. The shapes of the u_1 and u_2 curves are nearly unchanged. In Figure 2.14(b) we plot the scattering amplitude for the case of parallel illumination. We see that u_3 and u_4 obtain small resonances at $k_{10}a \approx 0.2$, $k_{10}a \approx 0.5$ and $k_{10}a \approx 0.3$. The shapes of u_1 and u_2 curves are again unchanged. In Figure 2.14(c) we plot the scattering amplitude for the case of perpendicular illumination. We see that the forms of u_1 and u_2 stay approximately the same, u_3 picks up a resonance at $k_{10}a = 0.25$ and u_4 also picks up a resonance at $k_{10}a = 0.25$.

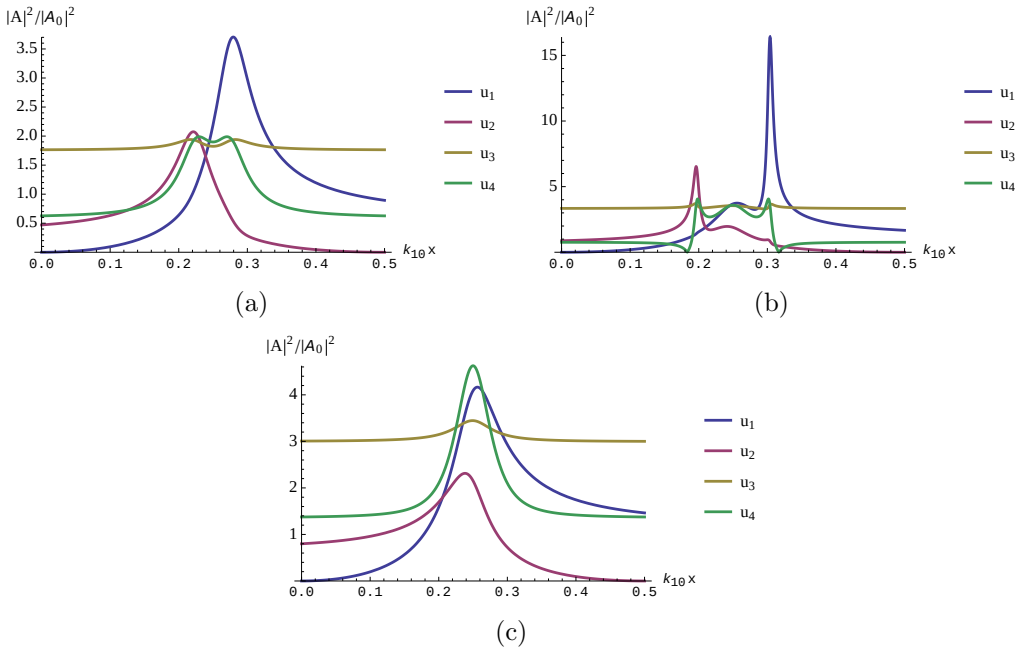

Figure 2.14: Frequency dependence of the scattering amplitudes in FWM. The parameters are given by $\eta^{(1)} = 2$, $\epsilon = \eta^{(3)} u_0/\eta^{(1)} = 0.1$. (a) One scatterer, (b) Two scatterers parallel to the incident wave, (c) Two scatterers perpendicular to the incident wave.

2.6 Discussion

We have investigated the theory of point scatterers in nonlinear optics. We considered in some detail the most important examples of quadratic and cubic nonlinearities, including second-harmonic generation, sum- and difference-frequency generation, three-wave mixing, Kerr effect, third-harmonic generation and four-wave mixing. Numerical results for the cases of one- and two-particle scattering were presented, emphasizing the manner in which scattering resonances are modified by the presence of nonlinearity. In future work, we plan to study the corresponding problems for the Maxwell equations. It may also be of interest to consider the extension to analogous problems in quantum optics, as was recently done for point scatterers in linear optics [78]. Finally, applications to nano-scale imaging with nonlinear contrast agents may be envisioned [52].

Appendix

2.A Bistability

In this Appendix we characterize the roots of the algebraic equation (2.98), which leads to conditions for bistability. To proceed, we suppose that $\eta^{(1)}$ and $\eta^{(3)}$ are real. We nondimensionalize (2.98) by writing

$$u/u_i = 1 + \frac{4\pi}{3} a^3 k^2 G_R (\eta^{(1)} u/u_i + 3\eta^{(3)} |u_i|^2 |u/u_i|^2 u/u_i) \ , \tag{2.127}$$

which can be rewritten as

$$\epsilon |z|^2 z + Az + B = 0 \ , \tag{2.128}$$

where $\epsilon = 3\eta^{(3)}|u_i|^2/\eta^{(1)}$, $z = u/u_i$, $A = 1/3 - B$, $B = 1/(4\pi a^3 k^2 G_R \eta^{(1)})$ and G_R is defined by (2.36). Next, we introduce the real variable

$$r = |z|^2 \ . \tag{2.129}$$

Eq. (2.128) thus becomes

$$\epsilon r z + Az + B = 0 \ . \tag{2.130}$$

Note that

$$z = \frac{-B}{A+\epsilon r} , \tag{2.131}$$

$$r = \frac{-Az-B}{\epsilon z} . \tag{2.132}$$

Eliminating z we have

$$r = \left| \frac{B}{A+\epsilon r} \right|^2 , \tag{2.133}$$

which can be written as

$$r((a_1+\epsilon r)^2 + a_2^2) - b_1^2 - b_2^2 = 0 , \tag{2.134}$$

where $a_1 = \mathrm{Re}A$, $a_2 = \mathrm{Im}A$, $b_1 = \mathrm{Re}B$ and $b_2 = \mathrm{Im}B$. Note that $a_1 = 1/3 - b_1$ and $a_2 = -b_2$ since $A = 1/3 - B$. The parameters b_1 and b_2 can be written in terms of ka and $\eta^{(1)}$ as

$$b_1 = \frac{3/2}{4\pi\eta^{(1)}(ka)^2(9/4+(ka)^2)} , \tag{2.135}$$

$$b_2 = -\frac{ka}{4\pi\eta^{(1)}(ka)^2(9/4+(ka)^2)} . \tag{2.136}$$

The corresponding inverse transformation is given by

$$ka = -\frac{3b_2}{2b_1} , \tag{2.137}$$

$$\eta^{(1)} = \frac{3/2}{4\pi b_1(ka)^2(9/4+(ka)^2)} . \tag{2.138}$$

Using the above results, we find that the conditions $ka > 0$ and $\eta^{(1)} \neq 0$ imply that $b_1 b_2 < 0$.

Making use of (2.129), (2.131) and (2.132), we see that the complex roots of (2.128) are in one to one correspondence to the real roots of (2.134), which is a cubic polynomial in r with

real coefficients. Recall that to determine the number of real roots of a cubic polynomial with real coefficients of the form

$$ax^3 + bx^2 + cx + d \ , \tag{2.139}$$

we examine the discriminant Δ, defined as

$$\Delta = b^2c^2 - 4ac^3 - 4b^3d - 27a^2d^2 + 18abcd \ . \tag{2.140}$$

If $\Delta > 0$, (2.139) has 3 distinct real roots; if $\Delta = 0$, (2.139) has 3 real roots, with at least two of them coinciding; if $\Delta < 0$, (2.139) has 1 real root and 2 complex roots. If we denote the discriminant of the left hand side of (2.134) by Δ_r, we obtain

$$\Delta_r = -\frac{1}{81}\epsilon^2 f(\epsilon) \ , \tag{2.141}$$

where

$$\begin{aligned} f(\epsilon) &= (2187b_1^4 + 4374b_1^2b_2^2 + 2187b_2^4)\epsilon^2 - 12(-1+3b_1)(b_1^2+b_2^2)((1-3b_1)^2 + 81b_2^2)\epsilon \\ &\quad +4b_2^2(1 - 6b_1 + 9b_1^2 + 9b_2^2)^2 \ . \end{aligned} \tag{2.142}$$

It follows that (2.134) has more than one real root on a nondegenerate interval only when $\Delta_r > 0$, namely when $f(\epsilon) < 0$. Note that $f(\epsilon)$ is a quadratic polynomial in ϵ whose leading coefficient is positive. The discriminant of $f(\epsilon)$, Δ_ϵ is given by

$$\Delta_\epsilon = 144((1-3b_1)^2 - 27b_2^2)^3(b_1^2+b_2^2)^2 \ . \tag{2.143}$$

Evidently, $\Delta_\epsilon > 0$ when $|1 - 3b_1| > \sqrt{27}|b_2|$. In this case, $f(\epsilon)$ has two real roots, which

we denote ϵ_1 and ϵ_2. For $\epsilon_2 < \epsilon < \epsilon_1$, we have that $f(\epsilon) < 0$ and $\Delta_r > 0$, so (2.134) has 3 distinct real roots and (2.128) has 3 distinct complex roots. Thus, the set of values of b_1 and

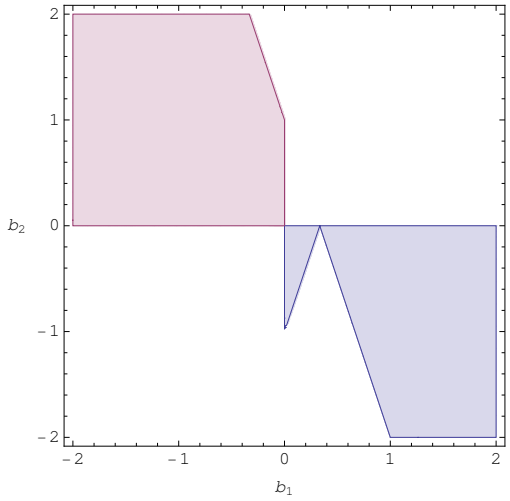

Figure 2.15: Illustrating the regions of multistability.

b_2 which allows (2.128) to have 3 roots for some values of ϵ is $|1-3b_1| > \sqrt{27}|b_2|$ and $b_1 b_2 < 0$ as shown by the shaded region in Fig. 2.15. The region in the second quadrant corresponds to negative values of $\eta^{(1)}$, whereas the part in the fourth quandrant corresponds to positive values of $\eta^{(1)}$. The condition (2.117) follows immediately from (2.135) and (2.136).

2.B Sum-difference frequency generation

The scattering amplitudes of sum-difference frequency generation with one or two small spherical scatterer(s) can be found in a strictly parallel manner to the method of Section 2.3.1. The steps can be sketched as follows. First write the solutions to (2.81) as integrals of the Greens function (2.15). Then using the fact that the scatterers are small balls, i.e., (2.30) and (2.33), we get that for one point scatterer, the scattering amplitudes are given by

$$A(\mathbf{r}, \Omega_1) \;=\; \frac{4\pi}{3} a^3 k^2(\Omega_1)(\eta^{(1)} u(\mathbf{0}, \Omega_1) + 2\eta^{(2)} u(\mathbf{0}, \Omega_3) u^*(\mathbf{0}, \Omega_2) + 2\eta^{(2)} u(\mathbf{0}, \Omega_4) u(\mathbf{0}, \Omega_2)) \;, \tag{2.144}$$

$$A(\mathbf{r},\Omega_2) = \frac{4\pi}{3}a^3k^2(\Omega_2)(\eta^{(1)}u(\mathbf{0},\Omega_2)+2\eta^{(2)}u(\mathbf{0},\Omega_3)u^*(\mathbf{0},\Omega_1)+2\eta^{(2)}u(\mathbf{0},\Omega_1)u^*(\mathbf{0},\Omega_4)) \ , \tag{2.145}$$

$$A(\mathbf{r},\Omega_3) = \frac{4\pi}{3}a^3k^2(\Omega_3)(\eta^{(1)}u(\mathbf{0},\Omega_3)+2\eta^{(2)}u(\mathbf{0},\Omega_1)u(\mathbf{0},\Omega_2)) \ , \tag{2.146}$$

$$A(\mathbf{r},\Omega_4) = \frac{4\pi}{3}a^3k^2(\Omega_4)(\eta^{(1)}u(\mathbf{0},\Omega_4)+2\eta^{(2)}u(\mathbf{0},\Omega_1)u^*(\mathbf{0},\Omega_2)) \ , \tag{2.147}$$

where the local fields $u(\mathbf{0},\Omega)$ and $u(\mathbf{0},2\Omega)$ satisfies the equations

$$\begin{aligned} u(\mathbf{0},\Omega_1) &= u_i(\mathbf{0},\Omega_1)+\frac{4\pi}{3}a^3k^2(\Omega_1)G_R(\Omega_1)(\eta^{(1)}u(\mathbf{0},\Omega_1) \\ &\quad +2\eta^{(2)}u(\mathbf{0},\Omega_3)u^*(\mathbf{0},\Omega_2)+2\eta^{(2)}u(\mathbf{0},\Omega_4)u(\mathbf{0},\Omega_2)) \ , \end{aligned} \tag{2.148}$$

$$\begin{aligned} u(\mathbf{0},\Omega_2) &= u_i(\mathbf{0},\Omega_2)+\frac{4\pi}{3}a^3k^2(\Omega_2)G_R(\Omega_2)(\eta^{(1)}u(\mathbf{0},\Omega_2) \\ &\quad +2\eta^{(2)}u(\mathbf{0},\Omega_3)u^*(\mathbf{0},\Omega_1)+2\eta^{(2)}u(\mathbf{0},\Omega_1)u^*(\mathbf{0},\Omega_4)) \ , \end{aligned} \tag{2.149}$$

$$u(\mathbf{0},\Omega_3) = \frac{4\pi}{3}a^3k^2(\Omega_3)G_R(\Omega_3)(\eta^{(1)}u(\mathbf{0},\Omega_3)+2\eta^{(2)}u(\mathbf{0},\Omega_1)u(\mathbf{0},\Omega_2)) \ , \tag{2.150}$$

$$u(\mathbf{0},\Omega_4) = \frac{4\pi}{3}a^3k^2(\Omega_4)G_R(\Omega_4)(\eta^{(1)}u(\mathbf{0},\Omega_4)+2\eta^{(2)}u(\mathbf{0},\Omega_1)u^*(\mathbf{0},\Omega_2)) \ , \tag{2.151}$$

and for two point scatterers, the scattering amplitudes are given by

$$\begin{aligned} A(\mathbf{r},\Omega_1) &= \frac{4\pi}{3}a^3k^2(\Omega_1)(\eta^{(1)}u(\mathbf{r}_1,\Omega_1) \\ &\quad +2\eta^{(2)}u(\mathbf{r}_1,\Omega_3)u^*(\mathbf{r}_1,\Omega_2)+2\eta^{(2)}u(\mathbf{r}_1,\Omega_4)u(\mathbf{r}_1,\Omega_2))e^{ik(\Omega_1)\widehat{\mathbf{r}}\cdot\mathbf{r}_1} \\ &\quad +\frac{4\pi}{3}a^3k^2(\Omega_1)(\eta^{(1)}u(\mathbf{r}_2,\Omega_1)+2\eta^{(2)}u(\mathbf{r}_2,\Omega_3)u^*(\mathbf{r}_2,\Omega_2) \\ &\quad +2\eta^{(2)}u(\mathbf{r}_2,\Omega_4)u(\mathbf{r}_2,\Omega_2))e^{ik(\Omega_1)\widehat{\mathbf{r}}\cdot\mathbf{r}_2} \ , \end{aligned} \tag{2.152}$$

$$\begin{aligned} A(\mathbf{r},\Omega_2) &= \frac{4\pi}{3}a^3k^2(\Omega_2)(\eta^{(1)}u(\mathbf{r}_1,\Omega_2)+2\eta^{(2)}u(\mathbf{r}_1,\Omega_3)u^*(\mathbf{r}_1,\Omega_1) \\ &\quad +2\eta^{(2)}u(\mathbf{r}_1,\Omega_1)u^*(\mathbf{r}_1,\Omega_4))e^{ik(\Omega_2)\widehat{\mathbf{r}}\cdot\mathbf{r}_1} \\ &\quad +\frac{4\pi}{3}a^3k^2(\Omega_2)(\eta^{(1)}u(\mathbf{r}_2,\Omega_2)+2\eta^{(2)}u(\mathbf{r}_2,\Omega_3)u^*(\mathbf{r}_2,\Omega_1) \\ &\quad +2\eta^{(2)}u(\mathbf{r}_2,\Omega_1)u^*(\mathbf{r}_2,\Omega_4))e^{ik(\Omega_2)\widehat{\mathbf{r}}\cdot\mathbf{r}_2} \ , \end{aligned} \tag{2.153}$$

$$
\begin{aligned}
A(\mathbf{r},\Omega_3) &= \frac{4\pi}{3}a^3k^2(\Omega_3)(\eta^{(1)}u(\mathbf{r}_1,\Omega_3)+2\eta^{(2)}u(\mathbf{r}_1,\Omega_1)u(\mathbf{r}_1,\Omega_2))e^{ik(\Omega_3)\widehat{\mathbf{r}}\cdot\mathbf{r}_1} \\
&\quad +\frac{4\pi}{3}a^3k^2(\Omega_3)(\eta^{(1)}u(\mathbf{r}_2,\Omega_3)+2\eta^{(2)}u(\mathbf{r}_2,\Omega_1)u(\mathbf{r}_2,\Omega_2))e^{ik(\Omega_3)\widehat{\mathbf{r}}\cdot\mathbf{r}_2}\ , \quad (2.154) \\
A(\mathbf{r},\Omega_4) &= \frac{4\pi}{3}a^3k^2(\Omega_4)(\eta^{(1)}u(\mathbf{r}_1,\Omega_4)+2\eta^{(2)}u(\mathbf{r}_1,\Omega_1)u^*(\mathbf{r}_1,\Omega_2))e^{ik(\Omega_4)\widehat{\mathbf{r}}\cdot\mathbf{r}_1} \\
&\quad +\frac{4\pi}{3}a^3k^2(\Omega_4)(\eta^{(1)}u(\mathbf{r}_2,\Omega_4)+2\eta^{(2)}u(\mathbf{r}_2,\Omega_1)u^*(\mathbf{r}_2,\Omega_2))e^{ik(\Omega_4)\widehat{\mathbf{r}}\cdot\mathbf{r}_2}\ , \quad (2.155)
\end{aligned}
$$

where the local fields $u(\mathbf{r}_1,\Omega_1)$, $u(\mathbf{r}_1,\Omega_2)$, $u(\mathbf{r}_1,\Omega_3)$ and $u(\mathbf{r}_1,\Omega_4)$, $u(\mathbf{r}_2,\Omega_1)$, $u(\mathbf{r}_2,\Omega_2)$, $u(\mathbf{r}_2,\Omega_3)$ and $u(\mathbf{r}_2,\Omega_4)$ satisfy the equations

$$
\begin{aligned}
u(\mathbf{r}_1,\Omega_1) &= u_i(\mathbf{r}_1,\Omega_1)+\frac{4\pi}{3}a^3k^2(\Omega_1)G_R(\Omega_1)(\eta^{(1)}u(\mathbf{r}_1,\Omega_1)+2\eta^{(2)}u(\mathbf{r}_1,\Omega_3)u^*(\mathbf{r}_1,\Omega_2) \\
&\quad +2\eta^{(2)}u(\mathbf{r}_1,\Omega_4)u(\mathbf{r}_1,\Omega_2))+\frac{4\pi}{3}a^3k^2(\Omega_1)G(\mathbf{r}_1,\mathbf{r}_2,\Omega_1)(\eta^{(1)}u(\mathbf{r}_2,\Omega_1) \\
&\quad +2\eta^{(2)}u(\mathbf{r}_2,\Omega_3)u^*(\mathbf{r}_2,\Omega_2)+2\eta^{(2)}u(\mathbf{r}_2,\Omega_4)u(\mathbf{r}_2,\Omega_2))\ , \quad (2.156) \\
u(\mathbf{r}_1,\Omega_2) &= u_i(\mathbf{r}_1,\Omega_2)+\frac{4\pi}{3}a^3k^2(\Omega_2)G_R(\Omega_2)(\eta^{(1)}u(\mathbf{r}_1,\Omega_2)+2\eta^{(2)}u(\mathbf{r}_1,\Omega_3)u^*(\mathbf{r}_1,\Omega_1) \\
&\quad +2\eta^{(2)}u(\mathbf{r}_1,\Omega_1)u^*(\mathbf{r}_1,\Omega_4))+\frac{4\pi}{3}a^3k^2(\Omega_2)G(\mathbf{r}_1,\mathbf{r}_2,\Omega_2)(\eta^{(1)}u(\mathbf{r}_2,\Omega_2) \\
&\quad +2\eta^{(2)}u(\mathbf{r}_2,\Omega_3)u^*(\mathbf{r}_2,\Omega_1)+2\eta^{(2)}u(\mathbf{r}_2,\Omega_1)u^*(\mathbf{r}_2,\Omega_4))\ , \quad (2.157) \\
u(\mathbf{r}_1,\Omega_3) &= \frac{4\pi}{3}a^3k^2(\Omega_3)G_R(\Omega_3)(\eta^{(1)}u(\mathbf{r}_1,\Omega_3)+2\eta^{(2)}u(\mathbf{r}_1,\Omega_1)u(\mathbf{r}_1,\Omega_2)) \\
&\quad +\frac{4\pi}{3}a^3k^2(\Omega_3)G(\mathbf{r}_1,\mathbf{r}_2,\Omega_3)(\eta^{(1)}u(\mathbf{r}_2,\Omega_3)+2\eta^{(2)}u(\mathbf{r}_2,\Omega_1)u(\mathbf{r}_2,\Omega_2))\ , \quad (2.158) \\
u(\mathbf{r}_1,\Omega_4) &= \frac{4\pi}{3}a^3k^2(\Omega_4)G_R(\Omega_4)(\eta^{(1)}u(\mathbf{r}_1,\Omega_4)+2\eta^{(2)}u(\mathbf{r}_1,\Omega_1)u^*(\mathbf{r}_1,\Omega_2)) \\
&\quad +\frac{4\pi}{3}a^3k^2(\Omega_4)G(\mathbf{r}_1,\mathbf{r}_2,\Omega_4)(\eta^{(1)}u(\mathbf{r}_2,\Omega_4)+2\eta^{(2)}u(\mathbf{r}_2,\Omega_1)u^*(\mathbf{r}_2,\Omega_2)) \quad (2.159) \\
u(\mathbf{r}_2,\Omega_1) &= u_i(\mathbf{r}_2,\Omega_1)+\frac{4\pi}{3}a^3k^2(\Omega_1)G(\mathbf{r}_2,\mathbf{r}_1,\Omega_1)(\eta^{(1)}u(\mathbf{r}_1,\Omega_1)\ , \\
&\quad +2\eta^{(2)}u(\mathbf{r}_1,\Omega_3)u^*(\mathbf{r}_1,\Omega_2)+2\eta^{(2)}u(\mathbf{r}_1,\Omega_4)u(\mathbf{r}_1,\Omega_2)) \\
&\quad +\frac{4\pi}{3}a^3k^2(\Omega_1)G_R(\Omega_1)(\eta^{(1)}u(\mathbf{r}_2,\Omega_1)+2\eta^{(2)}u(\mathbf{r}_2,\Omega_3)u^*(\mathbf{r}_2,\Omega_2) \\
&\quad +2\eta^{(2)}u(\mathbf{r}_2,\Omega_4)u(\mathbf{r}_2,\Omega_2))\ , \quad (2.160)
\end{aligned}
$$

$$
\begin{aligned}
u(\mathbf{r}_2,\Omega_2) &= u_i(\mathbf{r}_2,\Omega_2)+\frac{4\pi}{3}a^3k^2(\Omega_2)G(\mathbf{r}_2,\mathbf{r}_1,\Omega_2)(\eta^{(1)}u(\mathbf{r}_1,\Omega_2) \\
&\quad +2\eta^{(2)}u(\mathbf{r}_1,\Omega_3)u^*(\mathbf{r}_1,\Omega_1)+2\eta^{(2)}u(\mathbf{r}_1,\Omega_1)u^*(\mathbf{r}_1,\Omega_4)) \\
&\quad +\frac{4\pi}{3}a^3k^2(\Omega_2)G_R(\Omega_2)(\eta^{(1)}u(\mathbf{r}_2,\Omega_2)+2\eta^{(2)}u(\mathbf{r}_2,\Omega_3)u^*(\mathbf{r}_2,\Omega_1) \\
&\quad +2\eta^{(2)}u(\mathbf{r}_2,\Omega_1)u^*(\mathbf{r}_2,\Omega_4))\ , \qquad (2.161)\\
u(\mathbf{r}_2,\Omega_3) &= \frac{4\pi}{3}a^3k^2(\Omega_3)G(\mathbf{r}_2,\mathbf{r}_1,\Omega_3)(\eta^{(1)}u(\mathbf{r}_1,\Omega_3)+2\eta^{(2)}u(\mathbf{r}_1,\Omega_1)u(\mathbf{r}_1,\Omega_2)) \\
&\quad +\frac{4\pi}{3}a^3k^2(\Omega_3)G_R(\Omega_3)(\eta^{(1)}u(\mathbf{r}_2,\Omega_3)+2\eta^{(2)}u(\mathbf{r}_2,\Omega_1)u(\mathbf{r}_2,\Omega_2))\ , \qquad (2.162)\\
u(\mathbf{r}_2,\Omega_4) &= \frac{4\pi}{3}a^3k^2(\Omega_4)G(\mathbf{r}_2,\mathbf{r}_1,\Omega_4)(\eta^{(1)}u(\mathbf{r}_1,\Omega_4)+2\eta^{(2)}u(\mathbf{r}_1,\Omega_1)u^*(\mathbf{r}_1,\Omega_2)) \\
&\quad +\frac{4\pi}{3}a^3k^2(\Omega_4)G_R(\Omega_4)(\eta^{(1)}u(\mathbf{r}_2,\Omega_4)+2\eta^{(2)}u(\mathbf{r}_2,\Omega_1)u^*(\mathbf{r}_2,\Omega_2))\ . \qquad (2.163)
\end{aligned}
$$

2.C Three-wave mixing

Here we derive the scattering amplitude for three-wave mixing given in (2.85). For the case of one point scatterer, the scattering amplitudes are given by

$$
\begin{aligned}
A(\mathbf{r},\Omega_1) &= \frac{4\pi}{3}a^3k^2(\Omega_1)(\eta^{(1)}u(\mathbf{0},\Omega_1)+2\eta^{(2)}u(\mathbf{0},\Omega_3)u^*(\mathbf{0},\Omega_2))\ , \qquad (2.164)\\
A(\mathbf{r},\Omega_2) &= \frac{4\pi}{3}a^3k^2(\Omega_2)(\eta^{(1)}u(\mathbf{0},\Omega_2)+2\eta^{(2)}u(\mathbf{0},\Omega_3)u^*(\mathbf{0},\Omega_1))\ , \qquad (2.165)\\
A(\mathbf{r},\Omega_3) &= \frac{4\pi}{3}a^3k^2(\Omega_3)(\eta^{(1)}u(\mathbf{0},\Omega_3)+2\eta^{(2)}u(\mathbf{0},\Omega_1)u(\mathbf{0},\Omega_2))\ . \qquad (2.166)
\end{aligned}
$$

The local fields $u(\mathbf{0},\Omega)$ and $u(\mathbf{0},2\Omega)$ can be obtained by solving the equations perturbatively.

$$
u(\mathbf{0},\Omega_1) = u_i(\mathbf{0},\Omega_1)+\frac{4\pi}{3}a^3k^2(\Omega_1)G_R(\Omega_1)(\eta^{(1)}u(\mathbf{0},\Omega_1)+2\eta^{(2)}u(\mathbf{0},\Omega_3)u^*(\mathbf{0},\Omega_2))\ , \qquad (2.167)
$$

$$
u(\mathbf{0},\Omega_2) = u_i(\mathbf{0},\Omega_2)+\frac{4\pi}{3}a^3k^2(\Omega_2)G_R(\Omega_2)(\eta^{(1)}u(\mathbf{0},\Omega_2)+2\eta^{(2)}u(\mathbf{0},\Omega_3)u^*(\mathbf{0},\Omega_1))\ , \qquad (2.168)
$$

$$u(\mathbf{0},\Omega_3) = \frac{4\pi}{3}a^3k^2(\Omega_3)G_R(\Omega_3)(\eta^{(1)}u(\mathbf{0},\Omega_3)+2\eta^{(2)}u(\mathbf{0},\Omega_1)u(\mathbf{0},\Omega_2)) \ . \quad (2.169)$$

For the case of two point scatterers, the scattering amplitudes are given by

$$\begin{aligned}
A(\mathbf{r},\Omega_1) &= \frac{4\pi}{3}a^3k^2(\Omega_1)(\eta^{(1)}u(\mathbf{r}_1,\Omega_1)+2\eta^{(2)}u(\mathbf{r}_1,\Omega_3)u^*(\mathbf{r}_1,\Omega_2))e^{ik(\Omega_1)\widehat{\mathbf{r}}\cdot\mathbf{r}_1} \\
&\quad +\frac{4\pi}{3}a^3k^2(\Omega_1)(\eta^{(1)}u(\mathbf{r}_2,\Omega_1)+2\eta^{(2)}u(\mathbf{r}_2,\Omega_3)u^*(\mathbf{r}_2,\Omega_2))e^{ik(\Omega_1)\widehat{\mathbf{r}}\cdot\mathbf{r}_2} \ , (2.170) \\
A(\mathbf{r},\Omega_2) &= \frac{4\pi}{3}a^3k^2(\Omega_2)(\eta^{(1)}u(\mathbf{r}_1,\Omega_2)+2\eta^{(2)}u(\mathbf{r}_1,\Omega_3)u^*(\mathbf{r}_1,\Omega_1))e^{ik(\Omega_2)\widehat{\mathbf{r}}\cdot\mathbf{r}_1} \\
&\quad +\frac{4\pi}{3}a^3k^2(\Omega_2)(\eta^{(1)}u(\mathbf{r}_2,\Omega_2)+2\eta^{(2)}u(\mathbf{r}_2,\Omega_3)u^*(\mathbf{r}_2,\Omega_1))e^{ik(\Omega_2)\widehat{\mathbf{r}}\cdot\mathbf{r}_2} \ , (2.171) \\
A(\mathbf{r},\Omega_3) &= \frac{4\pi}{3}a^3k^2(\Omega_3)(\eta^{(1)}u(\mathbf{r}_1,\Omega_3)+2\eta^{(2)}u(\mathbf{r}_1,\Omega_1)u(\mathbf{r}_1,\Omega_2))e^{ik(\Omega_3)\widehat{\mathbf{r}}\cdot\mathbf{r}_1} \\
&\quad +\frac{4\pi}{3}a^3k^2(\Omega_3)(\eta^{(1)}u(\mathbf{r}_2,\Omega_3)+2\eta^{(2)}u(\mathbf{r}_2,\Omega_1)u(\mathbf{r}_2,\Omega_2))e^{ik(\Omega_3)\widehat{\mathbf{r}}\cdot\mathbf{r}_2} \ . \quad (2.172)
\end{aligned}$$

The local fields $u(\mathbf{r}_1,\Omega_1)$, $u(\mathbf{r}_1,\Omega_2)$, $u(\mathbf{r}_1,\Omega_3)$, $u(\mathbf{r}_2,\Omega_1)$, $u(\mathbf{r}_2,\Omega_2)$ and $u(\mathbf{r}_2,\Omega_3)$ can be obtained by solving the equations perturbatively.

$$\begin{aligned}
u(\mathbf{r}_1,\Omega_1) &= u_i(\mathbf{r}_1,\Omega_1)+\frac{4\pi}{3}a^3k^2(\Omega_1)G_R(\Omega_1)(\eta^{(1)}u(\mathbf{r}_1,\Omega_1) \\
&\quad +2\eta^{(2)}u(\mathbf{r}_1,\Omega_3)u^*(\mathbf{r}_1,\Omega_2))+\frac{4\pi}{3}a^3k^2(\Omega_1)G(\mathbf{r}_1,\mathbf{r}_2,\Omega_1)(\eta^{(1)}u(\mathbf{r}_2,\Omega_1) \\
&\quad +2\eta^{(2)}u(\mathbf{r}_2,\Omega_3)u^*(\mathbf{r}_2,\Omega_2)) \ , \quad (2.173) \\
u(\mathbf{r}_1,\Omega_2) &= u_i(\mathbf{r}_1,\Omega_2)+\frac{4\pi}{3}a^3k^2(\Omega_2)G_R(\Omega_2)(\eta^{(1)}u(\mathbf{r}_1,\Omega_2) \\
&\quad +2\eta^{(2)}u(\mathbf{r}_1,\Omega_3)u^*(\mathbf{r}_1,\Omega_1))+\frac{4\pi}{3}a^3k^2(\Omega_2)G(\mathbf{r}_1,\mathbf{r}_2,\Omega_2)(\eta^{(1)}u(\mathbf{r}_2,\Omega_2) \\
&\quad +2\eta^{(2)}u(\mathbf{r}_2,\Omega_3)u^*(\mathbf{r}_2,\Omega_1)) \ , \quad (2.174) \\
u(\mathbf{r}_1,\Omega_3) &= u_i(\mathbf{r}_1,\Omega_3)+\frac{4\pi}{3}a^3k^2(\Omega_3)G_R(\Omega_3)(\eta^{(1)}u(\mathbf{r}_1,\Omega_3) \\
&\quad +\eta^{(2)}u(\mathbf{r}_1,\Omega_1)u(\mathbf{r}_1,\Omega_2))+\frac{4\pi}{3}a^3k^2(\Omega_3)G(\mathbf{r}_1,\mathbf{r}_2,\Omega_3)(\eta^{(1)}u(\mathbf{r}_2,\Omega_3) \\
&\quad +2\eta^{(2)}u(\mathbf{r}_2,\Omega_1)u(\mathbf{r}_2,\Omega_2)) \ , \quad (2.175)
\end{aligned}$$

$$
\begin{aligned}
u(\mathbf{r}_2,\Omega_1) &= u_i(\mathbf{r}_2,\Omega_1) \\
&\quad +\frac{4\pi}{3}a^3k^2(\Omega_1)G(\mathbf{r}_2,\mathbf{r}_1,\Omega_1)(\eta^{(1)}u(\mathbf{r}_1,\Omega_1)+2\eta^{(2)}u(\mathbf{r}_1,\Omega_3)u^*(\mathbf{r}_1,\Omega_2)) \\
&\quad +\frac{4\pi}{3}a^3k^2(\Omega_1)G_R(\Omega_1)(\eta^{(1)}u(\mathbf{r}_2,\Omega_1)+2\eta^{(2)}u(\mathbf{r}_2,\Omega_3)u^*(\mathbf{r}_2,\Omega_2))\ , \quad (2.176) \\
u(\mathbf{r}_2,\Omega_2) &= u_i(\mathbf{r}_2,\Omega_2) \\
&\quad +\frac{4\pi}{3}a^3k^2(\Omega_2)G(\mathbf{r}_2,\mathbf{r}_1,\Omega_2)(\eta^{(1)}u(\mathbf{r}_1,\Omega_2)+2\eta^{(2)}u(\mathbf{r}_1,\Omega_3)u^*(\mathbf{r}_1,\Omega_1)) \\
&\quad +\frac{4\pi}{3}a^3k^2(\Omega_2)G_R(\Omega_2)(\eta^{(1)}u(\mathbf{r}_2,\Omega_2)+2\eta^{(2)}u(\mathbf{r}_2,\Omega_3)u^*(\mathbf{r}_2,\Omega_1))\ , \quad (2.177) \\
u(\mathbf{r}_2,\Omega_3) &= u_i(\mathbf{r}_2,\Omega_3) \\
&\quad +\frac{4\pi}{3}a^3k^2(\Omega_3)G(\mathbf{r}_2,\mathbf{r}_1,\Omega_3)(\eta^{(1)}u(\mathbf{r}_1,\Omega_3)+\eta^{(2)}u(\mathbf{r}_1,\Omega_1)u(\mathbf{r}_1,\Omega_2)) \\
&\quad +\frac{4\pi}{3}a^3k^2(\Omega_3)G_R(\Omega_3)(\eta^{(1)}u(\mathbf{r}_2,\Omega_3)+2\eta^{(2)}u(\mathbf{r}_2,\Omega_1)u(\mathbf{r}_2,\Omega_2))\ . \quad (2.178)
\end{aligned}
$$

2.D Third-harmonic generation

Here we derive the scattering amplitude for third-harmonic generation as given in (2.118). For the case of one point scatterer, the scattering amplitudes are of the form

$$
\begin{aligned}
A(\mathbf{r},\Omega) &= \frac{4\pi}{3}a^3k^2(\Omega)(\eta^{(1)}u(\mathbf{0},\Omega)+3\eta^{(3)}(u(\mathbf{0},\Omega))^2u^*(\mathbf{0},\Omega) \\
&\quad +3\eta^{(3)}u(\mathbf{0},3\Omega)(u^*(\mathbf{0},\Omega))^2)\ , \quad (2.179) \\
A(\mathbf{r},3\Omega) &= \frac{4\pi}{3}a^3k^2(3\Omega)(\eta^{(1)}u(\mathbf{0},3\Omega)+\eta^{(3)}(u(\mathbf{0},\Omega))^3)\ . \quad (2.180)
\end{aligned}
$$

The local fields $u(\mathbf{0},\Omega)$ and $u(\mathbf{0},2\Omega)$ can be obtained by solving the equations perturbatively. We thus obtain

$$
\begin{aligned}
u(\mathbf{0},\Omega) &= u_i(\mathbf{0},\Omega)+\frac{4\pi}{3}a^3k^2G_R(\Omega)(\eta^{(1)}u(\mathbf{0},\Omega) \\
&\quad +3\eta^{(3)}(u(\mathbf{0},\Omega))^2u^*(\mathbf{0},\Omega)+3\eta^{(3)}u(\mathbf{0},3\Omega)(u^*(\mathbf{0},\Omega))^2)\ , \quad (2.181) \\
u(\mathbf{0},3\Omega) &= \frac{4\pi}{3}a^3k^2G_R(3\Omega)(\eta^{(1)}u(\mathbf{0},3\Omega)+\eta^{(3)}(u(\mathbf{0},\Omega))^3)\ . \quad (2.182)
\end{aligned}
$$

For the case of two point scatterers, the scattering amplitudes are given by

$$\begin{aligned}
A(\mathbf{r},\Omega) &= \frac{4\pi}{3}a^3k^2(\Omega)(\eta^{(1)}u(\mathbf{r}_1,\Omega) \\
&\quad +3\eta^{(3)}(u(\mathbf{r}_1,\Omega))^2u^*(\mathbf{r}_1,\Omega)+3\eta^{(3)}u(\mathbf{r}_1,3\Omega)(u^*(\mathbf{r}_1,\Omega))^2)e^{ik(\Omega)\widehat{\mathbf{r}}\cdot\mathbf{r}_1} \\
&\quad +\frac{4\pi}{3}a^3k^2(\Omega)(\eta^{(1)}u(\mathbf{r}_2,\Omega)+3\eta^{(3)}(u(\mathbf{r}_2,\Omega))^2u^*(\mathbf{r}_2,\Omega) \\
&\quad +3\eta^{(3)}u(\mathbf{r}_2,3\Omega)(u^*(\mathbf{r}_2,\Omega))^2)e^{ik(\Omega)\widehat{\mathbf{r}}\cdot\mathbf{r}_2}\ , \qquad (2.183) \\
A(\mathbf{r},3\Omega) &= \frac{4\pi}{3}a^3k^2(3\Omega)(\eta^{(1)}u(\mathbf{r}_1,3\Omega)+\eta^{(3)}(u(\mathbf{r}_1,\Omega))^3)e^{ik(3\Omega)\widehat{\mathbf{r}}\cdot\mathbf{r}_1} \\
&\quad +\frac{4\pi}{3}a^3k^2(3\Omega)(\eta^{(1)}u(\mathbf{r}_2,3\Omega)+\eta^{(3)}(u(\mathbf{r}_2,\Omega))^3)e^{ik(3\Omega)\widehat{\mathbf{r}}\cdot\mathbf{r}_2}\ . \qquad (2.184)
\end{aligned}$$

The local fields $u(\mathbf{r}_1,\Omega)$, $u(\mathbf{r}_1,3\Omega)$, $u(\mathbf{r}_2,\Omega)$ and $u(\mathbf{r}_2,3\Omega)$ can be obtained by solving the equations perturbtively.

$$\begin{aligned}
u(\mathbf{r}_1,\Omega) &= u_i(\mathbf{r}_1,\Omega)+\frac{4\pi}{3}a^3k^2(\Omega)G_R(\Omega)(\eta^{(1)}u(\mathbf{r}_1,\Omega)+3\eta^{(3)}(u(\mathbf{r}_1,\Omega))^2u^*(\mathbf{r}_1,\Omega) \\
&\quad +3\eta^{(3)}u(\mathbf{r}_1,3\Omega)(u^*(\mathbf{r}_1,\Omega))^2)+\frac{4\pi}{3}a^3k^2(\Omega)G(\mathbf{r}_1,\mathbf{r}_2,\Omega)(\eta^{(1)}u(\mathbf{r}_2,\Omega) \\
&\quad +3\eta^{(3)}(u(\mathbf{r}_2,\Omega))^2u^*(\mathbf{r}_2,\Omega)+3\eta^{(3)}u(\mathbf{r}_2,3\Omega)(u^*(\mathbf{r}_2,\Omega))^2)\ , \qquad (2.185) \\
u(\mathbf{r}_1,3\Omega) &= \frac{4\pi}{3}a^3k^2(3\Omega)G_R(3\Omega)(\eta^{(1)}u(\mathbf{r}_1,3\Omega)+\eta^{(3)}(u(\mathbf{r}_1,\Omega))^3) \\
&\quad +\frac{4\pi}{3}a^3k^2(3\Omega)G(\mathbf{r}_1,\mathbf{r}_2,3\Omega)(\eta^{(1)}u(\mathbf{r}_2,3\Omega)+\eta^{(3)}(u(\mathbf{r}_2,\Omega))^3)\ , \qquad (2.186) \\
u(\mathbf{r}_2,\Omega) &= u_i(\mathbf{r}_2,\Omega)+\frac{4\pi}{3}a^3k^2(\Omega)G(\mathbf{r}_2,\mathbf{r}_1,\Omega)(\eta^{(1)}u(\mathbf{r}_1,\Omega) \\
&\quad +3\eta^{(3)}(u(\mathbf{r}_1,\Omega))^2u^*(\mathbf{r}_1,\Omega)+3\eta^{(3)}u(\mathbf{r}_1,3\Omega)(u^*(\mathbf{r}_1,\Omega))^2) \\
&\quad +\frac{4\pi}{3}a^3k^2(\Omega)G_R(\Omega)(\eta^{(1)}u(\mathbf{r}_2,\Omega)+3\eta^{(3)}(u(\mathbf{r}_2,\Omega))^2u^*(\mathbf{r}_2,\Omega) \\
&\quad +3\eta^{(3)}u(\mathbf{r}_2,3\Omega)(u^*(\mathbf{r}_2,\Omega))^2)\ , \qquad (2.187) \\
u(\mathbf{r}_2,3\Omega) &= \frac{4\pi}{3}a^3k^2(3\Omega)G(\mathbf{r}_2,\mathbf{r}_1,3\Omega)(\eta^{(1)}u(\mathbf{r}_1,3\Omega)+\eta^{(3)}(u(\mathbf{r}_1,\Omega))^3) \\
&\quad +\frac{4\pi}{3}a^3k^2(3\Omega)G_R(3\Omega)(\eta^{(1)}u(\mathbf{r}_2,3\Omega)+\eta^{(3)}(u(\mathbf{r}_2,\Omega))^3)\ . \qquad (2.188)
\end{aligned}$$

2.E Four-wave mixing

Here we derive the scattering amplitude for four-wave mixing given by (2.120). For the case of one point scatterer, the scattering amplitudes are of the form

$$A(\mathbf{r},\Omega_1) = \frac{4\pi}{3}a^3k^2(\Omega_1)(\eta^{(1)}u(\mathbf{0},\Omega_1)+6\eta^{(3)}u(\mathbf{0},\Omega_4)u^*(\mathbf{0},\Omega_3)u^*(\mathbf{0},\Omega_2)) \ , \quad (2.189)$$

$$A(\mathbf{r},\Omega_2) = \frac{4\pi}{3}a^3k^2(\Omega_2)(\eta^{(1)}u(\mathbf{0},\Omega_2)+6\eta^{(3)}u(\mathbf{0},\Omega_4)u^*(\mathbf{0},\Omega_3)u^*(\mathbf{0},\Omega_1)) \ , \quad (2.190)$$

$$A(\mathbf{r},\Omega_3) = \frac{4\pi}{3}a^3k^2(\Omega_3)(\eta^{(1)}u(\mathbf{0},\Omega_3)+6\eta^{(3)}u(\mathbf{0},\Omega_4)u^*(\mathbf{0},\Omega_2)u^*(\mathbf{0},\Omega_1)) \ , \quad (2.191)$$

$$A(\mathbf{r},\Omega_4) = \frac{4\pi}{3}a^3k^2(\Omega_4)(\eta^{(1)}u(\mathbf{0},\Omega_4)+6\eta^{(3)}u(\mathbf{0},\Omega_1)u(\mathbf{0},\Omega_2)u(\mathbf{0},\Omega_3)) \ . \quad (2.192)$$

The local fields can be obtained by solving the equations perturbatively.

$$\begin{aligned} u(\mathbf{0},\Omega_1) &= u_i(\mathbf{0},\Omega_1) \\ &\quad +\frac{4\pi}{3}a^3k^2(\Omega_1)G_R(\Omega_1)(\eta^{(1)}u(\mathbf{0},\Omega_1)+6\eta^{(3)}u(\mathbf{0},\Omega_4)u^*(\mathbf{0},\Omega_3)u^*(\mathbf{0},\Omega_2)) \ , \end{aligned} \quad (2.193)$$

$$\begin{aligned} u(\mathbf{0},\Omega_2) &= u_i(\mathbf{0},\Omega_2) \\ &\quad +\frac{4\pi}{3}a^3k^2(\Omega_2)G_R(\Omega_2)(\eta^{(1)}u(\mathbf{0},\Omega_2)+6\eta^{(3)}u(\mathbf{0},\Omega_4)u^*(\mathbf{0},\Omega_3)u^*(\mathbf{0},\Omega_1)) \ , \end{aligned} \quad (2.194)$$

$$\begin{aligned} u(\mathbf{0},\Omega_3 &= u_i(\mathbf{0},\Omega_3) \\ &\quad +\frac{4\pi}{3}a^3k^2(\Omega_3)G_R(\Omega_3)(\eta^{(1)}u(\mathbf{0},\Omega_3)+6\eta^{(3)}u(\mathbf{0},\Omega_4)u^*(\mathbf{0},\Omega_2)u^*(\mathbf{0},\Omega_1)) \ , \end{aligned} \quad (2.195)$$

$$\begin{aligned} u(\mathbf{0},\Omega_4) &= u_i(\mathbf{0},\Omega_4) \\ &\quad +\frac{4\pi}{3}a^3k^2(\Omega_4)G_R(\Omega_4)(\eta^{(1)}u(\mathbf{0},\Omega_4)+6\eta^{(3)}u(\mathbf{0},\Omega_1)u(\mathbf{0},\Omega_2)u(\mathbf{0},\Omega_3)) \ . \end{aligned} \quad (2.196)$$

For the case of two point scatterers, the scattering amplitudes are given by

$$\begin{aligned} A(\mathbf{r},\Omega_1) &= \frac{4\pi}{3}a^3k^2(\Omega_1)(\eta^{(1)}u(\mathbf{r}_1,\Omega_1)+6\eta^{(3)}u(\mathbf{r}_1,\Omega_4)u^*(\mathbf{r}_1,\Omega_3)u^*(\mathbf{r}_1,\Omega_2))e^{ik(\Omega_1)\widehat{\mathbf{r}}\cdot\mathbf{r}_1} \\ &\quad +\frac{4\pi}{3}a^3k^2(\Omega_1)(\eta^{(1)}u(\mathbf{r}_2,\Omega_1)+6\eta^{(3)}u(\mathbf{r}_2,\Omega_4)u^*(\mathbf{r}_2,\Omega_3)u^*(\mathbf{r}_2,\Omega_2))e^{ik(\Omega_1)\widehat{\mathbf{r}}\cdot\mathbf{r}_2}\ , \end{aligned} \tag{2.197}$$

$$\begin{aligned} A(\mathbf{r},\Omega_2) &= \frac{4\pi}{3}a^3k^2(\Omega_2)(\eta^{(1)}u(\mathbf{r}_1,\Omega_2)+6\eta^{(3)}u(\mathbf{r}_1,\Omega_4)u^*(\mathbf{r}_1,\Omega_3)u^*(\mathbf{r}_1,\Omega_1))e^{ik(\Omega_2)\widehat{\mathbf{r}}\cdot\mathbf{r}_1} \\ &\quad +\frac{4\pi}{3}a^3k^2(\Omega_2)(\eta^{(1)}u(\mathbf{r}_2,\Omega_2)+6\eta^{(3)}u(\mathbf{r}_2,\Omega_4)u^*(\mathbf{r}_2,\Omega_3)u^*(\mathbf{r}_2,\Omega_1))e^{ik(\Omega_2)\widehat{\mathbf{r}}\cdot\mathbf{r}_2}\ , \end{aligned} \tag{2.198}$$

$$\begin{aligned} A(\mathbf{r},\Omega_3) &= \frac{4\pi}{3}a^3k^2(\Omega_3)(\eta^{(1)}u(\mathbf{r}_1,\Omega_3)+6\eta^{(3)}u(\mathbf{r}_1,\Omega_4)u^*(\mathbf{r}_1,\Omega_2)u^*(\mathbf{r}_1,\Omega_1))e^{ik(\Omega_3)\widehat{\mathbf{r}}\cdot\mathbf{r}_1} \\ &\quad +\frac{4\pi}{3}a^3k^2(\Omega_3)(\eta^{(1)}u(\mathbf{r}_2,\Omega_3)+6\eta^{(3)}u(\mathbf{r}_2,\Omega_4)u^*(\mathbf{r}_2,\Omega_2)u^*(\mathbf{r}_2,\Omega_1))e^{ik(\Omega_3)\widehat{\mathbf{r}}\cdot\mathbf{r}_2}\ , \end{aligned} \tag{2.199}$$

$$\begin{aligned} A(\mathbf{r},\Omega_4) &= \frac{4\pi}{3}a^3k^2(\Omega_4)(\eta^{(1)}u(\mathbf{r}_1,\Omega_4)+6\eta^{(3)}u(\mathbf{r}_1,\Omega_1)u(\mathbf{r}_1,\Omega_2)u(\mathbf{r}_1,\Omega_3))e^{ik(\Omega_4)\widehat{\mathbf{r}}\cdot\mathbf{r}_1} \\ &\quad +\frac{4\pi}{3}a^3k^2(\Omega_4)(\eta^{(1)}u(\mathbf{r}_2,\Omega_4)+6\eta^{(3)}u(\mathbf{r}_2,\Omega_1)u(\mathbf{r}_2,\Omega_2)u(\mathbf{r}_2,\Omega_3))e^{ik(\Omega_4)\widehat{\mathbf{r}}\cdot\mathbf{r}_2}\ . \end{aligned} \tag{2.200}$$

The local fields $u(\mathbf{r}_1,\Omega_1)$, $u(\mathbf{r}_1,\Omega_2)$, $u(\mathbf{r}_1,\Omega_3)$ and $u(\mathbf{r}_1,\Omega_4)$, $u(\mathbf{r}_2,\Omega_1)$, $u(\mathbf{r}_2,\Omega_2)$, $u(\mathbf{r}_2,\Omega_3)$ and $u(\mathbf{r}_2,\Omega_4)$ can be obtained by solving the equations perturbatively.

$$\begin{aligned} u(\mathbf{r}_1,\Omega_1) &= u_i(\mathbf{r}_1,\Omega_1) \\ &\quad +\frac{4\pi}{3}a^3k^2(\Omega_1)G_R(\Omega_1)(\eta^{(1)}u(\mathbf{r}_1,\Omega_1)+6\eta^{(3)}u(\mathbf{r}_1,\Omega_4)u^*(\mathbf{r}_1,\Omega_3)u^*(\mathbf{r}_1,\Omega_2)) \\ &\quad +\frac{4\pi}{3}a^3k^2(\Omega_1)G(\mathbf{r}_1,\mathbf{r}_2,\Omega_1)(\eta^{(1)}u(\mathbf{r}_2,\Omega_1)+6\eta^{(3)}u(\mathbf{r}_2,\Omega_4)u^*(\mathbf{r}_2,\Omega_3)u^*(\mathbf{r}_2,\Omega_2))\ , \end{aligned} \tag{2.201}$$

$$
\begin{aligned}
u(\mathbf{r}_1,\Omega_2) &= u_i(\mathbf{r}_1,\Omega_2) \\
&\quad +\frac{4\pi}{3}a^3k^2(\Omega_2)G_R(\Omega_2)(\eta^{(1)}u(\mathbf{r}_1,\Omega_2)+6\eta^{(3)}u(\mathbf{r}_1,\Omega_4)u^*(\mathbf{r}_1,\Omega_3)u^*(\mathbf{r}_1,\Omega_1)) \\
&\quad +\frac{4\pi}{3}a^3k^2(\Omega_2)G(\mathbf{r}_1,\mathbf{r}_2,\Omega_2)(\eta^{(1)}u(\mathbf{r}_2,\Omega_2)+6\eta^{(3)}u(\mathbf{r}_2,\Omega_4)u^*(\mathbf{r}_2,\Omega_3)u^*(\mathbf{r}_2,\Omega_1)) \ ,
\end{aligned}
\tag{2.202}
$$

$$
\begin{aligned}
u(\mathbf{r}_1,\Omega_3) &= u_i(\mathbf{r}_1,\Omega_3) \\
&\quad +\frac{4\pi}{3}a^3k^2(\Omega_3)G_R(\Omega_3)(\eta^{(1)}u(\mathbf{r}_1,\Omega_3)+6\eta^{(3)}u(\mathbf{r}_1,\Omega_4)u^*(\mathbf{r}_1,\Omega_2)u^*(\mathbf{r}_1,\Omega_1)) \\
&\quad +\frac{4\pi}{3}a^3k^2(\Omega_3)G(\mathbf{r}_1,\mathbf{r}_2,\Omega_3)(\eta^{(1)}u(\mathbf{r}_2,\Omega_3)+6\eta^{(3)}u(\mathbf{r}_2,\Omega_4)u^*(\mathbf{r}_2,\Omega_2)u^*(\mathbf{r}_2,\Omega_1)) \ ,
\end{aligned}
\tag{2.203}
$$

$$
\begin{aligned}
u(\mathbf{r}_1,\Omega_4) &= u_i(\mathbf{r}_1,\Omega_4) \\
&\quad +\frac{4\pi}{3}a^3k^2(\Omega_4)G_R(\Omega_4)(\eta^{(1)}u(\mathbf{r}_1,\Omega_4)+6\eta^{(3)}u(\mathbf{r}_1,\Omega_1)u(\mathbf{r}_1,\Omega_2)u(\mathbf{r}_1,\Omega_3)) \\
&\quad +\frac{4\pi}{3}a^3k^2(\Omega_4)G(\mathbf{r}_1,\mathbf{r}_2,\Omega_4)(\eta^{(1)}u(\mathbf{r}_2,\Omega_4)+6\eta^{(3)}u(\mathbf{r}_2,\Omega_1)u(\mathbf{r}_2,\Omega_2)u(\mathbf{r}_2,\Omega_3)) \ ,
\end{aligned}
\tag{2.204}
$$

$$
\begin{aligned}
u(\mathbf{r}_2,\Omega_1) &= u_i(\mathbf{r}_2,\Omega_1) \\
&\quad +\frac{4\pi}{3}a^3k^2(\Omega_1)G(\mathbf{r}_2,\mathbf{r}_1,\Omega_1)(\eta^{(1)}u(\mathbf{r}_1,\Omega_1)+6\eta^{(3)}u(\mathbf{r}_1,\Omega_4)u^*(\mathbf{r}_1,\Omega_3)u^*(\mathbf{r}_1,\Omega_2)) \\
&\quad +\frac{4\pi}{3}a^3k^2(\Omega_1)G_R(\Omega_1)(\eta^{(1)}u(\mathbf{r}_2,\Omega_1)+6\eta^{(3)}u(\mathbf{r}_2,\Omega_4)u^*(\mathbf{r}_2,\Omega_3)u^*(\mathbf{r}_2,\Omega_2)) \ ,
\end{aligned}
\tag{2.205}
$$

$$
\begin{aligned}
u(\mathbf{r}_2,\Omega_2) &= u_i(\mathbf{r}_2,\Omega_2) \\
&\quad +\frac{4\pi}{3}a^3k^2(\Omega_2)G(\mathbf{r}_2,\mathbf{r}_1,\Omega_2)(\eta^{(1)}u(\mathbf{r}_1,\Omega_2)+6\eta^{(3)}u(\mathbf{r}_1,\Omega_4)u^*(\mathbf{r}_1,\Omega_3)u^*(\mathbf{r}_1,\Omega_1)) \\
&\quad +\frac{4\pi}{3}a^3k^2(\Omega_2)G_R(\Omega_2)(\eta^{(1)}u(\mathbf{r}_2,\Omega_2)+6\eta^{(3)}u(\mathbf{r}_2,\Omega_4)u^*(\mathbf{r}_2,\Omega_3)u^*(\mathbf{r}_2,\Omega_1)) \ ,
\end{aligned}
\tag{2.206}
$$

$$
\begin{aligned}
u(\mathbf{r}_2,\Omega_3) &= u_i(\mathbf{r}_2,\Omega_3) \\
&\quad +\frac{4\pi}{3}a^3k^2(\Omega_3)G(\mathbf{r}_2,\mathbf{r}_1,\Omega_3)(\eta^{(1)}u(\mathbf{r}_1,\Omega_3)+6\eta^{(3)}u(\mathbf{r}_1,\Omega_4)u^*(\mathbf{r}_1,\Omega_2)u^*(\mathbf{r}_1,\Omega_1)) \\
&\quad +\frac{4\pi}{3}a^3k^2(\Omega_3)G_R(\Omega_3)(\eta^{(1)}u(\mathbf{r}_2,\Omega_3)+6\eta^{(3)}u(\mathbf{r}_2,\Omega_4)u^*(\mathbf{r}_2,\Omega_2)u^*(\mathbf{r}_2,\Omega_1)) \ ,
\end{aligned}
\tag{2.207}
$$

$$
\begin{aligned}
u(\mathbf{r}_2,\Omega_4) &= u_i(\mathbf{r}_2,\Omega_4) \\
&\quad +\frac{4\pi}{3}a^3k^2(\Omega_4)G(\mathbf{r}_2,\mathbf{r}_1,\Omega_4)(\eta^{(1)}u(\mathbf{r}_1,\Omega_4)+6\eta^{(3)}u(\mathbf{r}_1,\Omega_1)u(\mathbf{r}_1,\Omega_2)u(\mathbf{r}_1,\Omega_3)) \\
&\quad +\frac{4\pi}{3}a^3k^2(\Omega_4)G_R(\Omega_4)(\eta^{(1)}u(\mathbf{r}_2,\Omega_4)+6\eta^{(3)}u(\mathbf{r}_2,\Omega_1)u(\mathbf{r}_2,\Omega_2)u(\mathbf{r}_2,\Omega_3))
\end{aligned}
\tag{2.208}
$$

Chapter 3

Optical Theorem for Nonlinear Media

3.1 Introduction

The optical theorem is a basic result in scattering theory that is of both fundamental interest and considerable applied importance [62]. It can be formulated in a variety of settings, including quantum mechanics, acoustics and electromagnetic theory. In its simplest form, the optical theorem relates the power extinguished from a plane wave incident on a scattering medium to the scattering amplitude in the forward direction of scattering. For the case of electromagnetic scattering, the extinguished power P_e is given by

$$P_e = \frac{c}{2k_0} \mathrm{Im}\mathbf{A} \cdot \mathbf{E}_0^* \ , \tag{3.1}$$

where k_0 is the wavenumber, $\mathbf{E}_0$ is the incident field and $\mathbf{A}$ is the scattering amplitude in the forward direction [90, 45, 16]. In physical terms, the loss of power from the incident field is due to interference between the incident field and the scattered field within the volume of the scatterer.

The standard derivation of the optical theorem makes use of the ansatz that the scattered

field $\mathbf{E}_s$ behaves asymptotically as an outgoing spherical wave of the form

$$\mathbf{E}_s \sim \mathbf{A}\frac{e^{ik_0 r}}{r} , \quad k_0 r \to \infty , \tag{3.2}$$

where A is the scattering amplitude which depends on the direction of observation. The above ansatz may be justified for the case of material media in which the polarization is related to the electric field by a *linear* constitutive relation. Moreover, in this situation, the optical theorem may be derived without invoking the asymptotic behavior of the scattered field [21, 53].

The optical theorem is normally considered within the framework of linear optics [16]. However, the ansatz (3.2) is very general. That is, all properties of the scatterer are encoded in its scattering amplitude, which can, in principle, be arbitrarily prescribed. Thus, there is no reason to restrict the optical theorem to the linear response regime. Making use of this observation, in this chapter we consider the optical theorem in the context of nonlinear media. We derive an expression for the extinguished power that holds when the polarization is an arbitrary function of the electric field. To some extent, this result may be expected on physical grounds. However, we provide a proper mathematical justification following the approach of Refs. [21, 53]. We specialize our result to the cases of quadratic and cubic nonlinearities. We also study in detail the processes of second-harmonic generation and the Kerr effect for small scatterers. Our results on scattering from small nonlinear particles are of independent interest, since exact solutions to nonlinear scattering problems are, to the best of our knowledge, known only in one dimension [81, 17].

The remainder of this chapter is organized as follows. In Sec. 3.2, we present some basic results in nonlinear optics and scattering theory that will be used later in the paper. Sec. 3.3 presents the derivation of the optical theorem in the form we require, without the use of asymptotics. In Sec. 3.4, we consider separately the cases of second- and third-order

nonlinearities. Numerical results for small scatterers are presented in Sec. 3.5. Finally, in Sec. 3.6 we consider applications to apertureless scanning near-field optical microscopy in which the tip exhibits a nonlinear optical response. We investigate the cases of second- and third-harmonic generation and characterize the achievable resolution for a model system consisting of two scatterers. A discussion of our results is presented in Sec. 3.7.

3.2 Preliminaries

In this section we collect several results in nonlinear optics and scattering theory that will be useful in the derivation of the generalized optical theorem. We begin by recalling that the Maxwell equations in a source-free nonmagnetic medium are of the form

$$\nabla \cdot \mathbf{D} = 0 \,, \tag{3.3}$$

$$\nabla \times \mathbf{E} + \frac{1}{c}\frac{\partial \mathbf{B}}{\partial t} = 0 \,, \tag{3.4}$$

$$\nabla \cdot \mathbf{B} = 0 \,, \tag{3.5}$$

$$\nabla \times \mathbf{B} - \frac{1}{c}\frac{\partial \mathbf{D}}{\partial t} = 0 \,. \tag{3.6}$$

Here $\mathbf{E}$ is the electric field, $\mathbf{B}$ is the magnetic field, $\mathbf{D}$ is the electric displacement field and $\mathbf{P}$ is the polarization. In addition, $\mathbf{D}$ and $\mathbf{P}$ satisfy the relation

$$\mathbf{D} = \mathbf{E} + 4\pi\mathbf{P} \,. \tag{3.7}$$

Throughout this chapter, we will use the following Fourier transformation convention:

$$f(\mathbf{r},\omega) = \int f(\mathbf{r},t)e^{i\omega t}dt \,, \tag{3.8}$$

$$f(\mathbf{r},t) = \frac{1}{2\pi}\int f(\mathbf{r},\omega)e^{-i\omega t}d\omega \,, \tag{3.9}$$

where the time and frequency dependence of all quantities are displayed explicitly. We note that if $f(\mathbf{r},t)$ is real-valued, then $f(\mathbf{r},-\omega)=f^*(\mathbf{r},\omega)$. Upon Fourier transforming (3.3)–(3.6) we obtain

$$\nabla\cdot\mathbf{D}(\mathbf{r},\omega) = 0\ , \tag{3.10}$$

$$\nabla\times\mathbf{E}(\mathbf{r},\omega)-ik(\omega)\mathbf{B}(\mathbf{r},\omega) = 0\ , \tag{3.11}$$

$$\nabla\cdot\mathbf{B}(\mathbf{r},\omega) = 0\ , \tag{3.12}$$

$$\nabla\times\mathbf{B}(\mathbf{r},\omega)+ik(\omega)\mathbf{D}(\mathbf{r},\omega) = 0\ , \tag{3.13}$$

where $k(\omega)=\omega/c$. Throughout this chapter, we consider only monochromatic incident fields with an $e^{-i\omega t}$ time dependence.

If the medium is linear, the polarization is given by

$$P_i(\mathbf{r},\omega)=\chi^{(1)}_{ij}(\mathbf{r};\omega)E_j(\mathbf{r},\omega)\ , \tag{3.14}$$

where $\chi^{(1)}_{ij}$ is the first-order susceptibility. Here we have adopted the summation convention, whereby repeated indices are summed. For the case of quadratic nonlinear media,

$$P_i(\mathbf{r},\omega)=\chi^{(1)}_{ij}(\mathbf{r};\omega)E_j(\omega)+\sum_{\omega_1+\omega_2=\omega}\chi^{(2)}_{ijk}(\mathbf{r};\omega_1,\omega_2)E_j(\mathbf{r},\omega_1)E_k(\mathbf{r},\omega_2)\ , \tag{3.15}$$

where $\chi^{(2)}_{ijk}$ is the second-order susceptibility. The sum implies that the electric field at the frequencies ω_1 and ω_2 contributes to the polarization at the frequency ω if $\omega_1+\omega_2=\omega$. For cubic nonlinear media,

$$P_i(\mathbf{r},\omega)=\chi^{(1)}_{ij}(\mathbf{r};\omega)E_j(\omega)+\sum_{\omega_1+\omega_2+\omega_3=\omega}\chi^{(3)}_{ijkl}(\mathbf{r};\omega_1,\omega_2,\omega_3)E_j(\mathbf{r},\omega_1)E_k(\mathbf{r},\omega_2)E_l(\mathbf{r},\omega_3)\ , \tag{3.16}$$

where $\chi^{(3)}_{ijkl}(\mathbf{r};\omega_1,\omega_2,\omega_3)$ are the third-order susceptibilities.

We will assume that the susceptibilities have over all permutation symmetry. This assumption is quite standard and holds for nonresonance frequencies in the classical anharmonic oscillator model and in quantum optics [81, 17]. However, we note that over all permutation symmetry, also known as Kleinman symmetry [17], can be broken in a variety of systems [32, 94, 87, 80, 82, 25].

The wave equation for the electric field $\mathbf{E}(\mathbf{r},\omega)$ is obtained by taking the curl of (3.4) and eliminating the magnetic field $\mathbf{B}(\mathbf{r},\omega)$ using (3.6). We then have

$$\nabla \times \nabla \times \mathbf{E}(\mathbf{r},\omega) - k^2(\omega)\mathbf{E}(\mathbf{r},\omega) = 4\pi k^2(\omega)\mathbf{P}(\mathbf{r},\omega) \ . \tag{3.17}$$

The solution of the wave equation (3.17) is given by

$$E_i(\mathbf{r},\omega) = E_{\mathrm{inc},i}(\mathbf{r},\omega) + k^2(\omega)\int d^3r' G_{ij}(\mathbf{r},\mathbf{r}';\omega)P_j(\mathbf{r}',\omega) \ , \tag{3.18}$$

where $\mathbf{E}_{\mathrm{inc}}(\mathbf{r},\omega)$ obeys (3.17) with $P = 0$. The Green's function G_{ij} is of the form [84]

$$G_{ij}(\mathbf{r},\mathbf{r}';\omega) = \left(\delta_{ij} + \frac{1}{k^2(\omega)}\partial_i\partial_j\right) G(\mathbf{r},\mathbf{r}';\omega) \ , \tag{3.19}$$

where

$$G(\mathbf{r},\mathbf{r}';\omega) = \frac{e^{ik(\omega)|\mathbf{r}-\mathbf{r}'|}}{|\mathbf{r}-\mathbf{r}'|} \ . \tag{3.20}$$

Straightforward calculation shows that the Green's function has the following asymptotic form

$$G_{ij}(\mathbf{r},\mathbf{r}';\omega) \sim \frac{e^{ik(\omega)r}}{r}(\delta_{ij} - \widehat{r}_i\widehat{r}_j)e^{-ik(\omega)\widehat{\mathbf{r}}\cdot\mathbf{r}'} \ , \tag{3.21}$$

when $r \gg r'$. Using this result, we find that the scattered field behaves as an outgoing spherical wave of the form

$$E_{s,i}(\mathbf{r},\omega) \sim \frac{e^{ik(\omega)r}}{r} A_i(\widehat{\mathbf{r}},\omega) \ , \tag{3.22}$$

where the scattering amplitude is defined by

$$A_i(\widehat{\mathbf{r}},\omega) = k^2(\omega)(\delta_{ij} - \widehat{r}_i\widehat{r}_j) \int d^3r' P_j(\mathbf{r}',\omega) e^{ik(\omega)\widehat{\mathbf{r}}\cdot\mathbf{r}'} \ . \tag{3.23}$$

Following standard procedures, the conservation of energy follows immediately from (3.17) and takes the form

$$\nabla \cdot \mathbf{S}(\mathbf{r},\omega) = \frac{ck(\omega)}{2\pi^2} \mathrm{Im}(\mathbf{E}^*(\mathbf{r},\omega) \cdot \mathbf{P}(\mathbf{r},\omega)) \ , \tag{3.24}$$

where the Poynting vector $\mathbf{S}$ is defined by

$$\mathbf{S}(\mathbf{r},\omega) = \frac{c}{8\pi^3} \mathrm{Re}(\mathbf{E}(\mathbf{r},\omega) \times \mathbf{B}^*(\mathbf{r},\omega)) \ . \tag{3.25}$$

We recall that the time-dependent Poynting vector is defined as

$$\mathbf{S}(\mathbf{r},t) = \frac{c}{4\pi} \mathbf{E}(\mathbf{r},t) \times \mathbf{B}(\mathbf{r},t) \ . \tag{3.26}$$

Note that by an abuse of notation, $\mathbf{S}(\mathbf{r},\omega)$ is not the Fourier transform of $\mathbf{S}(\mathbf{r},t)$.

For time-harmonic fields, the time average of the Poynting vector

$$\overline{\mathbf{S}} = \lim_{T\to\infty} \frac{1}{T} \int_0^T \mathbf{S}(\mathbf{r},t) dt \tag{3.27}$$

is well defined. It follows that

$$\overline{\mathbf{S}} = \sum_{\omega} \mathbf{S}(\mathbf{r}, \omega) \ . \tag{3.28}$$

We note that for nondispersive media, the analog of the Manley-Rowe relations can be shown to hold. That is, if the susceptibilities $\chi^{(1)}_{ij}$, $\chi^{(2)}_{ijk}$ and $\chi^{(3)}_{ijkl}$ are purely real, then $\nabla \cdot \overline{\mathbf{S}} = 0$. The proof is given in Appendix A.

3.3 Optical theorem

In this section we derive the optical theorem for nonlinear media following the approach of [21, 53]. We begin by recalling some basic facts from scattering theory [16]. We consider a general nonlinear medium, whose polarization is defined by either a quadratic or cubic nonlinearity. We suppose that a field $\mathbf{E}_{\text{inc}}$ is incident upon the medium and write the total electric field as the sum

$$\mathbf{E} = \mathbf{E}_{\text{inc}} + \mathbf{E}_s \ , \tag{3.29}$$

where $\mathbf{E}_s$ is the scattered field. It follows from (3.17) that $\mathbf{E}_s$ obeys

$$\nabla \times \nabla \times \mathbf{E}_s(\mathbf{r}, \omega) - k^2(\omega)\mathbf{E}_s(\mathbf{r}, \omega) = 4\pi k^2(\omega)\mathbf{P}(\mathbf{r}, \omega) \ . \tag{3.30}$$

The energy carried by the scattered field is associated with the Poynting vector $\mathbf{S}_s$, which is defined by

$$\mathbf{S}_s(\omega) = \frac{c}{8\pi^3}\text{Re}(\mathbf{E}_s(\omega) \times \mathbf{B}^*_s(\omega)) \ . \tag{3.31}$$

Evidently, $\mathbf{S}_s$ obeys the conservation law

$$\nabla \cdot \mathbf{S}_s(\mathbf{r},\omega) = \frac{ck(\omega)}{2\pi^2}\mathrm{Im}(\mathbf{E}_s^*(\mathbf{r},\omega)\cdot\mathbf{P}(\mathbf{r},\omega)) \ , \tag{3.32}$$

which is a consequence of (3.30).

Suppose that the scattering medium is contained in a volume V. Then the power absorbed by the medium is given by

$$P_a(\omega) = -\int_{\partial V} \mathbf{S}(\mathbf{r},\omega)\cdot\widehat{\mathbf{n}}d^2r \ , \tag{3.33}$$

where $\widehat{\mathbf{n}}$ is the outward unit normal to ∂V and the presence of the overall minus sign signifies that this is the flux of the Poynting vector of the wave traveling into the medium. Converting the above surface integral to a volume integral by means of the divergence theorem and making use of (3.24), we have

$$P_a(\omega) = \frac{ck(\omega)}{2\pi^2}\int_V \mathrm{Im}(\mathbf{E}^*(\mathbf{r}',\omega)\cdot\mathbf{P}(\mathbf{r}',\omega))d^3r' \ . \tag{3.34}$$

In a strictly similar manner, we define the scattered power as

$$P_s(\omega) = \int_{\partial V} \mathbf{S}_s(\mathbf{r}',\omega)\cdot\widehat{\mathbf{n}}d^2r' \ . \tag{3.35}$$

We then obtain from (3.32) that

$$P_s(\omega) = -\frac{ck(\omega)}{2\pi^2}\int_V \mathrm{Im}(\mathbf{E}_s^*(\mathbf{r}',\omega)\cdot\mathbf{P}(\mathbf{r}',\omega))d^3r' \ . \tag{3.36}$$

We define the extinguished power P_e to be the total power lost from the incident field due

to absorption and scattering:

$$P_e(\omega) = P_a(\omega) + P_s(\omega) \ . \tag{3.37}$$

It follows from (3.34) and (3.36) that the extinguished power is given by

$$P_e(\omega) = \frac{ck(\omega)}{2\pi^2} \int_V \mathrm{Im}(\mathbf{E}^*_{\mathrm{inc}}(\mathbf{r}', \omega) \cdot \mathbf{P}(\mathbf{r}', \omega)) d^3r' \ . \tag{3.38}$$

We note that if either Eqs. (3.15) or (3.16) for the polarization is inserted into the above expression, we see that the power extinguished from the incident field is due to interference between the incident field and the total field within the volume of the scatterer.

We can now rewrite (3.38) in terms of the scattering amplitude, provided that the incident field is a plane wave of the form

$$\mathbf{E}_{\mathrm{inc}}(\mathbf{r}, \omega) = \mathbf{E}_0(\omega) e^{ik(\omega)\widehat{\mathbf{s}} \cdot \mathbf{r}} \ , \tag{3.39}$$

where $\widehat{\mathbf{s}}$ is the direction of propagation. Upon comparing (3.38) and (3.23), we obtain the optical theorem

$$P_e(\omega) = \frac{c}{2\pi^2 k(\omega)} \mathrm{Im}\mathbf{A}(\widehat{\mathbf{s}}, \omega) \cdot \mathbf{E}^*_0(\omega) \ . \tag{3.40}$$

Using this result, we see that the time-averaged extinguished power is given by

$$\overline{P}_e = \sum_{\omega > 0} P_e(\omega) = \frac{c}{2\pi^2} \sum_{\omega > 0} \frac{1}{k(\omega)} \mathrm{Im}\mathbf{A}(\widehat{\mathbf{s}}, \omega) \cdot \mathbf{E}^*_0(\omega) \ . \tag{3.41}$$

We note that the optical theorem (3.40) applies to both linear and nonlinear media. In Sec. 3.4, we specialize this result to the cases of quadratic and cubic nonlinearities. Here

we remark that in the case of a linear medium with an incident monochromatic field of the form

$$\mathbf{E}_{\rm inc}(\mathbf{r},\omega) = e^{ik(\omega)\widehat{\mathbf{s}}\cdot\mathbf{r}}(\mathbf{E}_0\delta(\omega-\Omega)+\mathbf{E}_0^*\delta(\omega+\Omega)) \ , \tag{3.42}$$

(3.41) becomes

$$\overline{P}_e = \frac{c}{2\pi^2 k(\Omega)}{\rm Im}\mathbf{A}(\widehat{\mathbf{s}},\Omega)\cdot\mathbf{E}_0^* \ . \tag{3.43}$$

We have thus recovered the familiar form of the optical theorem (3.1). Finally, we note that (3.40) is an *exact* result. That is, it has not been derived by making use of the asymptotic behavior of the electric field.

3.4 Second- and third-order nonlinearities

Evidently, in order to apply the optical theorem (3.41) it is necessary to first obtain the scattering amplitude. In this section we calculate the scattering amplitude for second- and third-order nonlinearities. We begin with the case of second-order nonlinearity and, for simplicity, discuss only the problem of second-harmonic generation (SHG). In this setting, we analyze the scattering of an incident monochromatic wave from a spherical particle whose size is small compared to the wavelength. Next, we turn our attention to the case of third-order nonlinearity, where we restrict our attention to the Kerr effect. Once again, we calculate the extinguished power for a small particle and study the associated resonant scattering.

We note that the method we develop for calculating the scattering of light from a small nonlinear inhomogeneity may be of independent interest. In particular, it is readily extended to collections of small inhomogeneities, which is a physical setting that arises in applications to biomedical imaging and nonlinear microscopy [91, 85, 95, 96, 41, 67, 68]. We plan to report the results of such calculations elsewhere.

3.4.1 Second-order nonlinearity

We consider SHG excited by a monochromatic incident field of frequency Ω. We assume that the second-order susceptibility is sufficiently weak so that the condition

$$\sum_{\omega_1+\omega_2=\omega} \chi^{(2)}_{ijk}(\mathbf{r};\omega_1,\omega_2)E_j(\mathbf{r},\omega_1)E_k(\mathbf{r},\omega_2) \ll \chi^{(1)}_{ij}(\mathbf{r};\omega)E_j(\omega) \tag{3.44}$$

is obeyed. We then find that the wave equation (3.17) together with (3.15) and the permutation symmetry of $\chi^{(2)}_{ijk}$ gives rise to the pair of coupled wave equations

$$\begin{aligned} \nabla\times\nabla\times\mathbf{E}(\mathbf{r},\Omega) &- k^2(\Omega)\mathbf{E}(\mathbf{r},\Omega) = 4\pi k^2(\Omega)(\chi^{(1)}_{ij}(\mathbf{r},\Omega)E_j(\mathbf{r},\Omega) \\ &+ 2\chi^{(2)}_{ijk}(\mathbf{r},2\Omega,-\Omega)E_j(\mathbf{r},2\Omega)E^*_k(\mathbf{r},\Omega))\ , \qquad (3.45) \\ \nabla\times\nabla\times\mathbf{E}(\mathbf{r},2\Omega) &- k^2(2\Omega)\mathbf{E}(\mathbf{r},2\Omega) = 4\pi k^2(2\Omega)(\chi^{(1)}_{ij}(\mathbf{r},2\Omega)E_j(\mathbf{r},2\Omega) \\ &+ \chi^{(2)}_{ijk}(\mathbf{r},\Omega,\Omega)E_j(\mathbf{r},\Omega)E_k(\mathbf{r},\Omega))\ , \qquad (3.46) \end{aligned}$$

for the electric fields at the frequencies Ω and 2Ω. Note that we have not accounted for the formation of higher harmonics, consistent with the condition (3.44).

It follows immediately from (3.18) that the solutions to (3.45) and (3.46) are given by

$$\begin{aligned} E_i(\mathbf{r},\Omega) &= E_{\mathrm{inc},i}(\mathbf{r},\Omega) + k^2(\Omega)\int d^3r'\chi^{(1)}_{jk}(\mathbf{r}',\Omega)G_{ij}(\mathbf{r},\mathbf{r}';\Omega)E_k(\mathbf{r}',\Omega) \\ &+ 2k^2(\Omega)\int d^3r'\chi^{(2)}_{jkl}(\mathbf{r}',2\Omega,-\Omega)G_{ij}(\mathbf{r},\mathbf{r}';\Omega)E_k(\mathbf{r}',2\Omega)E^*_l(\mathbf{r}',\Omega)\ , \qquad (3.47) \\ E_i(\mathbf{r},2\Omega) &= k^2(2\Omega)\int d^3r'\chi^{(1)}_{jk}(\mathbf{r}',2\Omega)G_{ij}(\mathbf{r},\mathbf{r}';2\Omega)E_k(\mathbf{r}',2\Omega) \\ &+ k^2(2\Omega)\int d^3r'\chi^{(2)}_{jkl}(\mathbf{r}',\Omega,\Omega)G_{ij}(\mathbf{r},\mathbf{r}';2\Omega)E_k(\mathbf{r}',\Omega)E_l(\mathbf{r}',\Omega)\ . \qquad (3.48) \end{aligned}$$

Suppose that the scattering medium is a small ball of radius a with $k(\Omega)a \ll 1$ and $k(2\Omega)a \ll 1$. The susceptibilities are taken to be $\chi^{(1)}_{ij}(\mathbf{r};\omega) = \eta^{(1)}_{ij}$ and $\chi^{(2)}_{ijk}(\mathbf{r};\omega) = \eta^{(2)}_{ijk}$ for

$|\mathbf{r}| \leq a$ and to vanish for $|\mathbf{r}| > a$. Equations (3.47) and (3.48) thus become

$$\begin{aligned} E_i(\mathbf{r},\Omega) &= E_{\mathrm{inc},i}(\mathbf{r},\Omega) + k^2(\Omega)\eta^{(1)}_{jk}\int_{|\mathbf{r}'|\leq a} d^3r' G_{ij}(\mathbf{r},\mathbf{r}';\Omega)E_k(\mathbf{r}',\Omega) \\ &+ 2k^2(\Omega)\eta^{(2)}_{jkl}\int_{|\mathbf{r}'|\leq a} d^3r' G_{ij}(\mathbf{r},\mathbf{r}';\Omega)E_k(\mathbf{r}',2\Omega)E^*_l(\mathbf{r}',\Omega)\ , \qquad (3.49) \\ E_i(\mathbf{r},2\Omega) &= k^2(2\Omega)\eta^{(1)}_{jk}\int_{|\mathbf{r}'|\leq a} d^3r' G_{ij}(\mathbf{r},\mathbf{r}';2\Omega)E_k(\mathbf{r}',2\Omega) \\ &+ k^2(2\Omega)\eta^{(2)}_{jkl}\int_{|\mathbf{r}'|\leq a} d^3r' G_{ij}(\mathbf{r},\mathbf{r}';2\Omega)E_k(\mathbf{r}',\Omega)E_l(\mathbf{r}',\Omega)\ . \qquad (3.50) \end{aligned}$$

Using the asymptotic form of the Green's function given in (3.21), we find that the scattered fields are of the form

$$\begin{aligned} E^s_i(\mathbf{r},\Omega) &= A_i(\mathbf{r},\Omega)\frac{e^{ik(\Omega)r}}{r}\ , \qquad (3.51) \\ E_i(\mathbf{r},2\Omega) &= A_i(\mathbf{r},2\Omega)\frac{e^{ik(2\Omega)r}}{r}\ , \qquad (3.52) \end{aligned}$$

where the scattering amplitudes are defined by

$$\begin{aligned} A_i(\mathbf{r},\Omega) &= \frac{4\pi}{3}a^3(\delta_{ij}-\widehat{r}_i\widehat{r}_j)k^2(\Omega)(\eta^{(1)}_{jk}E_k(\mathbf{0},\Omega)+2\eta^{(2)}_{jkl}E_k(\mathbf{0},2\Omega)E^*_l(\mathbf{0},\Omega))\ , \qquad (3.53) \\ A_i(\mathbf{r},2\Omega) &= \frac{4\pi}{3}a^3(\delta_{ij}-\widehat{r}_i\widehat{r}_j)k^2(2\Omega)(\eta^{(1)}_{jk}E_j(\mathbf{0},2\Omega)+\eta^{(2)}_{jkl}E_k(\mathbf{0},\Omega)E_l(\mathbf{0},\Omega))\ . \qquad (3.54) \end{aligned}$$

Here we have used the fact that the radius of the scatterer is small, which leads to the identity

$$\int_{|\mathbf{r}'|\leq a} d^3r' e^{-ik(\omega)\widehat{\mathbf{r}}\cdot\mathbf{r}'}g(k(\omega)\mathbf{r}') = \frac{4\pi}{3}a^3 g(\mathbf{0})(1+O(k(\omega)a))\ , \qquad (3.55)$$

for some function g. The local fields $E_i(\mathbf{0},\Omega)$ and $E_i(\mathbf{0},2\Omega)$ can be calculated perturbatively as shown in Appendix 3.B.1.

3.4.2 Third-order nonlinearity

The treatment of the Kerr effect parallels that of SHG. We consider the Kerr effect excited by a monochromatic incident field of frequency Ω. We assume that the third-order susceptibility is sufficiently weak so that the condition

$$\sum_{\omega_1+\omega_2+\omega_3=\omega} \chi^{(3)}_{ijkl}(\mathbf{r};\omega_1,\omega_2)E_j(\mathbf{r},\omega_1)E_k(\mathbf{r},\omega_2)E_l(\mathbf{r},\omega_3) \ll \chi^{(1)}_{ij}(\mathbf{r};\omega)E_j(\omega) \tag{3.56}$$

is obeyed. We then find that (3.17) together with (3.16) and the permutation symmetry of $\chi^{(3)}_{ijkl}$ gives rise to the wave equation

$$\begin{aligned} \nabla\times\nabla\times\mathbf{E}(\mathbf{r},\Omega) &- k^2(\Omega)\mathbf{E}(\mathbf{r},\Omega) = 4\pi k^2(\Omega)(\chi^{(1)}_{ij}(\mathbf{r},\Omega)E_j(\mathbf{r},\Omega) \\ &+ 3\chi^{(3)}_{ijkl}(\mathbf{r},\Omega,\Omega,-\Omega)E_j(\mathbf{r},\Omega)E_k(\mathbf{r},\Omega)E^*_l(\mathbf{r},\Omega)) \ . \end{aligned} \tag{3.57}$$

Note that we have not accounted for the formation of higher harmonics, consistent with the condition (3.56). It follows immediately from (3.18) that the solution to (3.57) is given by

$$\begin{aligned} E_i(\mathbf{r},\Omega) = E_{\mathrm{inc},i}(\mathbf{r},\Omega) + k^2(\Omega)\int d^3r'\chi^{(1)}_{jk}(\mathbf{r}',\Omega)G_{ij}(\mathbf{r},\mathbf{r}';\Omega)E_k(\mathbf{r}',\Omega) \\ +3k^2(\Omega)\int d^3r'\chi^{(3)}_{jklm}(\mathbf{r}',\Omega,\Omega,-\Omega)G_{ij}(\mathbf{r},\mathbf{r}';\Omega)E_k(\mathbf{r}',\Omega)E_l(\mathbf{r}',\Omega)E^*_m(\mathbf{r}',\Omega) \ . \end{aligned} \tag{3.58}$$

Suppose that the scattering medium is a small ball of radius a with $k(\Omega)a \ll 1$. The susceptibilities are taken to be $\chi^{(1)}_{ij}(\mathbf{r};\omega) = \eta^{(1)}_{ij}$ and $\chi^{(3)}_{ijkl}(\mathbf{r};\omega) = \eta^{(3)}_{ijkl}$ for $|\mathbf{r}| \le a$ and to vanish for $|\mathbf{r}| > a$. Equation (3.58) thus become

$$\begin{aligned} E_i(\mathbf{r},\Omega) &= E_{\mathrm{inc},i}(\mathbf{r},\Omega) + k^2(\Omega)\eta^{(1)}_{jk}\int_{|\mathbf{r}'|\le a} d^3r'G_{ij}(\mathbf{r},\mathbf{r}';\Omega)E_k(\mathbf{r}',\Omega) \\ &+ 3k^2(\Omega)\eta^{(3)}_{jklm}\int_{|\mathbf{r}'|\le a} d^3r'G_{ij}(\mathbf{r},\mathbf{r}';\Omega)E_k(\mathbf{r}',\Omega)E_l(\mathbf{r}',\Omega)E^*_m(\mathbf{r}',\Omega)) \ . \end{aligned} \tag{3.59}$$

Using the asymptotic form of the Green's function given in (3.21), we find that the scattered field is of the form

$$E_i^s(\mathbf{r},\Omega) \;=\; A_i(\mathbf{r},\Omega)\frac{e^{ik(\Omega)r}}{r}\ . \tag{3.60}$$

where the scattering amplitude is defined by

$$A_i(\mathbf{r},\Omega) \;=\; \frac{4\pi}{3}a^3(\delta_{ij}-\widehat{r}_i\widehat{r}_j)k^2(\Omega)(\eta^{(1)}_{jk}E_k(\mathbf{0},\Omega)+3\eta^{(3)}_{jklm}E_k(\mathbf{0},\Omega)E_l(\mathbf{0},\Omega)E^*_m(\mathbf{0},\Omega))\ . \tag{3.61}$$

Once again, we calculate the local fields $E_i(\mathbf{0},\Omega)$ perturbatively, as shown in Appendix 3.B.2.

3.5 Numerical results

In this section we apply the optical theorem (3.41) to linear, second- and third-order nonlinear media. We present numerical results for several cases of interest, including second-harmonic generation and the Kerr effect. We will see that the effect of the nonlinearities is to modify the linear scattering resonance of small scatterers.

3.5.1 Linear response

We consider an isotropic medium with $\eta^{(1)}_{ij}=\eta^{(1)}\delta_{ij}$ and assume that all the higher-order susceptibilities vanish. The incident field is taken to be a unit-amplitude plane wave of the form $\mathbf{E}_{\rm inc}=\mathbf{E}_0\exp(ik_0\widehat{\mathbf{s}}\cdot\mathbf{r})$ with $\mathbf{E}_0=E_0\widehat{\mathbf{x}}$ and $\widehat{\mathbf{s}}=\widehat{\mathbf{z}}$. Using (98) and (91), the extinguished power becomes

$$P_e=\frac{8\Omega}{3}E_0^2a^3{\rm Im}\left(\frac{\eta^{(1)}}{1-\frac{4\pi}{3}k^2a^3\eta^{(1)}G_R}\right)\ . \tag{3.62}$$

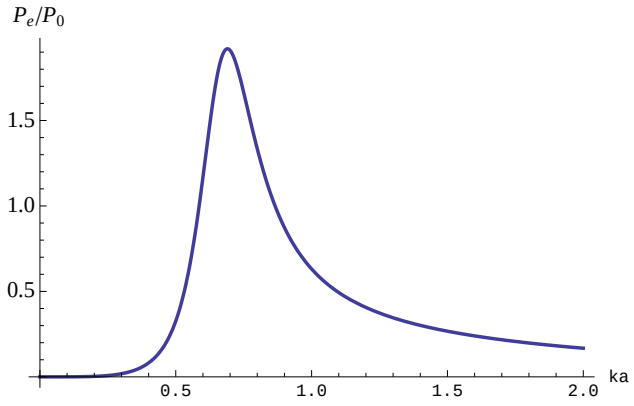

Figure 3.1: Frequency dependence of extinguished power for a single linear scatterer. Here $P_0 = a^2 c E_0^2$.

We can write the above formula in a more familiar form in terms of the renormalized polarizability α, which is defined as

$$\alpha = \frac{\alpha_0}{1 - k^2 \alpha_0 \left[1/a + i\frac{2}{3}k\right]} \ , \tag{3.63}$$

where α_0 is the zero-frequency polarizability, which is defined in terms of the linear dielectric permittivity $\epsilon^{(1)}$. Here

$$\alpha_0 = \frac{\epsilon^{(1)} - 1}{\epsilon^{(1)} + 2} a^3 \ , \tag{3.64}$$

where $\epsilon^{(1)} = 1 + 4\pi\eta^{(1)}$. We find that (3.62) becomes

$$P_e = \frac{2\Omega}{\pi} E_0^2 \mathrm{Im}\alpha \ . \tag{3.65}$$

In Figure 1 we illustrate the frequency dependence of the extinguished power for a dielectric scatterer of size $a = 100$nm with $\epsilon^{(1)} = -5.28$. We see that there is a scattering resonance at $ka \approx 0.7$.

3.5.2 Second-harmonic generation

We consider the case of a medium with isotropic $\eta^{(1)}$ and $\eta^{(2)}$ obeying permutation symmetry. That is, $\eta^{(1)}_{ij} = \eta^{(1)}\delta_{ij}$ and $\eta^{(2)}_{111} = \eta^{(2)}$, with the other $\eta^{(2)}_{ijk}$ vanishing. We also assume that the incident field $\mathbf{E}_{\rm inc}$ points in the x direction and the direction of observation $\widehat{\mathbf{s}}$ is taken to be in the z direction. It follows from (3.91) that the extinguished power P_e is given by

$$P_e = \frac{8\Omega}{3}a^3 \mathrm{Im}\left((\eta^{(1)}E_1^{(0)}(\mathbf{0},\Omega) + \eta^{(1)}E_1^{(2)}(\mathbf{0},\Omega) + 2\eta^{(2)}_{111}(E_1^{(0)}(\mathbf{0},\Omega))^* E_1^{(1)}(\mathbf{0},2\Omega))E^*_{\mathrm{inc},1}(\mathbf{0},\Omega)\right) . \tag{3.66}$$

In Figure 2 we illustrate the frequency dependence of the extinguished power for SHG. The scatterer size is $a = 100$nm and E_0 is taken to have unit amplitude. Plots are shown for $\epsilon = \eta^{(2)}E_0/\eta^{(1)} = 0, 0.1, 0.2, 0.3$. We see that the resonance shifts to lower frequencies and its amplitude increases by more than a factor of two relative to the linear case. The physical situation considered corresponds to the material β-BaB_2O_4 [17]. We note that there does not appear to be a simple physical argument to predict the extent or direction of the reported frequency shifts.

3.5.3 Kerr effect

We consider the case of a medium with isotropic $\eta^{(1)}$ and $\eta^{(3)}$ obeying the permutation symmetry. That is, $\eta^{(1)}_{ij} = \eta^{(1)}\delta_{ij}$ and $\eta^{(3)}_{1111} = \eta^{(3)}$, with all other $\eta^{(3)}_{ijkl}$ vanishing. We also assume that the incident field $\mathbf{E}_{\rm inc}$ points in the x direction and the direction of observation $\widehat{\mathbf{s}}$ is taken to be in the z direction. It follows from (3.103) that the extinguished power P_e is

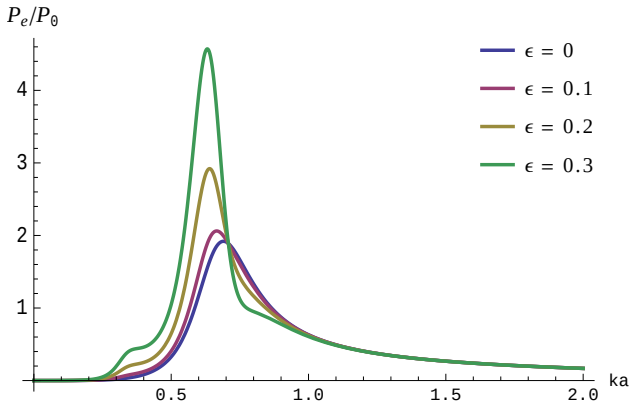

Figure 3.2: Frequency dependence of extinguished power for a single nonlinear scatterer with SHG. Here $P_0 = a^2 c E_0^2$.

given by

$$P_e = \frac{8\Omega}{3} a^3 \mathrm{Im}\Big((\eta^{(1)} E_1^{(0)}(\mathbf{0},\Omega) + \eta^{(1)} E_1^{(1)}(\mathbf{0},\Omega) \\ +3\eta^{(3)}_{1111} (E^*)_1^{(0)}(\mathbf{0},\Omega)(E)_1^{(0)}(\mathbf{0},\Omega)(E)_1^{(0)}(\mathbf{0},\Omega)) E^*_{\mathrm{inc},i}(\mathbf{0},\Omega) \Big) \ . \tag{3.67}$$

In Figure 3 we illustrate the frequency dependence of the extinguished power for the Kerr effect. The scatterer size is $a = 100$nm and E_0 is taken to have unit amplitude. Plots are shown for $\epsilon = \eta^{(3)} E_0^2/\eta^{(1)} = 0, 0.01, 0.02$. We see that the resonance shifts to higher frequencies relative to the linear case. As may be expected, the effect is less pronounced than in the case of SHG. As above, we do not know of a simple physical argument to predict the extent or direction of the reported frequency shifts.

3.6 Application to near-field microscopy

Near-field scanning optical microscopy (NSOM) is a widely used experimental tool to overcome the diffraction limit of optical microscopy [64]. In a typical experiment, an apertured

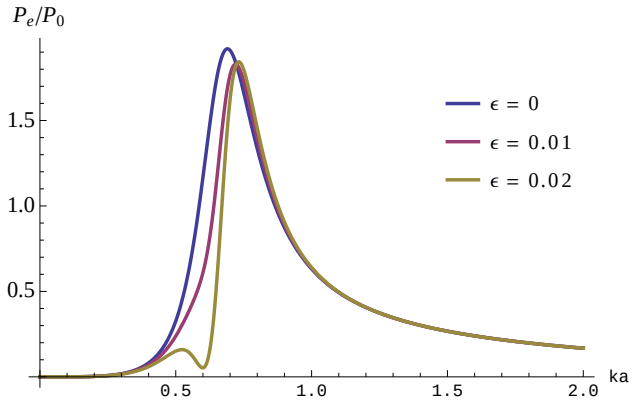

Figure 3.3: Frequency dependence of extinguished power for a single scatterer with Kerr nonlinearity. Here $P_0 = a^2 c E_0^2$.

probe (often a metallic coated optical fiber) is brought into the near-field of a sample and employed as an optical source. The image is formed by scanning the probe and recording the intensity of light scattered into the far-field. In a reciprocal arrangement, the probe may be used as a detector with the illumination incident from the far-field. In either case, the resolution of the resulting image is controlled by the size of the probe rather than the wavelength of light.

Apertureless NSOM is an alternative to the above approach in which the illumination and detection both take place in the far-field [64, 46]. The experimental setup is illustrated in Figure 3.4, in which an incident field illuminates a metallic tip that is placed in the near-field of the sample. The image is obtained by scanning the tip and measuring the scattered field with a detector that is placed in the far-field of the sample and the tip.

A refinement of apertureless NSOM is to introduce a fluorescent tip, which allows for the spectral isolation of the detected light and improvement in signal to noise ratio (SNR) by background suppression [51]. Spectral isolation may also be achieved by utilizing a tip that has a nonlinear optical response [91, 85, 95, 96, 41, 67, 68]. This approach has the advantage that it is not affected by fluorescent photobleaching. Experiments in which SHG, THG and four-wave mixing have been utilized for aptertureless NSOM in a dark-field configuration

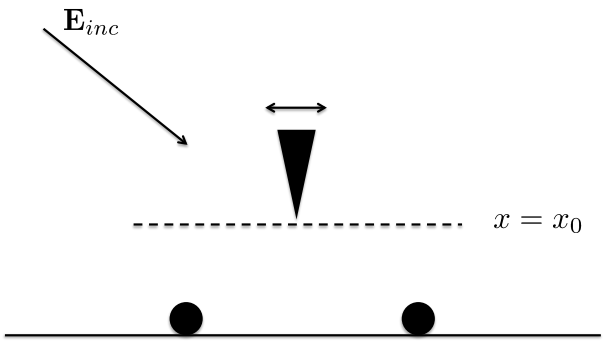

Figure 3.4: Illustrating the apertureless NSOM experiment.

have recently been reported [41].

In this section we develop a model for SHG and THG apertureless NSOM. We consider a system in which a nonlinear metallic tip is placed in the near-field of a pair of small dielectric particles, which are taken to have only a linear optical response. The setup is shown in Fig. 3.4 and the mathematical details are presented in Appendix C. We begin with the case of SHG. Denote the wavelength of the incident field by λ. The sample consists of a pair of dielectric spheres of radius $\lambda/(10\pi)$ and susceptibility $\widehat{\eta}^{(1)}_{ij} = 0.4\delta_{ij}$, located at the positions $\mathbf{r}_1 = (0, \frac{3\lambda}{20\pi}, 0)$ and $\mathbf{r}_2 = (0, -\frac{3\lambda}{20\pi}, 0)$, which corresponds to a separation of $\approx \lambda/10$. The tip has radius $a = \lambda/(10\pi)$, linear susceptibility $\eta^{(1)} = -0.4$, second-order susceptibility $\eta^{(2)}_{111}$ with $\eta^{(2)}_{111}E_0/\widehat{\eta}^{(1)} = 0.2$ and all other $\eta^{(2)}_{ijkl}$ vanishing, and is scanned in the planes $x = x_0$. In all numerical experiments, the incident electric field is a plane wave polarized in the x direction with wave vector $k(\Omega)\widehat{\mathbf{z}}$. In Fig. 3.5 images of the extinguished power are shown in three different scan planes corresponding to $x_0 = 2a$, $2.5a$ and $3a$. We see that the scatterers are well resolved with subwavelength separation in the closest scan plane and that the resolution degrades rapidly with distance from the plane $x = 0$. Qualitatively similar results are found for the intensity of scattered second-harmonic light, as illustrated in Fig. 3.7.

(a) $x_0 = \lambda/(5\pi)$ (b) $x_0 = \lambda/(4\pi)$ (c) $x_0 = 3\lambda/(10\pi)$

Figure 3.5: Apertureless NSOM images of the extinguished power P_e for SHG. The susceptibility of the tip is $\eta^{(2)}_{111}E_0/\widehat{\eta}^{(1)} = 0.2$. Images are shown in the planes $x = x_0$ as indicated. The field of view of each image is $3\lambda/(5\pi) \times 3\lambda/(5\pi)$. A linear scale is used in the colormap.

Next we consider the case of THG. The setup is the same as in the case of SHG, except that the third-order susceptibility of the tip is $\eta^{(3)}_{1111}$, with $\eta^{(3)}_{1111}E_0^2/\widehat{\eta}^{(1)} = 0.2$ and all other $\eta^{(3)}_{ijkl}$ vanishing. Once again, we find that the scatterers are better resolved in the closest scan plane. We also note that the relative extinguished power is smaller than in the case of SHG and that the intensity of the scattered third-harmonic is correspondingly greater. See Figs. 3.6 and 3.8. In Fig. 3.9 the extinguished power along a line in the closest scan plan is compared for SHG and THG. It is found that the the extinguished power for the case of a SHG tip is an order of magnitude larger than for a tip exhibiting THG. The corresponding result for the scattering amplitude is shown in Fig. 3.10.

3.7 Discussion

In this chapter we have presented a generalization of the optical theorem for the scattering of nonlinear electromagnetic waves. We consider in some detail the most important examples of quadratic and cubic nonlinearities. The theory is illustrated for the case of small inhomogeneities in the settings of second-harmonic generation and the Kerr effect. In par-

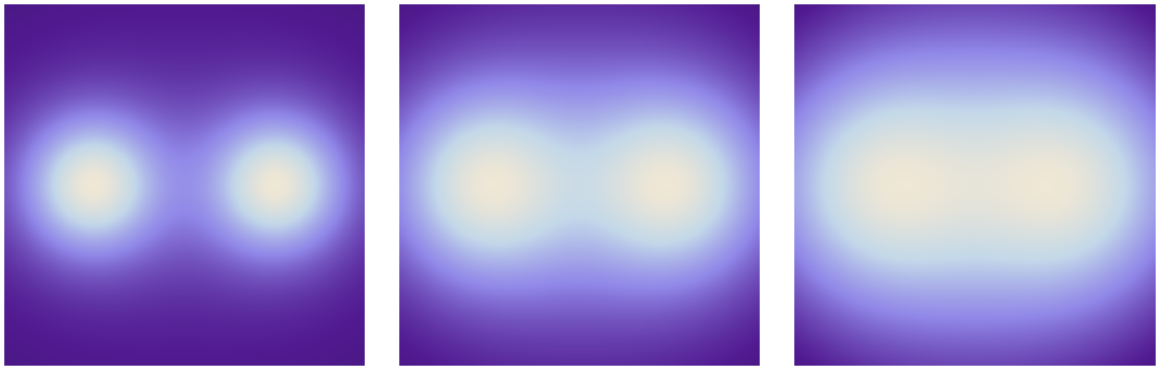

(a) $x_0 = \lambda/(5\pi)$ (b) $x_0 = \lambda/(4\pi)$ (c) $x_0 = 3\lambda/(10\pi)$

Figure 3.6: Apertureless NSOM images of the extinguished power P_e for THG. The susceptibility of the tip is $\eta^{(3)}_{1111} E_0/\widehat{\eta}^{(1)} = 0.2$. Images are shown in the planes $x = x_0$ as indicated. The field of view of each image is $3\lambda/(5\pi) \times 3\lambda/(5\pi)$. A linear scale is used in the colormap.

(a) $x_0 = \lambda/(5\pi)$ (b) $x_0 = \lambda/(4\pi)$ (c) $x_0 = 3\lambda/(10\pi)$

Figure 3.7: Apertureless NSOM images of the far-field intensity at frequency 2Ω in SHG. The susceptibility of the tip is $\eta^{(2)}_{111} E_0/\widehat{\eta}^{(1)} = 0.2$. Images are shown in the planes $x = x_0$ as indicated. The field of view of each image is $3\lambda/(5\pi) \times 3\lambda/(5\pi)$. A linear scale is used in the colormap.

(a) $x_0 = \lambda/(5\pi)$ (b) $x_0 = \lambda/(4\pi)$ (c) $x_0 = 3\lambda/(10\pi)$

Figure 3.8: Apertureless NSOM images of the far-field intensity at frequency 3Ω in THG. The susceptibility of the tip is $\eta^{(3)}_{1111}E_0/\widehat{\eta}^{(1)} = 0.2$. Images are shown in the planes $x = x_0$ as indicated. The field of view of each image is $3\lambda/(5\pi) \times 3\lambda/(5\pi)$. A linear scale is used in the colormap.

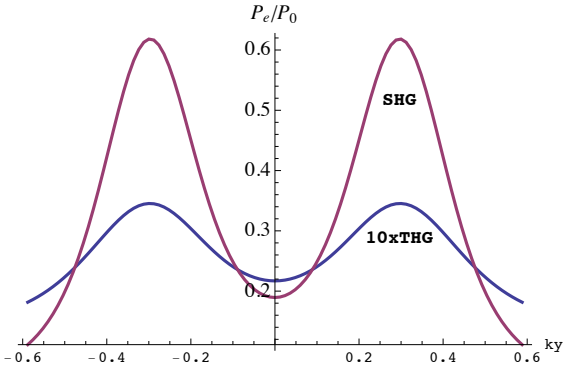

Figure 3.9: Extinguished power P_e/P_0 along the line defined by $x = \lambda/(5\pi)$ and $z = 0$, which corresponds to the closest scanning plane. Graphs are shown for SHG and THG. Here $P_0 = a^2cE_0^2$.

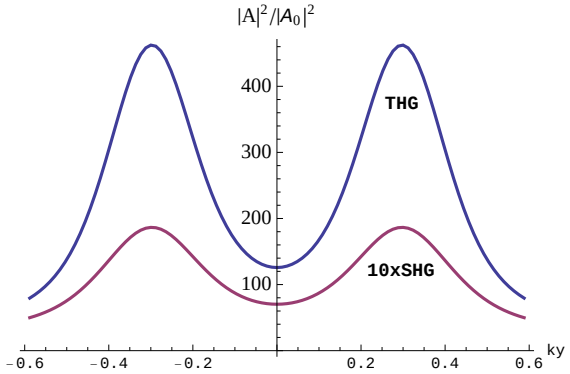

Figure 3.10: Far-field intensity along the line defined by $x = \lambda/(5\pi)$ and $z = 0$, which corresponds to the closest scanning plane. Graphs are shown for SHG and THG. Here $A_0 = aE_0$.

ticular, we describe the manner in which scattering resonances are modified by the presence of nonlinearity. As a second application, we consider the problem of computing the signal in a nonlinear near-field microscopy experiment. We note that the use of a tip with a nonlinear optical response affords the possibility of background suppression and spectral isolation of the detected signal. In future work, we plan to study the inverse problem for nonlinear near-field microscopy, whose goal is to reconstruct the linear optical properties of a sample illuminated by a nonlinear tip. This will necessitate the development of a scattering theory that incorporates contributions from the tip and the sample and their respective interactions, as was done for the corresponding linear problem [83].

Appendix

3.A Conservation of energy

Here we show that for nondispersive media, the analog of the Manley-Rowe relations hold [17]. That is, if the susceptibilities $\chi^{(1)}_{ij}$, $\chi^{(2)}_{ijk}$ and $\chi^{(3)}_{ijkl}$ are purely real, then $\nabla \cdot \overline{\mathbf{S}} = 0$. We treat the cases of quadratic and cubic nonlinearity separately. Note that for an incident field consisting of a sum of a finite number of frequencies, the integral in (3.28) becomes a sum.

3.A.1 Quadratic nonlinearity

We begin by inserting the quadratic polarization (3.15) into the statement of energy conservation (3.24). We then have

$$\begin{aligned} \nabla \cdot \mathbf{S}(\mathbf{r},\omega) &= \frac{\omega}{8\pi^3}\mathrm{Im}\left(E_i^*(\mathbf{r},\omega)\chi^{(1)}_{ij}(\mathbf{r};\omega)E_j(\omega)\right) \\ &+ \frac{\omega}{8\pi^3}\mathrm{Im}\left(\sum_{\omega_1+\omega_2=\omega}\chi^{(2)}_{ijk}(\mathbf{r};\omega_1,\omega_2)E_i^*(\mathbf{r},\omega)E_j(\mathbf{r},\omega_1)E_k(\mathbf{r},\omega_2)\right) . \quad (3.68) \end{aligned}$$

Making use of (3.28), the time-averaged divergence of energy current is

$$\begin{aligned} \nabla \cdot \overline{\mathbf{S}}(\mathbf{r}) &= \sum_{\omega}\frac{\omega}{8\pi^3}\mathrm{Im}(\chi^{(1)}_{ij}(\mathbf{r};\omega)E_i^*(\mathbf{r},\omega)E_j(\mathbf{r},\omega)) \\ &+ \sum_{\omega}\sum_{\omega_1+\omega_2=\omega}\frac{\omega}{8\pi^3}\mathrm{Im}(\chi^{(2)}_{ijk}(\mathbf{r};\omega_1,\omega_2)E_i^*(\mathbf{r},\omega)E_j(\mathbf{r},\omega_1)E_k(\mathbf{r},\omega_2)) . \quad (3.69) \end{aligned}$$

The first sum is zero since $\chi^{(1)}_{ij}(\mathbf{r};\omega)E^*_i(\mathbf{r},\omega)E_j(\mathbf{r},\omega)$ is real for each ω, due to the permutation symmetry of $\chi^{(1)}_{ij}$. The second sum vanishes as a consequence of the overall permutation symmetry of $\chi^{(2)}_{ijk}$ and the constraint $\omega_1+\omega_2=\omega$.

3.A.2 Cubic nonlinearity

For cubic nonlinearity we have

$$\nabla\cdot\overline{\mathbf{S}}(\mathbf{r}) = \sum_{\omega}\frac{\omega}{8\pi^3}\mathrm{Im}(\chi^{(1)}_{ij}(\mathbf{r};\omega)\mathbf{E}^*_i(\mathbf{r},\omega)\mathbf{E}_j(\mathbf{r},\omega))$$
$$+\sum_{\omega}\sum_{\omega_1+\omega_2+\omega_3=\omega}\frac{\omega}{8\pi^3}\mathrm{Im}(\chi^{(3)}_{ijkl}(\mathbf{r};\omega_1,\omega_2,\omega_3)\mathbf{E}^*_i(\mathbf{r},\omega)\mathbf{E}_j(\mathbf{r},\omega_1)\mathbf{E}_k(\mathbf{r},\omega_2)\mathbf{E}_l(\mathbf{r},\omega_3))\ . \quad (3.70)$$

The first sum is zero by the same argument as above. The second sum can be shown to be zero using the overall permutation symmetry of $\chi^{(3)}_{ijkl}$ and the constraint $\omega_1+\omega_2+\omega_3=\omega$.

3.B Calculation of local fields

Here we calculate the local fields of small scatterers for both second-harmonic generation and the Kerr effect.

3.B.1 Second-harmonic generation

We now calculate the local fields $E_i(\mathbf{0},\Omega)$ and $E_i(\mathbf{0},2\Omega)$. To proceed, we set $\mathbf{r}=0$ in (3.49) and (3.50) and thus obtain

$$\begin{aligned} E_i(\mathbf{0},\Omega) &= E_{\mathrm{inc},i}(\mathbf{0},\Omega)+k^2(\Omega)\eta^{(1)}_{jk}\int_{|\mathbf{r}'|\le a}d^3r' G_{ij}(\mathbf{0},\mathbf{r}';\Omega)E_k(\mathbf{r}',\Omega) \\ &+ 2k^2(\Omega)\eta^{(2)}_{jkl}\int_{|\mathbf{r}'|\le a}d^3r' G_{ij}(\mathbf{0},\mathbf{r}';\Omega)E_k(\mathbf{r}',\Omega)E^*_l(\mathbf{r}',2\Omega)\ , \end{aligned} \quad (3.71)$$

$$E_i(\mathbf{0},2\Omega) = k^2(2\Omega)\eta^{(1)}_{jk}\int_{|\mathbf{r}'|\le a} d^3r' G_{ij}(\mathbf{0},\mathbf{r}';2\Omega)E_k(\mathbf{r}',2\Omega) + k^2(\Omega)\eta^{(2)}_{jkl}\int_{|\mathbf{r}'|\le a} d^3r' G_{ij}(\mathbf{0},\mathbf{r}';2\Omega)E_k(\mathbf{r}',\Omega)E_l(\mathbf{r}',\Omega)\ . \quad (3.72)$$

Next, we use the fact that for a function g_j,

$$\int_{|\mathbf{r}'|\le a} d^3r' G_{ij}(\mathbf{0},\mathbf{r}';\omega)g_j(\mathbf{r}',\omega) = \frac{4\pi a^3}{3}\left(-\frac{1}{a^3k^2(\omega)}+\frac{1}{a}+i\frac{2}{3}k(\omega)+O(k^2(\omega)a)\right)g_i(\mathbf{0},\omega)\left(1+O(k(\omega)a)\right)\ , \quad (3.73)$$

which is derived in Appendix 3.B.3. We then find that (3.71) and (3.72) lead to a system of equations for the local fields which are of the form

$$E_i(\mathbf{0},\Omega) = E_{\mathrm{inc},i}(\mathbf{0},\Omega)+\frac{4\pi}{3}k^2(\Omega)a^3G_R(\Omega)(\eta^{(1)}_{ij}E_j(\mathbf{0},\Omega)+2\eta^{(2)}_{ijk}E_j(\mathbf{0},2\Omega)E^*_k(\mathbf{0},\Omega))\ , \quad (3.74)$$

$$E_i(\mathbf{0},2\Omega) = \frac{4\pi}{3}k^2(2\Omega)a^3G_R(2\Omega)(\eta^{(1)}_{ij}E_j(\mathbf{0},2\Omega)+\eta^{(2)}_{ijk}E_j(\mathbf{0},\Omega)E_k(\mathbf{0},\Omega))\ , \quad (3.75)$$

where

$$G_R(\omega) = -\frac{1}{a^3k^2(\omega)}+\frac{1}{a}+i\frac{2}{3}k(\omega)\ . \quad (3.76)$$

The above is a set of nonlinear algebraic equations which we solve perturbatively. To proceed, we introduce a parameter ϵ to scale the nonlinear terms in (3.74) and (3.75):

$$E_i(\mathbf{0},\Omega) = E_{\mathrm{inc},i}(\mathbf{0},\Omega)+\frac{4\pi}{3}k^2(\Omega)a^3G_R(\Omega)(\eta^{(1)}_{ij}E_j(\mathbf{0},\Omega)+2\epsilon\eta^{(2)}_{ijk}E_j(\mathbf{0},2\Omega)E^*_k(\mathbf{0},\Omega))\ , \quad (3.77)$$

$$E_i(\mathbf{0},2\Omega) = \frac{4\pi}{3}k^2(2\Omega)a^3G_R(2\Omega)(\eta^{(1)}_{ij}E_j(\mathbf{0},2\Omega)+\epsilon\eta^{(2)}_{ijk}E_j(\mathbf{0},\Omega)E_k(\mathbf{0},\Omega))\ . \quad (3.78)$$

We then introduce formal expansions for the fields of the form

$$E_i(0,\Omega) = E_i^{(0)}(0,\Omega) + \epsilon E_i^{(1)}(0,\Omega) + \epsilon^2 E_i^{(2)}(0,\Omega) + \cdots , \tag{3.79}$$

$$E_i(0,2\Omega) = E_i^{(0)}(0,2\Omega) + \epsilon E_i^{(1)}(0,2\Omega) + \epsilon^2 E_i^{(2)}(0,2\Omega) + \cdots . \tag{3.80}$$

For simplicity, we consider the case of isotropic $\eta^{(1)}$ and $\eta^{(2)}$ obeying permutation symmetry. That is, $\eta_{ij}^{(1)} = \eta^{(1)}\delta_{ij}$ and $\eta_{111}^{(2)} = \eta^{(2)}$, with the other $\eta_{ijk}^{(2)}$ vanishing. We also assume that the incident field $\mathbf{E}_{\rm inc}$ points in the x-direction and the direction of observation $\widehat{\mathbf{s}}$ is taken to be in the z-direction. To simplify the notation, we set $\Omega_1 = \Omega$, $\Omega_2 = 2\Omega$, and write $(E_i)_j = E_j(\mathbf{0},\Omega_i)$, $k_i = \Omega_i/c$, $(E_{\rm inc})_i = E_{{\rm inc},i}(\mathbf{0},\Omega)$ and $G_{Ri} = G_R(\Omega_i)$. Then (3.77) and (3.78) become

$$\begin{aligned}(E_1)_i &= (E_{\rm inc})_i + \frac{4\pi}{3}k_1^2 a^3 G_{R1}(\eta^{(1)}(E_1)_i + 2\epsilon\eta_{ijk}^{(2)}(E_1^*)_j(E_2)_k) \\ (E_2)_i &= \frac{4\pi}{3}k_2^2 a^3 G_{R2}(\eta^{(1)}(E_2)_i + \epsilon\eta_{ijk}^{(2)}(E_1)_j(E_1)_k) .\end{aligned} \tag{3.81}$$

Next, we expand the fields $(E_i)_j$ according to (3.74) and (3.75) and collect like powers of ϵ. At $O(1)$ we have that

$$\begin{aligned}(E_1)_i^{(0)} &= (E_{\rm inc})_i + \frac{4\pi}{3}k_1^2 a^3 G_{R1}\eta^{(1)}(E_1)_i^{(0)} \\ (E_2)_i^{(0)} &= 0 .\end{aligned} \tag{3.82}$$

Thus

$$(E_1)_1^{(0)} = \frac{(E_{\rm inc})_i}{1 - \frac{4\pi}{3}k_1^2 a^3 G_{R1}\eta^{(1)}} . \tag{3.83}$$

At $O(\epsilon)$ we have

$$(E_1)_i^{(1)} = \frac{4\pi}{3} k_1^2 a^3 G_{R1} \eta^{(1)} (E_1)_i^{(1)} \ , \tag{3.84}$$

$$(E_2)_i^{(1)} = \frac{4\pi}{3} k_2^2 a^3 G_{R2} (\eta^{(1)} (E_2)_i^{(1)} + \eta_{ijk}^{(2)} (E_1)_j^{(0)} (E_1)_k^{(0)}) \ , \tag{3.85}$$

which gives

$$(E_2)_1^{(1)} = \frac{4\pi}{3} k_2^2 a^3 G_{R2} (\eta^{(1)} (E_2)_3^{(1)} + \eta_{111}^{(2)} (E_1)_1^{(0)} (E_1)_1^{(0)}) \ . \tag{3.86}$$

Thus

$$(E_2)_1^{(1)} = \frac{\frac{4\pi}{3} k_2^2 a^3 G_{R2} \eta_{111}^{(2)} (E_1)_1^{(0)} (E_1)_1^{(0)}}{1 - \frac{4\pi}{3} k_2^2 a^3 G_{R2} \eta^{(1)}} \ . \tag{3.87}$$

At $O(\epsilon^2)$ we obtain

$$(E_1)_i^{(2)} = \frac{4\pi}{3} k_1^2 a^3 G_{R1} (\eta^{(1)} (E_1)_i^{(2)} + 2\eta_{ijk}^{(2)} (E_1^*)_j^{(0)} (E_2)_k^{(1)}) \ , \tag{3.88}$$

which gives

$$(E_1)_1^{(2)} = \frac{4\pi}{3} k_1^2 a^3 G_{R1} (\eta^{(1)} (E_1)_1^{(2)} + 2\eta_{111}^{(2)} (E_2)_1^{(1)} (E_1^*)_1^{(0)}) \ . \tag{3.89}$$

Thus

$$(E_1)_1^{(2)} = \frac{\frac{4\pi}{3} k_1^2 a^3 G_{R1} 2\eta_{111}^{(2)} (E_1^*)_1^{(0)} (E_2)_1^{(1)}}{1 - \frac{4\pi}{3} k_1^2 a^3 G_{R1} \eta^{(1)}} \ . \tag{3.90}$$

We can now calculate the extinguished power P_e from (3.40). We find that up to the order

$O(\epsilon^2)$

$$P_e = \frac{8\Omega_1}{3} a^3 \mathrm{Im}\left((\eta^{(1)}(E_1)_1^{(0)} + \eta^{(1)}(E_1)_1^{(2)} + 2\eta^{(2)}_{111}(E_1^*)_1^{(0)}(E_2)_1^{(1)})(E_{\mathrm{inc}})_1^* \right) \ . \tag{3.91}$$

3.B.2 Kerr effect

Here we calculate the local field $E_i(\mathbf{0}, \Omega)$. To proceed, we set $\mathbf{r} = 0$ in (3.59) and thus obtain

$$\begin{aligned} E_i(\mathbf{0},\Omega) &= E_{\mathrm{inc},i}(\mathbf{0},\Omega) + k^2(\Omega)\eta^{(1)}_{jk} \int_{|\mathbf{r}'|\le a} d^3r' G_{ij}(\mathbf{0},\mathbf{r}';\Omega) E_k(\mathbf{r}',\Omega) \\ &+ 3k^2(\Omega)\eta^{(3)}_{jklm} \int_{|\mathbf{r}'|\le a} d^3r' G_{ij}(\mathbf{0},\mathbf{r}';\Omega) E_k(\mathbf{r}',\Omega) E_l(\mathbf{r}',\Omega) E^*_m(\mathbf{r}',\Omega) \ . \end{aligned} \tag{3.92}$$

We then find that (3.92) leads to an equation for the local field which is of the form

$$\begin{aligned} E_i(\mathbf{0},\Omega) = \quad & E_{\mathrm{inc},i}(\mathbf{0},\Omega) + \frac{4\pi}{3} k^2 a^3(\Omega) G_R(\Omega)(\eta^{(1)} E_i(\mathbf{0},\Omega) \\ & + 3\eta^{(3)}_{ijkl} E^*_j(\mathbf{0},\Omega) E_k(\mathbf{0},\Omega) E_l(\mathbf{0},\Omega)) \ . \end{aligned} \tag{3.93}$$

The above is a nonlinear algebraic equation which we solve perturbatively. To proceed, we introduce a parameter ϵ to scale the nonlinear terms in (3.93):

$$\begin{aligned} E_i(\mathbf{0},\Omega) = \quad & E_{\mathrm{inc},i}(\mathbf{0},\Omega) + \frac{4\pi}{3} k^2 a^3(\Omega) G_R(\Omega)(\eta^{(1)} E_i(\mathbf{0},\Omega) \\ & + 3\epsilon\eta^{(3)}_{ijkl} E^*_j(\mathbf{0},\Omega) E_k(\mathbf{0},\Omega) E_l(\mathbf{0},\Omega)) \ . \end{aligned} \tag{3.94}$$

We then introduce formal expansions for the field of the form

$$E_i(0,\Omega) = E_i^{(0)}(0,\Omega) + \epsilon E_i^{(1)}(0,\Omega) + \epsilon^2 E_i^{(2)}(0,\Omega) + \cdots \ . \tag{3.95}$$

For simplicity, we consider the case of isotropic $\eta^{(1)}$ and $\eta^{(3)}$ obeying the permutation symmetry. That is, $\eta^{(1)}_{ij} = \eta^{(1)}\delta_{ij}$ and $\eta^{(3)}_{1111} = \eta^{(3)}$, with all other $\eta^{(3)}_{ijkl}$ vanishing. We also assume that the incident field $\mathbf{E}_{\text{inc}}$ points in the x-direction and the direction of observation $\widehat{\mathbf{s}}$ is taken to be in the z-direction. To simplify the notation, we write $(E)_j = E_j(\mathbf{0}, \Omega_i)$, $k = \Omega/c$ and $G_R = G_R(\Omega)$. Then (3.94) becomes

$$(E)_i = (E_{\text{inc}})_i + \frac{4\pi}{3}k^2a^3G_R(\eta^{(1)}(E)_i + 3\epsilon\eta^{(3)}_{ijkl}(E^*)_j(E)_k(E)_l) \ . \tag{3.96}$$

Next, we expand the fields $(E)_i$ according to (3.95) and collect like powers of ϵ. At $O(1)$ we have that

$$(E)^{(0)}_i = (E_{\text{inc}})_i + \frac{4\pi}{3}k^2a^3G_R\eta^{(1)}(E)^{(0)}_i \ . \tag{3.97}$$

Thus

$$(E)^{(0)}_1 = \frac{E_{\text{inc},i}}{1 - \frac{4\pi}{3}k^2a^3G_R\eta^{(1)}} \ . \tag{3.98}$$

At $O(\epsilon)$ we have

$$(E)^{(1)}_i = \frac{4\pi}{3}k^2a^3G_R(\eta^{(1)}(E)^{(1)}_i + 3\eta^{(3)}_{ijkl}(E^*)^{(0)}_j(E)^{(0)}_k(E)^{(0)}_l) \ , \tag{3.99}$$

which gives

$$(E)^{(1)}_i = \frac{4\pi}{3}k^2a^3G_R(\eta^{(1)}(E)^{(1)}_i + 3\eta^{(3)}_{i111}(E^*)^{(0)}_1(E)^{(0)}_1(E)^{(0)}_1) \ . \tag{3.100}$$

Thus

$$(E)_i^{(1)}(\mathbf{0}) = \frac{\frac{4\pi}{3}k^2a^3G_R 3\eta^{(3)}_{i111}(E^*)_1^{(0)}(0)(E)_1^{(0)}(0)(E)_1^{(0)}(0)}{1-\frac{4\pi}{3}k^2a^3G_R\eta^{(1)}} \tag{3.101}$$

and

$$(E)_1^{(1)}(\mathbf{0}) = \frac{\frac{4\pi}{3}k^2a^3G_R 3\eta^{(3)}_{1111}(E^*)_1^{(0)}(0)(E)_1^{(0)}(0)(E)_1^{(0)}(0)}{1-\frac{4\pi}{3}k^2a^3G_R\eta^{(1)}} \ . \tag{3.102}$$

We can now calculate the extinguished power P_e from (3.40). We find that up to the order $O(\epsilon)$

$$P_e = \frac{8\Omega_1}{3}a^3\mathrm{Im}\left((\eta^{(1)}(E)_1^{(0)} + \eta^{(1)}(E)_1^{(1)} + 3\eta^{(3)}_{1111}(E^*)_1^{(0)}(E)_1^{(0)}(E)_1^{(0)})(E_{\mathrm{inc}})_1^*\right) \ . \tag{3.103}$$

3.B.3 Evaluation of the Integral (3.73)

Here we show

$$\int_{|\mathbf{r}'|\le a} d^3r' G_{ij}(\mathbf{0},\mathbf{r}';\omega) = \frac{4\pi a^3}{3}\left(\frac{1}{a} + i\frac{2}{3}k(\omega) - \frac{1}{a^3k^2(\omega)} + O(k(\omega)a)\right) \ . \tag{3.104}$$

For notational convenience, we put $k = k(\Omega)$. Then

$$\int_{|\mathbf{r}'|\le a} d^3r' G_{ij}(\mathbf{0},\mathbf{r}';\omega) = \int_{|\mathbf{r}|\le a} d^3r \left(\delta_{ij} + \frac{1}{k^2}\partial_i\partial_j\right)\frac{e^{ikr}}{r} \tag{3.105}$$

The second term vanishes when $i \neq j$. Using the fact that

$$\left(\nabla^2 + k^2\right) \frac{e^{ikr}}{r} = -4\pi\delta(\mathbf{r}) \ , \tag{3.106}$$

we have

$$\begin{aligned} \int_{|\mathbf{r}|\leq a} d^3r \frac{1}{k^2}\partial_i\partial_j \frac{e^{ikr}}{r} &= \int_{|\mathbf{r}|\leq a} d^3r \delta_{ij} \frac{1}{k^2}\frac{1}{3}\left(-k^2\frac{e^{ikr}}{r} - 4\pi\delta(\mathbf{r})\right) \\ &= -\delta_{ij}\left(\int_{|\mathbf{r}|\leq a} d^3r \frac{e^{ikr}}{3r} + \frac{4\pi}{3k^2}\right) \ . \end{aligned} \tag{3.107}$$

So

$$\int_{|\mathbf{r}'|\leq a} d^3r' G_{ij}(\mathbf{0},\mathbf{r}';\omega) = \delta_{ij}\left(\int_{|\mathbf{r}|\leq a} d^3r \frac{2}{3}\frac{e^{ikr}}{r} - \frac{4\pi}{3k^2}\right) \ . \tag{3.108}$$

Since

$$\int_{|\mathbf{r}|\leq a} d^3r \frac{e^{ikr}}{r} = \frac{4\pi a^2}{3}\left(\frac{3}{2} + ika + O((ka)^2)\right) \ , \tag{3.109}$$

we obtain the required result.

3.C Near-field scanning optical microscopy

Here we derive the basic equations governing the NSOM experiments described in Sec. 3.6.

3.C.1 Second-harmonic generation

The sample and the tip are taken to be small balls of radius a centered at $\mathbf{r}_0$, $\mathbf{r}_1$ and $\mathbf{r}_2$. The corresponding susceptibilities are $\chi^{(1)}_{ij}(\mathbf{r};\omega) = \widehat{\eta}^{(1)}_{ij}$ for $|\mathbf{r}-\mathbf{r}_0| \leq a$, $\chi^{(1)}_{ij}(\mathbf{r};\omega) = \eta^{(1)}_{ij}$ for $|\mathbf{r}-\mathbf{r}_1| \leq a$ and $|\mathbf{r}-\mathbf{r}_2| \leq a$, and $\chi^{(2)}_{ijk}(\mathbf{r};\omega) = \eta^{(2)}_{ijk}$ for $|\mathbf{r}| \leq a$. In this setting, the solutions

to the wave equations of SHG (3.45) and (3.46) are

$$\begin{aligned}
E_i(\mathbf{r},\Omega) &= E_{\mathrm{inc},i}(\mathbf{r},\Omega) + k^2(\Omega)\widehat{\eta}^{(1)}_{jk}\int_{|\mathbf{r}'-\mathbf{r}_0|\le a} d^3r' G_{ij}(\mathbf{r},\mathbf{r}';\Omega)E_k(\mathbf{r}',\Omega) \\
&+ k^2(\Omega)\eta^{(1)}_{jk}\int_{|\mathbf{r}'-\mathbf{r}_1|\le a} d^3r' G_{ij}(\mathbf{r},\mathbf{r}';\Omega)E_k(\mathbf{r}',\Omega) \\
&+ k^2(\Omega)\eta^{(1)}_{jk}\int_{|\mathbf{r}'-\mathbf{r}_2|\le a} d^3r' G_{ij}(\mathbf{r},\mathbf{r}';\Omega)E_k(\mathbf{r}',\Omega) \\
&+ 2k^2(\Omega)\eta^{(2)}_{jkl}\int_{|\mathbf{r}'-\mathbf{r}_0|\le a} d^3r' G_{ij}(\mathbf{r},\mathbf{r}';\Omega)E_k(\mathbf{r}',2\Omega)E^*_l(\mathbf{r}',\Omega)\ , \qquad (3.110) \\
E_i(\mathbf{r},2\Omega) &= k^2(2\Omega)\widehat{\eta}^{(1)}_{jk}\int_{|\mathbf{r}'-\mathbf{r}_0|\le a} d^3r' G_{ij}(\mathbf{r},\mathbf{r}';\Omega)E_k(\mathbf{r}',2\Omega) \\
&+ k^2(2\Omega)\eta^{(1)}_{jk}\int_{|\mathbf{r}'-\mathbf{r}_1|\le a} d^3r' G_{ij}(\mathbf{r},\mathbf{r}';\Omega)E_k(\mathbf{r}',2\Omega) \\
&+ k^2(2\Omega)\eta^{(1)}_{jk}\int_{|\mathbf{r}'-\mathbf{r}_2|\le a} d^3r' G_{ij}(\mathbf{r},\mathbf{r}';\Omega)E_k(\mathbf{r}',2\Omega) \\
&+ k^2(2\Omega)\eta^{(2)}_{jkl}\int_{|\mathbf{r}'-\mathbf{r}_0|\le a} d^3r' G_{ij}(\mathbf{r},\mathbf{r}';\Omega)E_k(\mathbf{r}',\Omega)E_l(\mathbf{r}',\Omega)\ . \qquad (3.111)
\end{aligned}$$

Using the asymptotic form of the Green's function given in (3.21), we find that the scattered fields are of the form

$$E^s_i(\mathbf{r},\Omega) = A_i(\mathbf{r},\Omega)\frac{e^{ik(\Omega)r}}{r}\ , \qquad (3.112)$$

$$E^s_i(\mathbf{r},2\Omega) = A_i(\mathbf{r},2\Omega)\frac{e^{ik(2\Omega)r}}{r}\ , \qquad (3.113)$$

where the scattering amplitudes are defined by

$$\begin{aligned} A_i(\mathbf{r},\Omega) &= \frac{4\pi}{3}a^3(\delta_{ij}-\widehat{r}_i\widehat{r}_j)k^2(\Omega)(\widehat{\eta}^{(1)}_{jk}E_k(\mathbf{r}_0,\Omega)+2\eta^{(2)}_{jkl}E_k(\mathbf{r}_0,2\Omega)E^*_l(\mathbf{r}_0,\Omega))e^{ik(\Omega)\widehat{\mathbf{r}}\cdot\mathbf{r}_0} \\ &+ \frac{4\pi}{3}a^3(\delta_{ij}-\widehat{r}_i\widehat{r}_j)k^2(\Omega)\eta^{(1)}_{jk}E_k(\mathbf{r}_1,\Omega)e^{ik(\Omega)\widehat{\mathbf{r}}\cdot\mathbf{r}_1} \\ &+ \frac{4\pi}{3}a^3(\delta_{ij}-\widehat{r}_i\widehat{r}_j)k^2(\Omega)\eta^{(1)}_{jk}E_k(\mathbf{r}_2,\Omega)e^{ik(\Omega)\widehat{\mathbf{r}}\cdot\mathbf{r}_2}\ , \end{aligned} \tag{3.114}$$

$$\begin{aligned} A_i(\mathbf{r},2\Omega) &= \frac{4\pi}{3}a^3(\delta_{ij}-\widehat{r}_i\widehat{r}_j)k^2(2\Omega)(\widehat{\eta}^{(1)}_{jk}E_j(\mathbf{r}_0,2\Omega)+\eta^{(2)}_{jkl}E_k(\mathbf{r}_0,\Omega)E_l(\mathbf{r}_0,\Omega))e^{ik(\Omega)\widehat{\mathbf{r}}\cdot\mathbf{r}_0} \\ &+ \frac{4\pi}{3}a^3(\delta_{ij}-\widehat{r}_i\widehat{r}_j)k^2(2\Omega)\eta^{(1)}_{jk}E_k(\mathbf{r}_1,2\Omega)e^{ik(2\Omega)\widehat{\mathbf{r}}\cdot\mathbf{r}_1} \\ &+ \frac{4\pi}{3}a^3(\delta_{ij}-\widehat{r}_i\widehat{r}_j)k^2(2\Omega)\eta^{(1)}_{jk}E_k(\mathbf{r}_2,2\Omega)e^{ik(2\Omega)\widehat{\mathbf{r}}\cdot\mathbf{r}_2}\ . \end{aligned} \tag{3.115}$$

Setting $\mathbf{r}=\mathbf{r}_0$, $\mathbf{r}=\mathbf{r}_1$ and $\mathbf{r}=\mathbf{r}_2$ in (3.110) and (3.111), and carrying out the indicated integrations we obtain

$$\begin{aligned} E_i(\mathbf{r}_0,\Omega) &= E_{\mathrm{inc},i}(\mathbf{r}_0,\Omega)+\frac{4\pi}{3}k^2(\Omega)a^3G_R(\Omega)(\widehat{\eta}^{(1)}_{ij}E_j(\mathbf{r}_0,\Omega)+2\eta^{(2)}_{ijk}E_j(\mathbf{r}_0,2\Omega)E^*_k(\mathbf{r}_0,\Omega)) \\ &+ \frac{4\pi}{3}k^2(\Omega)a^3G_{ij}(\mathbf{r}_1,\mathbf{r}_0;\Omega)\eta^{(1)}_{jk}E_k(\mathbf{r}_1,\Omega)+\frac{4\pi}{3}k^2(\Omega)a^3G_{ij}(\mathbf{r}_2,\mathbf{r}_0;\Omega)\eta^{(1)}_{jk}E_k(\mathbf{r}_2,\Omega)\ , \end{aligned} \tag{3.116}$$

$$\begin{aligned} E_i(\mathbf{r}_0,2\Omega) &= \frac{4\pi}{3}k^2(2\Omega)a^3G_R(2\Omega)(\widehat{\eta}^{(1)}_{ij}E_j(\mathbf{r}_0,2\Omega)+\eta^{(2)}_{ijk}E_j(\mathbf{r}_0,\Omega)E_k(\mathbf{r}_0,\Omega)) \\ &+ \frac{4\pi}{3}k^2(2\Omega)a^3G_{ij}(\mathbf{r}_1,\mathbf{r}_0;2\Omega)\eta^{(1)}_{jk}E_k(\mathbf{r}_1,2\Omega) \\ &+ \frac{4\pi}{3}k^2(2\Omega)a^3G_{ij}(\mathbf{r}_2,\mathbf{r}_0;2\Omega)\eta^{(1)}_{jk}E_k(\mathbf{r}_2,2\Omega)\ , \end{aligned} \tag{3.117}$$

$$
\begin{aligned}
E_i(\mathbf{r}_1,\Omega) &= E_{\mathrm{inc},i}(\mathbf{r}_1,\Omega)+\frac{4\pi}{3}k^2(\Omega)a^3G_R(\Omega)\eta^{(1)}_{ij}E_j(\mathbf{r}_1,\Omega)\ , \\
&+ \frac{4\pi}{3}k^2(\Omega)a^3G_{ij}(\mathbf{r}_1,\mathbf{r}_0;\Omega)(\widehat{\eta}^{(1)}_{jk}E_k(\mathbf{r}_0,\Omega)+2\eta^{(2)}_{jkl}E_k(\mathbf{r}_0,2\Omega)E^*_l(\mathbf{r}_0,\Omega))) \\
&+ \frac{4\pi}{3}k^2(\Omega)a^3G_{ij}(\mathbf{r}_1,\mathbf{r}_2;\Omega)\eta^{(1)}_{jk}E_k(\mathbf{r}_2,\Omega)\ , \qquad (3.118) \\
E_i(\mathbf{r}_1,2\Omega) &= \frac{4\pi}{3}k^2(2\Omega)a^3G_R(2\Omega)\eta^{(1)}_{ij}E_j(\mathbf{r}_1,2\Omega) \\
&+ \frac{4\pi}{3}k^2(2\Omega)a^3G_{ij}(\mathbf{r}_1,\mathbf{r}_0;2\Omega)(\widehat{\eta}^{(1)}_{jk}E_k(\mathbf{r}_0,2\Omega)+\eta^{(2)}_{jkl}E_k(\mathbf{r}_0,\Omega)E_l(\mathbf{r}_0,\Omega)) \\
&+ \frac{4\pi}{3}k^2(2\Omega)a^3G_{ij}(\mathbf{r}_1,\mathbf{r}_2;2\Omega)\eta^{(1)}_{jk}E_k(\mathbf{r}_2,2\Omega)\ , \qquad (3.119) \\
E_i(\mathbf{r}_2,\Omega) &= E_{\mathrm{inc},i}(\mathbf{r}_2,\Omega)+\frac{4\pi}{3}k^2(\Omega)a^3G_R(\Omega)\eta^{(1)}_{ij}E_j(\mathbf{r}_2,\Omega)\ , \\
&+ \frac{4\pi}{3}k^2(\Omega)a^3G_{ij}(\mathbf{r}_2,\mathbf{r}_0;\Omega)(\widehat{\eta}^{(1)}_{jk}E_k(\mathbf{r}_0,\Omega)+2\eta^{(2)}_{jkl}E_k(\mathbf{r}_0,2\Omega)E^*_l(\mathbf{r}_0,\Omega)) \\
&+ \frac{4\pi}{3}k^2(\Omega)a^3G_{ij}(\mathbf{r}_2,\mathbf{r}_1;\Omega)\eta^{(1)}_{jk}E_k(\mathbf{r}_1,\Omega)\ , \qquad (3.120) \\
E_i(\mathbf{r}_2,2\Omega) &= \frac{4\pi}{3}k^2(2\Omega)a^3G_R(2\Omega)\eta^{(1)}_{ij}E_j(\mathbf{r}_2,2\Omega) \\
&+ \frac{4\pi}{3}k^2(2\Omega)a^3G_{ij}(\mathbf{r}_2,\mathbf{r}_0;2\Omega)(\widehat{\eta}^{(1)}_{jk}E_k(\mathbf{r}_0,2\Omega)+\eta^{(2)}_{jkl}E_k(\mathbf{r}_0,\Omega)E_l(\mathbf{r}_0,\Omega)) \\
&+ \frac{4\pi}{3}k^2(2\Omega)a^3G_{ij}(\mathbf{r}_2,\mathbf{r}_1;2\Omega)\eta^{(1)}_{jk}E_k(\mathbf{r}_1,2\Omega)\ , \qquad (3.121)
\end{aligned}
$$

Following the procedure indicated in Appendix B, the above equations can be solved perturbatively for the local fields.

3.C.2 Third-harmonic generation

As above, the sample and the tip are small balls of radius a centered at $\mathbf{r}_0$, $\mathbf{r}_1$ and $\mathbf{r}_2$. The susceptibilities are $\chi^{(1)}_{ij}(\mathbf{r};\omega)=\widehat{\eta}^{(1)}_{ij}$ for $|\mathbf{r}-\mathbf{r}_0|\le a$, $\chi^{(1)}_{ij}(\mathbf{r};\omega)=\eta^{(1)}_{ij}$ for $|\mathbf{r}-\mathbf{r}_1|\le a$ and $|\mathbf{r}-\mathbf{r}_2|\le a$, and $\chi^{(3)}_{ijkl}(\mathbf{r};\omega)=\eta^{(3)}_{ijkl}$ for $|\mathbf{r}|\le a$. We begin with the general cubic-nonlinear wave equations which are correct to order ϵ:

$$
\begin{aligned}
\nabla\times\nabla\times\mathbf{E}(\mathbf{r},\Omega) &- k^2(\Omega)\mathbf{E}(\mathbf{r},\Omega)=4\pi k^2(\Omega)(\chi^{(1)}_{ij}(\mathbf{r},\Omega)E_j(\mathbf{r},\Omega) \\
&+ 3\chi^{(3)}_{ijkl}(\mathbf{r},\Omega,\Omega,-\Omega)E_j(\mathbf{r},\Omega)E_k(\mathbf{r},\Omega)E^*_l(\mathbf{r},\Omega))\ . \qquad (3.122)
\end{aligned}
$$

$$\nabla \times \nabla \times \mathbf{E}(\mathbf{r}, 3\Omega) - k^2(3\Omega)\mathbf{E}(\mathbf{r}, 3\Omega) = 4\pi k^2(3\Omega)(\chi^{(1)}_{ij}(\mathbf{r}, 3\Omega)E_j(\mathbf{r}, 3\Omega) + \chi^{(3)}_{ijkl}(\mathbf{r}, \Omega, \Omega, \Omega)E_j(\mathbf{r}, \Omega)E_k(\mathbf{r}, \Omega)E_l(\mathbf{r}, \Omega)) \ . \tag{3.123}$$

It follows immediately from (3.18) that the solution to (3.122) and (3.123) is given by

$$E_i(\mathbf{r}, \Omega) = E_{\mathrm{inc},i}(\mathbf{r}, \Omega) + k^2(\Omega)\int d^3r' \chi^{(1)}_{jk}(\mathbf{r}', \Omega)G_{ij}(\mathbf{r}, \mathbf{r}'; \Omega)E_k(\mathbf{r}', \Omega) + 3k^2(\Omega)\int d^3r' \chi^{(3)}_{jklm}(\mathbf{r}', \Omega, \Omega, -\Omega)G_{ij}(\mathbf{r}, \mathbf{r}'; \Omega)E_k(\mathbf{r}', \Omega)E_l(\mathbf{r}', \Omega)E^*_m(\mathbf{r}', \Omega)) \ , \tag{3.124}$$

$$E_i(\mathbf{r}, 3\Omega) = k^2(3\Omega)\int d^3r' \chi^{(1)}_{jk}(\mathbf{r}', 3\Omega)G_{ij}(\mathbf{r}, \mathbf{r}'; 3\Omega)E_k(\mathbf{r}', 3\Omega) + 3k^2 3(\Omega)\int d^3r' \chi^{(3)}_{jklm}(\mathbf{r}', \Omega, \Omega, \Omega)G_{ij}(\mathbf{r}, \mathbf{r}'; 3\Omega)E_k(\mathbf{r}', \Omega)E_l(\mathbf{r}', \Omega)E_m(\mathbf{r}', \Omega)) \ , \tag{3.125}$$

For the specific set up described at the beginning of this section, Equations (3.124) and (3.125) become

$$\begin{aligned} E_i(\mathbf{r}, \Omega) &= E_{\mathrm{inc},i}(\mathbf{r}, \Omega) + k^2(\Omega)\widehat{\eta}^{(1)}_{jk}\int_{|\mathbf{r}'-\mathbf{r}_0|\le a} d^3r' G_{ij}(\mathbf{r}, \mathbf{r}'; \Omega)E_k(\mathbf{r}', \Omega) \\ &+ k^2(\Omega)\eta^{(1)}_{jk}\int_{|\mathbf{r}'-\mathbf{r}_1|\le a} d^3r' G_{ij}(\mathbf{r}, \mathbf{r}'; \Omega)E_k(\mathbf{r}', \Omega) \\ &+ k^2(\Omega)\eta^{(1)}_{jk}\int_{|\mathbf{r}'-\mathbf{r}_2|\le a} d^3r' G_{ij}(\mathbf{r}, \mathbf{r}'; \Omega)E_k(\mathbf{r}', \Omega) \\ &+ 3k^2(\Omega)\eta^{(3)}_{jklm}\int_{|\mathbf{r}'-\mathbf{r}_0|\le a} d^3r' G_{ij}(\mathbf{r}, \mathbf{r}'; \Omega)E_k(\mathbf{r}', \Omega)E_l(\mathbf{r}', \Omega)E^*_m(\mathbf{r}', \Omega)) \end{aligned} \tag{3.126}$$

$$
\begin{aligned}
E_i(\mathbf{r},3\Omega) &= k^2(3\Omega)\widehat{\eta}^{(1)}_{jk}\int_{|\mathbf{r}'-\mathbf{r}_0|\le a} d^3r' G_{ij}(\mathbf{r},\mathbf{r}';3\Omega)E_k(\mathbf{r}',3\Omega) \\
&+ k^2(3\Omega)\eta^{(1)}_{jk}\int_{|\mathbf{r}'-\mathbf{r}_1|\le a} d^3r' G_{ij}(\mathbf{r},\mathbf{r}';3\Omega)E_k(\mathbf{r}',3\Omega) \\
&+ k^2(3\Omega)\eta^{(1)}_{jk}\int_{|\mathbf{r}'-\mathbf{r}_2|\le a} d^3r' G_{ij}(\mathbf{r},\mathbf{r}';3\Omega)E_k(\mathbf{r}',3\Omega) \\
&+ k^2(3\Omega)\eta^{(3)}_{jklm}\int_{|\mathbf{r}'-\mathbf{r}_0|\le a} d^3r' G_{ij}(\mathbf{r},\mathbf{r}';3\Omega)E_k(\mathbf{r}',\Omega)E_l(\mathbf{r}',\Omega)E_m(\mathbf{r}',\Omega)) \qquad (3.127)
\end{aligned}
$$

Using the asymptotic form of the Green's function given in (3.21), we find that the scattered field is of the form

$$
\begin{aligned}
E^s_i(\mathbf{r},\Omega) &= A_i(\mathbf{r},\Omega)\frac{e^{ik(\Omega)r}}{r} \qquad (3.128) \\
E^s_i(\mathbf{r},3\Omega) &= A_i(\mathbf{r},3\Omega)\frac{e^{ik(3\Omega)r}}{r}\ , \qquad (3.129)
\end{aligned}
$$

where the scattering amplitude is defined by

$$
\begin{aligned}
A_i(\mathbf{r},\Omega) &= \frac{4\pi}{3}a^3(\delta_{ij}-\widehat{r}_i\widehat{r}_j)k^2(\Omega)(\widehat{\eta}^{(1)}_{jk}E_k(\mathbf{r}_0,\Omega)+3\eta^{(3)}_{jklm}E_k(\mathbf{r}_0,\Omega)E_l(\mathbf{r}_0,\Omega)E^*_m(\mathbf{r}_0,\Omega)) \\
&+ \frac{4\pi}{3}a^3(\delta_{ij}-\widehat{r}_i\widehat{r}_j)k^2(\Omega)\eta^{(1)}_{jk}E_k(\mathbf{r}_1,\Omega)e^{ik(\Omega)\widehat{\mathbf{r}}\cdot\mathbf{r}_1} \\
&+ \frac{4\pi}{3}a^3(\delta_{ij}-\widehat{r}_i\widehat{r}_j)k^2(\Omega)\eta^{(1)}_{jk}E_k(\mathbf{r}_2,\Omega)e^{ik(\Omega)\widehat{\mathbf{r}}\cdot\mathbf{r}_2}\ , \qquad (3.130) \\
A_i(\mathbf{r},3\Omega) &= \frac{4\pi}{3}a^3(\delta_{ij}-\widehat{r}_i\widehat{r}_j)k^2(3\Omega)(\widehat{\eta}^{(1)}_{jk}E_k(\mathbf{r}_0,3\Omega)+\eta^{(3)}_{jklm}E_k(\mathbf{r}_0,\Omega)E_l(\mathbf{r}_0,\Omega)E_m(\mathbf{r}_0,\Omega)) \\
&+ \frac{4\pi}{3}a^3(\delta_{ij}-\widehat{r}_i\widehat{r}_j)k^2(3\Omega)\eta^{(1)}_{jk}E_k(\mathbf{r}_1,3\Omega)e^{ik(3\Omega)\widehat{\mathbf{r}}\cdot\mathbf{r}_1} \\
&+ \frac{4\pi}{3}a^3(\delta_{ij}-\widehat{r}_i\widehat{r}_j)k^2(3\Omega)\eta^{(1)}_{jk}E_k(\mathbf{r}_2,3\Omega)e^{ik(3\Omega)\widehat{\mathbf{r}}\cdot\mathbf{r}_2}\ . \qquad (3.131)
\end{aligned}
$$

Setting $\mathbf{r}=\mathbf{r}_0$, $\mathbf{r}=\mathbf{r}_1$ and $\mathbf{r}=\mathbf{r}_2$ in (3.127) and (3.127), and carrying out the indicated

integrations we find that

$$
\begin{aligned}
E_i(\mathbf{r}_0,\Omega) &= E_{\mathrm{inc},i}(\mathbf{r}_0,\Omega) + \frac{4\pi}{3}a^3k^2(\Omega)\widehat{\eta}^{(1)}_{ij}G_R(\Omega)E_j(\mathbf{r}_0,\Omega) \\
&+ \frac{4\pi}{3}a^3k^2(\Omega)\eta^{(1)}_{jk}G_{ij}(\mathbf{r}_0,\mathbf{r}_1;\Omega)E_k(\mathbf{r}_1,\Omega) \\
&+ \frac{4\pi}{3}a^3k^2(\Omega)\eta^{(1)}_{jk}G_{ij}(\mathbf{r},\mathbf{r}_2;\Omega)E_k(\mathbf{r}_2,\Omega) \\
&+ \frac{4\pi}{3}a^3k^2(\Omega)3\eta^{(3)}_{ijkl}G_R(\Omega)E_j(\mathbf{r}_0,\Omega)E_k(\mathbf{r}_0,\Omega)E^*_l(\mathbf{r}_0,\Omega))\ , \qquad (3.132) \\
E_i(\mathbf{r}_1,\Omega) &= E_{\mathrm{inc},i}(\mathbf{r}_1,\Omega) + \frac{4\pi}{3}a^3k^2(\Omega)\widehat{\eta}^{(1)}_{jk}G_{ij}(\mathbf{r}_1,\mathbf{r}_0;\Omega)E_k(\mathbf{r}_0,\Omega) \\
&+ \frac{4\pi}{3}a^3k^2(\Omega)\eta^{(1)}_{ij}G_R(\mathbf{r},\mathbf{r}_1;\Omega)E_j(\mathbf{r}',\Omega) \\
&+ \frac{4\pi}{3}a^3k^2(\Omega)\eta^{(1)}_{jk}G_{ij}(\mathbf{r}_1,\mathbf{r}_2;\Omega)E_k(\mathbf{r}_2,\Omega) \\
&+ \frac{4\pi}{3}a^3k^2(\Omega)3\eta^{(3)}_{jklm}G_{ij}(\mathbf{r}_1,\mathbf{r}_0;\Omega)E_k(\mathbf{r}_0,\Omega)E_l(\mathbf{r}_0,\Omega)E^*_m(\mathbf{r}_0,\Omega))\ , \qquad (3.133) \\
E_i(\mathbf{r}_2,\Omega) &= E_{\mathrm{inc},i}(\mathbf{r}_2,\Omega) + \frac{4\pi}{3}a^3k^2(\Omega)\widehat{\eta}^{(1)}_{jk}G_{ij}(\mathbf{r}_2,\mathbf{r}_0;\Omega)E_k(\mathbf{r}_0,\Omega) \\
&+ \frac{4\pi}{3}a^3k^2(\Omega)\eta^{(1)}_{jk}G_{ij}(\mathbf{r}_2,\mathbf{r}_1;\Omega)E_k(\mathbf{r}_1,\Omega) \\
&+ \frac{4\pi}{3}a^3k^2(\Omega)\eta^{(1)}_{ij}G_R(\Omega)E_j(\mathbf{r}_2,\Omega) \\
&+ \frac{4\pi}{3}a^3k^2(\Omega)3\eta^{(3)}_{jklm}G_{ij}(\mathbf{r}_2,\mathbf{r}_0;\Omega)E_k(\mathbf{r}_0,\Omega)E_l(\mathbf{r}_0,\Omega)E^*_m(\mathbf{r}_0,\Omega))\ , \qquad (3.134) \\
E_i(\mathbf{r}_0,3\Omega) &= \frac{4\pi}{3}a^3k^2(3\Omega)\widehat{\eta}^{(1)}_{ij}G_R(3\Omega)E_j(\mathbf{r}_0,3\Omega) \\
&+ \frac{4\pi}{3}a^3k^2(3\Omega)\eta^{(1)}_{jk}G_{ij}(\mathbf{r}_0,\mathbf{r}_1;3\Omega)E_k(\mathbf{r}_1,3\Omega) \\
&+ \frac{4\pi}{3}a^3k^2(3\Omega)\eta^{(1)}_{jk}G_{ij}(\mathbf{r}_0,\mathbf{r}_2;3\Omega)E_k(\mathbf{r}_2,3\Omega) \\
&+ \frac{4\pi}{3}a^3k^2(3\Omega)\eta^{(3)}_{jklm}G_R(3\Omega)E_k(\mathbf{r}_0,\Omega)E_l(\mathbf{r}_0,\Omega)E_m(\mathbf{r}_0,\Omega))\ , \qquad (3.135)
\end{aligned}
$$

$$
\begin{aligned}
E_i(\mathbf{r}_1,3\Omega) &= \frac{4\pi}{3}a^3k^2(3\Omega)\widehat{\eta}^{(1)}_{jk}G_{ij}(\mathbf{r}_1,\mathbf{r}_0;3\Omega)E_k(\mathbf{r}_0,3\Omega) \\
&+ \frac{4\pi}{3}a^3k^2(3\Omega)\eta^{(1)}_{ij}G_R(3\Omega)E_j(\mathbf{r}_1,3\Omega) \\
&+ \frac{4\pi}{3}a^3k^2(3\Omega)\eta^{(1)}_{jk}G_{ij}(\mathbf{r}_1,\mathbf{r}_2;3\Omega)E_k(\mathbf{r}_2,3\Omega) \\
&+ \frac{4\pi}{3}a^3k^2(3\Omega)\eta^{(3)}_{jklm}G_{ij}(\mathbf{r}_1,\mathbf{r}_0;3\Omega)E_k(\mathbf{r}_0,\Omega)E_l(\mathbf{r}_0,\Omega)E_m(\mathbf{r}_0,\Omega)) \ , \quad (3.136) \\
E_i(\mathbf{r}_2,3\Omega) &= \frac{4\pi}{3}a^3k^2(3\Omega)\widehat{\eta}^{(1)}_{jk}G_{ij}(\mathbf{r}_2,\mathbf{r}_0;3\Omega)E_k(\mathbf{r}_0,3\Omega) \\
&+ \frac{4\pi}{3}a^3k^2(3\Omega)\eta^{(1)}_{jk}G_{ij}(\mathbf{r}_2,\mathbf{r}_1;3\Omega)E_k(\mathbf{r}_1,3\Omega) \\
&+ \frac{4\pi}{3}a^3k^2(3\Omega)\eta^{(1)}_{ij}G_R(3\Omega)E_k(\mathbf{r}_2,3\Omega) \\
&+ \frac{4\pi}{3}a^3k^2(3\Omega)\eta^{(3)}_{jklm}G_{ij}(\mathbf{r}_2,\mathbf{r}_0;3\Omega)E_k(\mathbf{r}_0,\Omega)E_l(\mathbf{r}_0,\Omega)E_m(\mathbf{r}_0,\Omega)) \ . \quad (3.137)
\end{aligned}
$$

Following the procedure indicated in Appendix B, the above equations can be solved perturbatively for the local fields.

Chapter 4

Second-harmonic Imaging in Random Media

4.1 Introduction

We consider imaging of N small nonlinear scatterers at locations $\boldsymbol{y}_j$, for $j = 1, \ldots, N_{\boldsymbol{y}}$, in a medium occupying a bounded domain $V \subset \mathbb{R}^m$ with piecewise smooth boundary ∂V, for $m \geq 2$. We restrict our attention to the case of second harmonic generation (SHG), but more general quadratic or cubic nonlinearities could be treated similarly. The data-gathering setup is illustrated in Fig. 4.1. The medium is illuminated by monochromatic plane waves at frequency ω, in the directions of the unit vectors $\boldsymbol{\theta}_j$, for $j = 1, \ldots, N_\theta$. These vectors belong to a cone C with axis along the unit vector $\boldsymbol{\vartheta}$ and small opening angle α. The illuminated part of the boundary of V is assumed smooth, with small curvature. Moreover, $\boldsymbol{\vartheta}$ is almost in the normal direction of the boundary of V, so the plane waves penetrate the domain. The resulting waves are measured by an array of receivers located at points $\boldsymbol{x}_s$ in the array aperture A, for $s = 1, \ldots, N_{\boldsymbol{x}}$. The array lies on one side of the boundary ∂V, and the scatterers are confined to a small region R near the center of V, at distance of order L from

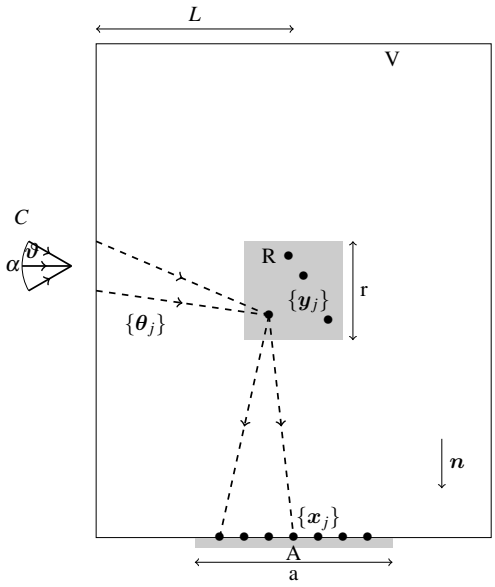

Figure 4.1: Setup of the imaging problem. Here A denotes the array, C the cone of incident directions, R the search region and V the imaging domain.

∂V. The linear size (diameter) of R is $r \ll L$. The linear size a of the array aperture A is small with respect to L, and the unit vector $\boldsymbol{n}$, pointing from the center of R to the center of A, is oriented at a nearly right angle with respect to the directions of the incident plane waves.

The imaging problem is to estimate the locations of the $N_{\boldsymbol{y}}$ nonlinear scatterers from the measurements at the array of the wave fields at frequency ω and the second harmonic 2ω. When the medium in V is known and non-scattering, we can image with coherent methods known as matched filtering in the signal processing [86] and radar literature [63], migration in seismic imaging [8], and backprojection in tomography [61]. These methods assume a linearized (Born) data model, and form an image by superposing the array measurements backpropagated in the known medium to points $\boldsymbol{y}^R$ in the imaging region R. The backpropagation is done analytically when the Green's function is known, or numerically, and its purpose is to compensate the phases of the measurements at points $\boldsymbol{y}^R$ near a scatterer location, so that they add constructively there, and the imaging function displays a peak.

We refer henceforth to such imaging as migration, and note that it is robust with respect to additive, Gaussian noise [9].

We are interested in imaging in heterogeneous media, containing numerous small inhomogeneities that interact with the waves. An inhomogeneity by itself is much weaker than any of the scatterers that we wish to image. However, when the waves propagate at a large enough distance L, the cumulative scattering of the inhomogeneities becomes significant and must be taken into account in imaging. This is difficult because in applications it is impossible to know the microstructure of the medium (the inhomogeneities) and we cannot hope to determine it from the data. Thus, imaging is carried in an uncertain environment. We incorporate this uncertainty in the data model by studying imaging in random media. The goal is to understand if it is possible to obtain robust estimates of the nonlinear scatterer locations from the measurements gathered by the array in one fixed realization of the random medium. Such robustness is known as statistical stability, and it means that the images vary little from one realization to another.

We study with analysis and numerical simulations imaging of nonlinear scatterers embedded in random media, in two regimes where cumulative scattering by the inhomogeneities causes large distortion of the wave field measured at the array. In physical terms, this means that the distance L is larger than the scattering mean free path S, which is the characteristic length scale on which the waves randomize [74]. The analysis uses a geometrical optics model [75], where the typical size ℓ of the inhomogeneities is large with respect to the wavelength λ, and $L > S > \ell$, so that the net scattering effects in the medium amount to large random wavefront distortions. In the numerics, we consider a regime with $\ell \sim \lambda$, where the waves interact more efficiently with the inhomogeneities. Because we are interested in coherent imaging, we take L smaller than the transport mean free path, which is the characteristic distance at which the waves forget their initial direction [74] due to scattering. At larger distances the waves are in a radiative transfer or diffusion regime, and only incoherent imaging

methods would work [4].

Both the analysis and numerical simulations show that the random distortions of the array measurements are very different than additive noise, and cannot be mitigated just by summation, as in migration. Ideally, the distortions would be mitigated by the backpropagation of the measurements in the true medium, as in time reversal [35]. However, this cannot be done in imaging because the medium is unknown. We can only backpropagate in the hypothetical reference medium with known and smooth wave velocity, as in migration.

The coherent interferometric (CINT) method [11, 12] is designed to mitigate random wave distortions by imaging with cross-correlations of the measurements instead of the measurements themselves. The CINT imaging function is given by the superposition of cross-correlations backpropagated in the reference medium to the imaging points $\boldsymbol{y}^R$. Its mathematical expression resembles that of the time reversal function analyzed in [70, 69], and its statistical stability and resolution are studied in [12, 13]. Unlike in time reversal, where super-resolution of focusing occurs, the stability of CINT comes at the expense of resolution, which is determined by two characteristic scales in the random medium: the decoherence frequency and length. These quantify the frequency offsets and receiver separations over which the waves become statistically uncorrelated, and must be taken into account in the calculation of the cross-correlations [11]. Moreover, they determine the conditions under which CINT is statistically stable. This can be formally understood as a consequence of the law of large numbers, due to the summation in the imaging function of many statistically uncorrelated terms, when the array aperture a is much larger than the decoherence length and the probing signals have bandwidth that is larger than the decoherence frequency [12].

In this chapter we study CINT imaging with time harmonic waves, so there is no summation over the frequencies. Such summation is essential for the statistical stability of CINT, and of time reversal for that matter [10], when scattering in the medium causes significant reverberations (delay spread). Here we consider weaker scattering regimes, like random

geometrical optics, where imaging can be done at a single frequency [13].

4.2 Formulation of the problem

In this section we describe the model of the data and define the migration and CINT imaging functions analyzed theoretically and numerically in the following sections.

4.2.1 Random model of the array data

We consider for simplicity scalar waves, modeled by Helmholtz's equation with random wave speed $c(\boldsymbol{x})$ defined by

$$\frac{1}{c^2(\boldsymbol{x})} = \frac{1}{c_o^2}\left[1 + 4\pi\eta(\boldsymbol{x})\right], \tag{4.1}$$

where c_o is the reference speed, assumed constant, and $\eta(\boldsymbol{x})$ is the linear susceptibility of the medium, a mean zero, stationary random process that is bounded almost surely so that the right hand side in (4.1) remains positive. We also assume that $\eta(\boldsymbol{x})$ is mixing [47, Section 4.6.2], which means in particular that its autocorrelation function is integrable. The $N_{\boldsymbol{y}}$ small scatterers embedded in the random medium are modeled by the linear susceptibility $\eta_1(\boldsymbol{x})$ and the nonlinear one $\eta_2(\boldsymbol{x})$. These functions have small amplitude and support concentrated near the points $\boldsymbol{y}_j$, for $j = 1, \ldots, N_{\boldsymbol{y}}$, and satisfy the weak nonlinearity assumption $\|\eta_2\|_\infty \ll \|\eta_1\|_\infty$, which allows us to write the following quadratic model of the waves as derived in Ch. 2:

$$\Delta u_1(\boldsymbol{x};\boldsymbol{\theta}) + k^2[1 + 4\pi\eta(\boldsymbol{x})]u_1(\boldsymbol{x};\boldsymbol{\theta}) = -4\pi k^2[\eta_1(\boldsymbol{x})u_1(\boldsymbol{x};\boldsymbol{\theta}) + 2\eta_2(\boldsymbol{x})u_2(\boldsymbol{x};\boldsymbol{\theta})u_1^*(\boldsymbol{x};\boldsymbol{\theta})]\ , \tag{4.2}$$

$$\Delta u_2(\boldsymbol{x};\boldsymbol{\theta}) + (2k)^2[1 + 4\pi\eta(\boldsymbol{x})]u_2(\boldsymbol{x};\boldsymbol{\theta}) = -4\pi(2k)^2[\eta_1(\boldsymbol{x})u_2(\boldsymbol{x};\boldsymbol{\theta}) + \eta_2(\boldsymbol{x})u_1^2(\boldsymbol{x};\boldsymbol{\theta})], \tag{4.3}$$

for $\boldsymbol{x} \in V$, with excitation by an incoming plane wave at frequency ω

$$u_1^{(i)}(\boldsymbol{x};\boldsymbol{\theta}) = e^{ik\boldsymbol{\theta}\cdot\boldsymbol{x}}, \tag{4.4}$$

where $k = \omega/c_o$ is the wavenumber, $\boldsymbol{\theta}$ is a unit wave vector, and the star denotes complex conjugate. We denote by $u_1(\boldsymbol{x};\boldsymbol{\theta})$ the generated wave at frequency ω, and by $u_2(\boldsymbol{x};\boldsymbol{\theta})$ the wave at the second harmonic 2ω. This is emitted at the nonlinear scatterers modeled by the susceptibility $\eta_2(\boldsymbol{x})$. The scattered waves $u_1(\boldsymbol{x};\boldsymbol{\theta}) - u_1^{(i)}(\boldsymbol{x};\boldsymbol{\theta})$ and $u_2(\boldsymbol{x};\boldsymbol{\theta})$ also satisfy outgoing boundary conditions at ∂V, because outside V the medium is homogeneous, with wave speed c_o.

As illustrated in Fig. 4.1, we consider N_θ illuminations of the medium by plane waves travelling in directions $\boldsymbol{\theta}_j$, for $j = 1, \ldots, N_\theta$, and denote by $\mathcal{U}$ the "ideal data set", given by the wave fields at the receivers,

$$\mathcal{U} = \{u_1(\boldsymbol{x}_s, \boldsymbol{\theta}_q),\ u_2(\boldsymbol{x}_s, \boldsymbol{\theta}_q), \quad s = 1, \ldots, N_{\boldsymbol{x}},\ \ q = 1, \ldots, N_\theta\}\,. \tag{4.5}$$

Note that u_1 and u_2 are random fields, and the actual array measurements are for a single realization of the medium. These are the data used to form images, as explained in the next sections. We only use the set $\mathcal{U}$ for the statistical analysis of the imaging functions.

4.2.2 Migration imaging

The migration image formation assumes that the medium in V is homogeneous ($\eta \equiv 0$), and that the recorded waves scatterer only once at the unknown scatterers. If the medium were homogeneous, we could write the solution of (4.2)-(4.3), denoted by $u_{1,o}$ and $u_{2,o}$, using

Lippmann-Schwinger's equation

$$u_{1,o}(\boldsymbol{x};\boldsymbol{\theta}) = u_1^{(i)}(\boldsymbol{x};\boldsymbol{\theta}) + k^2 \int_V d\boldsymbol{y}\, G_o(\boldsymbol{x},\boldsymbol{y};\omega)[\eta_1(\boldsymbol{y})u_{1,o}(\boldsymbol{y};\boldsymbol{\theta}) + 2\eta_2(\boldsymbol{y})u_{2,o}(\boldsymbol{y};\boldsymbol{\theta})u^*_{1,o}(\boldsymbol{y};\boldsymbol{\theta})] \ , \tag{4.6}$$

$$u_{2,o}(\boldsymbol{x};\boldsymbol{\theta}) = (2k)^2 \int_V d\boldsymbol{y}\, G_o(\boldsymbol{x},\boldsymbol{y};2\omega)[\eta_1(\boldsymbol{y})u_{2,o}(\boldsymbol{y};\boldsymbol{\theta}) + \eta_2(\boldsymbol{y})u^2_{1,o}(\boldsymbol{y};\boldsymbol{\theta})] \ , \tag{4.7}$$

where G_o is the outgoing Green's function multiplied by 4π. It is given by

$$G_o(\boldsymbol{x},\boldsymbol{y};\omega) = \frac{e^{ik|\boldsymbol{x}-\boldsymbol{y}|}}{|\boldsymbol{x}-\boldsymbol{y}|} \tag{4.8}$$

in three dimensions, and by

$$G_o(\boldsymbol{x},\boldsymbol{y};\omega) = i\pi H_0^{(1)}(k|\boldsymbol{x}-\boldsymbol{y}|) \tag{4.9}$$

in two dimensions, where $H_0^{(1)}$ is the Hankel function of the first kind.

The linear forward model for the scattered waves, assumed equal to $u_{1,o} - u_1^{(i)}$ and $u_{2,o}$, is obtained from the Born approximation of (4.6)-(4.7). Since we have two wave fields and two unknown susceptibilities, we introduce two forward mappings

$$F_j[\eta_j](\boldsymbol{x}_s,\boldsymbol{\theta}_q) = (jk)^2 \int_V d\boldsymbol{y}\, \eta_j(\boldsymbol{y}) G_o(\boldsymbol{x}_s,\boldsymbol{y};j\omega) e^{ijk\boldsymbol{\theta}_q\cdot\boldsymbol{y}}. \tag{4.10}$$

These take the susceptibilities η_j to the the scattered waves at the receiver sensors indexed by $s = 1,\ldots,N_{\boldsymbol{x}}$, for the illuminations indexed by $q = 1,\ldots,N_\theta$, and frequencies $j\omega$, for $j = 1, 2$.

Let us denote by d_1 and d_2 the array data, given by

$$d_1(\boldsymbol{x}_s, \boldsymbol{\theta}_q) = u_1^{(real)}(\boldsymbol{x}_s; \boldsymbol{\theta}_q) - u_1^{(i)}(\boldsymbol{x}_s; \boldsymbol{\theta}_q) + \mathfrak{n}_1(\boldsymbol{x}_s; \boldsymbol{\theta}_q), \tag{4.11}$$

$$d_2(\boldsymbol{x}_s, \boldsymbol{\theta}_q) = u_2^{(real)}(\boldsymbol{x}_s; \boldsymbol{\theta}_q) + \mathfrak{n}_2(\boldsymbol{x}_s; \boldsymbol{\theta}_q), \qquad s = 1, \ldots, N_{\boldsymbol{x}}, \quad q = 1, \ldots, N_\theta, \tag{4.12}$$

where $u_j^{(real)}$, for $j = 1, 2$, denote the waves in the real medium, one realization of the random model, and $\mathfrak{n}_1$ and $\mathfrak{n}_2$ model additive Gaussian noise (due to the measurement of the data), uncorrelated and identically distributed. Using the forward mappings (4.10), we formulate the linear output least squares minimizations

$$\eta_j^{LS} = \arg\min_{\eta_j} \|d_j - F_j[\eta_j]\|_2^2, \tag{4.13}$$

that estimate the unknown susceptibilities η_j by η_j^{LS}, for $j = 1, 2$. The minimizers η_j^{LS} satisfy the normal equations

$$F_j^H F_j[\eta_j^{LS}](\boldsymbol{y}^R) = F_j^H[d_j](\boldsymbol{y}^R) = (jk)^2 \sum_{s=1}^{N_{\boldsymbol{x}}} \sum_{q=1}^{N_\theta} G_o^\star(\boldsymbol{y}^R, \boldsymbol{x}_s; j\omega) e^{-ijk\boldsymbol{\theta}_q \cdot \boldsymbol{y}^R} d_j(\boldsymbol{x}_s, \boldsymbol{\theta}_q), \tag{4.14}$$

where the index H denotes the adjoint with respect to the Euclidian inner product, and the star denotes complex conjugate. The integral (normal) operators $F_j^H F_j$ map η_j^{LS} to

$$F_j^H F_j[\eta_j^{LS}](\boldsymbol{y}^R) = \int_V d\boldsymbol{y}\, \eta_j^{LS}(\boldsymbol{y}) \mathcal{K}_j(\boldsymbol{y}^R, \boldsymbol{y}), \tag{4.15}$$

and their integral kernels

$$\mathcal{K}_j(\boldsymbol{y}^R, \boldsymbol{y}) = (jk)^4 \sum_{s=1}^{N_{\boldsymbol{x}}} \sum_{q=1}^{N_\theta} G_o(\boldsymbol{x}_s, \boldsymbol{y}; j\omega) G_o^\star(\boldsymbol{y}^R, \boldsymbol{x}_s; j\omega) e^{ijk\boldsymbol{\theta}_q \cdot (\boldsymbol{y} - \boldsymbol{y}^R)} \tag{4.16}$$

are equal, up to constant factors, to the time reversal point spread functions at frequencies

$j\omega$, for $j = 1, 2$.

In our setting, the kernels (4.16) peak along the diagonal $\boldsymbol{y}^R = \boldsymbol{y}$, so we can replace formally the left hand side in (4.14) by $\eta_j^{LS}(\boldsymbol{y}^R)$ multiplied by some constant. In imaging we are interested in the support of the sussceptibility, so we can neglect the constants and obtain from (4.16) the migration imaging functions

$$\mathcal{I}_j^M(\boldsymbol{y}^R) = \sum_{s=1}^{N_{\boldsymbol{x}}} \sum_{q=1}^{N_\theta} G_o^\star(\boldsymbol{y}^R, \boldsymbol{x}_s; j\omega) e^{-ijk\boldsymbol{\theta}_q \cdot \boldsymbol{y}^R} d_j(\boldsymbol{x}_s, \boldsymbol{\theta}_q), \qquad j = 1, 2. \tag{4.17}$$

Because $k|\boldsymbol{y}^R - \boldsymbol{x}_s| \gg 1$ and the array aperture a is much smaller than $|\boldsymbol{x}_s - \boldsymbol{y}^R| = O(L)$ for $\boldsymbol{y}^R$ in the search region R (recall Fig. 4.1), we can approximate the Green's function in (4.17) by

$$G_0(\boldsymbol{y}^R, \boldsymbol{x}_s; j\omega) \approx C_j e^{ijk|\boldsymbol{y}^R - \boldsymbol{x}_s|}, \tag{4.18}$$

for constant C_j, and $j = 1, 2$. This is both in three and two dimensions, as follows from the asymptotics of the Hankel function in (4.9). Thus, the right hand side in (4.17) is the superposition of the measurements, with phases compensated relative to the imaging point $\boldsymbol{y}^R$. The superposition is needed for focusing the image and averaging out the noise. When $\boldsymbol{y}^R$ is close to a scatterer location, and the medium in V is either homogeneous or has negligible effect on the waves so that their propagation is approximated by G_o, the phases in the coherent part of d_j are cancelled approximately. Then, the terms add constructively and the imaging function displays a peak.

We are interested in imaging in stronger scattering media, where G_o is not a good model for wave propagation, and the migration imaging function (4.17) either does not focus or gives spurious peaks at locations that may not be close to the scatterers.

4.2.3 Coherent interferometric imaging

Let us define the backpropagated data to the imaging point $\boldsymbol{y}^R$ by

$$b_j(\boldsymbol{x}_s, \boldsymbol{\theta}_q, \boldsymbol{y}^R) = d_j(\boldsymbol{x}_s, \boldsymbol{\theta}_q) G_o^\star(\boldsymbol{y}^R, \boldsymbol{x}_s; j\omega) e^{-ijk\boldsymbol{\theta}_q \cdot \boldsymbol{y}^R}, \qquad s = 1, \ldots, N_{\boldsymbol{x}},\ q = 1, \ldots, N_\theta,\ j = 1, 2. \tag{4.19}$$

The CINT imaging function is formed by superposition of local cross-correlations of b_j, as we now explain. By local we mean that we cross-correlate only at nearby receivers and for nearby incoming illuminations

$$|\boldsymbol{x}_s - \boldsymbol{x}_{s'}| \leq X, \qquad |\boldsymbol{\theta}_q - \boldsymbol{\theta}_{q'}| \leq \Theta, \tag{4.20}$$

where Θ and X are scales that account for the decorrelation of the waves due to scattering in the random medium [11]. Intuitively, waves travelling along very different trajectories interact with different parts of the random medium, assumed to have no long range correlations (i.e., mixing), so they are decorrelated. Note that in practice the decorrelation parameters are usually unknown, so they must be estimated from the data, either using statistical data analysis or by optimization, which seeks to improve the focusing of CINT images, as explained in [11]. We denote henceforth the true decorrelation parameters in the medium by $X_{d,j}$ and Θ_d, to distinguish them from those used in the calculation of the cross-correlations, and assume that

$$X/X_{d,j} = O(1), \quad \Theta/\Theta_d = O(1). \tag{4.21}$$

We also refer to $X_{d,j}$ as decoherence lengths and Θ_d as decoherence angles. Note that the decoherence length is proportional to the wavelength, so it depends on j. We suppress for simplicity of notation the dependence of the thresholding parameter X on j.

Let us introduce the center and offset sensor locations

$$\overline{\boldsymbol{x}}_{ss'} = (\boldsymbol{x}_s + \boldsymbol{x}_{s'})/2, \qquad \widetilde{\boldsymbol{x}}_{ss'} = \boldsymbol{x}_s - \boldsymbol{x}_{s'}, \qquad s, s' = 1, \ldots, N_{\boldsymbol{x}}, \tag{4.22}$$

and direction vectors

$$\overline{\boldsymbol{\theta}}_{qq'} = (\boldsymbol{\theta}_q + \boldsymbol{\theta}'_q)/2, \qquad \widetilde{\boldsymbol{\theta}}_{qq'} = \boldsymbol{\theta}_q - \boldsymbol{\theta}_{q'}, \qquad q, q' = 1, \ldots, N_\theta. \tag{4.23}$$

We count the center variables by $\overline{s} = 1, \ldots, \overline{N}_{\boldsymbol{x}}$ and $\overline{q} = 1, \ldots, \overline{N}_{\boldsymbol{\theta}}$, and the offsets by $\widetilde{s} = 1, \ldots, \widetilde{N}_{\boldsymbol{x}}$ and $\widetilde{q} = 1, \ldots, \widetilde{N}_{\boldsymbol{\theta}}$. The local cross-correlations are

$$\mathcal{C}_j(\overline{\boldsymbol{x}}_{\overline{s}}, \overline{\boldsymbol{\theta}}_{\overline{q}}, \boldsymbol{y}^R) = \sum_{\widetilde{s}=1}^{\widetilde{N}_{\boldsymbol{x}}} \sum_{\widetilde{q}=1}^{\widetilde{N}_\theta} \Phi\Big(\frac{\widetilde{\boldsymbol{x}}_{\widetilde{s}}}{X}\Big) \Phi\Big(\frac{\widetilde{\boldsymbol{\theta}}_{\widetilde{q}}}{\Theta}\Big) b_j\Big(\overline{\boldsymbol{x}}_{\overline{s}} + \frac{\widetilde{\boldsymbol{x}}_{\widetilde{s}}}{2}, \overline{\boldsymbol{\theta}}_{\overline{q}} + \frac{\widetilde{\boldsymbol{\theta}}_{\widetilde{q}}}{2}, \boldsymbol{y}^R\Big) b_j^\star\Big(\overline{\boldsymbol{x}}_{\overline{r}} - \frac{\widetilde{\boldsymbol{x}}_{\widetilde{s}}}{2}, \overline{\boldsymbol{\theta}}_{\overline{q}} - \frac{\widetilde{\boldsymbol{\theta}}_{\widetilde{q}}}{2}, \boldsymbol{y}^R\Big), \tag{4.24}$$

where Φ is a smooth window of support of order one, used to limit the receiver and director offsets by X and Θ.

The CINT imaging function is formed by the superposition of (4.24). To explain why, consider the model backpropagated data in the reference medium,

$$b_{j,o}(\boldsymbol{x}_s, \boldsymbol{\theta}_q, \boldsymbol{y}^R) = (jk)^2 \int_V d\boldsymbol{y}\, \eta_j(\boldsymbol{y}) G_o(\boldsymbol{y}, \boldsymbol{x}_s; j\omega) G_o^\star(\boldsymbol{y}^R, \boldsymbol{x}_s; j\omega) e^{ijk\boldsymbol{\theta}_q \cdot (\boldsymbol{y} - \boldsymbol{y}^R)}, \tag{4.25}$$

and use it to form the cross-correlations $\mathcal{C}_{j,o}$, the analogues of (4.24). If we had a point scatterer at imaging point $\boldsymbol{y}^R$, modeled by $\eta_j(\boldsymbol{y}) = \langle \eta_{j,\boldsymbol{y}^R} \rangle\, \delta(\boldsymbol{y} - \boldsymbol{y}^R)$, we would obtain that

$$\mathcal{C}_{j,o}(\overline{\boldsymbol{x}}_{\overline{s}}, \overline{\boldsymbol{\theta}}_{\overline{q}}, \boldsymbol{y}^R) = \rho_j(\boldsymbol{y}^R) \mathcal{L}_j(\overline{\boldsymbol{x}}_{\overline{s}}, \overline{\boldsymbol{\theta}}_{\overline{q}}, \boldsymbol{y}^R), \tag{4.26}$$

with

$$\rho_j(\boldsymbol{y}^R) = (jk)^4 \left| \langle \eta_{j,\boldsymbol{y}^R} \rangle \right|^2.$$

and

$$\mathcal{L}_j(\overline{\boldsymbol{x}}_{\overline{s}}, \overline{\boldsymbol{\theta}}_{\overline{q}}, \boldsymbol{y}^R) = \sum_{\widetilde{s}=1}^{\widetilde{N}_{\boldsymbol{x}}} \sum_{\widetilde{q}=1}^{\widetilde{N}_\theta} \Phi\Big(\frac{\widetilde{\boldsymbol{x}}_{\widetilde{s}}}{X}\Big)\Phi\Big(\frac{\widetilde{\boldsymbol{\theta}}_{\widetilde{q}}}{\Theta}\Big)\Big|G_o\Big(\overline{\boldsymbol{x}}_{\overline{s}}+\frac{\widetilde{\boldsymbol{x}}_{\widetilde{s}}}{2}, \overline{\boldsymbol{\theta}}_{\overline{q}}+\frac{\widetilde{\boldsymbol{\theta}}_{\widetilde{q}}}{2}, \boldsymbol{y}^R\Big)\Big|^2\Big|G_o\Big(\overline{\boldsymbol{x}}_{\overline{s}}-\frac{\widetilde{\boldsymbol{x}}_{\widetilde{s}}}{2}, \overline{\boldsymbol{\theta}}_{\overline{q}}-\frac{\widetilde{\boldsymbol{\theta}}_{\widetilde{q}}}{2}, \boldsymbol{y}^R\Big)\Big|^2. \tag{4.27}$$

Let then $\mathcal{M}_j$ be the linear mapping that takes ρ_j to the model cross-correlations (4.26),

$$\mathcal{M}_j[\rho](\overline{\boldsymbol{x}}_{\overline{s}}, \overline{\boldsymbol{\theta}}_{\overline{q}}, \boldsymbol{y}^R) = \rho(\boldsymbol{y}^R)\mathcal{L}_j(\overline{\boldsymbol{x}}_{\overline{s}}, \overline{\boldsymbol{\theta}}_{\overline{q}}, \boldsymbol{y}^R), \tag{4.28}$$

and formulate the least squares problem

$$\arg\min_{\rho_j} \sum_{\overline{s}=1}^{\overline{N}_{\boldsymbol{x}}} \sum_{\overline{q}=1}^{\overline{N}_\theta} \int_R d\boldsymbol{y}^R \left|\mathcal{C}_j(\overline{\boldsymbol{x}}_{\overline{s}}, \overline{\boldsymbol{\theta}}_{\overline{q}}, \boldsymbol{y}^R) - \mathcal{M}_j[\rho](\overline{\boldsymbol{x}}_{\overline{s}}, \overline{\boldsymbol{\theta}}_{\overline{q}}, \boldsymbol{y}^R)\right|^2, \qquad j = 1, 2. \tag{4.29}$$

As in the case of migration, this involves a linearization in the unknown susceptibility, as it assumes that the contribution of multiple scatterers is additive. The minimizer solves the normal equations

$$\mathcal{M}_j^H \mathcal{M}_j[\rho_j](\boldsymbol{y}^R) = \mathcal{M}_j^H[\mathcal{C}_j](\boldsymbol{y}^R) = \sum_{\overline{s}=1}^{\overline{N}_{\boldsymbol{x}}} \sum_{\overline{q}=1}^{\overline{N}_\theta} \mathcal{C}_j(\overline{\boldsymbol{x}}_{\overline{s}}, \overline{\boldsymbol{\theta}}_{\overline{q}}, \boldsymbol{y}^R)\mathcal{L}_j(\overline{\boldsymbol{x}}_{\overline{s}}, \overline{\boldsymbol{\theta}}_{\overline{q}}, \boldsymbol{y}^R), \tag{4.30}$$

which have a simple form in our setting, where the Green's function may be approximated as in (4.18), and the mapping $\mathcal{M}_j$ becomes a multiple of the indentity

$$\mathcal{M}_j[\rho](\overline{\boldsymbol{x}}_{\overline{s}}, \overline{\boldsymbol{\theta}}_{\overline{q}}, \boldsymbol{y}^R) \approx C_j \rho_j(\boldsymbol{y}^R), \tag{4.31}$$

with redefined constants C_j. Neglecting the constants, we obtain from (4.30) the CINT imaging function

$$\mathcal{I}_j^{CINT}(\boldsymbol{y}^R) = \sum_{\overline{s}=1}^{\overline{N}_s} \sum_{\overline{q}=1}^{\overline{N}_\theta} \mathcal{C}_j(\overline{\boldsymbol{x}}_{\overline{s}}, \overline{\boldsymbol{\theta}}_{\overline{q}}, \boldsymbol{y}^R). \tag{4.32}$$

Remark: Model (4.25) assumes the complete removal of the direct waves that have not interacted with the scatterers that we wish to image. In homogeneous media this is achieved by the subtraction of the incident wave from the measurements. However, in random media the direct wave reaching the array is not close to $u_1^{(i)}$, so the subtraction in (4.11) does not achieve its purpose. The unwanted direct wave may be removed in our geometrical setting if the array of sensors can differentiate among arrival directions and the scattering medium is not strong enough to mix the directions of the waves, as is the case in the geometrical optics regime considered in our analysis. Such differentiation may be achieved for example by an approximate plane wave decomposition of the measurements, using a discrete Fourier transform with respect to the coordinates of the receivers in the surface of the array. We do not make any differentiation here, and work instead with (4.12), to illustrate the effect of the unwanted direct arrivals on the imaging of η_1. This problem does not extend to the second harmonic wave, which is emitted at the nonlinear scatterers.

4.3 Analysis of the migration and CINT point spread functions

In this section we analyze the migration and CINT imaging functions (4.17) and (4.32), for a point-like scatterer in the random medium, in a geometrical optics regime with large random wavefront fluctuations. The analysis is basically the same in two and three dimensions, so we focus attention on the three dimensional case.

We model the susceptibility of the medium by

$$4\pi\eta(\boldsymbol{x}) = \sigma\mu\left(\frac{\boldsymbol{x}}{\ell}\right), \tag{4.33}$$

using a random, stationary process μ of dimensionless argument, with mean zero and Gaus-

sian autocorrelation

$$\mathbb{E}[\mu(\boldsymbol{h})\mu(\mathbf{0})] = e^{-\frac{|\boldsymbol{h}|^2}{2}}. \tag{4.34}$$

This autocorrelation is convenient for the analysis, because it allows us to obtain explicit expressions of the statistical moments of the imaging functions. The process μ is normalized so that the maximum of (4.34) equals one, and

$$\int_{\mathbb{R}^3} d\boldsymbol{x}\, \mathbb{E}\left[\mu\left(\frac{\boldsymbol{x}}{\ell}\right)\mu(\mathbf{0})\right] = (2\pi)^{3/2}\ell^3.$$

Thus, the scale σ in (4.33) quantifies the amplitude of the random fluctuations of the susceptibility, and ℓ quantifies the correlation length, the typical size of the inhomogeneities.

We begin with the scaling in section 4.3.1 and then describe in section 4.3.2 the random geometrical optics model of wave propagation. We base our imaging on the linearized data model defined in section 4.3.3, justified by the weak nonlinearity. With this model we calculate in sections 4.3.4 and 4.3.5 the expectation and variance of the migration and CINT images, in order to study their resolution and statistical stability.

4.3.1 Scaling

Let $\boldsymbol{y}$ be the location of the point-like scatterer, assumed to lie near the center of the domain V, and let L to be the distance between $\boldsymbol{y}$ and the center of the array, so that

$$|\boldsymbol{x}_s - \boldsymbol{y}| \approx L, \qquad |\boldsymbol{y} - \boldsymbol{y}^{(i)}(\boldsymbol{\theta}_q)| \approx L, \qquad s = 1, \ldots, N_{\boldsymbol{x}}, \quad q = 1, \ldots, N_\theta,$$

where we denote by $\boldsymbol{y}^{(i)}(\boldsymbol{\theta}_q)$ the incident point on ∂V of the ray entering the domain in the direction $\boldsymbol{\theta}_q$ and passing through $\boldsymbol{y}$. The unit vector $\boldsymbol{n}$ points from $\boldsymbol{y}$ to the center of the array aperture A, and for simplicity we suppose that the array is square planar, and orthogonal to $\boldsymbol{n}$. We take the origin of the system of coordinates at the center of A, with

one axis parallel to $\boldsymbol{n}$, so that we can write henceforth

$$\boldsymbol{x} = (\boldsymbol{x}_\perp, 0), \quad \forall\, \boldsymbol{x} \in A, \tag{4.35}$$

with two dimensional vectors $\boldsymbol{x}_\perp$ in the plane of the array.

The random geometrical optics wave propagation model described in the next section applies to the regime of separation of scales

$$\lambda \ll \ell \ll L, \tag{4.36}$$

with small amplitude σ of the fluctuations of the susceptibility, satisfying

$$\sigma \ll (\ell/L)^{3/2}, \qquad \sigma \ll \sqrt{\lambda \ell}/L. \tag{4.37}$$

As shown in [75, Chapter 1], the first bound in (4.37) is needed so that the waves propagate along straight rays, and the variance of the amplitude of the Green's function is negligible. The second bound ensures that the second order (in σ) corrections of the travel time are negligible. We estimate in the next section that the standard deviation of the random travel time fluctuations is of order $\sigma\sqrt{\ell L}/c_o$, so to see large wavefront distortions we assume

$$\sigma \gg \frac{\lambda}{\sqrt{\ell L}}. \tag{4.38}$$

This is consistent with (4.37) when $\ell \gg \sqrt{\lambda L}$.

We already stated that the array aperture a is small with respect to L. To simplify the

calculations, we consider a paraxial regime[1] with

$$a \ll (\lambda L^3)^{1/4} \ll L. \tag{4.39}$$

The illumination directions belong to the cone C with axis along the unit vector ϑ that is assumed orthogonal to $\boldsymbol{n}$. The opening angle α of the cone satisfies

$$\alpha = O\left(\frac{a}{L}\right). \tag{4.40}$$

The search region R is centered at $\boldsymbol{y}$. It is a cube of side length r satisfying

$$r \ll \frac{\lambda L^2}{a^2} \ll a, \tag{4.41}$$

so that we can use the following approximation of the Green's function in the reference medium

$$G_o(\boldsymbol{x}, \boldsymbol{y}^R; j\omega) \approx \frac{1}{L} \exp\left[ijk\left(y_\parallel^R + \frac{|\boldsymbol{x}_\perp - \boldsymbol{y}_\perp^R|^2}{2L}\right)\right], \qquad \forall\, \boldsymbol{y}^R \in R. \tag{4.42}$$

Here we wrote $\boldsymbol{y}^R = (\boldsymbol{y}_\perp^R, y_\parallel^R)$, with $y_\parallel^R$ equal to the distance of $\boldsymbol{y}^R$ from the array, along $\boldsymbol{n}$, and $\boldsymbol{y}_\perp^R$ the two dimensional vector orthogonal to $\boldsymbol{n}$. With this notation we note that $y_\parallel = L$.

We expect from the analysis in [13] that to obtain statistically stable CINT images we need $a \gg \ell$. There are many scalings that allow $\sqrt{\lambda L} \ll \ell \ll a$, so we choose one that simplifies slightly the moment calculations of the random travel time corrections. Specifically,

[1] Imaging may be done with larger apertures and wider opening angles of the illumination cone C, but the expressions of the imaging functions become complicated. The analysis presented here may be used in such cases, after segmenting the aperture and illumination cone in subsets satisfying our assumptions. The results apply for each subset, and the images are obtained by summation over the subsets.

we consider the length scale ordering

$$\lambda \ll \sqrt{\lambda L} \ll \ell \ll (\lambda L^2)^{1/3} \ll a \ll (\lambda L^3)^{1/4} \ll L, \tag{4.43}$$

and gather the assumptions (4.37)-(4.38) on σ in

$$\frac{\lambda}{\sqrt{\ell L}} \ll \sigma \ll \frac{\sqrt{\lambda \ell}}{L}. \tag{4.44}$$

Here we used that

$$\frac{(\ell/L)^{3/2}}{\sqrt{\lambda\ell}/L} = \frac{\ell}{\sqrt{\lambda L}} \gg 1,$$

and we note that (4.43) is consistent because

$$\frac{\sqrt{\lambda L}}{(\lambda L^2)^{1/3}} = \left(\frac{\lambda}{L}\right)^{1/6} \ll 1, \qquad \frac{(\lambda L^2)^{1/3}}{(\lambda L^3)^{1/4}} = \left(\frac{\lambda}{L}\right)^{1/12} \ll 1.$$

4.3.2 The random geometrical optics model

We refer to [75, Chapter 1] and [13, Appendix A] for the derivation of the geometrical optics model. It holds in the scaling regime defined by (4.43)-(4.44).

The geometrical optics approximation of the Green's function, denoted by G, is

$$G(\boldsymbol{x}, \boldsymbol{y}; j\omega) = G_o(\boldsymbol{x}, \boldsymbol{y}; j\omega) e^{ijk\nu(\boldsymbol{x},\boldsymbol{y})}, \qquad \forall\, \boldsymbol{x} \in A, \tag{4.45}$$

where G_o is given by (4.8), and the random phase ν is given by the integral of the fluctuations μ along the straight rays

$$\nu(\boldsymbol{x}, \boldsymbol{y}) = \frac{\sigma|\boldsymbol{x} - \boldsymbol{y}|}{2} \int_0^1 dt\, \mu\Big(\frac{(1-t)\boldsymbol{y}}{\ell} + \frac{t\boldsymbol{x}}{\ell}\Big). \tag{4.46}$$

The approximation of the direct wave, which enters the medium as the plane wave (4.4), is

$$u_1^{(d)}(\boldsymbol{x};\boldsymbol{\theta}) = e^{ik\boldsymbol{\theta}\cdot\boldsymbol{x}+ik\gamma(\boldsymbol{x},\boldsymbol{\theta})}, \tag{4.47}$$

with random phase

$$\gamma(\boldsymbol{x},\boldsymbol{\theta}) = \frac{\sigma|\boldsymbol{x}-\boldsymbol{x}^{(i)}(\boldsymbol{\theta})|}{2}\int_0^1 dt\,\mu\Big(\frac{(1-t)\boldsymbol{x}}{\ell}+\frac{t\boldsymbol{x}^{(i)}(\boldsymbol{\theta})}{\ell}\Big). \tag{4.48}$$

Because

$$|\boldsymbol{x}-\boldsymbol{y}|\approx L,\quad \forall\,\boldsymbol{x}\in A,\ \text{ and }\ |\boldsymbol{x}-\boldsymbol{x}^{(i)}(\boldsymbol{\theta})| = O(L),\quad \forall\,\boldsymbol{x}\in A\cup\{\boldsymbol{y}\},$$

we can use [13, Lemma 3.1] to conclude that the normalized processes

$$\widetilde{\nu}(\boldsymbol{x},\boldsymbol{y}) = \frac{2}{(2\pi)^{1/4}}\frac{\nu(\boldsymbol{x},\boldsymbol{y})}{\sigma\sqrt{\ell|\boldsymbol{x}-\boldsymbol{y}|}},\qquad \widetilde{\gamma}(\boldsymbol{x},\boldsymbol{\theta}) = \frac{2}{(2\pi)^{1/4}}\frac{\gamma(\boldsymbol{x},\boldsymbol{\theta})}{\sigma\sqrt{\ell|\boldsymbol{x}-\boldsymbol{x}^{(i)}(\boldsymbol{\theta})|}}, \tag{4.49}$$

converge in distribution to Gaussian ones in the limit $\ell/L\to 0$. Obviously, (4.49) are mean zero, with variance

$$\mathbb{E}[\widetilde{\nu}^2(\boldsymbol{x},\boldsymbol{y})] = \frac{|\boldsymbol{x}-\boldsymbol{y}|}{\ell\sqrt{2\pi}}\int_0^1 dt\int_0^1 dt'\exp\left[-\frac{(t-t')^2|\boldsymbol{x}-\boldsymbol{y}|^2}{2\ell^2}\right]\approx 1, \tag{4.50}$$

$$\mathbb{E}[\widetilde{\gamma}^2(\boldsymbol{x},\boldsymbol{\theta})] = \frac{|\boldsymbol{x}-\boldsymbol{x}^{(i)}(\boldsymbol{\theta})|}{\ell\sqrt{2\pi}}\int_0^1 dt\int_0^1 dt'\exp\left[-\frac{(t-t')^2|\boldsymbol{x}-\boldsymbol{x}^{(i)}(\boldsymbol{\theta})|^2}{2\ell^2}\right]\approx 1, \tag{4.51}$$

where we used (4.34). Thus, the variance of the random phase fluctuations in (4.45) and

(4.47) is

$$k^2\mathbb{E}[\nu^2(\boldsymbol{x},\boldsymbol{y})] \approx \frac{\sqrt{2\pi}\sigma^2k^2\ell|\boldsymbol{x}-\boldsymbol{y}|}{4} = O\left(\sigma^2\frac{\ell L}{\lambda^2}\right), \tag{4.52}$$

$$k^2\mathbb{E}[\gamma^2(\boldsymbol{x},\boldsymbol{\theta})] \approx \frac{\sqrt{2\pi}\sigma^2k^2\ell|\boldsymbol{x}-\boldsymbol{x}^{(i)}(\boldsymbol{\theta})|}{4} = O\left(\sigma^2\frac{\ell L}{\lambda^2}\right), \tag{4.53}$$

and we conclude from the assumption (4.44) that cumulative scattering in the medium has a significant net effect on the waves, manifested as large random wavefront distortions.

Randomization of the waves

Because the processes (4.49) are approximately Gaussian for $\ell \ll L$, we can approximate the expectation of the Green's function (4.45) by

$$\begin{aligned}\mathbb{E}\left[G(\boldsymbol{x},\boldsymbol{y};j\omega)\right] &= G_o(\boldsymbol{x},\boldsymbol{y};j\omega)\mathbb{E}\left[\exp\left[ijk\nu(\boldsymbol{x},\boldsymbol{y})\right]\right] \\ &\approx G_o(\boldsymbol{x},\boldsymbol{y};j\omega)\exp\left[-\frac{(jk)^2\mathbb{E}[\nu^2(\boldsymbol{x},\boldsymbol{y})]}{2}\right] \\ &= G_o(\boldsymbol{x},\boldsymbol{y};j\omega)\exp\left[-\frac{|\boldsymbol{x}-\boldsymbol{y}|}{S_j}\right],\end{aligned} \tag{4.54}$$

where S_j are the scattering mean free paths

$$S_j = \frac{8}{\sqrt{2\pi}\sigma^2(jk)^2\ell}, \qquad j = 1, 2. \tag{4.55}$$

The scaling relation (4.38) ensures that $S_j \ll |\boldsymbol{x}-\boldsymbol{y}| \approx L$, so the mean Green's function is exponentially small. Clearly,

$$|G(\boldsymbol{x},\boldsymbol{y};j\omega)| = |G_o(\boldsymbol{x},\boldsymbol{y};j\omega)|,$$

so the standard deviation is

$$\mathrm{std}\left[G(\boldsymbol{x},\boldsymbol{y};j\omega)\right]=\sqrt{\left|G_o(\boldsymbol{x},\boldsymbol{y};j\omega)\right|^2-\left|\mathbb{E}\left[G(\boldsymbol{x},\boldsymbol{y};j\omega)\right]\right|^2}\approx\left|G_o(\boldsymbol{x},\boldsymbol{y};j\omega)\right|. \tag{4.56}$$

This is much larger than (4.54), so the wave is randomized by scattering in the random medium. In our regime the randomization arises due to the large phase $jk\nu$ in (4.45).

A similar calculation for the direct wave (4.47) gives

$$\begin{aligned}\mathbb{E}\left[u_1^{(d)}(\boldsymbol{x};\boldsymbol{\theta})\right]&=e^{ik\boldsymbol{\theta}\cdot\boldsymbol{x}}\mathbb{E}\left[\exp\left[ik\gamma(\boldsymbol{x},\boldsymbol{\theta})\right]\right]\\&\approx u_1^{(i)}(\boldsymbol{x};\boldsymbol{\theta})\exp\left[-\frac{k^2\mathbb{E}[\gamma^2(\boldsymbol{x},\boldsymbol{\theta})]}{2}\right]\\&=\exp\left[ik\boldsymbol{\theta}\cdot\boldsymbol{x}-\frac{|\boldsymbol{x}-\boldsymbol{x}^{(i)}(\boldsymbol{\theta})|}{S_1}\right],\end{aligned} \tag{4.57}$$

and since $|\boldsymbol{x}-\boldsymbol{x}^{(i)}(\boldsymbol{\theta})|=O(L)\gg S_1$ and $\left|u_1^{(d)}(\boldsymbol{x};\boldsymbol{\theta})\right|=1$, we conclude that $u_1^{(d)}$ is randomized and therefore very different than the incident plane wave $u_1^{(i)}$.

Decorrelation of the waves

The statistical moments of the wave fields are determined by the second moments of the phases (4.46) and (4.48), which are approximately Gaussian. These moments are derived in appendix 4.A.1, using the assumptions (4.43)-(4.44). We use them in appendix 4.A.2 to derive the second moments stated in the next lemmas.

Lemma 4.3.1 *Let $\boldsymbol{x},\boldsymbol{x}'$ be two points in A. The second moments of the Green's function* (4.45) *are*

$$\mathbb{E}\left[G(\boldsymbol{x},\boldsymbol{y};j\omega)G^{\star}(\boldsymbol{x}',\boldsymbol{y};j\omega)\right]\approx\frac{1}{L^2}\exp\left[ijk\left(L+\frac{|\boldsymbol{x}_\perp-\boldsymbol{y}_\perp|^2}{2L}\right)-\frac{|\boldsymbol{x}'_\perp-\boldsymbol{x}_\perp|^2}{2X_{d,j}^2}\right], \tag{4.58}$$

where we recall that $\boldsymbol{x}_\perp$ and $\boldsymbol{y}_\perp$ are the components of $\boldsymbol{x}$ and $\boldsymbol{y}$ in the plane orthogonal to $\boldsymbol{n}$,

and L is the distance from $\boldsymbol{y}$ to the center of the array. The length scales $X_{d,j}$ are given by

$$X_{d,j} = \ell\sqrt{\frac{3S_j}{2L}} = O\left(\frac{\lambda\sqrt{\ell}}{\sigma\sqrt{L}}\right) \ll \ell. \tag{4.59}$$

The decay in (4.58) with the receiver offsets models the decorrelation of the waves due to scattering in the random medium, so we call $X_{d,j}$ the decoherence lengths. The next lemma quantifies the decorrelation of the waves travelling in different directions.

Lemma 4.3.2 *Let $\boldsymbol{x}, \boldsymbol{x}'$ be two points in A, and $\boldsymbol{\theta}$ and $\boldsymbol{\theta}'$ be two illumination directions in the cone C. The second moments of the direct wave are*

$$\begin{aligned}\mathbb{E}\left[u_1^d(\boldsymbol{x},\boldsymbol{\theta})\overline{u_1^d(\boldsymbol{x}',\boldsymbol{\theta}')}\right] &\approx e^{ik(\boldsymbol{x}\cdot\boldsymbol{\theta}-\boldsymbol{x}'\cdot\boldsymbol{\theta}')} \\ &\quad\times \exp\Big(-\frac{3|\boldsymbol{P}_{\boldsymbol{\vartheta}}\widetilde{\boldsymbol{x}}|^2 - 3|\boldsymbol{x}-\boldsymbol{x}^{(i)}(\boldsymbol{\theta})|\widetilde{\boldsymbol{x}}\cdot\boldsymbol{P}_{\boldsymbol{\vartheta}}\widetilde{\boldsymbol{\theta}} + |\boldsymbol{x}-\boldsymbol{x}^{(i)}(\boldsymbol{\theta})|^2|\boldsymbol{P}_{\boldsymbol{\vartheta}}\widetilde{\boldsymbol{\theta}}|^2}{2X_{d,1}^2}\Big),\end{aligned} \tag{4.60}$$

with $X_{d,1}$ defined as in (4.59)*, the notation $\widetilde{\boldsymbol{x}} = \boldsymbol{x} - \boldsymbol{x}'$, $\widetilde{\boldsymbol{\theta}} = \boldsymbol{\theta} - \boldsymbol{\theta}'$, and the orthogonal projection*

$$\boldsymbol{P}_{\boldsymbol{\vartheta}} = I - \boldsymbol{\vartheta}\boldsymbol{\vartheta}^T. \tag{4.61}$$

The second moments of the waves impinging on the scatterer at $\boldsymbol{y}$ are

$$\mathbb{E}\left[u_1^d(\boldsymbol{y},\boldsymbol{\theta})\overline{u_1^d(\boldsymbol{y},\boldsymbol{\theta}')}\right] \approx e^{ik\boldsymbol{y}\cdot\widetilde{\boldsymbol{\theta}} - \frac{|\boldsymbol{P}_{\boldsymbol{\vartheta}}\widetilde{\boldsymbol{\theta}}|^2}{2\Theta_d^2}}, \tag{4.62}$$

with

$$\Theta_d = \frac{X_{d,1}}{|\boldsymbol{y}-\boldsymbol{y}^{(i)}(\boldsymbol{\vartheta})|} = O\left(\frac{\lambda\sqrt{\ell}}{\sigma\sqrt{L^3}}\right) \ll \frac{\ell}{L} \ll 1. \tag{4.63}$$

The dimensionless scale Θ_d defines the direction offset over which the incoming plane waves remain statistically correlated when they reach the scatterer at $\boldsymbol{y}$. Note that in our

scaling we have

$$X_{d,j} \ll \ell \ll a, \qquad \Theta_d \ll \frac{\ell}{L} \ll \alpha = O\left(\frac{a}{L}\right).$$

This is essential for obtaining statistically stable CINT images, as we show later.

We state next one more wave decorrelation result needed in the next sections. It says that the Green's function from the scatterer to the array and the direct wave impinging on the scatterer are statistically decorrelated. This is expected because these waves traverse different parts of the random medium.

Lemma 4.3.3 *Let $\boldsymbol{x}$ be a point in A and $\boldsymbol{\theta}$ a unit vector in the illumination cone C. We have*

$$\mathbb{E}\left[G(\boldsymbol{x},\boldsymbol{y};j\omega)e^{ijk\gamma(\boldsymbol{y},\boldsymbol{\theta})}\right] \approx \mathbb{E}\left[G(\boldsymbol{x},\boldsymbol{y};j\omega)\right]\mathbb{E}\left[e^{ijk\gamma(\boldsymbol{y},\boldsymbol{\theta})}\right] \approx G_o(\boldsymbol{x},\boldsymbol{y};j\omega)e^{-\frac{|\boldsymbol{x}-\boldsymbol{y}|}{S_j}-\frac{|\boldsymbol{y}-\boldsymbol{y}^{(i)}(\boldsymbol{\theta})|}{S_j}} \approx 0. \tag{4.64}$$

The proof is in appendix 4.A.2.

4.3.3 The linearized data model in the random medium

Using the weak nonlinearity assumption, we can write approximately the solutions of equations (4.2)-(4.3) as

$$u_1(\boldsymbol{x};\boldsymbol{\theta}) \approx u_1^{(d)}(\boldsymbol{x};\boldsymbol{\theta}) + k^2\left\langle\eta_1\right\rangle G(\boldsymbol{x},\boldsymbol{y};\omega)u_1^{(d)}(\boldsymbol{y};\boldsymbol{\theta}), \tag{4.65}$$

$$u_2(\boldsymbol{x};\boldsymbol{\theta}) \approx (2k)^2\left\langle\eta_2\right\rangle G(\boldsymbol{x},\boldsymbol{y};2\omega)[u_1^{(d)}(\boldsymbol{y};\boldsymbol{\theta})]^2, \tag{4.66}$$

where we modeled the point-like scatterer by the net susceptibilities $\langle\eta_j\rangle$, given by the integral of η_j over its small support contained inside a ball centered at $\boldsymbol{y}$, of radius much smaller

than λ:

$$\langle \eta_j \rangle = \int_V d\boldsymbol{y}\, \eta_j(\boldsymbol{y}) \ , \quad j = 1, 2.$$

The Green's function in equations (4.65)-(4.66) models the propagation of the waves in the medium, from the scatterer to the array, and it is modeled by (4.45). The direct wave $u_1^{(d)}$ models the incident plane wave distorted by the random medium, as given in equation (4.47).

The random model of the data (4.11)-(4.12) at the array is

$$d_1(\boldsymbol{x}, \boldsymbol{\theta}) = e^{ik\boldsymbol{x}\cdot\boldsymbol{\theta}} \left[e^{ik\gamma(\boldsymbol{x},\boldsymbol{\theta})} - 1 \right] + k^2 \langle \eta_1 \rangle G(\boldsymbol{x}, \boldsymbol{y}; \omega) e^{ik\boldsymbol{y}\cdot\boldsymbol{\theta} + ik\gamma(\boldsymbol{y},\boldsymbol{\theta})}, \tag{4.67}$$

$$d_2(\boldsymbol{x}, \boldsymbol{\theta}) = 4k^2 \langle \eta_2 \rangle G(\boldsymbol{x}, \boldsymbol{y}; 2\omega) e^{i2k\boldsymbol{y}\cdot\boldsymbol{\theta} + i2k\gamma(\boldsymbol{y},\boldsymbol{\theta})}, \tag{4.68}$$

for $\boldsymbol{x} \in A$ and $\boldsymbol{\theta}$ in the cone C with axis along $\boldsymbol{\vartheta}$ and opening angle α. We neglect for simplicity the additive, uncorrelated noise, which is much easier to mitigate than the random medium distortions.

4.3.4 Analysis of migration imaging

We assume in this and the following section that the number $N_{\boldsymbol{x}}$ of sensors in the array aperture A is large, so that we can replace the sums over the receivers by integrals over the aperture

$$\sum_{s=1}^{N_{\boldsymbol{x}}} \sim \int_A d\boldsymbol{x}_\perp,$$

where the symbol "$\sim$" denotes approximate, up to multiplication by a constant. Recall that $\boldsymbol{x}_\perp$ is the two dimensional vector in the square aperture A of side a. We also approximate the sums over the incident directions $\boldsymbol{\theta}_q$ by integrals over the unit vectors $\boldsymbol{\theta}$ in the cone C, parametrized by the polar angle $\varphi \in (0, \alpha)$ between $\boldsymbol{\theta}$ and $\boldsymbol{\vartheta}$ and the azimuthal angle

$\beta \in [0, 2\pi]$

$$\sum_{q=1}^{N_\theta} \sim \int_C d\boldsymbol{\theta} = \int_0^\alpha d\varphi \, \sin\varphi \int_0^{2\pi} d\beta.$$

The migration imaging function (4.17) at search points $\boldsymbol{y}^R \in R$ is modeled (up to multiplicative constants) by

$$\mathcal{I}_j^M(\boldsymbol{y}^R) = \int_A d\boldsymbol{x}_\perp \int_C d\boldsymbol{\theta} \, d_j(\boldsymbol{x}, \boldsymbol{\theta}) G_o^\star(\boldsymbol{y}^R, \boldsymbol{x}; j\omega) e^{-ijk\boldsymbol{y}\cdot\boldsymbol{\theta}}, \tag{4.69}$$

with d_j given by (4.67)-(4.68). We describe first its focusing in homogeneous media, and then consider random media.

Homogeneous media

The model of the migration imaging function in homogeneous media is

$$\mathcal{I}_{o,j}^M(\boldsymbol{y}^R) = (jk)^2 \langle \eta_j \rangle \int_A d\boldsymbol{x}_\perp \, G_o(\boldsymbol{x}, \boldsymbol{y}; j\omega) G_o^\star(\boldsymbol{y}^R, \boldsymbol{x}; j\omega) \int_C d\boldsymbol{\theta} \, e^{ijk\boldsymbol{\theta}\cdot(\boldsymbol{y}-\boldsymbol{y}^R)}. \tag{4.70}$$

It has a separable form, given by the product of two integrals over the array aperture A and the cone C of illuminations.

The integral over the aperture is

$$\begin{aligned}\int_A d\boldsymbol{x}_\perp \, G_o(\boldsymbol{x}, \boldsymbol{y}; j\omega) G_o^\star(\boldsymbol{y}^R, \boldsymbol{x}; j\omega) \approx \frac{a^2}{L^2} e^{ijk\left(y_\parallel - y_\parallel^s + \frac{|\boldsymbol{y}_\perp|^2 - |\boldsymbol{y}^R|^2}{2L}\right)} \\ \times \operatorname{sinc}\Big(\frac{jka(y-y^s)_1}{2L}\Big) \operatorname{sinc}\Big(\frac{jka(y-y^s)_2}{2L}\Big),\end{aligned} \tag{4.71}$$

where we used the paraxial approximation (4.42), and indexed by 1 and 2 the components of $\boldsymbol{y}_\perp$ and $\boldsymbol{y}_\perp^R$ in the plane orthogonal to $\boldsymbol{n}$, for coordinate axes parallel to the sides of the square aperture. This is the classic calculation of the point spread function of time reversal in homogeneous media. It localizes the scatterer in the plane orthogonal to $\boldsymbol{n}$ with resolution

of the order $\lambda L/(ja)$.

The integral over the cone C of illuminations is

$$\int_C d\boldsymbol{\theta}\, e^{ijk\boldsymbol{\theta}\cdot(\boldsymbol{y}-\boldsymbol{y}^R)} = \int_0^\alpha d\varphi\, \sin\varphi\, e^{ijk\cos\varphi\,\boldsymbol{\vartheta}\cdot(\boldsymbol{y}-\boldsymbol{y}^R)} \int_0^{2\pi} d\beta\, e^{ijk\sin\varphi\cos\beta|\boldsymbol{P}_{\boldsymbol{\vartheta}}(\boldsymbol{y}-\boldsymbol{y}^R)|}, \tag{4.72}$$

and we can simplify it using the assumptions (4.40) and (4.41) on the small opening angle α and the linear size r of the search domain. We approximate

$$k\cos\varphi\,\boldsymbol{\vartheta}\cdot(\boldsymbol{y}-\boldsymbol{y}^R) = k\boldsymbol{\vartheta}\cdot(\boldsymbol{y}-\boldsymbol{y}^R) + O\left(\frac{ra^2}{\lambda L^2}\right) \approx k\boldsymbol{\vartheta}\cdot(\boldsymbol{y}-\boldsymbol{y}^R),$$

and

$$k\sin\varphi\,\cos\beta|\boldsymbol{P}_{\boldsymbol{\vartheta}}(\boldsymbol{y}-\boldsymbol{y}^R)| = k\varphi\cos\beta|\boldsymbol{P}_{\boldsymbol{\vartheta}}(\boldsymbol{y}-\boldsymbol{y}^R)| + O\left(\frac{a^3 r}{\lambda L^3}\right) \approx k\varphi\cos\beta|\boldsymbol{P}_{\boldsymbol{\vartheta}}(\boldsymbol{y}-\boldsymbol{y}^R)|,$$

and obtain that

$$\begin{aligned}
\int_C d\boldsymbol{\theta}\, e^{ijk\boldsymbol{\theta}\cdot(\boldsymbol{y}-\boldsymbol{y}^R)} &\approx e^{ijk\boldsymbol{\vartheta}\cdot(\boldsymbol{y}-\boldsymbol{y}^R)} \int_0^\alpha d\varphi\,\varphi \int_0^{2\pi} d\beta\, e^{ijk\varphi\cos\beta|\boldsymbol{P}_{\boldsymbol{\vartheta}}(\boldsymbol{y}-\boldsymbol{y}^R)|} \\
&= 2\pi\, e^{ijk\boldsymbol{\vartheta}\cdot(\boldsymbol{y}-\boldsymbol{y}^R)} \int_0^\alpha d\varphi\,\varphi J_0\left(jk\varphi|\boldsymbol{P}_{\boldsymbol{\vartheta}}(\boldsymbol{y}-\boldsymbol{y}^R)|\right) \\
&= 2\pi\, e^{ijk\boldsymbol{\vartheta}\cdot(\boldsymbol{y}-\boldsymbol{y}^R)} \alpha \frac{J_1\left(jk\alpha|\boldsymbol{P}_{\boldsymbol{\vartheta}}(\boldsymbol{y}-\boldsymbol{y}^R)|\right)}{jk|\boldsymbol{P}_{\boldsymbol{\vartheta}}(\boldsymbol{y}-\boldsymbol{y}^R)|},
\end{aligned} \tag{4.73}$$

where J_q are the Bessel functions of the first kind for $q = 0, 1$. This expression is large when

$$|\boldsymbol{P}_{\boldsymbol{\vartheta}}(\boldsymbol{y}-\boldsymbol{y}^R)| = O\left(\frac{\lambda}{j\alpha}\right) = O\left(\frac{\lambda L}{ja}\right),$$

and gives the focusing in the plane orthogonal to $\boldsymbol{\vartheta}$, and therefore along $\boldsymbol{n}$.

The imaging function is the product of (4.71) and (4.72), and it focuses at $\boldsymbol{y}$ with resolution $\lambda L/(ja)$.

The migration image in random media

To analyze the behavior of the migration imaging function in random media, we calculate in appendix 4.B its expectation and standard deviation. The result is summarized in the following proposition.

Proposition 1 *The expectation* $\mathbb{E}\big[\mathcal{I}_j^M(\boldsymbol{y})\big]$ *of the migration imaging function* (4.69) *evaluated at the scatterer location* $\boldsymbol{y}$ *is exponentially smaller than its standard deviation. The signal to noise ratio (SNR), which is the ratio of the expectation to the standard deviation, is proportional to*

$$\exp\left[-\frac{L}{S_j}\right], \tag{4.74}$$

where S_j *is defined in* (4.55) *. We will refer to terms proportional to* (4.74) *as "exponentially small".*

This result means that we cannot draw any conclusion about the focusing of the migration image by studying its statistical expectation. Because the waves that reach the array are randomized in our scaling, as stated in section 4.3.2, the migration image is also randomized, and has very large fluctuations with respect to its mean. This manifests in practice by the fact that the image may not be focused and reproducible, as it changes unpredictably with the realizations of the random medium. Migration does not work due to this lack statistical stability. This is because that there is no mechanism for mitigating the wave randomization in the migration image formation. The integration over the array aperture and over the illumination directions only takes care of additive and uncorrelated noise, but it cannot deal with the large random wave distortions due to scattering in the medium.

4.3.5 Analysis of CINT imaging

The CINT imaging function is as defined in (4.32), with the sums replaced by integrals over the aperture A and the cone C, except for one modification motivated by Lemma 4.3.2. This says that the waves decorrelate over offsets $\widetilde{\boldsymbol{\theta}} = \boldsymbol{\theta} - \boldsymbol{\theta}'$ in the plane orthogonal to $\boldsymbol{\vartheta}$, so we replace the windowing in (4.32) by

$$\Phi\Big(\frac{\widetilde{\boldsymbol{\theta}}}{\Theta}\Big) \rightsquigarrow \Phi\Big(\frac{\boldsymbol{P}_{\boldsymbol{\vartheta}}\widetilde{\boldsymbol{\theta}}}{\Theta}\Big),$$

where $\boldsymbol{P}_{\boldsymbol{\vartheta}}$ is as defined in (4.61). We also take a Gaussian window $\Phi(\boldsymbol{z}) = \exp(-|\boldsymbol{z}|^2/2)$ to simplify the calculations. The thresholding parameters X and Θ are of the same order as the decoherence scales $X_{d,1}$ and Θ_d, and we recall that $\boldsymbol{\vartheta}$ and $\boldsymbol{n}$ are orthogonal.

The CINT image is formed with cross-correlations of the measurements at points $\boldsymbol{x} \pm \widetilde{\boldsymbol{x}}/2 \in A$, and for incident plane waves with unit wave vectors $\boldsymbol{\theta} \pm \widetilde{\boldsymbol{\theta}}/2 \in C$. In our system of coordinates with origin at the center of A, which is planar square of side a, we have $\boldsymbol{x} = (\boldsymbol{x}_\perp, 0)$ and $\widetilde{\boldsymbol{x}} = (\widetilde{\boldsymbol{x}}_\perp, 0)$, with

$$(\boldsymbol{x}_\perp, \widetilde{\boldsymbol{x}}_\perp) \in \Big\{(\boldsymbol{z}, \widetilde{\boldsymbol{z}}) \in \mathbb{R}^4 : \ |z_j| \le \frac{a}{2}, \text{ and } \ |\widetilde{z}_j| \le \min\{a - 2|z_j|, 3X\}, \ j = 1, 2\Big\}. \tag{4.75}$$

Here we used that the offset is limited by the essential support of the Gaussian window

$$\Phi(\widetilde{\boldsymbol{x}}) = \exp\Big(-\frac{|\widetilde{\boldsymbol{x}}|^2}{2X^2}\Big) = \exp\Big(-\frac{|\widetilde{\boldsymbol{x}}_\perp|^2}{2X^2}\Big),$$

which is three times its standard deviation. Note that since $X \sim X_{d,1} \ll a$, the offsets $\widetilde{\boldsymbol{x}}_\perp$ are limited by $3X$ for most center points $\boldsymbol{x}_\perp$, so we can obtain a good approximation of the imaging function by using the simpler set

$$\mathcal{A} = \Big\{(\boldsymbol{z}, \widetilde{\boldsymbol{z}}) \in \mathbb{R}^4 : \ |z_j| \le \frac{a}{2}, \text{ and } \ |\widetilde{z}_j| \le 3X, \ j = 1, 2\Big\}. \tag{4.76}$$

We denote by $\iint_{\mathcal{A}} d\boldsymbol{x}_\perp d\widetilde{\boldsymbol{x}}_\perp$ the integral over $\mathcal{A}$.

To define the set that supports $\boldsymbol{\theta}$ and $\widetilde{\boldsymbol{\theta}}$, we use the orthonormal basis $\{\boldsymbol{\vartheta}, \boldsymbol{\eta}, \boldsymbol{\zeta}\}$, with vector $\boldsymbol{\eta}$ aligned with the projection $\boldsymbol{P}_{\boldsymbol{\vartheta}}\boldsymbol{\theta}$, so that

$$\boldsymbol{\theta} = |\boldsymbol{\theta}|(\boldsymbol{\vartheta}\cos\varphi + \boldsymbol{\eta}\sin\varphi), \qquad \varphi \in (0, \alpha). \tag{4.77}$$

Since $|\boldsymbol{\theta} \pm \widetilde{\boldsymbol{\theta}}/2| = 1$, we have

$$\boldsymbol{\theta} \cdot \widetilde{\boldsymbol{\theta}} = 0, \quad |\boldsymbol{\theta}| = \sqrt{1 - |\widetilde{\boldsymbol{\theta}}|^2/4}, \tag{4.78}$$

and using the decomposition

$$\widetilde{\boldsymbol{\theta}} = \widetilde{\theta}_{\vartheta}\boldsymbol{\vartheta} + \widetilde{\theta}_{\eta}\boldsymbol{\eta} + \widetilde{\theta}_{\zeta}\boldsymbol{\zeta}, \tag{4.79}$$

we can solve for the component of $\widetilde{\boldsymbol{\theta}}$ along the axis of the cone C,

$$\widetilde{\theta}_{\vartheta} = -\tan\varphi\,\widetilde{\theta}_{\eta}. \tag{4.80}$$

This gives that

$$|\widetilde{\boldsymbol{\theta}}|^2 = \widetilde{\theta}_{\zeta}^2 + \frac{\widetilde{\theta}_{\eta}^2}{\cos^2\varphi} = \widetilde{\theta}_{\zeta}^2 + \widetilde{\theta}_{\eta}^2 + O(\alpha^2\Theta_d^2), \qquad |\boldsymbol{\theta}| = 1 + O(\Theta_d^2), \tag{4.81}$$

where we used that

$$|\boldsymbol{P}_{\boldsymbol{\vartheta}}\widetilde{\theta}|^2 = \widetilde{\theta}_{\zeta}^2 + \widetilde{\theta}_{\eta}^2 = O(\Theta_d^2),$$

due to the Gaussian thresholding window with $\Theta = O(\Theta_d)$. We write then that $(\boldsymbol{\theta}, \widetilde{\boldsymbol{\theta}}) \in \mathcal{C}$, the set defined by vectors $\boldsymbol{\theta}$ of the form (4.77), with norm as in (4.81), and

$$\widetilde{\boldsymbol{\theta}} = \widetilde{\theta}_{\eta}\,(\boldsymbol{\eta} - \boldsymbol{\vartheta}\tan\varphi) + \widetilde{\theta}_{\zeta}\boldsymbol{\zeta}. \tag{4.82}$$

We parametrize $\mathcal{C}$ by the polar angle $\varphi \in (0, \alpha)$, the azimuthal angle $\beta \in (0, 2\pi)$, and the components $\widetilde{\theta}_\eta$ and $\widetilde{\theta}_\zeta$ of $\widetilde{\boldsymbol{\theta}}$. The angle β determines the unit vectors $\boldsymbol{\eta}$ and $\boldsymbol{\zeta}$ in polar coordinates, in the plane orthogonal to $\boldsymbol{\vartheta}$. We also denote by $\iint_{\mathcal{C}} d\boldsymbol{\theta} d\widetilde{\boldsymbol{\theta}}$ the integral over $\mathcal{C}$.

The analysis of CINT in homogeneous media is not interesting. This is because the windowing of the receiver and direction offsets is not necessary, and once we remove it, the CINT imaging function becomes the square of the migration function. We analyze separately the imaging of the linear and quadratic susceptibilities in random media. The calculations are similar, except that in the linear case data (4.67) have an extra term due to the randomly distorted direct wave. We begin with the imaging of the quadratic susceptibility, which uses the simpler data model (4.68).

Imaging of the quadratic susceptibility

Data (4.68) backpropagated to $\boldsymbol{y}^R \in R$ are modeled by

$$b_2\Big(\boldsymbol{x}\pm\frac{\widetilde{\boldsymbol{x}}}{2}, \boldsymbol{\theta}\pm\frac{\widetilde{\boldsymbol{\theta}}}{2}, \boldsymbol{y}^R\Big) = 4k^2 \left\langle \eta_2 \right\rangle G\Big(\boldsymbol{x}\pm\frac{\widetilde{\boldsymbol{x}}}{2}, \boldsymbol{y}; 2\omega\Big) G_o^\star\Big(\boldsymbol{x}\pm\frac{\widetilde{\boldsymbol{x}}}{2}, \boldsymbol{y}^R; 2\omega\Big) e^{i2k\left(\boldsymbol{\theta}+\frac{\tilde{\boldsymbol{\theta}}}{2}\right)\cdot(\boldsymbol{y}-\boldsymbol{y}^R)+i2k\gamma\left(\boldsymbol{y},\boldsymbol{\theta}\pm\frac{\tilde{\boldsymbol{\theta}}}{2}\right)}, \tag{4.83}$$

for $\boldsymbol{x} = (\boldsymbol{x}_\perp, 0)$ and $\widetilde{\boldsymbol{x}} = (\widetilde{\boldsymbol{x}}_\perp, 0)$ with $(\boldsymbol{x}_\perp, \widetilde{\boldsymbol{x}}_\perp) \in \mathcal{A}$, and $(\boldsymbol{\theta}, \widetilde{\boldsymbol{\theta}}) \in \mathcal{C}$. The image is formed with the cross-correlations of (4.83)

$$\begin{aligned}\mathcal{I}_2^{CINT}(\boldsymbol{y}^R) = \iint_{\mathcal{A}} d\boldsymbol{x}_\perp d\widetilde{\boldsymbol{x}}_\perp \iint_{\mathcal{C}} d\boldsymbol{\theta} d\widetilde{\boldsymbol{\theta}}\, e^{-\frac{|\widetilde{\boldsymbol{x}}_\perp|^2}{2X^2} - \frac{|\boldsymbol{P}_{\boldsymbol{\vartheta}}\widetilde{\boldsymbol{\theta}}|^2}{2\Theta^2}} \\ \times b_2\Big(\boldsymbol{x}+\frac{\widetilde{\boldsymbol{x}}}{2}, \boldsymbol{\theta}+\frac{\widetilde{\boldsymbol{\theta}}}{2}, \boldsymbol{y}^R\Big) b_2^\star\Big(\boldsymbol{x}-\frac{\widetilde{\boldsymbol{x}}}{2}, \boldsymbol{\theta}-\frac{\widetilde{\boldsymbol{\theta}}}{2}, \boldsymbol{y}^R\Big),\end{aligned} \tag{4.84}$$

and its focusing and statistical stability are described in the next proposition proved in appendix 4.C.

Proposition 2 *The expectation of the CINT imaging function is given by*

$$\mathbb{E}\left[\mathcal{I}_2^{CINT}(\boldsymbol{y}^R)\right] \approx \frac{(2\pi)^3}{2}\left(4k^2\langle\eta_2\rangle^2\alpha\Theta_e\frac{aX_e}{L^2}\right)^2 \times \exp\left[-\frac{1}{2}\left(\frac{2kX_e|\boldsymbol{y}_\perp-\boldsymbol{y}_\perp^R|}{L}\right)^2-\frac{1}{2}\left(2k\Theta_e|\boldsymbol{P}_{\boldsymbol{\vartheta}}(\boldsymbol{y}-\boldsymbol{y}_s^R)|\right)^2\right] \tag{4.85}$$

where X_e and Θ_e are defined by

$$\frac{1}{X_e^2}=\frac{1}{X^2}+\frac{1}{X_{d,2}^2}, \qquad \frac{1}{\Theta_e^2}=\frac{1}{\Theta^2}+\frac{4}{\Theta_d^2}.$$

The SNR of the imaging function evaluated at the scatterer location is of the order $(a/\ell)^2$.

Since in our scaling $\ell \ll a$, the SNR of the CINT image is very high, meaning that

$$\mathcal{I}_2^{CINT}(\boldsymbol{y}^R) \approx \mathbb{E}\left[\mathcal{I}_2^{CINT}(\boldsymbol{y}^R)\right].$$

This is the statement of statistical stability. The focusing of the image is determined by the exponential in (4.85). The first term gives the focusing in the plane of the array, and the second in the plane orthogonal to $\boldsymbol{\vartheta}$, which is orthogonal to the normal $\boldsymbol{n}$ to the array. By assumption (4.21) we have $X_e \sim X_{d,2}$ and $\Theta \sim \Theta_d$, and using definition (4.63) of Θ_d we conclude that the CINT resolution is

$$|\boldsymbol{y}-\boldsymbol{y}^R| \le O\left(\frac{\lambda L}{X_e}\right) \gg \frac{\lambda L}{a}. \tag{4.86}$$

The cost of stability comes at the expense of resolution, which is worse than in homogeneous media. Note that

$$\frac{\lambda L/X_e}{\lambda L^2/a^2}=O\left(\frac{a^2}{LX_{d,2}}\right)=O\left(\frac{a^2\sigma}{\lambda\sqrt{\ell L}}\right)\ll\frac{a^2}{\sqrt{\lambda L^3}}\ll 1,$$

so the peak of the CINT image can be observed in the search region R with linear size r satisfying (4.41).

Imaging of the linear susceptibility

The backpropagated data (4.67) to $\boldsymbol{y}^R \in R$ is

$$b_1\Big(\boldsymbol{x} \pm \frac{\widetilde{\boldsymbol{x}}}{2}, \boldsymbol{\theta} \pm \frac{\widetilde{\boldsymbol{\theta}}}{2}, \boldsymbol{y}^R\Big) = \left[e^{ik\gamma\left(\boldsymbol{x}\pm\frac{\widetilde{\boldsymbol{x}}}{2}, \boldsymbol{\theta}\pm\frac{\widetilde{\boldsymbol{\theta}}}{2}\right)} - 1\right] G_o^\star\big(\boldsymbol{x} \pm \frac{\widetilde{\boldsymbol{x}}}{2}, \boldsymbol{y}^R; \omega\big) e^{ik\left(\boldsymbol{\theta}\pm\frac{\widetilde{\boldsymbol{\theta}}}{2}\right)\cdot\left(\boldsymbol{x}\pm\frac{\widetilde{\boldsymbol{x}}}{2}-\boldsymbol{y}^R\right)}$$
$$+ k^2 \langle \eta_1 \rangle G\big(\boldsymbol{x} \pm \frac{\widetilde{\boldsymbol{x}}}{2}, \boldsymbol{y}; \omega\big) G_o^\star\big(\boldsymbol{x} \pm \frac{\widetilde{\boldsymbol{x}}}{2}, \boldsymbol{y}^R; \omega\big) e^{ik\left(\boldsymbol{\theta}\pm\frac{\widetilde{\boldsymbol{\theta}}}{2}\right)\cdot(\boldsymbol{y}-\boldsymbol{y}^R)+ik\gamma\left(\boldsymbol{y},\boldsymbol{\theta}+\frac{\widetilde{\boldsymbol{\theta}}}{2}\right)}. \tag{4.87}$$

The first term is due to the uncompensated direct wave which has not interacted with the scatterer at $\boldsymbol{y}$. The second term is the useful one in inversion. The imaging function is given by the superposition of the cross-correlations of (4.87),

$$\mathcal{I}_1^{CINT}(\boldsymbol{y}^R) = \iint_{\mathcal{A}} d\widetilde{\boldsymbol{x}} d\widetilde{\boldsymbol{x}}_\perp \iint_{\mathcal{C}} d\boldsymbol{\theta} d\widetilde{\boldsymbol{\theta}}\, e^{-\frac{|\widetilde{\boldsymbol{x}}_\perp|^2}{2X^2} - \frac{|\boldsymbol{P}_{\boldsymbol{\vartheta}}\widetilde{\boldsymbol{\theta}}|^2}{2\Theta^2}}$$
$$\times b_1\Big(\boldsymbol{x} + \frac{\widetilde{\boldsymbol{x}}}{2}, \boldsymbol{\theta} + \frac{\widetilde{\boldsymbol{\theta}}}{2}, \boldsymbol{y}^R\Big) b_1^\star\Big(\boldsymbol{x} - \frac{\widetilde{\boldsymbol{x}}}{2}, \boldsymbol{\theta} - \frac{\widetilde{\boldsymbol{\theta}}}{2}, \boldsymbol{y}^R\Big), \tag{4.88}$$

with the same notation as in the previous section. The following proposition, proved in appendix

Proposition 3 *The expectation of the imaging function* (4.88) *evaluated at points* $\boldsymbol{y}^R$ *in the imaging region* R *is given by*

$$\mathbb{E}\Big[\mathcal{I}_1^{CINT}(\boldsymbol{y}^R)\Big] \approx \frac{(2\pi)^3}{2}\left(k^2 \langle \eta_1 \rangle^2 \alpha \Theta_e \frac{aX_e}{L^2}\right)^2$$
$$\times \exp\left[-\frac{1}{2}\left(\frac{kX_e|\boldsymbol{y}_\perp - \boldsymbol{y}_\perp^R|}{L}\right)^2 - \frac{1}{2}\left(k\Theta_e|\boldsymbol{P}_{\boldsymbol{\vartheta}}(\boldsymbol{y}-\boldsymbol{y}^R)|\right)^2\right], \tag{4.89}$$

with X_e and Θ_e defined by

$$\frac{1}{X_e^2} = \frac{1}{X^2} + \frac{1}{X_{d,1}^2}, \qquad \frac{1}{\Theta_e^2} = \frac{1}{\Theta^2} + \frac{1}{\Theta_d^2}.$$

Moreover, the SNR of the imaging function evaluated at the scatterer location is very large, of the order $(a/\ell)^2$.

The uncompensated direct wave in (4.87) does not play a role in this result because we limit the search points $\boldsymbol{y}^R$ to the small region R centered at $\boldsymbol{y}$. If we searched in the whole domain, we would see the effect of the direct waves at points $\boldsymbol{y}^R$ near the array, as stated in the next proposition.

Proposition 4 *The expectation of the imaging function* (4.88) *is large at points $\boldsymbol{y}^R$ near the array. Moreover, the set of such points grows as we increase the aperture size and the opening angle of the cone of illuminations, in the sense that the larger these are, the further the points from the array that contribute to the image.*

We refer to the end of appendix 4.C.2 for the proof, and to the numerical simulations in the next section that verify this statement. Proposition 4 is interesting because it says that while in general it is advantageous to have a diverse set of illuminations and a larger aperture, this is not so when we cannot eliminate from the measurements the direct waves that have not interacted with the scatterers that we wish to image. These lead to spurious image peaks that cover a larger and larger neighborhood of the array as we increase the opening angle of the cone of illuminations and the aperture, and make it difficult to locate the scatterers unless we know approximately where to search, and they are located in a favorable position.

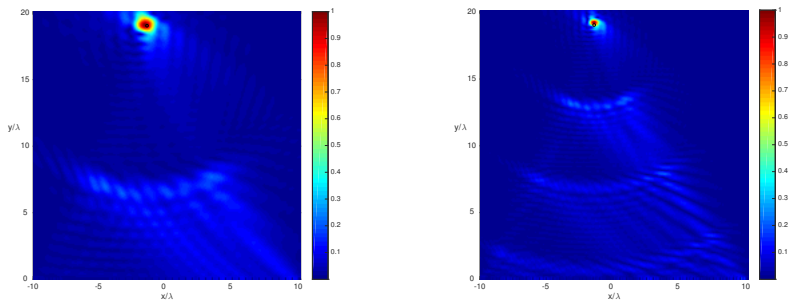

Figure 4.2: The migration images in a homogeneous medium of $\eta^{(1)}$ (left) and $\eta^{(2)}$ (right).

4.4 Numerical results

In this section we present numerical results with data calculated by solving the nonlinear equations (4.2)-(4.3), as explained in appendix 4.D. To decrease the computational cost, the numerical study is in two dimensions. The setup is like in Figure 4.1, but the scaling regime is different than the one used in the analysis section 4.3. This is for two reasons. The first is that the scaling there requires very long distances of propagation of the waves, over many wavelengths, which makes the forward solver in appendix 4.D prohibitively expensive. The second reason is that we wish to explore numerically a different scattering regime, that is difficult to analyze theoretically, and yet gives qualitatively similar results to those predicted by the theory in section 4.3.

We consider a square domain V of side length 20λ. The array covers the entire bottom side of V, and the system of coordinates has the origin at the center of the array, with the x_1-axis pointing horizontally to the right. Denote the wavelength of the incident field by λ. The domain V contains one small scatterer modeled by a disk of radius 0.1λ, centered at $\boldsymbol{y} = (-1.5\lambda, 19\lambda)$. The linear susceptibility of the scatterer is 1, and the quadratic susceptibility of the scatterer is 0.01. We take a wide cone C of illuminations, parametrized by the angle $\varphi \in [-\frac{\pi}{4}, \frac{\pi}{4}]$, with center direction $\boldsymbol{\vartheta}$ pointing horizontally, to the right. We use 20 incident angles and 81 sensors in the aperture $a = 20\lambda$.

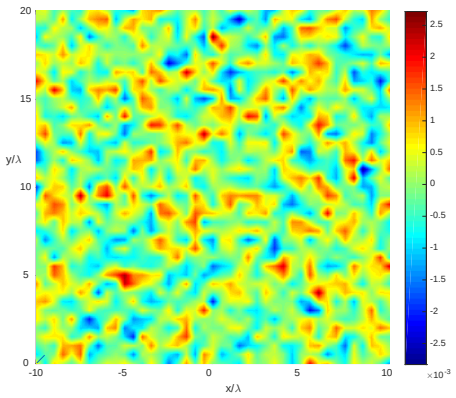

Figure 4.3: One realization of the susceptibility μ.

The migration images of η_1 and η_2 in a homogeneous medium are shown in Fig. 4.2. They peak at the scatterer location denoted by the circle. We observe that the resolution of the images is of the order of the wavelength. Since this is smaller for the second harmonic, the resolution of the image of η_2 is better.

We study imaging in a random medium, generated numerically with random Fourier series [34] for the Gaussian autocorrelation function (4.34) with correlation length $\ell = 0.3\lambda$, and amplitude $\sigma = 0.01 \times (4\pi)$. We display in Figure 4.3 one realization of η. The migration and CINT images of η_1 and η_2 in a small search region near the scatterer are shown in Figures 4.4 and 4.5, for two realizations of the random medium. The thresholding parameters in the CINT image formation are $X_1 = 2X_2 = 7\lambda$ and $\Theta = \frac{\pi}{5}$. We observe that as predicted by the theory in section 4.3, the peaks of the migration images dance around the location of the scatterer, from one realization to another, whereas the peak of the CINT images of η_1 and η_2 is more stable and near the scatter. Moreover, the statistical stabilization comes at the expense of resolution, as the CINT images are blurrier than those in homogeneous media displayed in Figure 4.2.

The images of the quadratic susceptibility, displayed in Figure 4.5 are slightly better than those of the linear susceptibility, shown in Figure 4.5. This is because we limited the search domain to the vicinity of the scatterer, and as predicted by the theory in section 4.3,

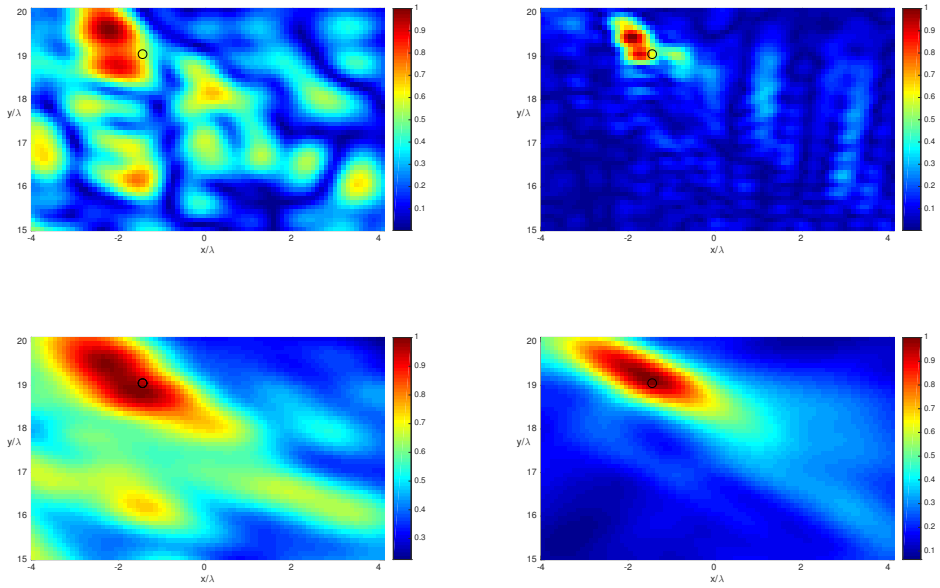

Figure 4.4: The migration (top row) and CINT (bottom) row images of the linear susceptibility η_1 in two realizations of the random medium. The scatterer location is shown with a black circle.

the uncompensated direct waves in the array data do not have an effect far from the array. However, as shown in Figure 4.6, these waves cause strong artifacts of the images of the linear susceptibility over a large set of points. As predicted by the theory, the image of the quadratic susceptibility is clearly better and it has the highest peak at the scatterer.

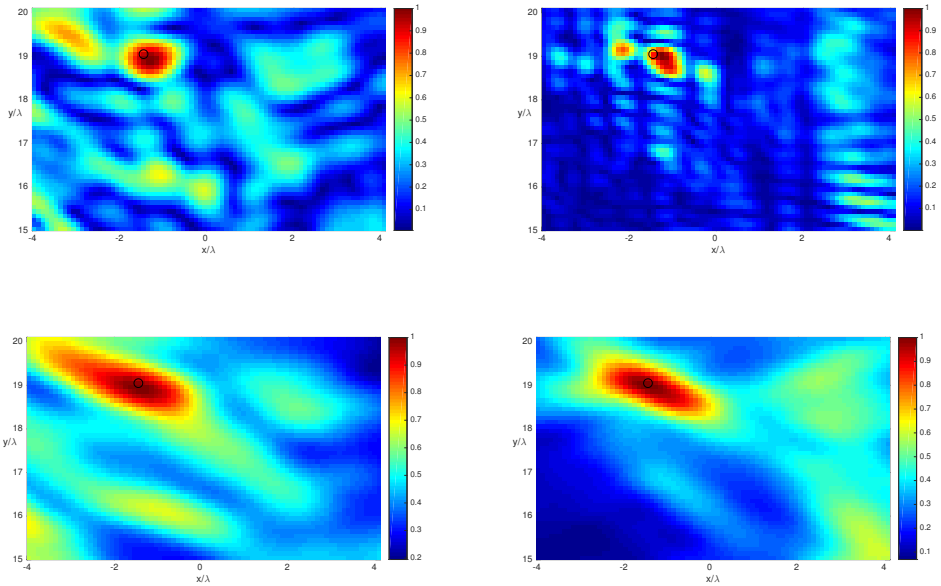

Figure 4.5: The migration (top row) and CINT (bottom) row images of the quadratic susceptibility η_2 in two realizations of the random medium. The scatterer location is shown with a black circle.

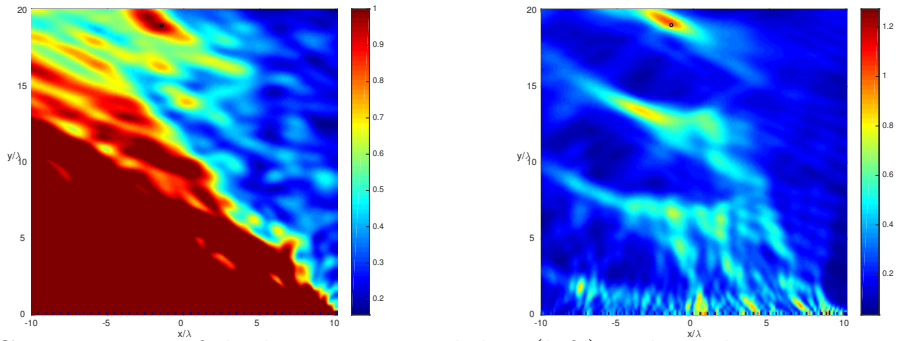

Figure 4.6: CINT images of the linear susceptibility (left) and quadratic susceptibility (right).

Appendix

4.A Statistical moments

In this appendix we calculate the statistical moments of the wave fields. We begin in section 4.A.1 with the second moments of the random phases, which are approximately Gaussian distributed in our scaling regime. Then we calculate the second moments of the waves in section 4.A.2.

4.A.1 Moments of the random phases

We prove here the following lemma.

Lemma 4.A.1 *Let $\boldsymbol{x}, \boldsymbol{x}'$ be two points in the array aperture A. The second moments of the processes* (4.46) *and* (4.48) *are approximated by*

$$\mathbb{E}[\nu(\boldsymbol{x},\boldsymbol{y})\nu(\boldsymbol{x}',\boldsymbol{y})] \approx \frac{\sqrt{2\pi}\sigma^2\ell|\boldsymbol{x}'-\boldsymbol{y}|}{4}\int_0^1 dt\, e^{-\frac{t^2}{2\ell^2}\left|\boldsymbol{x}'_\perp-\boldsymbol{x}_\perp\right|^2}, \tag{4.90}$$

and

$$\mathbb{E}[\gamma(\boldsymbol{x},\boldsymbol{\theta})\gamma(\boldsymbol{x}',\boldsymbol{\theta}')] \approx \frac{\sqrt{2\pi}\sigma^2\ell|\boldsymbol{x}'-\boldsymbol{x}'^{(i)}(\boldsymbol{\theta}')|}{4}\int_0^1 dt\, e^{-\frac{1}{2\ell^2}\left|\boldsymbol{P}_{\boldsymbol{\vartheta}}\left[(1-t)(\boldsymbol{x}'^{(i)}(\boldsymbol{\theta}')-\boldsymbol{x}^{(i)}(\boldsymbol{\theta}))+t(\boldsymbol{x}'-\boldsymbol{x})\right]\right|^2}. \tag{4.91}$$

The cross-moments satisfy

$$|\mathbb{E}[\gamma(\boldsymbol{x},\boldsymbol{\theta})\nu(\boldsymbol{x}',\boldsymbol{y})]| \ll \lambda^2, \qquad |\mathbb{E}[\gamma(\boldsymbol{y},\boldsymbol{\theta})\nu(\boldsymbol{x}',\boldsymbol{y})]| \ll \lambda^2. \tag{4.92}$$

Proof: Definition (4.46) and the Gaussian autocorrelation (4.34) give

$$\begin{aligned}\mathbb{E}[\nu(\boldsymbol{x},\boldsymbol{y})\nu(\boldsymbol{x}',\boldsymbol{y})] &= \frac{\sigma^2|\boldsymbol{x}-\boldsymbol{y}||\boldsymbol{x}'-\boldsymbol{y}|}{4}\int_0^1 dt\int_0^1 dt'\,\mathbb{E}\left[\mu\left(\frac{(1-t)\boldsymbol{y}}{\ell}+\frac{t\boldsymbol{x}}{\ell}\right)\mu\left(\frac{(1-t')\boldsymbol{y}}{\ell}+\frac{t'\boldsymbol{x}'}{\ell}\right)\right]\\ &= \frac{\sigma^2|\boldsymbol{x}-\boldsymbol{y}||\boldsymbol{x}'-\boldsymbol{y}|}{4}\int_0^1 dt\int_0^1 dt'\,e^{-\frac{1}{2\ell^2}|(t'-t)(\boldsymbol{x}-\boldsymbol{y})+t'(\boldsymbol{x}'-\boldsymbol{x})|^2},\end{aligned} \tag{4.93}$$

for $\boldsymbol{x},\boldsymbol{x}' \in A$. We change variables

$$(t,t') \rightsquigarrow (\widetilde{t},t'), \quad \widetilde{t} = (t'-t)|\boldsymbol{x}-\boldsymbol{y}|/\ell,$$

with $t' \in (0,1)$ and $\widetilde{t} \in (-(1-t')|\boldsymbol{x}-\boldsymbol{y}|/\ell, t'|\boldsymbol{x}-\boldsymbol{y}|/\ell)$, and use that $|\boldsymbol{x}-\boldsymbol{y}|/\ell \approx L/\ell \gg 1$ to extend the $\widetilde{t}$ integral to the real line. We obtain

$$\mathbb{E}[\nu(\boldsymbol{x},\boldsymbol{y})\nu(\boldsymbol{x}',\boldsymbol{y})] \approx \frac{\sqrt{2\pi}\ell|\boldsymbol{x}'-\boldsymbol{y}|}{4}\int_0^1 dt' e^{-\frac{1}{2\ell^2}|t'\boldsymbol{P}(\boldsymbol{x}'-\boldsymbol{x})|^2}, \tag{4.94}$$

where $\boldsymbol{P}$ is the orthogonal projection on the plane orthogonal to $\boldsymbol{x}-\boldsymbol{y}$. In our setting we have

$$\left|\frac{\boldsymbol{x}-\boldsymbol{y}}{|\boldsymbol{x}-\boldsymbol{y}|}-\boldsymbol{n}\right| = O\left(\frac{a}{L}\right) \ll 1, \tag{4.95}$$

and we can estimate the projection in (4.94) by

$$\frac{\boldsymbol{P}(\boldsymbol{x}'-\boldsymbol{x})}{\ell} = \frac{\boldsymbol{P}_{\boldsymbol{n}}(\boldsymbol{x}'-\boldsymbol{x})}{\ell} + O\left(\frac{a^2}{\ell L}\right), \qquad \boldsymbol{P}_n = I - \boldsymbol{n}\boldsymbol{n}^T. \tag{4.96}$$

The residual in (4.37) is negligible by assumption (4.43), that gives

$$\frac{a^2}{\ell L} \ll \frac{\sqrt{\lambda L}}{\ell} \ll 1.$$

Equation (4.90) follows from (4.94) and (4.96).

The derivation of (4.91) is essentially the same, so let us calculate the cross-moments. We obtain from (4.46), (4.48) and the Gaussian autocorrelation (4.34) that

$$\mathbb{E}[\gamma(\boldsymbol{x},\boldsymbol{\theta})\nu(\boldsymbol{x}',\boldsymbol{y})] = \frac{\sigma^2|\boldsymbol{x}-\boldsymbol{x}^{(i)}(\boldsymbol{\theta})||\boldsymbol{x}'-\boldsymbol{y}|}{4}\int_0^1 dt\int_0^1 dt'\, e^{-\frac{1}{2}\left|\frac{t'(\boldsymbol{x}-\boldsymbol{x}^{(i)}(\boldsymbol{\theta}))}{\ell}+\frac{t(\boldsymbol{x}'-\boldsymbol{y})}{\ell}+\frac{\boldsymbol{y}-\boldsymbol{x}}{\ell}\right|^2}, \tag{4.97}$$

where the result is obviously positive, so no absolute value is needed. Changing variables

$$(t,t') \rightsquigarrow (T,T'), \quad T = t\frac{|\boldsymbol{x}'-\boldsymbol{y}|}{\ell}, \quad T' = t'\frac{|\boldsymbol{x}-\boldsymbol{x}^{(i)}(\boldsymbol{\theta})|}{\ell},$$

and extending the integrals to the real line, we obtain the upper bound

$$\mathbb{E}[\gamma(\boldsymbol{x},\boldsymbol{\theta})\nu(\boldsymbol{x}',\boldsymbol{y})] \le \frac{\sigma^2\ell^2}{4}\int_{-\infty}^{\infty} dT\int_{-\infty}^{\infty} dT'\, e^{-\frac{1}{2}\left|T'\boldsymbol{\theta}+T\frac{(\boldsymbol{x}'-\boldsymbol{y})}{|\boldsymbol{x}'-\boldsymbol{y}|}+\frac{\boldsymbol{y}-\boldsymbol{x}}{\ell}\right|^2}. \tag{4.98}$$

Expanding the square in the exponent,

$$\left|T'\boldsymbol{\theta}+T\left(\frac{\boldsymbol{x}'-\boldsymbol{y}}{|\boldsymbol{x}'-\boldsymbol{y}|}\right)+\frac{\boldsymbol{y}-\boldsymbol{x}}{\ell}\right|^2 = \left[T'+T\frac{\boldsymbol{\theta}\cdot(\boldsymbol{x}'-\boldsymbol{y})}{|\boldsymbol{x}'-\boldsymbol{y}|}+\frac{\boldsymbol{\theta}\cdot(\boldsymbol{y}-\boldsymbol{x})}{\ell}\right]^2 + \left|\boldsymbol{P}_{\boldsymbol{\theta}}\left[T\frac{(\boldsymbol{x}'-\boldsymbol{y})}{|\boldsymbol{x}'-\boldsymbol{y}|}+\frac{\boldsymbol{y}-\boldsymbol{x}}{\ell}\right]\right|^2$$

with $\boldsymbol{P}_{\boldsymbol{\theta}} = I - \boldsymbol{\theta}\boldsymbol{\theta}^T$, we obtain after integrating in T' that

$$\mathbb{E}[\gamma(\boldsymbol{x},\boldsymbol{\theta})\nu(\boldsymbol{x}',\boldsymbol{y})] \le \frac{\sqrt{2\pi}\sigma^2\ell^2}{4}\int_{-\infty}^{\infty} dT e^{-\frac{1}{2}\left|\boldsymbol{P}_{\boldsymbol{\theta}}\left[T\frac{(\boldsymbol{x}'-\boldsymbol{y})}{|\boldsymbol{x}'-\boldsymbol{y}|}+\frac{\boldsymbol{y}-\boldsymbol{x}}{\ell}\right]\right|^2}. \tag{4.99}$$

To evaluate the T integral we proceed similarly, by decomposing the vector $\boldsymbol{P_\theta}(\boldsymbol{y}-\boldsymbol{x})$ in two parts: One along the vector $\boldsymbol{P_\theta}(\boldsymbol{x}'-\boldsymbol{y})$ and the other orthogonal to it. Then, we expand the square in (4.99) and obtain after integration in T the upper bound

$$\mathbb{E}[\gamma(\boldsymbol{x},\boldsymbol{\theta})\nu(\boldsymbol{x}',\boldsymbol{y})] \leq \frac{2\pi\sigma^2\ell^2}{4\left|\boldsymbol{P_\theta}\frac{(\boldsymbol{x}'-\boldsymbol{y})}{|\boldsymbol{x}'-\boldsymbol{y}|}\right|}. \tag{4.100}$$

Equation (4.92) follows from the assumptions (4.40), $\boldsymbol{\vartheta} \perp \boldsymbol{n}$ and equation (4.96) which give

$$\left|\boldsymbol{P_\theta}\frac{(\boldsymbol{x}'-\boldsymbol{y})}{|\boldsymbol{x}'-\boldsymbol{y}|}\right| = O(1),$$

so that the right hand side in (4.100) is $O(\sigma^2\ell^2)$. But by assumption (4.44),

$$\sigma^2\ell^2 \ll \frac{\lambda\ell^3}{L^2} \ll \lambda^2,$$

with the last inequality implied by the upper bound on ℓ in (4.43). This concludes the proof of Lemma 4.A.1. $\square$

4.A.2 Second moments of the wave fields

Let us suppose in this section that

$$|\boldsymbol{x}-\boldsymbol{y}| \geq |\boldsymbol{x}'-\boldsymbol{y}|, \qquad |\boldsymbol{x}-\boldsymbol{x}^{(i)}(\boldsymbol{\theta})| \geq |\boldsymbol{x}'-\boldsymbol{x}'^{(i)}(\boldsymbol{\theta}')|, \tag{4.101}$$

and use the results of Lemma 4.A.1 to derive the second moments of the wave fields. Note that the first inequality in (4.101) is only involved in the proof of (4.58) and the second inequality in (4.101) is only involved in the proof of (4.60), thus if the distances satisfy the opposite of inequality (4.101), the same analysis applies once we exchange the primed

quantities with the unprimed ones in the statement of Lemma 4.A.1 and its proof.

Proof of Lemma 4.3.1: Using that the phases are approximately Gaussian,

$$\mathbb{E}\left[G(\boldsymbol{x},\boldsymbol{y};j\omega)G^{\star}(\boldsymbol{x}',\boldsymbol{y};j\omega)\right] \approx G_o(\boldsymbol{x},\boldsymbol{y};j\omega)G_o^{\star}(\boldsymbol{x}',\boldsymbol{y};j\omega)e^{-\frac{(jk)^2}{2}\mathbb{E}\left\{[\nu(\boldsymbol{x},\boldsymbol{y})-\nu(\boldsymbol{x}',\boldsymbol{y})]^2\right\}}, \quad (4.102)$$

with exponent written using (4.90) and (4.55) as follows

$$\frac{(jk)^2}{2}\mathbb{E}\left\{\left[\nu(\boldsymbol{x},\boldsymbol{y})-\nu(\boldsymbol{x}',\boldsymbol{y})\right]^2\right\} = \frac{|\boldsymbol{x}-\boldsymbol{y}|}{S_j}+\frac{|\boldsymbol{x}'-\boldsymbol{y}|}{S_j}-\frac{2|\boldsymbol{x}'-\boldsymbol{y}|}{S_j}\int_0^1 dt\, e^{-\frac{t^2}{2\ell^2}\left|\boldsymbol{x}'_{\perp}-\boldsymbol{x}_{\perp}\right|^2}.$$

Since $|\boldsymbol{x}-\boldsymbol{y}|, |\boldsymbol{x}'-\boldsymbol{y}| \approx L \gg S_j$, this is very large and therefore (4.102) is negligible, unless the integral is close to one. This happens when

$$\left|\boldsymbol{x}'_{\perp}-\boldsymbol{x}_{\perp}\right| \ll \ell, \quad (4.103)$$

in which case we can use a Taylor expansion of the exponential and obtain the approximation

$$\int_0^1 dt\, e^{-\frac{t^2}{2\ell^2}\left|\boldsymbol{x}'_{\perp}-\boldsymbol{x}_{\perp}\right|^2} \approx 1-\frac{\left|\boldsymbol{x}'_{\perp}-\boldsymbol{x}_{\perp}\right|^2}{6\ell^2}.$$

Substituting in (4.102), we get

$$\mathbb{E}\left[G(\boldsymbol{x},\boldsymbol{y};j\omega)G^{\star}(\boldsymbol{x}',\boldsymbol{y};j\omega)\right] \approx G_o(\boldsymbol{x},\boldsymbol{y};j\omega)G_o^{\star}(\boldsymbol{x}',\boldsymbol{y};j\omega)e^{-\frac{||\boldsymbol{x}-\boldsymbol{y}|-|\boldsymbol{x}'-\boldsymbol{y}||}{S_j}-\frac{|\boldsymbol{x}'_{\perp}-\boldsymbol{x}_{\perp}|^2}{2X_{d,j}^2}}, \quad (4.104)$$

with

$$X_{d,j} = \ell\sqrt{\frac{3S_j}{2|\boldsymbol{x}'-\boldsymbol{y}|}} \approx \ell\sqrt{\frac{3S_j}{2L}}. \quad (4.105)$$

We also have

$$|\boldsymbol{x}-\boldsymbol{y}|-|\boldsymbol{x}'-\boldsymbol{y}| \approx \frac{(\boldsymbol{x}-\boldsymbol{y})}{|\boldsymbol{x}-\boldsymbol{y}|}\cdot(\boldsymbol{x}-\boldsymbol{x}') = \boldsymbol{n}\cdot(\boldsymbol{x}-\boldsymbol{x}')+O\left(\frac{a^2}{L}\right)=O\left(\frac{a^2}{L}\right), \quad (4.106)$$

where we used (4.95) and that A is orthogonal to $\boldsymbol{n}$. But definition (4.55) of S_j and assumptions (4.43)-(4.44) give

$$\frac{||\boldsymbol{x}-\boldsymbol{y}|-|\boldsymbol{x}'-\boldsymbol{y}||}{S_j} = O\left(\frac{a^2}{LS_j}\right) = O\left(\frac{a^2\ell\sigma^2}{L\lambda^2}\right) \ll \frac{a^2\ell^2}{\lambda L^3} \ll \frac{a^4}{\lambda L^3} \ll 1, \tag{4.107}$$

so the first term in the exponent of (4.104) is negligible. Equation (4.58) follows from (4.104), (4.106) and the paraxial approximation (4.42) of G_o. This formula is derived under assumption (4.103). If this doesn't hold, the moment is exponentially small, as explained above. This is captured in the expression (4.106) be the exponential decay on the scale $X_{d,j}$, which is much smaller than ℓ because $S_j \ll L$. $\square$

Proof of Lemma 4.3.2: Again, using the approximate Gaussianity of the phases, we obtain from definition (4.47)

$$\mathbb{E}\left[u_1^d(\boldsymbol{x},\boldsymbol{\theta})\overline{u_1^d(\boldsymbol{x}',\boldsymbol{\theta}')}\right] \approx e^{ik(\boldsymbol{x}\cdot\boldsymbol{\theta}-\boldsymbol{x}'\cdot\boldsymbol{\theta}')-\frac{k^2}{2}\mathbb{E}\left\{[\gamma(\boldsymbol{x},\boldsymbol{\theta})-\gamma(\boldsymbol{x}',\boldsymbol{\theta}')]^2\right\}}, \tag{4.108}$$

with the last term in the exponent following from (4.91)

$$\frac{k^2}{2}\mathbb{E}\left\{[\gamma(\boldsymbol{x},\boldsymbol{\theta})-\gamma(\boldsymbol{x}',\boldsymbol{\theta}')]^2\right\} \approx \frac{|\boldsymbol{x}-\boldsymbol{x}^{(i)}(\boldsymbol{\theta})|}{S_1} + \frac{|\boldsymbol{x}'-\boldsymbol{x}'^{(i)}(\boldsymbol{\theta}')|}{S_1} - \frac{2|\boldsymbol{x}'-\boldsymbol{x}'^{(i)}(\boldsymbol{\theta}')|}{S_1}$$
$$\times \int_0^1 dt\, e^{-\frac{1}{2\ell^2}\left|\boldsymbol{P}_{\boldsymbol{\vartheta}}\left[(1-t)(\boldsymbol{x}'^{(i)}(\boldsymbol{\theta}')-\boldsymbol{x}^{(i)}(\boldsymbol{\theta}))+t(\boldsymbol{x}'-\boldsymbol{x})\right]\right|^2}. \tag{4.109}$$

We conclude as above that since $|\boldsymbol{x}-\boldsymbol{x}^{(i)}(\boldsymbol{\theta})|, |\boldsymbol{x}'-\boldsymbol{x}'^{(i)}(\boldsymbol{\theta})| \gg S_1$, the right hand side in (4.108) is small unless

$$\frac{|\boldsymbol{P}_{\boldsymbol{\vartheta}}(\boldsymbol{x}'-\boldsymbol{x})|}{\ell} \ll 1, \qquad \frac{|\boldsymbol{P}_{\boldsymbol{\vartheta}}(\boldsymbol{x}'^{(i)}(\boldsymbol{\theta}')-\boldsymbol{x}^{(i)}(\boldsymbol{\theta}))|}{\ell} \ll 1. \tag{4.110}$$

By definition

$$\boldsymbol{x}^{(i)}(\boldsymbol{\theta}) = \boldsymbol{x} - |\boldsymbol{x} - \boldsymbol{x}^{(i)}(\boldsymbol{\theta})|\boldsymbol{\theta}, \qquad \boldsymbol{x}'^{(i)}(\boldsymbol{\theta}') = \boldsymbol{x}' - |\boldsymbol{x}' - \boldsymbol{x}'^{(i)}(\boldsymbol{\theta}')|\boldsymbol{\theta}', \tag{4.111}$$

so the last inequality in (4.110) implies that the angle between $\boldsymbol{\theta}$ and $\boldsymbol{\theta}'$ must be small.

With the assumption (4.110), we can approximate the integral using the Taylor expansion of the exponential,

$$e^{-\frac{k^2}{2}\mathbb{E}\left\{[\gamma(\boldsymbol{x},\boldsymbol{\theta})-\gamma(\boldsymbol{x}',\boldsymbol{\theta}')]^2\right\}} \approx e^{-\frac{\left||\boldsymbol{x}-\boldsymbol{x}^{(i)}(\boldsymbol{\theta})|-|\boldsymbol{x}'-\boldsymbol{x}'^{(i)}(\boldsymbol{\theta}')|\right|}{S_1} - \frac{|\boldsymbol{P}_{\boldsymbol{\vartheta}}\widetilde{\boldsymbol{x}}|^2+\widetilde{\boldsymbol{x}}\cdot\boldsymbol{P}_{\boldsymbol{\vartheta}}\widetilde{\boldsymbol{x}}^{(i)}+|\boldsymbol{P}_{\boldsymbol{\vartheta}}\widetilde{\boldsymbol{x}}^{(i)}|^2}{2X_{d,1}^2}}, \tag{4.112}$$

with S_1 defined in (4.55), $X_{d,1}$ defined in (4.105), $\widetilde{\boldsymbol{x}} = \boldsymbol{x} - \boldsymbol{x}'$, and $\widetilde{\boldsymbol{x}}^{(i)} = \boldsymbol{x}^{(i)}(\boldsymbol{\theta}) - \boldsymbol{x}'^{(i)}(\boldsymbol{\theta}')$. The first term in the exponential in (4.112) is of the same order as in the estimate (4.107), and is negligible. The second term can be rewritten using (4.111), which gives

$$\widetilde{\boldsymbol{x}}^{(i)} = \widetilde{\boldsymbol{x}} - \left(|\boldsymbol{x} - \boldsymbol{x}^{(i)}(\boldsymbol{\theta})| - |\boldsymbol{x}' - \boldsymbol{x}'^{(i)}(\boldsymbol{\theta}')|\right)\overline{\boldsymbol{\theta}} - \frac{\left(|\boldsymbol{x} - \boldsymbol{x}^{(i)}(\boldsymbol{\theta})| + |\boldsymbol{x}' - \boldsymbol{x}'^{(i)}(\boldsymbol{\theta}')\right)}{2}\widetilde{\boldsymbol{\theta}}, \tag{4.113}$$

where $\overline{\boldsymbol{\theta}} = (\boldsymbol{\theta} + \boldsymbol{\theta}')/2$ and $\widetilde{\boldsymbol{\theta}} = \boldsymbol{\theta} - \boldsymbol{\theta}'$. Note that

$$\frac{\left||\boldsymbol{x} - \boldsymbol{x}^{(i)}(\boldsymbol{\theta})| - |\boldsymbol{x}' - \boldsymbol{x}'^{(i)}(\boldsymbol{\theta}')|\right|}{X_{d,1}} = O\left(\frac{a^2}{LX_{d,1}}\right) = O\left(\frac{a^2\sigma}{\lambda\sqrt{\ell L}}\right) \ll \frac{a^2}{\sqrt{\lambda L^3}} \ll 1,$$

where we used the definition of $X_{d,1}$ and the scaling assumptions (4.43)-(4.44). Thus, we can neglect the second term in the right hand-side of (4.113), and get

$$\widetilde{\boldsymbol{x}}^{(i)} \approx \widetilde{\boldsymbol{x}} - |\boldsymbol{x} - \boldsymbol{x}^{(i)}(\boldsymbol{\theta})|\widetilde{\boldsymbol{\theta}}. \tag{4.114}$$

Gathering the results we obtain

$$e^{-\frac{k^2}{2}\mathbb{E}\left\{[\gamma(\boldsymbol{x},\boldsymbol{\theta})-\gamma(\boldsymbol{x}',\boldsymbol{\theta}')]^2\right\}} \approx \exp\left(-\frac{3|\boldsymbol{P}_{\vartheta}\widetilde{\boldsymbol{x}}|^2 - 3|\boldsymbol{x}-\boldsymbol{x}^{(i)}(\boldsymbol{\theta})|\widetilde{\boldsymbol{x}}\cdot\boldsymbol{P}_{\vartheta}\widetilde{\boldsymbol{\theta}} + |\boldsymbol{x}-\boldsymbol{x}^{(i)}(\boldsymbol{\theta})|^2|\boldsymbol{P}_{\vartheta}\widetilde{\boldsymbol{\theta}}|^2}{2X_{d,1}^2}\right), \tag{4.115}$$

as stated in the lemma. □

Proof of Lemma 4.3.3: We calculate that

$$\begin{aligned}\mathbb{E}\left[G(\boldsymbol{x},\boldsymbol{y};j\omega)e^{ijk\gamma(\boldsymbol{y},\boldsymbol{\theta})}\right] &\approx G_o(\boldsymbol{x},\boldsymbol{y};j\omega)e^{-\frac{(jk)^2}{2}\mathbb{E}\left\{[\nu(\boldsymbol{x},\boldsymbol{y})-\gamma(\boldsymbol{y},\boldsymbol{\theta})]^2\right\}} \\ &\approx G_o(\boldsymbol{x},\boldsymbol{y};j\omega)e^{-\frac{|\boldsymbol{x}-\boldsymbol{y}|}{S_j}-\frac{|\boldsymbol{y}-\boldsymbol{y}^{(i)}(\boldsymbol{\theta})|}{S_j}},\end{aligned} \tag{4.116}$$

where the first approximation is because the phases are approximately Gaussian, and the second approximation is because, as shown in Lemma 4.A.1,

$$k^2\left|\mathbb{E}\left[\nu(\boldsymbol{x},\boldsymbol{y})\gamma(\boldsymbol{y},\boldsymbol{\theta})\right]\right| \ll 1. \tag{4.117}$$

The statement of the lemma follows. □

4.B Statistics of the migration image

To prove Proposition 1 we use Lemmas 4.3.1-4.3.3, and the following estimates implied by the estimate (4.117),

$$\begin{aligned}&\mathbb{E}\left[G(\boldsymbol{x},\boldsymbol{y};j\omega)G^{\star}(\boldsymbol{x}',\boldsymbol{y};j\omega)e^{ijk[\gamma(\boldsymbol{y},\boldsymbol{\theta})-\gamma(\boldsymbol{y},\boldsymbol{\theta}')]}\right] \\ &\quad\approx \mathbb{E}\left[G(\boldsymbol{x},\boldsymbol{y};j\omega)G^{\star}(\boldsymbol{x}',\boldsymbol{y};j\omega)\right]\mathbb{E}\left[e^{ijk[\gamma(\boldsymbol{y},\boldsymbol{\theta})-\gamma(\boldsymbol{y},\boldsymbol{\theta}')]}\right],\end{aligned} \tag{4.118}$$

and

$$\mathbb{E}\left[G^\star(\boldsymbol{x}',\boldsymbol{y};j\omega)e^{ijk[\gamma(\boldsymbol{y},\boldsymbol{\theta}')-\gamma(\boldsymbol{x},\boldsymbol{\theta})]}\right] \approx \mathbb{E}\left[G^\star(\boldsymbol{x}',\boldsymbol{y};j\omega)\right]\mathbb{E}\left[e^{ijk[\gamma(\boldsymbol{y},\boldsymbol{\theta}')-\gamma(\boldsymbol{x},\boldsymbol{\theta})]}\right]. \tag{4.119}$$

We analyze separately the imaging of the linear and quadratic susceptibilities.

4.B.1 Imaging of the linear susceptibility

Definitions (4.67) and (4.69), and the estimates (4.57), (4.64) give that the expectation of the image is

$$\begin{aligned}\mathbb{E}\left[\mathcal{I}_1^M(\boldsymbol{y}^R)\right] \approx &\int_A d\boldsymbol{x}_\perp \int_C d\boldsymbol{\theta}\, G_o^\star(\boldsymbol{x},\boldsymbol{y}^R;\omega)e^{ik\boldsymbol{\theta}\cdot(\boldsymbol{x}-\boldsymbol{y}^R)}\left[e^{-\frac{|\boldsymbol{x}-\boldsymbol{x}^{(i)}(\boldsymbol{\theta})|}{S_1}}-1\right]\\ &+k^2\langle\eta_1\rangle\int_A d\boldsymbol{x}_\perp\int_C d\boldsymbol{\theta}\, G_o(\boldsymbol{x},\boldsymbol{y};\omega)G_o^\star(\boldsymbol{x},\boldsymbol{y}^R;\omega)e^{ik\boldsymbol{\theta}\cdot(\boldsymbol{y}-\boldsymbol{y}^R)-\frac{|\boldsymbol{x}-\boldsymbol{y}|}{S_1}-\frac{|\boldsymbol{y}-\boldsymbol{y}^{(i)}(\boldsymbol{\theta})|}{S_1}}.\end{aligned} \tag{4.120}$$

All the terms but one in this expression are exponentially small. But even this one gives a small contribution because of the large phase

$$k\left[|\boldsymbol{x}-\boldsymbol{y}^R|-\boldsymbol{\theta}\cdot(\boldsymbol{x}-\boldsymbol{y}^R)\right]=k|\boldsymbol{x}-\boldsymbol{y}^R|\left[1-\boldsymbol{\theta}\cdot\frac{(\boldsymbol{x}-\boldsymbol{y}^R)}{|\boldsymbol{x}-\boldsymbol{y}^R|}\right]=O(L/\lambda)\gg 1,$$

where we used that $\boldsymbol{\vartheta}\perp\boldsymbol{n}$.

The second moment of the imaging function at the scatterer location is

$$\begin{aligned}\mathbb{E}\left[\left|\mathcal{I}_1^M(\boldsymbol{y})\right|^2\right] \approx &\int_A d\boldsymbol{x}_\perp\int_A d\boldsymbol{x}'_\perp\int_C d\boldsymbol{\theta}\int_C d\boldsymbol{\theta}'\, G_o(\boldsymbol{x}',\boldsymbol{y};\omega)G_o^\star(\boldsymbol{x},\boldsymbol{y};\omega)\Big\{e^{ik[\boldsymbol{\theta}\cdot\boldsymbol{x}-\boldsymbol{\theta}'\cdot\boldsymbol{x}'-\boldsymbol{y}\cdot(\boldsymbol{\theta}-\boldsymbol{\theta}')]}\\ &\times\left[\mathbb{E}\left[e^{ik[\gamma(\boldsymbol{x},\boldsymbol{\theta})-\gamma(\boldsymbol{x}',\boldsymbol{\theta}')]}\right]+1\right]+(k^2\langle\eta_1\rangle)^2\mathbb{E}\left[G(\boldsymbol{x},\boldsymbol{y};\omega)G^\star(\boldsymbol{x}',\boldsymbol{y};\omega)\right]\mathbb{E}\left[e^{ik[\gamma(\boldsymbol{y},\boldsymbol{\theta})-\gamma(\boldsymbol{y},\boldsymbol{\theta}')]}\right]\Big\},\end{aligned}$$

where we dropped all the exponentially small terms. Using Lemmas 4.3.1 and 4.3.2, we

see that the result is clearly much larger than the square of (4.120). Thus, the standard deviation of the image

$$\mathrm{std}[\mathcal{I}_1^M(\boldsymbol{y})] = \sqrt{\mathbb{E}\left[\left|\mathcal{I}_1^M(\boldsymbol{y})\right|^2\right] - \left|\mathbb{E}\left[\mathcal{I}_1^M(\boldsymbol{y})\right]\right|^2} \approx \sqrt{\mathbb{E}\left[\left|\mathcal{I}_1^M(\boldsymbol{y})\right|^2\right]}$$

is much larger than its mean, as stated in Proposition 1.

4.B.2 Imaging of the quadratic susceptibility

We obtain similarly from definitions (4.68) and (4.69), and the estimates (4.57) and (4.64) that

$$\mathbb{E}\left[\mathcal{I}_2^M(\boldsymbol{y}^R)\right] \approx 4k^2 \langle \eta_2 \rangle \int_A d\boldsymbol{x}_\perp \int_C d\boldsymbol{\theta}\, G_o(\boldsymbol{x}, \boldsymbol{y}; 2\omega) G_o^\star(\boldsymbol{x}, \boldsymbol{y}^R; 2\omega) e^{i2k\boldsymbol{\theta}\cdot(\boldsymbol{y}-\boldsymbol{y}^R) - \frac{|\boldsymbol{x}-\boldsymbol{y}|}{S_2} - \frac{|\boldsymbol{y}-\boldsymbol{y}^{(i)}(\boldsymbol{\theta})|}{S_2}}. \tag{4.121}$$

This peaks at $\boldsymbol{y} = \boldsymbol{y}$, where the phase cancells out, but the peak there is exponentially small, because $|\boldsymbol{x}-\boldsymbol{y}|$ and $|\boldsymbol{y}-\boldsymbol{y}^{(i)}(\boldsymbol{\theta})|$ are much larger than S_2. The second moment at the scatterer location is

$$\begin{aligned}\mathbb{E}\left[\left|\mathcal{I}_2^M(\boldsymbol{y})\right|^2\right] \approx (4k^2|\eta|_2)^2 \int_A d\boldsymbol{x}_\perp \int_A d\boldsymbol{x}'_\perp \int_C d\boldsymbol{\theta} \int_C d\boldsymbol{\theta}'\, G_o(\boldsymbol{x}', \boldsymbol{y}; 2\omega) G_o^\star(\boldsymbol{x}, \boldsymbol{y}; 2\omega) \\ \times \mathbb{E}\left[G(\boldsymbol{x}, \boldsymbol{y}; 2\omega) G^\star(\boldsymbol{x}', \boldsymbol{y}; 2\omega)\right] \mathbb{E}\left[e^{i2k[\gamma(\boldsymbol{y},\boldsymbol{\theta}) - \gamma(\boldsymbol{y},\boldsymbol{\theta}')]}\right],\end{aligned} \tag{4.122}$$

with the expectations in the second line given by (4.122). These expectations are large for nearby points in the array and nearby directions of illumination, and substituting in (4.122) and comparing with (4.121) leads us to the conclusion

$$\mathrm{std}[\mathcal{I}_2^M(\boldsymbol{y})] = \sqrt{\mathbb{E}\left[\left|\mathcal{I}_2^M(\boldsymbol{y})\right|^2\right] - \left|\mathbb{E}\left[\mathcal{I}_2^M(\boldsymbol{y})\right]\right|^2} \approx \sqrt{\mathbb{E}\left[\left|\mathcal{I}_2^M(\boldsymbol{y})\right|^2\right]}.$$

The statement in Proposition 1 follows. □

4.C Statistics of the CINT image

We calculate here the mean and variance of the CINT imaging functions $\mathcal{I}_j^{CINT}$, for $j = 1, 2$. The expression of the mean is needed to quantify the focusing of the image, and the variance is needed to assess the robustness with respect to different realizations of the random medium.

4.C.1 CINT image of the quadratic susceptibility

The expression of the CINT imaging function is obtained by substituting (4.83) in (4.84)

$$\begin{aligned}\mathcal{I}_2^{CINT}(\boldsymbol{y}^R) = (4k^2\langle\eta_2\rangle)^2 \\ \times \iint_{\mathcal{C}} d\boldsymbol{\theta} d\widetilde{\boldsymbol{\theta}}\, e^{-\frac{|\boldsymbol{P}_{\boldsymbol{\vartheta}}\widetilde{\boldsymbol{\theta}}|^2}{2\Theta^2}+i2k[(\boldsymbol{\theta}+\widetilde{\boldsymbol{\theta}}/2)\cdot(\boldsymbol{y}-\boldsymbol{y}^R)-(\boldsymbol{\theta}-\widetilde{\boldsymbol{\theta}}/2)\cdot(\boldsymbol{y}-\boldsymbol{y}^R)]+i2k[\gamma(\boldsymbol{y},\boldsymbol{\theta}+\widetilde{\boldsymbol{\theta}}/2)-\gamma(\boldsymbol{y},\boldsymbol{\theta}-\widetilde{\boldsymbol{\theta}}/2)]} \\ \iint_A d\boldsymbol{x}_\perp d\widetilde{\boldsymbol{x}}_\perp\, e^{-\frac{|\widetilde{\boldsymbol{x}}_\perp|^2}{2X^2}} G\Big(\boldsymbol{x}+\frac{\widetilde{\boldsymbol{x}}}{2},\boldsymbol{y};2\omega\Big)G^\star\Big(\boldsymbol{x}-\frac{\widetilde{\boldsymbol{x}}}{2},\boldsymbol{y};2\omega\Big) \\ \times G_o^\star\Big(\boldsymbol{x}+\frac{\widetilde{\boldsymbol{x}}}{2},\boldsymbol{y}^R;2\omega\Big)G_o\Big(\boldsymbol{x}-\frac{\widetilde{\boldsymbol{x}}}{2},\boldsymbol{y}^R;2\omega\Big)\,. \end{aligned} \tag{4.123}$$

It is given by the product of the integrals over the direction vectors and the receiver coordinates. Because of the statistical decorrelation stated in Lemma 4.3.3 (see also estimate (4.117)) we can study separately the statistics of these integrals, denoted by

$$\begin{aligned}\mathcal{J}_{\mathcal{A}}(\boldsymbol{y}^R) = \iint_{\mathcal{A}} d\boldsymbol{x}_\perp d\widetilde{\boldsymbol{x}}_\perp e^{-\frac{|\widetilde{\boldsymbol{x}}_\perp|^2}{2X^2}} G\Big(\boldsymbol{x}+\frac{\widetilde{\boldsymbol{x}}}{2},\boldsymbol{y};2\omega\Big)G^\star\Big(\boldsymbol{x}-\frac{\widetilde{\boldsymbol{x}}}{2},\boldsymbol{y};2\omega\Big)G_o^\star\Big(\boldsymbol{x}+\frac{\widetilde{\boldsymbol{x}}}{2},\boldsymbol{y}^R;2\omega\Big) \\ \times G_o\Big(\boldsymbol{x}-\frac{\widetilde{\boldsymbol{x}}}{2},\boldsymbol{y}^R;2\omega\Big),\end{aligned} \tag{4.124}$$

and

$$\mathcal{J}_{\mathcal{C}}(\boldsymbol{y}^R) = \iint_{\mathcal{C}} d\boldsymbol{\theta} d\widetilde{\boldsymbol{\theta}}_\perp \, e^{-\frac{|\boldsymbol{P}_{\boldsymbol{\vartheta}}\widetilde{\boldsymbol{\theta}}|^2}{2\Theta^2} + i2k[(\boldsymbol{\theta}+\widetilde{\boldsymbol{\theta}}/2)\cdot(\boldsymbol{y}-\boldsymbol{y}^R) - (\boldsymbol{\theta}-\widetilde{\boldsymbol{\theta}}/2)\cdot(\boldsymbol{y}-\boldsymbol{y}^R)] + i2k[\gamma(\boldsymbol{y},\boldsymbol{\theta}+\widetilde{\boldsymbol{\theta}}/2) - \gamma(\boldsymbol{y},\boldsymbol{\theta}-\widetilde{\boldsymbol{\theta}}/2)]}. \tag{4.125}$$

The expectation of the imaging function

The integral $\mathcal{J}_A(\boldsymbol{y}^R)$ models the CINT point spread function for a source at $\boldsymbol{y}$, and has been studied in [13]. Its expectation follows easily from Lemma 4.3.1 and the definition (4.76) of the set $\mathcal{A}$,

$$\mathbb{E}\left[\mathcal{J}_A(\boldsymbol{y}^R)\right] \approx \frac{1}{L^4}\int_A d\boldsymbol{x}_\perp \int_{\mathbb{R}^2} d\widetilde{\boldsymbol{x}}_\perp e^{-\frac{|\widetilde{\boldsymbol{x}}_\perp|^2}{2X_e^2} + i2k\widetilde{\boldsymbol{x}}_\perp\cdot(\boldsymbol{y}_\perp^R - \boldsymbol{y}_\perp)} \approx \frac{2\pi a^2 X_e^2}{L^4} e^{-\frac{1}{2}\left(\frac{2kX_e|\boldsymbol{y}_\perp - \boldsymbol{y}_\perp^R|}{L}\right)^2}, \tag{4.126}$$

with X_e defined as in Proposition 2. Here we extended the $\widetilde{\boldsymbol{x}}_\perp$ integral to the whole plane using that $X_e \sim X_{d,2} \ll a$.

Similarly, using Lemma 4.3.2 we get

$$\begin{aligned}\mathbb{E}\left[\mathcal{J}_C(\boldsymbol{y}^R)\right] &\approx \iint_{\mathcal{C}} d\boldsymbol{\theta} d\widetilde{\boldsymbol{\theta}}_\perp \, e^{-\frac{|\boldsymbol{P}_{\boldsymbol{\vartheta}}\widetilde{\boldsymbol{\theta}}|^2}{2\Theta_e^2} + i2k\widetilde{\boldsymbol{\theta}}\cdot(\boldsymbol{y}-\boldsymbol{y}^R)} \\ &= \iint_{\mathcal{C}} d\boldsymbol{\theta} d\widetilde{\boldsymbol{\theta}}_\perp \, e^{-\frac{\left(\widetilde{\theta}_\eta^2 + \widetilde{\theta}_\zeta^2\right)}{2\Theta_e^2} + i2k\widetilde{\theta}_\zeta\boldsymbol{\zeta}\cdot(\boldsymbol{y}-\boldsymbol{y}^R) + 2ik\widetilde{\theta}_\eta\left(\boldsymbol{\eta} - \tan\varphi\boldsymbol{\vartheta}\right)\cdot(\boldsymbol{y}-\boldsymbol{y}^R)}\end{aligned} \tag{4.127}$$

with Θ_e as in Proposition 2, and $\widetilde{\theta}_\eta$, $\widetilde{\theta}_\zeta$, φ parametrizing $\boldsymbol{\theta}$ and $\widetilde{\boldsymbol{\theta}}$ as in equations (4.77)-(4.82). To write the integral over the set $\mathcal{C}$, we recall from (4.77) and (4.81) that

$$\boldsymbol{\theta} = \boldsymbol{\vartheta}\cos\varphi + \boldsymbol{\eta}(\beta)\sin\varphi + O(\Theta_d^2),$$

with azimuthal angle β parametrizing the vectors $\boldsymbol{\eta}(\beta)$ and $\boldsymbol{\zeta}(\beta)$. In the calculation of the

Jacobian of the transformation we may neglect the residual in this equation, and obtain

$$d\boldsymbol{\theta} \rightsquigarrow \sin\varphi d\varphi d\beta.$$

We also see from equation (4.82) that for any given φ and β we have, using $\varphi = O(\alpha) = O(a/L) \ll 1$, that

$$\partial_{\widetilde{\theta}_\eta}\widetilde{\boldsymbol{\theta}} \approx \boldsymbol{\eta}(\beta) \quad \text{and} \quad \partial_{\widetilde{\theta}_\zeta}\widetilde{\boldsymbol{\theta}} \approx \boldsymbol{\zeta}(\beta),$$

and since $\boldsymbol{\eta}(\beta)$ and $\boldsymbol{\zeta}(\beta)$ are orthonormal, we get

$$d\widetilde{\boldsymbol{\theta}} \rightsquigarrow d\widetilde{\theta}_\eta d\widetilde{\theta}_\zeta.$$

The integrals over $\widetilde{\theta}_\eta$ and $\widetilde{\theta}_\zeta$ may be extended to the real line, because the Gaussians are negligible outside $\mathcal{C}$, and the result is

$$\mathbb{E}\left[\mathcal{J}_C(\boldsymbol{y}^R)\right] \approx 2\pi\Theta_e^2 \int_0^\alpha d\varphi \, \sin\varphi \int_0^{2\pi} d\beta e^{-\frac{(2k\Theta_e)^2}{2}\left\{\left[(\boldsymbol{y}-\boldsymbol{y}^R)\cdot\boldsymbol{\zeta}(\beta)\right]^2+\left[(\boldsymbol{y}-\boldsymbol{y}^R)\cdot\boldsymbol{\eta}(\beta)-\tan\varphi(\boldsymbol{y}-\boldsymbol{y}^R)\cdot\boldsymbol{\vartheta}\right]^2\right\}}. \tag{4.128}$$

We are interested only in the points $\boldsymbol{y}^R$ for which $\mathcal{J}_{\mathcal{A}}(\boldsymbol{y}^R)$ is large, so

$$|(\boldsymbol{y}-\boldsymbol{y}^R)\cdot\boldsymbol{\vartheta}| = O\left(\frac{L}{kX_e}\right).$$

Since $\Theta_e \approx X_e/L$ and $\varphi \leq \alpha \ll 1$, we have

$$k\Theta_e \tan\varphi |(\boldsymbol{y}-\boldsymbol{y}^R)\cdot\boldsymbol{\vartheta}| \leq O(\alpha) \ll 1,$$

so we can neglect the φ dependent term in the exponential in (4.128). We also note that

$$\big[(\boldsymbol{y}-\boldsymbol{y}^R)\cdot\boldsymbol{\zeta}(\beta)\big]^2+\big[(\boldsymbol{y}-\boldsymbol{y}^R)\cdot\boldsymbol{\eta}(\beta)\big]^2=\big|\boldsymbol{P}_{\boldsymbol{\vartheta}}(\boldsymbol{y}-\boldsymbol{y}^R)\big|^2$$

is independent of β, so we obtain

$$\mathbb{E}\left[\mathcal{J}_C(\boldsymbol{y}^R)\right]\approx 2\pi\Theta_e^2 e^{-\frac{\left[2k\Theta_e\left|\boldsymbol{P}_{\boldsymbol{\vartheta}}(\boldsymbol{y}-\boldsymbol{y}^R)\right|\right]^2}{2}}\int_0^\alpha d\varphi\,\sin\varphi\int_0^{2\pi}d\beta=2\pi^2\Theta_e^2\alpha^2 e^{-\frac{\left[2k\Theta_e\left|\boldsymbol{P}_{\boldsymbol{\vartheta}}(\boldsymbol{y}-\boldsymbol{y}^R)\right|\right]^2}{2}}. \tag{4.129}$$

Proposition 2 follows. □

The variance of the imaging function

The variance of $\mathcal{J}_A$ is calculated in [13, Appendix E], so we revisit here the main ideas. The calculation involves the fourth moments of the Green's function (4.45), which are determined by

$$\mathbb{E}\Big\{e^{i2k\left[\nu\left(\boldsymbol{x}+\frac{\widetilde{\boldsymbol{x}}}{2},\boldsymbol{y}\right)-\nu\left(\boldsymbol{x}-\frac{\widetilde{\boldsymbol{x}}}{2},\boldsymbol{y}\right)-\nu\left(\boldsymbol{x}'+\frac{\widetilde{\boldsymbol{x}}'}{2},\boldsymbol{y}\right)+\nu\left(\boldsymbol{x}'-\frac{\widetilde{\boldsymbol{x}}'}{2},\boldsymbol{y}\right)\right]}\Big\}\approx e^{-\tau/2}, \tag{4.130}$$

where we introduced the notation

$$\tau=(2k)^2\mathbb{E}\big\{\big[\nu\big(\boldsymbol{x}+\frac{\widetilde{\boldsymbol{x}}}{2},\boldsymbol{y}\big)-\nu\big(\boldsymbol{x}-\frac{\widetilde{\boldsymbol{x}}}{2},\boldsymbol{y}\big)-\nu\big(\boldsymbol{x}'+\frac{\widetilde{\boldsymbol{x}}'}{2},\boldsymbol{y}\big)+\nu\big(\boldsymbol{x}'-\frac{\widetilde{\boldsymbol{x}}'}{2},\boldsymbol{y}\big)\big]^2\big\}, \tag{4.131}$$

and used the approximate Gaussianity of the phases. We need the second moments (4.90), rewritten as

$$(2k)^2\mathbb{E}\left[\nu(\boldsymbol{x},\boldsymbol{y})\nu(\boldsymbol{x}',\boldsymbol{y})\right]=\frac{3\ell^2}{X_{d,2}^2}h\left(\frac{|\boldsymbol{x}_\perp-\boldsymbol{x}'_\perp|}{\ell}\right),\qquad h(z)=\frac{1}{z}\int_0^z dt\,e^{-\frac{t^2}{2}}, \tag{4.132}$$

using the definition (4.59) of the decoherence length. The expression (4.131) becomes

$$\tau = \frac{6\ell^2}{X_{d,2}^2}\left[2 - h\Big(\frac{\widetilde{\boldsymbol{x}}_\perp}{\ell}\Big) - h\Big(\frac{\widetilde{\boldsymbol{x}}'_\perp}{\ell}\Big) + h\Big(\frac{\boldsymbol{x}_\perp - \boldsymbol{x}'_\perp}{\ell} + \frac{\widetilde{\boldsymbol{x}}_\perp + \widetilde{\boldsymbol{x}}'_\perp}{2\ell}\Big) + h\Big(\frac{\boldsymbol{x}_\perp - \boldsymbol{x}'_\perp}{\ell} - \frac{\widetilde{\boldsymbol{x}}_\perp + \widetilde{\boldsymbol{x}}'_\perp}{2\ell}\Big)\right.$$
$$\left. - h\Big(\frac{\boldsymbol{x}_\perp - \boldsymbol{x}'_\perp}{\ell} + \frac{\widetilde{\boldsymbol{x}}_\perp - \widetilde{\boldsymbol{x}}'_\perp}{2\ell}\Big) - h\Big(\frac{\boldsymbol{x}_\perp - \boldsymbol{x}'_\perp}{\ell} - \frac{\widetilde{\boldsymbol{x}}_\perp - \widetilde{\boldsymbol{x}}'_\perp}{2\ell}\Big)\right],$$

and we can simplify it because $|\widetilde{\boldsymbol{x}}_\perp|, |\widetilde{\boldsymbol{x}}'_\perp| \lesssim X_{d,2} \ll \ell$, due to the windowing in the calculation of the cross-correlations. Expanding in $\widetilde{\boldsymbol{x}}_\perp/\ell$ and $\widetilde{\boldsymbol{x}}'/\ell'$ we get

$$\tau \approx \frac{6}{X_{d,2}^2}\left[\frac{|\widetilde{\boldsymbol{x}}_\perp|^2 + |\widetilde{\boldsymbol{x}}'_\perp|^2}{6} + \widetilde{\boldsymbol{x}}_\perp \cdot H\Big(\frac{\boldsymbol{x}_\perp - \boldsymbol{x}'_\perp}{\ell}\Big)\widetilde{\boldsymbol{x}}'_\perp\right], \tag{4.133}$$

where H is the Hessian of h, evaluated at $(\boldsymbol{x}_\perp - \boldsymbol{x}'_\perp)/\ell$.

Because the Hessian decays, we note that the phase differences at points satisfying $|\boldsymbol{x}_\perp - \boldsymbol{x}'_\perp| \gg \ell$ are decorrelated

$$\tau \approx \frac{|\widetilde{\boldsymbol{x}}_\perp|^2 + |\widetilde{\boldsymbol{x}}'_\perp|^2}{X_{d,2}^2} = (2k)^2\mathbb{E}\Big\{\Big[\nu\Big(\boldsymbol{x} + \frac{\widetilde{\boldsymbol{x}}}{2}, \boldsymbol{y}\Big) - \nu\Big(\boldsymbol{x} - \frac{\widetilde{\boldsymbol{x}}}{2}, \boldsymbol{y}\Big)\Big]^2\Big\} + (2k)^2\mathbb{E}\Big\{\Big[\nu\Big(\boldsymbol{x}' + \frac{\widetilde{\boldsymbol{x}}'}{2}, \boldsymbol{y}\Big)$$
$$-\nu\Big(\boldsymbol{x}' - \frac{\widetilde{\boldsymbol{x}}'}{2}, \boldsymbol{y}\Big)\Big]^2\Big\}.$$

It is only for $|\boldsymbol{x}_\perp - \boldsymbol{x}'_\perp| \lesssim \ell$ that the Hessian contributes to (4.133). Thus, when calculating the variance of the CINT imaging function, we get a contribution only from the set of points

$$\{\boldsymbol{x}, \boldsymbol{x}' \in A, \quad |\boldsymbol{x}_\perp - \boldsymbol{x}'_\perp| \lesssim \ell\}.$$

This is why the SNR of $\mathcal{J}_A$ is of order a/ℓ. We refer to [13, Appendix E] for more details.

The calculation of the variance of $\mathcal{J}_C$ is similar, and the SNR is of the same order.

4.C.2 CINT image of the linear susceptibility

The expression of the imaging function is obtained by substituting (4.87) in (4.88),

$$\begin{aligned}
&\mathcal{I}_1^{CINT}(\boldsymbol{y}^R)\\
&= \iint_{\mathcal{A}} d\boldsymbol{x}_\perp d\widetilde{\boldsymbol{x}}_\perp \iint_{\mathcal{C}} d\boldsymbol{\theta} d\widetilde{\boldsymbol{\theta}}\, e^{-\frac{|\widetilde{\boldsymbol{x}}_\perp|^2}{2X^2}-\frac{|\boldsymbol{P}_{\vartheta}\widetilde{\boldsymbol{\theta}}|^2}{2\Theta^2}} G_o^\star\Big(\boldsymbol{x}+\frac{\widetilde{\boldsymbol{x}}}{2},\boldsymbol{y}^R;\omega\Big) G_o\Big(\boldsymbol{x}-\frac{\widetilde{\boldsymbol{x}}}{2},\boldsymbol{y}^R;\omega\Big) e^{-ik\widetilde{\boldsymbol{\theta}}\cdot\boldsymbol{y}^R}\\
&\times\Big\{\Big[e^{ik\gamma\left(\boldsymbol{x}+\frac{\widetilde{\boldsymbol{x}}}{2},\boldsymbol{\theta}+\frac{\widetilde{\boldsymbol{\theta}}}{2}\right)}-1\Big] e^{ik\left(\boldsymbol{\theta}+\frac{\widetilde{\boldsymbol{\theta}}}{2}\right)\cdot\left(\boldsymbol{x}+\frac{\widetilde{\boldsymbol{x}}}{2}\right)} + k^2\langle\eta_1\rangle\, G\Big(\boldsymbol{x}+\frac{\widetilde{\boldsymbol{x}}}{2},\boldsymbol{y};\omega\Big) e^{ik\left(\boldsymbol{\theta}+\frac{\widetilde{\boldsymbol{\theta}}}{2}\right)\cdot\boldsymbol{y}+ik\gamma\left(\boldsymbol{y},\boldsymbol{\theta}+\frac{\widetilde{\boldsymbol{\theta}}}{2}\right)}\Big\}\\
&\times\Big\{\Big[e^{-ik\gamma\left(\boldsymbol{x}-\frac{\widetilde{\boldsymbol{x}}}{2},\boldsymbol{\theta}-\frac{\widetilde{\boldsymbol{\theta}}}{2}\right)}-1\Big] e^{-ik\left(\boldsymbol{\theta}-\frac{\widetilde{\boldsymbol{\theta}}}{2}\right)\cdot\left(\boldsymbol{x}-\frac{\widetilde{\boldsymbol{x}}}{2}\right)} + k^2\langle\eta_1\rangle\, G^\star\Big(\boldsymbol{x}-\frac{\widetilde{\boldsymbol{x}}}{2},\boldsymbol{y};\omega\Big) e^{-ik\left(\boldsymbol{\theta}-\frac{\widetilde{\boldsymbol{\theta}}}{2}\right)\cdot\boldsymbol{y}-ik\gamma\left(\boldsymbol{y},\boldsymbol{\theta}-\frac{\widetilde{\boldsymbol{\theta}}}{2}\right)}\Big\}.
\end{aligned} \tag{4.134}$$

Using Lemmas 4.3.1-4.3.3, we obtain its expectation

$$\begin{aligned}
\mathbb{E}\Big[\mathcal{I}_1^{CINT}(\boldsymbol{y}^R)\Big] \approx \iint_{\mathcal{A}} d\boldsymbol{x}_\perp d\widetilde{\boldsymbol{x}}_\perp \iint_{\mathcal{C}} d\boldsymbol{\theta} d\widetilde{\boldsymbol{\theta}}\, e^{-\frac{|\widetilde{\boldsymbol{x}}_\perp|^2}{2X^2}-\frac{|\boldsymbol{P}_{\vartheta}\widetilde{\boldsymbol{\theta}}|^2}{2\Theta^2}} G_o^\star\Big(\boldsymbol{x}+\frac{\widetilde{\boldsymbol{x}}}{2},\boldsymbol{y}^R;\omega\Big) G_o\Big(\boldsymbol{x}-\frac{\widetilde{\boldsymbol{x}}}{2},\boldsymbol{y}^R;\omega\Big)\\
\times e^{-ik\widetilde{\boldsymbol{\theta}}\cdot\boldsymbol{y}^R}\Big\{ e^{ik\boldsymbol{\theta}\cdot\widetilde{\boldsymbol{x}}+ik\widetilde{\boldsymbol{\theta}}\cdot\boldsymbol{x}}\Big[\mathbb{E}\Big[e^{ik\left[\gamma\left(\boldsymbol{x}+\frac{\widetilde{\boldsymbol{x}}}{2},\boldsymbol{\theta}+\frac{\widetilde{\boldsymbol{\theta}}}{2}\right)-\gamma\left(\boldsymbol{x}+\frac{\widetilde{\boldsymbol{x}}}{2},\boldsymbol{\theta}+\frac{\widetilde{\boldsymbol{\theta}}}{2}\right)\right]}\Big]+1\Big]\\
+ k^4\langle\eta_1\rangle^2 e^{ik\widetilde{\boldsymbol{\theta}}\cdot\boldsymbol{y}}\mathbb{E}\Big[G\Big(\boldsymbol{x}+\frac{\widetilde{\boldsymbol{x}}}{2},\boldsymbol{y};\omega\Big)G^\star\Big(\boldsymbol{x}-\frac{\widetilde{\boldsymbol{x}}}{2},\boldsymbol{y};\omega\Big)\Big]\mathbb{E}\Big[e^{ik\left[\gamma\left(\boldsymbol{y},\boldsymbol{\theta}+\frac{\widetilde{\boldsymbol{\theta}}}{2}\right)-\gamma\left(\boldsymbol{y},\boldsymbol{\theta}+\frac{\widetilde{\boldsymbol{\theta}}}{2}\right)\right]}\Big]\Big\},
\end{aligned} \tag{4.135}$$

where we neglected the exponentially small terms. We write the right hand side as the sum of three terms

$$\mathbb{E}\Big[\mathcal{I}_1^{CINT}(\boldsymbol{y}^R)\Big] \approx \mathcal{T}_1(\boldsymbol{y}^R)+\mathcal{T}_2(\boldsymbol{y}^R)+\mathcal{T}_3(\boldsymbol{y}^R). \tag{4.136}$$

The first two are due to the uncompensated direct wave, and are given by

$$\mathcal{T}_1(\boldsymbol{y}^R) = \frac{1}{L^2}\iint_{\mathcal{A}} d\boldsymbol{x}_\perp d\widetilde{\boldsymbol{x}}_\perp \int_{\mathcal{C}} d\boldsymbol{\theta} d\widetilde{\boldsymbol{\theta}}\, e^{ik\widetilde{\boldsymbol{x}}\cdot\boldsymbol{\theta}-ik\frac{\widetilde{\boldsymbol{x}}_\perp\cdot(\boldsymbol{x}_\perp-\boldsymbol{y}_\perp^R)}{L}+ik\widetilde{\boldsymbol{\theta}}\cdot(\boldsymbol{x}-\boldsymbol{y}^R)-\frac{|\widetilde{\boldsymbol{x}}_\perp|^2}{2X^2}-\frac{|\boldsymbol{P}_{\vartheta}\widetilde{\boldsymbol{\theta}}|^2}{2\Theta^2}}, \tag{4.137}$$

and

$$\mathcal{T}_2(\boldsymbol{y}^R) = \frac{1}{L^2}\iint_{\mathcal{A}} d\boldsymbol{x}_\perp d\widetilde{\boldsymbol{x}}_\perp \int_{\mathcal{C}} d\boldsymbol{\theta} d\widetilde{\boldsymbol{\theta}}\, e^{ik\widetilde{\boldsymbol{x}}\cdot\boldsymbol{\theta} - ik\frac{\widetilde{\boldsymbol{x}}_\perp\cdot(\boldsymbol{x}_\perp-\boldsymbol{y}_\perp^R)}{L}\big) + ik\widetilde{\boldsymbol{\theta}}\cdot(\boldsymbol{x}-\boldsymbol{y}^R) - \frac{|\widetilde{\boldsymbol{x}}_\perp|^2}{2X^2} - \frac{|\boldsymbol{P}_{\boldsymbol{\vartheta}}\widetilde{\boldsymbol{\theta}}|^2}{2\Theta^2}}$$
$$\times e^{-\frac{|\boldsymbol{P}_{\boldsymbol{\vartheta}}\widetilde{\boldsymbol{\theta}}|^2}{2[X_{d,1}/|\boldsymbol{x}-\boldsymbol{x}^{(i)}(\boldsymbol{\theta})|]^2} - \frac{3}{2}\frac{|\boldsymbol{P}_{\boldsymbol{\vartheta}}\widetilde{\boldsymbol{x}}|^2}{X_{d,1}^2} + \frac{3}{2}\frac{\boldsymbol{P}_{\boldsymbol{\vartheta}}\widetilde{\boldsymbol{x}}}{X_{d,1}}\cdot\frac{\boldsymbol{P}_{\boldsymbol{\vartheta}}\widetilde{\boldsymbol{\theta}}}{X_{d,1}/|\boldsymbol{x}-\boldsymbol{x}^{(i)}(\boldsymbol{\theta})|}}. \qquad (4.138)$$

Here we used the paraxial approximation (4.42) and moment formula (4.60). The third term is similar to the expectation of the imaging function for the quadratic susceptibility $\mathbb{E}[\mathcal{I}_2^{CINT}(\boldsymbol{y}^R)]$, so we write it directly,

$$\mathcal{T}_3(\boldsymbol{y}^R) = \frac{(2\pi)^3}{2}\left(k^2\langle\eta_1\rangle^2\alpha\Theta_e\frac{aX_e}{L^2}\right)^2 \exp\left[-\frac{1}{2}\left(\frac{kX_e|\boldsymbol{y}_\perp-\boldsymbol{y}_\perp^R|}{L}\right)^2 - \frac{1}{2}\left(k\Theta_e|\boldsymbol{P}_{\boldsymbol{\vartheta}}(\boldsymbol{y}-\boldsymbol{y}^R)|\right)^2\right], \qquad (4.139)$$

with X_e and Θ_e defined as in Proposition 3.

To calculate (4.137) we recall the definition (4.76) of the set $\mathcal{A}$ and the parametrization of the set $\mathcal{C}$ described in equations (4.77)-(4.82). We integrate over $\widetilde{\boldsymbol{x}}_\perp$ using that $\widetilde{\boldsymbol{x}}$ is orthogonal to $\boldsymbol{n}$, and

$$k\widetilde{\boldsymbol{x}}\cdot\boldsymbol{\theta} = k|\boldsymbol{\theta}|\widetilde{\boldsymbol{x}}\cdot(\cos\varphi\,\boldsymbol{\vartheta} + \sin\varphi\,\boldsymbol{\eta}(\beta)) = k\widetilde{\boldsymbol{x}}_\perp(\cos\varphi\,\boldsymbol{\vartheta}_\perp + \sin\varphi\,\boldsymbol{\eta}_\perp(\beta)) + O(kX_{d,1}\Theta_d^2),$$

with two dimensional vectors $\boldsymbol{\vartheta}_\perp$ and $\boldsymbol{\eta}_\perp$ of components of $\boldsymbol{\vartheta}$ and $\boldsymbol{\eta}$ in the plane orthogonal to $\boldsymbol{n}$. The residual is negligible by equations (4.59), (4.63) and assumption (4.43),

$$kX_{d,1}\Theta_d^2 = O\left(\frac{X_{d,1}^3}{\lambda L^2}\right) \ll \frac{\ell^3}{\lambda L^2} \ll 1.$$

To integrate over $\widetilde{\boldsymbol{\theta}}$, more precisely over $\widetilde{\theta}_\eta$ and $\widetilde{\theta}_\zeta$, we use that

$$|\boldsymbol{P}_{\boldsymbol{\vartheta}}\widetilde{\boldsymbol{\theta}}|^2 = \widetilde{\theta}_\eta^2 + \widetilde{\theta}_\zeta^2, \qquad \widetilde{\boldsymbol{\theta}}\cdot(\boldsymbol{x}-\boldsymbol{y}) = \widetilde{\theta}_\eta(\boldsymbol{x}-\boldsymbol{y}^R)\cdot\big(\boldsymbol{\eta}-\boldsymbol{\vartheta}\tan\varphi\big) + \widetilde{\theta}_\zeta(\boldsymbol{x}-\boldsymbol{y}^R)\cdot\boldsymbol{\zeta}.$$

We obtain that

$$\mathcal{T}_1(\boldsymbol{y}^R) \approx \frac{(2\pi)^2 X^2 \Theta^2}{L^2} \int_A d\boldsymbol{x}_\perp \int_0^\alpha d\varphi \, \sin\varphi \int_0^\beta d\beta e^{-\frac{(kX)^2}{2}\left| \cos\varphi \, \boldsymbol{\vartheta}_\perp - \frac{\boldsymbol{x}_\perp - \boldsymbol{y}_\perp^R}{L} + \sin\varphi \boldsymbol{\eta}_\perp(\beta)\right|^2} \\ \times e^{-\frac{(k\Theta)^2}{2}\left\{ \left[(\boldsymbol{x}-\boldsymbol{y}^R)\cdot\boldsymbol{\zeta}(\beta)\right]^2 + \left[(\boldsymbol{x}-\boldsymbol{y}^R)\cdot\boldsymbol{\eta}(\beta) - \tan\varphi(\boldsymbol{x}-\boldsymbol{y}^R)\cdot\boldsymbol{\vartheta}\right]^2\right\}}, \quad (4.140)$$

and note that the result is exponentially small. The first exponential is small because

$$\left| \cos\varphi \, \boldsymbol{\vartheta}_\perp - \frac{\boldsymbol{x}_\perp - \boldsymbol{y}_\perp^R}{L} + \sin\varphi \boldsymbol{\eta}_\perp(\beta)\right| = \cos\varphi + O\left(\frac{a}{L}\right) \approx 1,$$

and by definition (4.59) and assumptions (4.43)-(4.44), we have

$$kX = O\left(\frac{X_{d,1}}{\lambda}\right) = O\left(\frac{\sqrt{\ell}}{\sigma\sqrt{L}}\right) \gg \sqrt{\frac{L}{\lambda}} \gg 1.$$

The second exponential is small because

$$k\Theta\sqrt{\left[(\boldsymbol{x}-\boldsymbol{y}^R)\cdot\boldsymbol{\zeta}(\beta)\right]^2 + \left[(\boldsymbol{x}-\boldsymbol{y}^R)\cdot\boldsymbol{\eta}(\beta) - \tan\varphi(\boldsymbol{x}-\boldsymbol{y}^R)\cdot\boldsymbol{\vartheta}\right]^2} = O(k\Theta L) = O(kX_{d,1}) \gg 1.$$

The calculation of (4.138) is similar, slightly more involved, and the result is exponentially small for points $\boldsymbol{y}^R$ in the imaging region R.

The calculation of the variance of $\mathcal{I}_1^{CINT}(\boldsymbol{y}^R)$ is very similar to that described in appendix 4.C.1. It shows that the direct wave has a negligible effect at points $\boldsymbol{y}^R \in R$, due to the large deterministic uncompensated phases. The variance is approximately equal to that of the useful term in the imaging function, which focuses at the scatterer, and the SNR is of order $(a/\ell)^2$, as in the case of quadratic susceptibility. This is the statement in Proposition 3. $\square$.

It remains to verify Proposition 4, by studying the imaging function (4.134) at points $\boldsymbol{y}^R$ outside the small search region R. It suffices to consider only the terms that involve the

direct waves, because we know from the analysis above that the the waves that interact with the scatterer at $\boldsymbol{y}$ contribute to the image only in the vicinity of $\boldsymbol{y}$. We obtain from (4.134) that the contribution of the direct waves to the expectation of the image is given by the sum of two terms

$$\mathcal{T}_1(\boldsymbol{y}^R) = \iint_{\mathcal{A}} d\boldsymbol{x}_\perp d\widetilde{\boldsymbol{x}}_\perp \iint_{\mathcal{C}} d\boldsymbol{\theta} d\widetilde{\boldsymbol{\theta}}\, e^{-\frac{|\widetilde{\boldsymbol{x}}_\perp|^2}{2X^2} - \frac{|\boldsymbol{P}_{\boldsymbol{\vartheta}}\widetilde{\boldsymbol{\theta}}|^2}{2\Theta^2}} G_o^\star\Big(\boldsymbol{x} + \frac{\widetilde{\boldsymbol{x}}}{2}, \boldsymbol{y}^R; \omega\Big) \times G_o\Big(\boldsymbol{x} - \frac{\widetilde{\boldsymbol{x}}}{2}, \boldsymbol{y}^R; \omega\Big) e^{ik\widetilde{\boldsymbol{\theta}}\cdot(\boldsymbol{x}-\boldsymbol{y}^R) + ik\boldsymbol{\theta}\cdot\widetilde{\boldsymbol{x}}}\,, \tag{4.141}$$

and

$$\mathcal{T}_2(\boldsymbol{y}^R) = \iint_{\mathcal{A}} d\boldsymbol{x}_\perp d\widetilde{\boldsymbol{x}}_\perp \iint_{\mathcal{C}} d\boldsymbol{\theta} d\widetilde{\boldsymbol{\theta}}\, e^{-\frac{|\widetilde{\boldsymbol{x}}_\perp|^2}{2X^2} - \frac{|\boldsymbol{P}_{\boldsymbol{\vartheta}}\widetilde{\boldsymbol{\theta}}|^2}{2\Theta^2}} G_o^\star\Big(\boldsymbol{x} + \frac{\widetilde{\boldsymbol{x}}}{2}, \boldsymbol{y}^R; \omega\Big) G_o\Big(\boldsymbol{x} - \frac{\widetilde{\boldsymbol{x}}}{2}, \boldsymbol{y}^R; \omega\Big) \times e^{ik\widetilde{\boldsymbol{\theta}}\cdot(\boldsymbol{x}-\boldsymbol{y}^R) + ik\boldsymbol{\theta}\cdot\widetilde{\boldsymbol{x}} - \frac{|\boldsymbol{P}_{\boldsymbol{\vartheta}}\widetilde{\boldsymbol{\theta}}|^2}{2[X_{d,1}/|\boldsymbol{x}-\boldsymbol{x}^{(i)}(\boldsymbol{\theta})|]^2} - \frac{3}{2}\frac{|\boldsymbol{P}_{\boldsymbol{\vartheta}}\widetilde{\boldsymbol{x}}|^2}{X_{d,1}^2} + \frac{3}{2}\frac{\boldsymbol{P}_{\boldsymbol{\vartheta}}\widetilde{\boldsymbol{x}}}{X_{d,1}}\cdot\frac{\boldsymbol{P}_{\boldsymbol{\vartheta}}\widetilde{\boldsymbol{\theta}}}{X_{d,1}/|\boldsymbol{x}-\boldsymbol{x}^{(i)}(\boldsymbol{\theta})|}}\,. \tag{4.142}$$

The product of the Green's functions in these expressions is approximated by

$$G_o^\star\Big(\boldsymbol{x} + \frac{\widetilde{\boldsymbol{x}}}{2}, \boldsymbol{y}^R; \omega\Big) G_o\Big(\boldsymbol{x} - \frac{\widetilde{\boldsymbol{x}}}{2}, \boldsymbol{y}^R; \omega\Big) \approx \frac{1}{|\boldsymbol{y} - \boldsymbol{y}^R|^2} e^{ik\widetilde{\boldsymbol{x}}\cdot\frac{(\boldsymbol{x}-\boldsymbol{y})}{|\boldsymbol{x}-\boldsymbol{y}|}}\,, \tag{4.143}$$

because

$$k\Big(\Big|\boldsymbol{x} + \frac{\widetilde{\boldsymbol{x}}}{2} - \boldsymbol{y}^R\Big| - \Big|\boldsymbol{x} - \frac{\widetilde{\boldsymbol{x}}}{2} - \boldsymbol{y}^R\Big|\Big) = k\widetilde{\boldsymbol{x}}\cdot\frac{(\boldsymbol{x}-\boldsymbol{y}^R)}{|\boldsymbol{x}-\boldsymbol{y}^R|} + O\left(\frac{|\widetilde{\boldsymbol{x}}|^3 (y_\parallel^R)^2 |\boldsymbol{x}_\perp - \boldsymbol{y}_\perp^R|}{\lambda|\boldsymbol{x}-\boldsymbol{y}^R|^5}\right), \tag{4.144}$$

assuming $|\boldsymbol{x}-\boldsymbol{y}^R| \gg X$, which holds for a fixed $\boldsymbol{y}^R$ at all $\boldsymbol{x}$ in the aperture, with the possible exception of a small set, of radius of order X, which makes a negligible contribution to the integrals in (4.141) and (4.142). Under this condition we see that the residual in (4.144) is negligible for search points near the array (with small enough $y_\parallel^R$), and we can approximate the integrals (4.141) and (4.142) using the approximation (4.143).

Substituting (4.143) in (4.141), and integrating over $\widetilde{\boldsymbol{x}}$ and $\widetilde{\boldsymbol{\theta}}$ we get that

$$\mathcal{T}_1(\boldsymbol{y}^R) \approx (2\pi X\Theta/2)^2 \int_A d\boldsymbol{x}_\perp \frac{1}{|\boldsymbol{x}-\boldsymbol{y}^R|^2} \int_0^\alpha d\varphi \, \sin\varphi \int_0^{2\pi} d\beta e^{-\frac{(kX)^2}{2}\left|\boldsymbol{P_n}\left(\boldsymbol{\theta}-\frac{\boldsymbol{y}^R-\boldsymbol{x}}{|\boldsymbol{y}^R-\boldsymbol{x}|}\right)\right|^2} \times e^{-\frac{(k\Theta)^2}{2}\left\{[(\boldsymbol{x}-\boldsymbol{y}^R)\cdot\boldsymbol{\zeta}(\beta)]^2+[(\boldsymbol{x}-\boldsymbol{y}^R)\cdot(\boldsymbol{\eta}(\beta)-\tan\varphi\boldsymbol{\vartheta})]^2\right\}}, \quad (4.145)$$

with $\boldsymbol{\theta}$ parametrized as in equations (4.77) and (4.77). It is difficult to evaluate these integrals explicitly, unless we make further scaling assumptions on the location of $\boldsymbol{y}^R$. However, it is clear that (4.145) is large when

$$\left|\boldsymbol{P_n}\left(\boldsymbol{\theta}-\frac{\boldsymbol{y}^R-\boldsymbol{x}}{|\boldsymbol{y}^R-\boldsymbol{x}|}\right)\right| \lesssim \frac{1}{kX} = O\left(\frac{\lambda}{X_{d,1}}\right) \ll 1, \quad (4.146)$$

for most directions $\boldsymbol{\theta}$ in the cone of illuminations. Equations (4.77) and (4.77), and the assumed orthogonality of $\boldsymbol{\vartheta}$ and $\boldsymbol{n}$ give that

$$\boldsymbol{P_n}\boldsymbol{\theta} = \cos\varphi\boldsymbol{\vartheta} + \sin\varphi\boldsymbol{P_n}\boldsymbol{\eta}(\beta),$$

and since $\varphi \le \alpha = O(a/L) \ll 1$, we see that the image is large when

$$\boldsymbol{\vartheta}\cdot\frac{(\boldsymbol{y}^R-\boldsymbol{x})}{|\boldsymbol{y}^R-\boldsymbol{x}|} \approx \cos\varphi \approx 1. \quad (4.147)$$

This can hold only at points $\boldsymbol{y}^R$ near the array. The second exponential in (4.145) is large when

$$\left|\boldsymbol{P}_{\boldsymbol{\vartheta}}(\boldsymbol{x}-\boldsymbol{y}^R)\right| \lesssim \frac{1}{k\Theta} = O\left(\frac{\lambda L}{X_{d,1}}\right),$$

which is consistent with (4.147).

The calculation of (4.142) is similar, and leads to the same conclusion. We end with the remark that the set of points where $\mathcal{T}_1(\boldsymbol{y}^R)$ and $\mathcal{T}_2(\boldsymbol{y}^R)$ are large depends on the aperture

size and the opening angle of the cone of illuminations. Indeed, equation (4.147) gives that the image is large when

$$\boldsymbol{\vartheta} \cdot \frac{(\boldsymbol{y}^R - \boldsymbol{x})}{|\boldsymbol{y}^R - \boldsymbol{x}|} = O(\cos\alpha),$$

so the larger α is, the further from the array $\boldsymbol{y}^R$ can be. Moreover, the larger the aperture is, the more points $\boldsymbol{y}^R$ satisfy this equation, for at least some subset of the receiver locations in the array. $\square$

4.D Numerical solution of the forward problem

To solve the system of nonlinear Helmholtz equations (4.2)-(4.3) numerically we employ the fixed point iteration described below. Denote by H_k and H_{2k} respectively the linear operators in (4.2)-(4.3):

$$H_k = \Delta + k^2(1 + 4\pi\eta(\boldsymbol{x}) + 4\pi\eta_1(\boldsymbol{x})), \tag{4.148}$$

$$H_{2k} = \Delta + (2k)^2(1 + 4\pi\eta(\boldsymbol{x}) + 4\pi\eta_1(\boldsymbol{x})). \tag{4.149}$$

We also introduce the successive approximations to the solutions of (4.2)-(4.3) as

$$u^{(j)}(\boldsymbol{x}) \approx u_1(\boldsymbol{x}) - u_i(\boldsymbol{x}), \tag{4.150}$$

$$v^{(j)}(\boldsymbol{x}) \approx u_2(\boldsymbol{x}). \tag{4.151}$$

We substitute (4.150)–(4.151) into (4.2)-(4.3), and obtain for $j = 0, 1, \ldots$ the following fixed point iteration

$$u^{(j+1)} = -4\pi k^2 H_k^{-1}\left[2\eta_2(\boldsymbol{x})v^{(j)}(\boldsymbol{x})(u^{(j)}(\boldsymbol{x}) + u_i(\boldsymbol{x}))^* + (\eta_0(\boldsymbol{x}) + \eta_1(\boldsymbol{x}))u_i(\boldsymbol{x})\right], \tag{4.152}$$

$$v^{(j+1)} = -16\pi k^2 H_{2k}^{-1}\left[\eta_2(\boldsymbol{x})(u^{(j+1)}(\boldsymbol{x}) + u_i(\boldsymbol{x}))^2\right], \tag{4.153}$$

where we start with $u^{(0)}(\boldsymbol{x}) \equiv v^{(0)}(\boldsymbol{x}) \equiv 0$. Note that for convergence of the fixed point iteration it is crucial to include all linear terms into the definition of H_k and H_{2k}, in particular $4\pi\eta_0(\boldsymbol{x}) + 4\pi\eta^{(1)}(\boldsymbol{x})$.

The inverses in (4.152)–(4.153) mean that we have to solve the PDEs with operators (4.148)–(4.149) in the whole space, both inside and outside the rectangular region V. This can be done by discretizing (4.148)–(4.149) inside V and then placing a perfectly matched layer (PML) around it to account for $\mathbb{R}^d \setminus V$. To that effect we replace the operators H_k and H_{2k} in (4.152)–(4.153) with their PML counterparts. Following [28], in the case $d = 2$ we define the PML analogues of H_k and H_{2k} as

$$H_k^{\text{PML}} = \frac{\partial}{\partial x}\left(\frac{e_y(\boldsymbol{x})}{e_x(\boldsymbol{x})}\frac{\partial}{\partial x}\right) + \frac{\partial}{\partial y}\left(\frac{e_x(\boldsymbol{x})}{e_y(\boldsymbol{x})}\frac{\partial}{\partial y}\right) + k^2 e_x(\boldsymbol{x})e_y(\boldsymbol{x})(1 + 4\pi\eta_0(\boldsymbol{x}) + 4\pi\eta^{(1)}(\boldsymbol{x})), \tag{4.154}$$

$$H_{2k}^{\text{PML}} = \frac{\partial}{\partial x}\left(\frac{e_y(\boldsymbol{x})}{e_x(\boldsymbol{x})}\frac{\partial}{\partial x}\right) + \frac{\partial}{\partial y}\left(\frac{e_x(\boldsymbol{x})}{e_y(\boldsymbol{x})}\frac{\partial}{\partial y}\right) + (2k)^2 e_x(\boldsymbol{x})e_y(\boldsymbol{x})(1 + 4\pi\eta_0(\boldsymbol{x}) + 4\pi\eta^{(1)}(\boldsymbol{x})), \tag{4.155}$$

where $e_x(\boldsymbol{x})$ and $e_y(\boldsymbol{x})$ are defined by

$$e_x(\boldsymbol{x}) = \begin{cases} 1 - ia_0\left(\dfrac{d_x(\boldsymbol{x})}{L_x}\right)^2, & \text{if } \boldsymbol{x} \in V_x^{\text{PML}} \\ 1, & \text{otherwise} \end{cases}, \; e_y(\boldsymbol{x}) = \begin{cases} 1 - ia_0\left(\dfrac{d_y(\boldsymbol{x})}{L_y}\right)^2, & \text{if } \boldsymbol{x} \in V_y^{\text{PML}} \\ 1, & \text{otherwise} \end{cases} \tag{4.156}$$

Here V_x^{PML} and V_y^{PML} each contain two PML layers that we surround V with in x and y directions respectively. The layers in V_x^{PML} have widths L_x, the layers in V_y^{PML} have widths L_y. In the numerical experiments we take $L_x = L_y = 1.5\lambda$. The functions $d_x(\boldsymbol{x})$ and $d_y(\boldsymbol{x})$ compute the distances from a point $\boldsymbol{x}$ in the corresponding PML layer to ∂V. The constant $a_0 = 1.79$ is chosen according to [28].

Finally, to apply the fixed point iteration (4.152)–(4.153) numerically, we discretize

(4.154)–(4.155) on a tensor product finite difference grid with a five point stencil. Both H_k^{PML} and H_{2k}^{PML} are discretized on the same grid. Thus, the grid should be refined enough to properly resolve the higher wavenumber operator H_{2k}^{PML}. In the numerical experiments we take equal grid steps in x and y directions $h_x = h_y = \frac{\lambda}{20}$.

Chapter 5

Conclusion

5.1 Closely related works

Here we summarize the current research status in fields that are most related to our work.

5.1.1 On scattering from small nonlinear particles

Scattering of waves from a collection of small nonlinear scatterers is of broad interest [23, 42]. Although no exact solutions are known in three dimensional space, this problem has been investigated by many numerical methods [19] and analytical approximations [31, 66, 40, 7]. An important branch of analytical approximations was originated from Foldy and Lax, who modeled the susceptibility of the scatterers as a sum of delta functions [36, 49]. The Foldy-Lax model captures some multiple scattering effects and therefore allows resonances, which is its key advantage over the Born approximation. In the original papers [36, 49], linear scatterers were considered and self-interaction was omitted, which means that the field at one scatterer explicitly depends on the incident field at that scatterer and the total fields at the other scatterers. The Foldy-Lax method has been generalized to weakly nonlinear scatterers by linearization in the weak nonliearity [40]. It has also been generalized to

include self-interaction by assigning the scatterers finite volumes [7]. In Ref. [7], Bass used the generalized Foldy-Lax method with self-interaction to study the shift of resonances in the presence of scatterers of weak Kerr nonlinearity. Our method is a close analogue of Bass's work [7], where more general nonlinearities in the setting of the Maxwell equations were taken into consideration.

5.1.2 Optical theorem for nonlinear media

The optical theorem is a conservation law that shows up in a variety of settings including optics, acoustics, quantum mechanics and quantum field theory [16, 58, 1, 72]. The optical theorem for light has only been shown to hold in linear media [90, 45, 16]. But in fact, the assumption that the material media respond to light linearly is not essential. We consider polarization densities as arbitrary functions of the electric field, and derive the generalized optical theorem in scalar wave theory and for the Maxwell equations following a similar approach to [21, 53]. Note that for the polarization density to be an arbitrary function of the electric field, the nonlinearity can not be too strong, since strong nonlinearity yields effects such as shock wave formation and phase mismatch [23].

5.1.3 Imaging of nonlinear scatterers

Nonlinear scatterers are promising tools for improving imaging results since nonlinearity gives a richer structure of the scattering process [88, 60]. However in the setting of random media, the only literature is [2] to the best of our knowledge. There it was shown that the image of the nonlinear susceptibility is indeed superior. In this work, the scatterers exhibit SGH, and the illumination is direction resolved time harmonic plane waves. The waves are assumed to be two dimensional functions and specific polarizations are chosen, such that the wave equations are two-dimensional Helmholtz equations where the inhomogeneity shows

up in the derivative. Migration type imaging functions are considered, and the analysis of the effect of the random medium was based on the Born approximation. Our work is done in a similar set up, with the following three fundamental differences. First, we consider the full three-dimensional problem within the scalar theory developed in chapter 1. Second, in addition to investigating migration imaging functions, we also study CINT imaging. Third, our analysis is carried out in the random geometrical optics model, where the effect of the random background is to generate random phases as the waves propagate.

5.2 Contributions

In this thesis, we first presented a method of solving the direct scattering problem from a finite number of nonlinear particles in the scalar theory. This method holds when the nonlinearity is weak and the size of the particles is much less than the wavelength of the incident fields. The solutions given by this method are explicit and analytic. We showed that for common types of quadratic and cubic nonlinear processes in the presence of one and two scatterers, the resonances of the intensity of the scattered fields are modified, and that the energy is transferred among frequency components. We also showed that when a single particle of Kerr nonlinearity is involved, the scattering process displays bistability for a certain set of parameters that we exactly characterize.

We then considered scattering problems in the full Maxwell system. We showed that the optical theorem holds exactly for polarization densities as arbitrary functions of the electric fields. We generalized the method of solving the direct scattering problem from small weakly nonlinear scatterers to the full Maxwell system. We applied our results to modeling near-field scanning optical microscopy (NSOM). We showed that with proper choice of the direction and polarization of the illumination field, NSOM with nonlinear tips is a background-free microscopy technique that yields subwavelength resolution.

We finally provided a method of robustly locating small nonlinear scatterers in random media. To find a few quadratically nonlinear scatterers, we illuminate the medium by monochromatic plane waves at a fixed frequency from multiple directions. The total fields at the incident frequency and the second harmonic frequency are measured by receivers located on the boundary of the random medium. We showed that the coherent interferometry (CINT) image of the nonlinear susceptibility is stable for propagation distances within a few transport mean free path, and does not suffer from the destructive randomized incident field. We analytically derived these results in a specific scaling regime, and numerically observed these phenomena in another specific scaling regime. This was done within the scalar model.

5.3 Future research

The following are possible problems that can be addressed in the future.

5.3.1 Rigorous asymptotics

The method of calculating the scattering amplitudes presented in Ch. 1 and Ch. 2 involves two approximations: (1) the field inside each scatterer is replaced by a constant, and (2) the higher order terms in the weak nonlinearity are truncated. The validity of these two approximations should be rigorously analyzed.

For approximation (1), we have a confirmative result in the scalar model when there is only one scatterer exhibiting Kerr nonlinearity. The idea is to first establish the existence and uniqueness of the solutions to the Lippmann-Schwinger equation (2.90) for sufficiently small scatterers, and then control the remainder of the Taylor expansion of the field by estimating the size of the derivative of the field. We will try to generalize this idea to multiple scatterers and to the full Maxwell system.

5.3.2 Time dependent nonlinear scattering

The analysis of scattering processes in this thesis is done for steady states, where the fields are time harmonic functions with time independent amplitudes. The steady state analysis reveals important features of physical systems but all scattering processes involve time in principle. Thus we plan to study scattering processes that depend on time, and try to answer time related questions such as: how does the energy flow when it is injected into a scattering system, what does it mean for a solution to be stable or unstable, and which branch of the solution does the field choose for a given initial condition in a bistable system.

5.3.3 Inverse problem of near-field scattering optical microscopy

In a NSOM experiment, one could consider the inverse problem of reconstructing the linear susceptibility of the sample from the measured scattered fields. This problem has been solved when the tip is a linear scatterer that is much stronger than the sample in Ref. [83], where the contributions from the tip, the sample and the interaction of the tip and sample are carefully estimated and properly summed. We plan to analyze this problem similarly for NSOM with nonlinear tips.

5.3.4 Radiative transfer equation in nonlinear media

In a random medium, the radiative transport equation (RTE) is an extensively used macroscopic equation. In the scalar model, the RTE takes the form

$$\frac{1}{c}\frac{\partial I(\mathbf{r},\widehat{\mathbf{k}})}{\partial t}+\widehat{\mathbf{k}}\cdot\nabla I(\mathbf{r},\widehat{\mathbf{k}})+(\mu_s+\mu_a)I(\mathbf{r},\widehat{\mathbf{k}})=\mu_s\int d\widehat{\mathbf{k}'}p(\widehat{\mathbf{k}},\widehat{\mathbf{k}'})I(\mathbf{r},\widehat{\mathbf{k}'})\ , \tag{5.1}$$

where $I(\mathbf{r}, \widehat{\mathbf{k}})$ is the intensity of light at $\mathbf{r}$ in the direction of $\widehat{\mathbf{k}}$, μ_s is the scattering coefficient, μ_a is the absorption coefficient, and $p(\widehat{\mathbf{k}}, \widehat{\mathbf{k}'})$ is the phase function. The RTE describes that energy is lost due to absorption and scattering and is also gained by scattering. Derivations of the RTE from the scalar wave equations in a linear random media has been given heuristically by diagrammatic method [22] and asymptotic method [76], and rigorously from first principles [14]. An outline of the asymptotic proof is to consider the Wigner transform in a proper scaling regime and equate the angularly resolved intensity with the expectation of the leading term in a multiscale expansion. The idea of the rigorous derivation is to consider a random medium under specific scaling constraints, and consider waves that travel in a wide cone with opening angle less then 180 degrees. I plan to generalize the RTE for Kerr-type random media.

5.3.5 Variations of imaging nonlinear scatterers in random media

We considered imaging of small scatterers exhibiting SHG in the scalar model. We could consider similar problems with other nonlinear processes within the scalar model, or within the full Maxwell model, or in the presence of a mixture of scatterers with different nonlinearities. We expect the analysis to be more complicated but qualitatively the same.

The illumination that we used is time harmonic plane waves. We could consider other illuminations such as beams, chirps or pulses. As mentioned in Sec. 4.1, these illuminations will induce an average over the frequencies, which may help the CINT imaging function remain stable for stronger inhomogeneities.

Bibliography

[1] E. Abers, *Quantum Mechanics*, Pearson Education, (2003).

[2] H. Ammari, J. Garnier, and P. Millien, Backpropagation imaging in nonlinear harmonic holography in the presence of measurement and medium noises, *SIAM Journal on Imaging Sciences*, **7**, 239–276 (2014).

[3] P. Anger, P. Bharadwaj, and L. Novotny, Enhancement and quenching of single-molecule fluorescence, *Physical Review Letters*, **96**, 113002 (2006).

[4] S. R. Arridge and J. C. Schotland, Optical tomography: forward and inverse problems, *Inverse Problems*, **25**, 123010 (2009).

[5] A Babin and A Figotin, Multilinear spectral decomposition for nonlinear Maxwell equations, *Translations of the American Mathematical Society-Series 2*, **206**, 1–28 (2002).

[6] A. Babin and A. Figotin, Nonlinear maxwell equations in inhomogeneous media, *Communications in Mathematical Physics*, **241**, 519–581 (2003).

[7] F. G. Bass, V. D. Freilikher, and V. V. Prosentsov, Small nonlinear particles in waveguides and resonators, *Journal of Electromagnetic Waves and Applications*, **14**, 1723–1741 (2000).

[8] B. Biondi, *3D Seismic Imaging*, Society of Exploration Geophysicists Tulsa, Okla, USA, (2006).

[9] N. Bleistein, J. K. Cohen, W John Jr, et al., *Mathematics of multidimensional seismic imaging, migration, and inversion*, Springer Science & Business Media, (2013).

[10] P. Blomgren, G. Papanicolaou, and H. Zhao, Super-resolution in time-reversal acoustics, *The Journal of the Acoustical Society of America*, **111**, 230–248 (2002).

[11] L Borcea, G Papanicolaou, and C Tsogka, Adaptive interferometric imaging in clutter and optimal illumination, *Inverse Problems*, **22**, 1405 (2006).

[12] L Borcea, G Papanicolaou, and C Tsogka, Asymptotics for the space-time Wigner transform with applications to imaging, *Stochastic Differential Equations: Theory and Applications (in Honor of Prof. Boris L. Rozovskii), Interdiscip. Math. Sci*, **2**, 91–112 (2007).

[13] L Borcea, J Garnier, G Papanicolaou, and C Tsogka, Enhanced statistical stability in coherent interferometric imaging, *Inverse Problems*, **27**, 085004 (2011).

[14] L. Borcea and J. Garnier, Derivation of a one-way radiative transfer equation in random media, *Physical Review E*, **93**, 022115 (2016).

[15] L. Borcea, G. Papanicolaou, and C. Tsogka, Interferometric array imaging in clutter, *Inverse Problems*, **21**, 1419 (2005).

[16] M. Born and E. Wolf, *Principles of Optics*, UK, Cambridge University Press, (1999).

[17] R. W. Boyd, *Nonlinear Optics*, London, Academic Press, (2008).

[18] M. L. Brongersma, J. W. Hartman, and H. A. Atwater, Electromagnetic energy transfer and switching in nanoparticle chain arrays below the diffraction limit, *Physical Review B*, **62**, R16356–R16359 (2000).

[19] S. Caorsi, A. Massa, and M. Pastorino, Method of moments as applied to arbitrarily shaped bounded nonlinear scatterers, *Journal de Physique III*, **4**, 87–97 (1994).

[20] R. Carminati, J.-J. Greffet, C Henkel, and J. M. Vigoureux, Radiative and non-radiative decay of a single molecule close to a metallic nanoparticle, *Optics Communications*, **261**, 368–375 (2006).

[21] P. S. Carney, J. C. Schotland, and E. Wolf, Generalized optical theorem for reflection, transmission, and extinction of power for scalar fields, *Physical Review E*, **70**, 036611 (2004).

[22] A Cazé and J. C. Schotland, Diagrammatic and asymptotic approaches to the origins of radiative transport theory: tutorial, *JOSA A*, **32**, 1475–1484 (2015).

[23] D. Censor, Scattering by weakly nonlinear objects, *SIAM Journal on Applied Mathematics*, **43**, 1400–1417 (1983).

[24] R. R. Chance, A Prock, and R Silbey, Molecular fluorescence and energy transfer near interfaces, *Adv. Chem. Phys*, **37**, 65 (1978).

[25] D. S. Chemla and J Jerphagnon, Optical Second-Harmonic Generation in Paratellurite and Kleinman's Symmetry Relations, *Applied Physics Letters*, **20**, 222–223 (1972).

[26] W. Chen and D. L. Mills, Optical response of a nonlinear dielectric film, *Physical Review B*, **35**, 524 (1987).

[27] W. Chen and D. L. Mills, Optical response of nonlinear multilayer structures: bilayers and superlattices, *Physical Review B*, **36**, 6269 (1987).

[28] Z. Chen, D. Cheng, W. Feng, and T. Wu, An optimal 9-point finite difference scheme for the Helmholtz equation with PML, *Int. J. Numer. Anal. Model*, **10**, 389–410 (2013).

[29] K. B. Crozier, E. Togan, E. Simsek, and T. Yang, Experimental measurement of the dispersion relations of the surface plasmon modes of metal nanoparticle chains, *Optics Express*, **15**, 17482–17493 (2007).

[30] J. I. Dadap, J. Shan, and T. F. Heinz, Theory of optical second-harmonic generation from a sphere of centrosymmetric material: small-particle limit, *JOSA B*, **21**, 1328–1347 (2004).

[31] J. I. Dadap, J. Shan, K. B. Eisenthal, and T. F. Heinz, Second-harmonic Rayleigh scattering from a sphere of centrosymmetric material, *Physical Review Letters*, **83**, 4045 (1999).

[32] C. A. Dailey, B. J. Burke, and G. J. Simpson, The general failure of Kleinman symmetry in practical nonlinear optical applications, *Chemical Physics Letters*, **390**, 8–13 (2004).

[33] P Debye, The diffraction theory of aberrations, *Ann. Phys.(Leipzig)*, **30**, 59–62 (1909).

[34] L. Devroye, Nonuniform random variate generation, *Handbooks in Operations Research and Management Science*, **13**, 83–121 (2006).

[35] M. Fink, Time reversal of ultrasonic fields. I. Basic principles, *IEEE Transactions on Ultrasonics, Ferroelectrics, and Frequency Control*, **39**, 555–566 (1992).

[36] L. L. Foldy, The Multiple Scattering of Waves. I. General Theory of Isotropic Scattering by Randomly Distributed Scatterers, *Physical Review*, **67**, 107–119 (1945).

[37] Y. N. Gartstein and V. M. Agranovich, Excitons in long molecular chains near the reflecting interface, *Physical Review B*, **76**, 115329 (2007).

[38] A. A. Govyadinov and V. A. Markel, From slow to superluminal propagation: Dispersive properties of surface plasmon polaritons in linear chains of metallic nanospheroids, *Physical Review B*, **78**, 035403 (2008).

[39] W. T. Grandy, *Scattering of Waves from Large Spheres*, Cambridge University Press, (1992).

[40] B. Grémaud and T. Wellens, Speckle instability: Coherent effects in nonlinear disordered media, *Physical Review Letters*, **104**, 133901 (2010).

[41] H. Harutyunyan, S. Palomba, J. Renger, R. Quidant, and L. Novotny, Nonlinear dark-field microscopy, *Nano Letters*, **10**, 5076–5079 (2010).

[42] R. O. Hstger, Harmonic radar systems for near-ground in-foliage nonlinear scatterers, *IEEE Transactions on Aerospace and Electronic Systems*, 230–245 (1976).

[43] A. Ishimaru, Theory and application of wave propagation and scattering in random media, *Proceedings of the IEEE*, **65**, 1030–1061 (1977).

[44] A. Ishimaru, Wave propagation and scattering in random media and rough surfaces, *Proceedings of the IEEE*, **79**, 1359–1366 (1991).

[45] D. S. Jones, CIX. On the scattering cross section of an obstacle, *The London, Edinburgh, and Dublin Philosophical Magazine and Journal of Science*, **46**, 957–962 (1955).

[46] F. Keilmann and R. Hillenbrand, Near-field microscopy by elastic light scattering from a tip, *Philosophical Transactions of Royal Society of London Series A :Mathematica, Physical and Engineering Sciences*, 787–806 (2004).

[47] H. Kushner, *Approximation and Weak Convergence Methods for Random Processes*, Cambridge, MIT Press, (1984).

[48] P. K. Kwan and Y. Y. Lu, Computing optical bistability in one-dimensional nonlinear structures, *Optics Communications*, **238**, 169–175 (2004).

[49] M. Lax, Multiple scattering of waves, *Reviews of Modern Physics*, **23**, 287 (1951).

[50] M. Lax, Multiple scattering of waves. II. The effective field in dense systems, *Physical Review*, **85**, 621–629 (1952).

[51] A. Lewis and K. Lieberman, Near-field optical imaging with a non-evanescently excited high-brightness light source of sub-wavelength dimensions, *Nature*, **354**, 214–216 (1991).

[52] W. Li and J. C. Schotland, Optical theorem for nonlinear media, *Physical Review A*, **92**, 043824 (2015).

[53] D. R. I. Lytle, P. S. Carney, J. C. Schotland, and E. Wolf, Generalized optical theorem for reflection, transmission, and extinction of power for electromagnetic fields, *Physical Review E*, **71**, 056610 (2005).

[54] S. A. Maier, P. G. Kik, and H. A. Atwater, Observation of coupled plasmon-polariton modes in Au nanoparticle chain waveguides of different lengths: Estimation of waveguide loss, *Applied Physics Letters*, **81**, 1714–1716 (2002).

[55] S. A. Maier, P. G. Kik, H. A. Atwater, S. Meltzer, E. Harel, B. E. Koel, and A. A. Requicha, Local detection of electromagnetic energy transport below the diffraction limit in metal nanoparticle plasmon waveguides, *Nature Materials*, **2**, 229–232 (2003).

[56] J. H. Marburger and F. S. Felber, Theory of a lossless nonlinear Fabry-Perot interferometer, *Physical Review A*, **17**, 335 (1978).

[57] V. A. Markel and A. K. Sarychev, Propagation of surface plasmons in ordered and disordered chains of metal nanospheres, *Physical Review B*, **75**, 085426 (2007).

[58] P. L. Marston, Generalized optical theorem for scatterers having inversion symmetry: Applications to acoustic backscattering, *The Journal of the Acoustical Society of America*, **109**, 1291–1295 (2001).

[59] G. Mie, Beiträge zur Optik trüber Medien, speziell kolloidaler Metallösungen, *Annalen der physik*, **330**, 377–445 (1908).

[60] W. Min, C. W. Freudiger, S. Lu, and X. S. Xie, Coherent nonlinear optical imaging: beyond fluorescence microscopy, *Annual Review of Physical Chemistry*, **62**, 507 (2011).

[61] F. Natterer, *The Mathematics of Computerized Tomography*, Siam, (1986).

[62] R. G. Newton, *Scattering Theory of Waves and Particles*, Berlin Heidelberg, Springer-Verlag, (1982).

[63] C. J. Nolan and M. Cheney, Synthetic aperture inversion, *Inverse Problems*, **18**, 221 (2002).

[64] L. Novotny and B. Hecht, *Principles of Nano-Optics*, Cambridge University Press, (2012).

[65] H. M. Nussenzveig, *Diffraction Effects in Semiclassical Scattering*, Cambridge University Press, (1992).

[66] D Östling, P Stampfli, and K. H. Bennemann, Theory of nonlinear optical properties of small metallic spheres, *Zeitschrift für Physik D Atoms, Molecules and Clusters*, **28**, 169–175 (1993).

[67] S. Palomba, M. Danckwerts, and L. Novotny, Nonlinear plasmonics with gold nanoparticle antennas, *Journal of Optics A: Pure and Applied Optics*, **11**, 114030 (2009).

[68] S. Palomba and L. Novotny, Near-field imaging with a localized nonlinear light source, *Nano Letters*, **9**, 3801–3804 (2009).

[69] G. Papanicolaou, L. Ryzhik, and K. Sølna, Self-averaging from lateral diversity in the Itô-Schrödinger equation, *Multiscale Modeling & Simulation*, **6**, 468–492 (2007).

[70] G. Papanicolaou, L. Ryzhik, and K. Sølna, Statistical stability in time reversal, *SIAM Journal on Applied Mathematics*, **64**, 1133–1155 (2004).

[71] Y Pavlyukh and W Hübner, Nonlinear Mie scattering from spherical particles, *Physical Review B*, **70**, 245434 (2004).

[72] M. E. Peskin and D. V. Schroeder, *An Introduction to Quantum Field Theory*, Addison-Wesley Publishing Company, (1995).

[73] E. M. Purcell and C. R. Pennypacker, Scattering and absorption of light by nonspherical dielectric grains, *The Astrophysical Journal*, **186**, 705–714 (1973).

[74] M. C. W. van Rossum and T. M. Nieuwenhuizen, Multiple scattering of classical waves: microscopy, mesoscopy, and diffusion, *Reviews of Modern Physics*, **71**, 313 (1999).

[75] S. M. Rytov, Y. A. Kravtsov, and V. I. Tatarskii. *Principle of statistical radiophysics IV: Wave propagation through random media. Chapter 4*. 1989.

[76] L. Ryzhik, G. Papanicolaou, and J. B. Keller, Transport equations for elastic and other waves in random media, *Wave Motion*, **24**, 327–370 (1996).

[77] B. E. A. Saleh and M. C. Teich, *Fundamentals of Photonics*, Wiley-Interscience, (1991).

[78] J. C. Schotland, A Cazé, and T. B. Norris, Scattering of entangled two-photon states, *Optics Letters*, **41**, 444–447 (2016).

[79] V. I. Shcheslavskiy, S. M. Saltiel, A. Faustov, G. I. Petrov, and V. V. Yakovlev, Third-harmonic Rayleigh scattering: theory and experiment, *Journal of the Optical Society of America B*, **22**, 2402–2408 (2005).

[80] D. Shelton and Z. Lu, Kleinman symmetry deviations for hydrogen, *Physical Review A*, **37**, 2231 (1988).

[81] Y.-R. Shen, *Principles of Nonlinear Optics*, New York, Wiley-Interscience, (1984).

[82] S Singh, W. A. Bonner, and L. G. Van Uitert, Violation of Kleinman's symmetry condition in paratellurite, *Physics Letters A*, **38**, 407–408 (1972).

[83] J. Sun, P. S. Carney, and J. C. Schotland, Strong tip effects in near-field scanning optical tomography, *Journal of Applied Physics*, **102**, 103103 (2007).

[84] C.-T. Tai, *Dyadic Green functions in electromagnetic theory*, Institute of Electrical & Electronics Engineers (IEEE), (1994).

[85] S. Takahashi and A. V. Zayats, Near-field second-harmonic generation at a metal tip apex, *Applied Physics Letters*, **80**, 3479–3481 (2002).

[86] C. W. Therrien, *Discrete random signals and statistical signal processing*, Prentice Hall PTR, (1992).

[87] N. Tsutsumi, T. Mizutani, W. Sakai, T. Watanabe, and S. Miyata, Precise study of nonlinear optical coefficients and hyperpolarizabilities in cold-drawn and poled ferroelectric Nylon 11 films, *The Journal of Chemical Physics*, **108**, 9839–9850 (1998).

[88] V. V. Tuchin and V Tuchin, *Tissue Optics: Light Scattering Methods and Instruments for Medical Diagnosis*, SPIE Press Bellingham, (2007).

[89] H. C. Van De Hulst, *Light Scattering by Small Particles*, Courier Corporation, (1957).

[90] H. C. Van De Hulst, On the attenuation of plane waves by obstacles of arbitrary size and form, *Physica*, **15**, 740–746 (1949).

[91] J. Vigoureux, C Girard, and F Depasse, Nonlinear near field optics, *Journal of Modern Optics*, **41**, 49–58 (1994).

[92] P. de Vries, D. V. van Coevorden, and A. Lagendijk, Point scatterers for classical waves, *Reviews of Modern Physics*, **70**, 447–466 (1998).

[93] H. G. Winful, J. H. Marburger, and E Garmire, Theory of bistability in nonlinear distributed feedback structures, *Applied Physics Letters*, **35**, 379–381 (1979).

[94] M. Xu and S. Jiang, Breaking of the overall permutation symmetry in nonlinear optical susceptibilities of one-dimensional periodic dimerized Hückel model, *Journal of Physics: Condensed Matter*, **18**, 8987 (2006).

[95] A. V. Zayats and V. Sandoghdar, Apertureless scanning near-field second-harmonic microscopy, *Optics Communications*, **178**, 245–249 (2000).

[96] A. Zayats and V Sandoghdar, Apertureless near-field optical microscopy via local second-harmonic generation, *Journal of Microscopy*, **202**, 94–99 (2001).

[97] H. Zhou, I Honma, J. W. Haus, H Sasabe, and H Komiyama, Synthesis and optical properties of coated nanoparticle composites, *Journal of luminescence*, **70**, 21–34 (1996).